

EUROPEAN SPACE AGENCY



Final Report

INDREX-II Indonesian Radar Experiment Campaign over Tropical Forest in L- and P-band



WAGENINGEN UNIVERSITY
WAGENINGEN WUR

DATE: 14 June 2006

Version 1

Contacts:

Dr. Irena Hajnsek
German Aerospace Center
Microwave and Radar Institute
Department: SAR Technology
Pol-InSAR Research Group
P.O. Box 1116, 82234 Wessling, Germany
Tel.: +49 8153 28 2363
Fax.: +49 8153 28 1135
Email: irena.hajnsek@dlr.de

Dr. Dirk Hoekman
Borneo Orangutan Survival Foundation (BOS)
& Wageningen University (WUR)
Department of Environmental Sciences
Nieuwe Kanaal 11,
6709 PA Wageningen, Netherlands
Tel.: +31 317 482894
Fax.: +31 317 484885
Email: dirk.hoekman@wur.nl

Contents

1 Introduction.....	5
2 Objectives of the INDREX-II Experiment.....	6
3 Consolidates Tropical Test Site	7
4 Test Site Description	7
4.1 Overview of the Test Area at Kalimantan	7
4.1.1 General description of the Mawas area.....	8
4.1.2 General description of the Balikpapan area	8
4.2 Bio-/Geo-Physical Characterisation of the Test Site.....	9
4.3 Specific Objectives of the Test Sites	13
4.4 Test Site Location.....	14
5 Data Acquisition	18
5.1 Ground Data Acquisition	18
5.1.1 Background Test Sites	18
5.1.2 In Situ Measurements Performed during the Flight Campaign.....	18
5.1.3 Some details of measurement approach.....	20
5.2 Synthetic Aperture Radar Data Acquisition	21
5.2.1 Mission Logistics	21
5.2.2 Ferry flight of the Do228.....	21
5.2.3 Transfer of the E-SAR Equipment.....	22
5.2.4 Installation of the E-SAR system on board the Do228	23
5.2.5 Calibration of the E-SAR system.....	23
5.2.6 Main Measurement Campaign	25
5.2.7 First Test Processing on Site	26
5.2.8 Flight schedule.....	27
5.2.9 Measurement flight configuration	27
5.3 Data Acquisition Flight Tracks	28
5.4 Radar Data Acquisition.....	31
6 Data Description and Processing.....	39
6.1 Ground Data Description	39
6.1.1 Gross data structure	39
6.1.2 GIS data.....	41
6.1.3 Hydrology data.....	41
6.1.4 Aerial photography data	45
6.1.5 Field photography data	45

6.1.6 Tree transect field data	45
6.1.7 Biomass and allometry.....	48
6.1.8 Tree transect data quality.....	50
6.1.9 Summary and concluding remarks field data collection	53
6.2 Radar Data Processing and Description	53
6.2.1 Calibration.....	54
6.2.1.1 The calibration test-site	54
6.2.2 Homogeneous tropical rain forest test-site.....	55
6.2.2.1 Calibration Performance	57
6.2.3 Segmentation and Processing Strategy.....	62
6.2.3.1 Large Data Take Handling Problem	62
6.2.4 Segmentation Aspects	63
6.2.5 Test Site Definition and Processing Strategy.....	64
6.2.6 Other Site Definitions	64
6.2.7 Data Segmentation for INDREX-II	65
6.2.8 Summary of Data Delivery	66
6.2.9 Test-Site Samboja Lestari.....	67
6.2.9.1 DEM-Processing.....	67
6.2.9.2 Geocoded Image Processing	67
6.2.9.3 Repeat-Pass Interferometric Processing.....	68
6.2.10 Sungai Wain (North).....	69
6.2.10.1 DEM-Processing	69
6.2.10.2 Geocoded Image Processing	70
6.2.10.3 Repeat-Pass Interferometric Processing.....	71
6.2.11 Sungai Wain (South).....	73
6.2.11.1 DEM-Processing	73
6.2.11.2 Geocoded Image Processing	74
6.2.11.3 Repeat-Pass Interferometric Processing.....	74
6.2.12 Mawas-A	76
6.2.12.1 DEM-Processing	76
6.2.12.2 Geocoded Image Processing	77
6.2.12.3 Repeat-Pass Interferometric Processing.....	78
6.2.13 Mawas-C.....	80
6.2.13.1 DEM-Processing	80
6.2.13.2 Geocoded Image Processing	80
6.2.13.3 Repeat-Pass Interferometric Processing.....	81
6.2.14 Mawas-E	83

6.2.14.1	DEM-Processing	83
6.2.14.2	Geocoded Image Processing	83
6.2.14.3	Repeat-Pass Interferometric Processing.....	84
6.2.15	Meratus	86
6.2.15.1	DEM-Processing	86
6.2.15.2	Geocoded Image Processing	87
6.2.15.3	Repeat-Pass Interferometric Processing.....	87
6.2.16	Summary.....	88
7	Data Analysis	89
7.1	Radar Backscattering Evaluation	89
7.1.1	Mawas research transect.....	89
7.1.2	Balikpapan sites.....	90
7.2	Classification Analysis	93
7.3	Polarimetric SAR and Interferometric SAR Analysis	96
7.3.1	Test Sites and Data Selection	96
7.3.2	Pol-InSAR Processing Flow.....	96
7.3.3	Pol-InSAR Data Discussion	97
7.3.4	Conclusions	121
7.3.5	Quantitative Pol-InSAR Data Analysis	121
7.3.6	Performance Comparison and Discussion	135
8	Summary and Conclusions	137
9	Recommendation.....	139
9.1.1	Ground measurements and Radar backscattering analysis.....	139
9.1.2	Pol-InSAR analysis	139
10	Publications	140
11	Reference	141

1 Introduction

This document aims to describe the airborne experiment for radar data acquisition carried out in Indonesia at the Island Kalimantan. The campaign is named INDREX-II that stays for Indonesian Airborne Radar Experiments. Already in 1996 an airborne Radar experiment in co-operation between the company DORNIER (now EADS Dornier) and the Indonesian Ministry of Forest has been successfully carried out under the name INDREX. The objective of INDREX has been to generate a digital elevation model over a non-accessible region in order to model environmental changes. INDREX-II was a following up campaign conducted under the umbrella of a cooperation agreement between the Indonesian Ministry of Forest and the European Space Agency.

The first planning of INDREX-II started in March 2004 and the main execution phase has been between 24th of October to the 19th of December 2004, whereas the main ground measurements campaign started in the beginning of September 2004 and was longing until March 2005.



INDREX-II has been a successful campaign in terms of experiment planning, radar data and ground measurement acquisition and radar data quality. All suggested experiments could be performed as described in the Experimental Plan submitted to ESA. The planned time schedule could be kept and no major technical problem occur during the INDREX-II campaign.

The successful execution of such a challenging campaign requires the involvement of many committed persons. We like to thank ESA for their continuously support, not only financial but also for their advice and quick response in critical situations, throughout the project. INDREX-II could be not performed without the help of the Indonesian Ministry of Forest, which has been the driving force for the project execution. Further we like to thank AIR AMPERA, an Indonesian handler, for their guidance through the Indonesian administration jungle. The ground and on site activities has been supported by the Borneo Orangutan Survival Foundation (BOS) and the Indonesian remote sensing company SARVISION. All ground activities has been coordinated and performed by the 4 person team from the Wageningen University form The Netherlands. The airborne activities, which included the permission preparation, sensor transport and integration into the aircraft, the aircraft transfer and radar data acquisition has been coordinated by a 20 person team from the Microwaves and Radar Institute, from DLR in Germany.

The final report summarises the objectives of INDREX-II, the description of the tropical forest test site, the radar data and ground data acquisition, as well as the processing and the first results of the INDREX-II campaign.

2 Objectives of the INDREX-II Experiment

The objective of INDREX-II was to build up a data base for the investigation and validation of bio-/geo-physical parameters obtained from L- and P-band polarimetric SAR interferometry (Pol-InSAR) acquired over tropical forests and to secure with this data set that feedback to the European Agency regarding the optimal SAR sensor configuration and algorithms for biomass retrieval and monitoring in tropical areas can be provided.

Over a variety of forest types (Boreal, Mediterranean and Temperate) Pol-InSAR data has been already acquired with L-band and investigations with regards to bio-/geo-physical forest parameter retrieval are ongoing. The big unknown forest type is tropical and subtropical forest in term of data availability and parameter estimation feasibility. Tropical forests are the most complex structured and heterogeneous forest types and representing therefore the highest challenge for their observation. SAR in general seems to be the only observing instrument, which could provide vertical structure and surface ground information using long wavelength SAR. The combination of long wavelength and polarimetric interferometry SAR seems to be an unbeatable technique for quantitative parameter estimation over forest areas and is to be investigated to answer open questions to the radar community.

In a first line this campaign should be able to give the following first order answers to the questions in a short time:

- 1. *Is there an empirical relation between the radar backscatter and the forest biomass using L- and/or P-band?***
- 2. *Does L or/and P-band penetrates though the dense tropical forest and shows reflection from the ground?***
- 3. *Is it possible to estimate forest height with L- and/or P-band over tropical forest?***

In order to answer these crucial questions repeat pass polarimetric SAR interferometry in L- and P-band has been flown with the Experimental Synthetic Aperture Radar (E-SAR) of the German Aerospace Center (DLR), Microwaves and Radar Institute (HR). Additionally, for the support single pass X-band for the digital elevation model generation and dual polarimetric C-band mode has been flown and acquired. In advance and parallel to the flight campaign an extensive ground measurement campaign is performed estimating forest height and forest biomass in different test areas. In Figure 4.1 a matrix for the INDREX-II campaign is drafted presenting the chosen SAR observables, the methodology how to retrieve the bio-/geo-physical forest parameters and the ground as well as the SAR estimated parameters. For the forest biomass retrieval two methods has been chosen, one empirical relation linking the ground measured forest biomass to the radar backscatter and using a classification procedure to support the regional separation of different forest biomass classes and one Pol-InSAR model based approach using the well known 'Random Volume over Ground model' to estimate directly forest height and take the allometric relation to forest biomass estimation in tropical forest into account.

In a long term, for example in a frame of other studies, this data set can be used for a wide range of forest studies, from field ecologists to global ecological modelling. Where on the one side hopefully scientific questions could be answered, perhaps also new ideas in terms of algorithm development can be expressed and on the other side probably new questions will be rising.

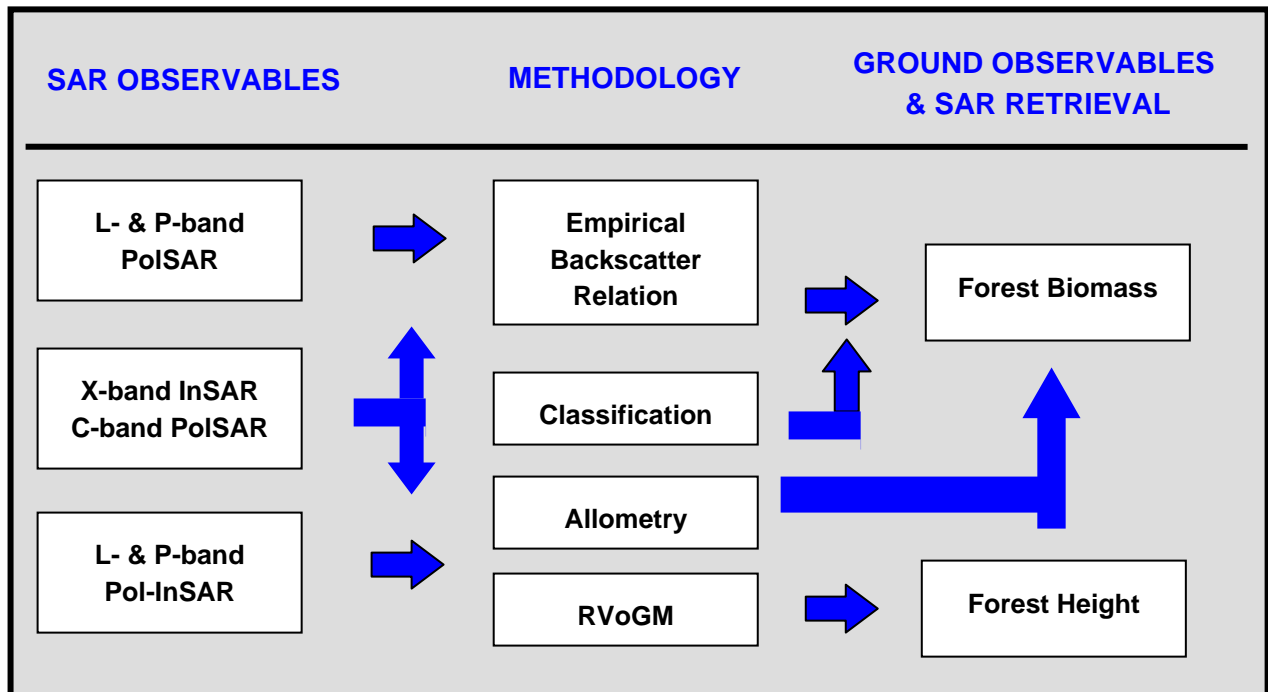


Fig. 4.1: INDREX-II Objective Matrix with intended SAR Observables, chosen methodology, taking ground measurements and estimating/validating the SAR retrievals (PoISAR: Polarimetric SAR, InSAR: Interferometric SAR, Pol-InSAR: Polarimetric SAR Interferometry, RVoGM: Random Volume over Ground Model).

3 Consolidates Tropical Test Site

The Indonesian tropical forest has been chosen as already long term ongoing research on the ground since 1993 is performed. From the first airborne radar flight within the Indonesian Radar Experiment (INDREX) numerous remote sensing data could be collected and are available in a data base. Simultaneous to the remote sensing data, ground measurements have been collected and are available. Several ground acquisitions from periods between the remote sensing acquisitions are as well available. Hence, Kalimantan is the most suitable test site in terms of tropical forest diversity and availability of remote sensing as well as ground data. The description of the test site is available in Section 4.

Additionally, in Indonesia a good collaboration with the Indonesian Ministry of Forestry is already established and together with non-governmental organisations as the Borneo Orangutan Survival foundation (BOS) and SARVISION Indonesia a strong support in terms of delivering up to date required ground measured forest parameters was given.

4 Test Site Description

4.1 Overview of the Test Area at Kalimantan

Two test areas have been selected. The first area is the Mawas conservation area located in the province Central Kalimantan in the vicinity of its capital city Palangkaraya. The second area is located in the Province East Kalimantan in the vicinity of the province's largest city Balikpapan. These two

areas comprise all the main broad forest types: lowland Dipterocarp forest, peat swamp forest and mangrove, as well as a variety of the common types of plantations such as oil palm and rubber.

4.1.1 General description of the Mawas area

Southern Borneo is largely flat, gradually sloping towards the sea and is dissected by large parallel rivers running from north to south. As a result of the low altitude extensive coastal swamps have developed during the last 10,000 years (since the last ice age), creating massive peat domes, and elevating the land above the present sea level. The Mawas conservation area comprises several large (ombrogenous) peat domes covered by tropical peat swamp forest types. Typically these range very gradually from a relatively tall (30 m) and dense forest type at the edges towards small (15 m or lower) and open forest types at the centre of a dome. Along the large rivers mixed swamp forests (some are topogenous) and floodplain forests are found. Most of the area is intact. The southern and eastern parts are disturbed by excessive drainage (through canals) and peat and forest fires. Efforts are conducted by BOS and Wetlands International Indonesia to restore the area by blocking canals and reforestation. BOS manages this large area and protects one of the last large populations of wild orang-utans. Major funding is generated through carbon offset trading.

The Mawas area is typical for a large biome, 27 million ha is size in Indonesia alone, comprising enormous stocks of carbon (peat layers often are in excess of 10 m), and comprising unique biodiversity.

4.1.2 General description of the Balikpapan area

The Balikpapan area was originally covered by lowland Dipterocarp forest and some mangrove forest. These forest types are typical for SE Asia, however, disappear at alarming rates. During the last decades the acreage of the lowland forest in the Balikpapan area decreased strongly due to intensive selective logging, illegal logging, conversion to plantations and the vast ENSO (El Niño) induced forest fires of 1982 and 1998. Some large pockets of pristine lowland Dipterocarp forest remain in the Sungai Wain reserve (10.000 ha) and the Gunung Meratus reserve (over 100.000 ha). Both areas are protected by BOS, which uses them as orang-utan reintroduction sites. Large mangrove areas adjacent to the Sungai Wain reserve are still largely intact.

Because of the relatively good accessibility, large variety of typical tropical land cover types, and the excellent logistic support - first by the *Tropenbos* Foundation, later continued by BOS - a lot of remote sensing related research has been conducted in this area. In 1996 the ESA-MOFEC INDREX campaign was conducted with the Dornier high-resolution (1.5 m) InSAR. In 2000 NASA's second 'Pacific Rim' campaign (PacRim 2) was executed here, yielding AirSAR data in TopSAR and PolSAR mode.



Fig. 4.2: Location of the test sites at Kalimantan (Mawas, Sungai Wain, Meratus, Samboja Lestari) and the two main airports (Balikpapan, Palangkaraya)

4.2 Bio-/Geo-Physical Characterisation of the Test Site

Within the measuring campaign eight appropriate test sites have been identified for bio-/geo-physical parameter retrieval. The first two are located in the Mawas area; the remaining six in the Balikpapan area.

1. Mawas Reserve – Undisturbed
2. Mawas Reserve – Disturbed
3. Sungai Wain Reserve
4. Balikpapan Bay Mangrove area
5. Oil Palm Plantation, located in Penajam
6. Samboja Lestari Plantation
7. Gunung Meratus Reserve
8. Rubber Tree Plantation, located in Penajam

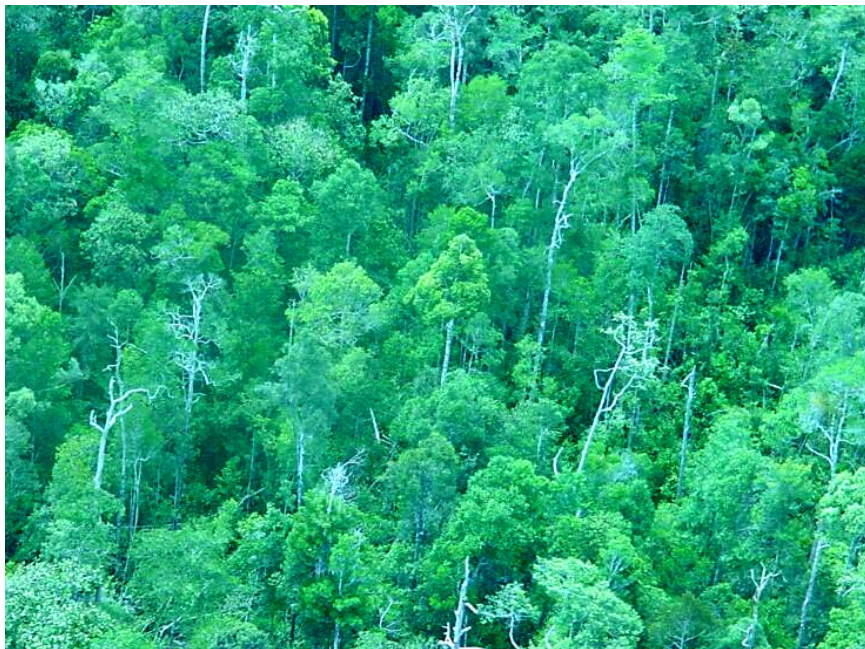
In the following each test site is listed with its characteristics:

<p>(1) Mawas reserve (undisturbed part) Central Kalimantan, 540,000 ha Vegetation: Tropical peat swamp forest types Topography: Almost perfectly flat (slopes < 0.1%) Biomass range: 50-400 ton/ha Height range: 5-25 m Location centre: 114° 36'E, 2° 12'S Extent: +/- 30 km in all directions</p>	<p>(5) Oil Palm plantation, Penajam Vegetation: Oil palm, alang-alang (grass) Topography: Flat to undulating Biomass range: 100-300 ton/ha. Height range: 3-10 m. Location centre: 116° 37'E, 1° 22'S Extent: +/- 5 km in all directions</p>
<p>(2) Mawas reserve (disturbed part) Central Kalimantan Vegetation: Tropical peat swamp forest types, shrubs Topography: Almost perfectly flat (slopes < 0.1%) Biomass range: 5-100 ton/ha Height range: 1-20 m Location centre: 114° 22'E, 2° 15'S Extent: +/- 10 km in all directions</p>	<p>(6) Samboja Lestari reforestation area East Kalimantan, 1,600 ha Vegetation: Plantation forest, many species, age: 1-5 year; Some regenerating forest remnants; Alang-alang (grass) Topography: Undulating - Hilly Biomass range: 30-150 ton/ha. Height range: 2-15 m. Location centre: 116° 59'E, 1° 02'S Extent: +/- 3 km in all directions</p>
<p>(3) Sungai Wain reserve East Kalimantan, 10,000 ha Vegetation: Tropical Dipterocarp lowland forest, swamp forest, mangroves Topography: Hilly (lowland forest) to flat (mangrove and swamp forest) Biomass range: 100-400 ton/ha. Height range: 10-50 m. Location centre: 116° 50'E, 1° 05'S Extent: +/- 10 km in all directions</p>	<p>(7) Gunung Meratus reserve East Kalimantan, 100,000 ha Vegetation: Tropical Dipterocarp forest (lowland and mountain) Topography: Hilly to steep Biomass range: 100-400 ton/ha. Height range: 10-50 m. Location centre: 116° 15'E, 1° 00'S Extent: +/- 20 km in all directions</p>
<p>(4) Balikpapan Bay Mangrove area Vegetation: Mangrove, Nipah Topography: Flat Biomass range: 50-150 ton/ha. Height range: 10-20 m. Location centre: 116° 45'E, 1° 11'S Extent: +/- 10 km in all directions</p>	<p>(8) Rubber Tree plantation, Penajam Vegetation: Rubber Topography: Flat to undulating Biomass range: 100-200 ton/ha. Height range: 10-20 m. Location centre: 116° 37'E, 1° 22'S Extent: +/- 5 km in all directions</p>

Fig. 4.3: Some example photographs from the test sites



Site 3. Sungai Wain Reserve. Lowland Dipterocarp forest type



Site 1. Mawas Reserve – Undisturbed. Peat swamp forest type



Site 7. Gunung Meratus Reserve. Dipterocarp forest in mountainous area



Site 2. Mawas Reserve – Disturbed. Peat swamp forest remnants, shrubs, canals, drought damage, peat fires

4.3 Specific Objectives of the Test Sites

Site 1. Mawas Reserve – Undisturbed

This site has some excellent conditions for research. A 23 km research transect crosses a dome and connects two research field stations. The terrain is very flat (slopes less than 0.1%), the forest canopy is undisturbed and very regular, and slowly changes from a relatively dense and high forest type at both ends of the 23 km transect towards a relatively low and open forest type at the centre of the transect. The biomass variation over a dome typically ranges from 150-300 ton/ha at the edges to 50-100 ton/ha in the centre, which is considered to be the range where P-band is still sensitive. Therefore, this site could be very suitable for the development of biomass estimation algorithms (L- and P-band) and Pol-InSAR (L- and P-band) forest height estimation techniques.

Site 2. Mawas Reserve – Disturbed

Many peat lands are disturbed or damaged beyond recovery by excess drainage through canals. These canals were constructed in the recent past to open such areas for logging and conversion to agricultural use. In dry periods forests collapse along canals, and peat fires occur at large scale. In the El Niño year 1997 an estimated amount of 1-2 Gt Carbon was released to the atmosphere, in Indonesia alone, and mainly through combustion of peat. This is enormous by all measures considering the average global atmospheric annual increase of 3 Gt C.

Since the success of agriculture is limited, and the environmental damage is large in many respects, efforts are ongoing to restore the ecology and hydrology of these areas. To assess the condition of these areas, which is sometimes very critical, and to be able to take action, information from L-band radar seems to be extremely useful. L-band (and P-band) monitoring gives relevant information on forest and flooding conditions, which are crucial to proper understanding.

These processes can be studied in Mawas, where BOS assisted by Wetlands International Indonesia, carries out restoration activities by blocking canals and reforestation.

Site 7. Gunung Meratus reserve

This reserve, part of the large Meratus mountain chain at the border of the provinces East and Central Kalimantan, and extending to the province South Kalimantan, is located around the mountain Gunung Meratus (1230 m in height). It comprises a large area of the remaining lowland Dipterocarp forest and some steep slopes and higher elevation areas in the centre. This very typical and common forest type is more dense and higher than the peat swamp forests. The site would be suitable to test the PolInSAR techniques under more difficult circumstances, and to assess possible limitations.

Along the edges of the reserve large illegal logging activities are common practice. In mountainous areas like Meratus cloud cover is almost permanent around the year. Radar monitoring techniques provide the only practical and realistic information source to combat illegal logging by enabling effective law enforcement.

Site 5-4-3 Sungai Wain, Mangroves, and Oil Palm

These three sites line up at a short distance and can be covered in one track, identical to the track flown by the NASAS/JPL AirSAR in 2000. The Sungai Wain forest reserve contains a wide variety of forests including, Dipterocarp forest and several types of swamp forests. The 1998 (El Niño induced) huge forest fires affected a relatively small part of this area. Other parts of this strip include two large stretches of mangrove forests along both sides of the Balikpapan bay, rice fields, wastelands, a rubber plantation, a large area of oil palm plantations, shrimp ponds, beaches, the Bukit Bangkirai forest reserve and the Wanariset research station.

This site would be ideal to study the mangrove forest biome and a large variety of other typical tropical land cover types. Even the important topic of land cover change could be addressed through comparison with the 2000 AirSAR data.

Site 6. Samboja Lestari plantation

This area comprises tree plantations, most of them monocultures, planted 1-5 years before the campaign. With more than hundred species the variety is large; plots are typically 2-10 ha. Some fast growing species reached levels up to 150 ton/ha already.

This site would be very suitable to study the robustness of Pol-InSAR and biomass estimation techniques in the low biomass range. It is also noted that many tropical species have structures very distinct from species in temperate areas and, therefore, results from the latter areas cannot be simply extrapolated.

Site 8. Rubber Tree Plantation

Together with oil palm, which is the main cash crop in SE Asia, rubber tree plantations cover very large areas and are of large economic importance. A large rubber plantation area is located in Penajam, just south of the Balikpapan bay, i.e. the same area as the oil palm plantations (site 5).

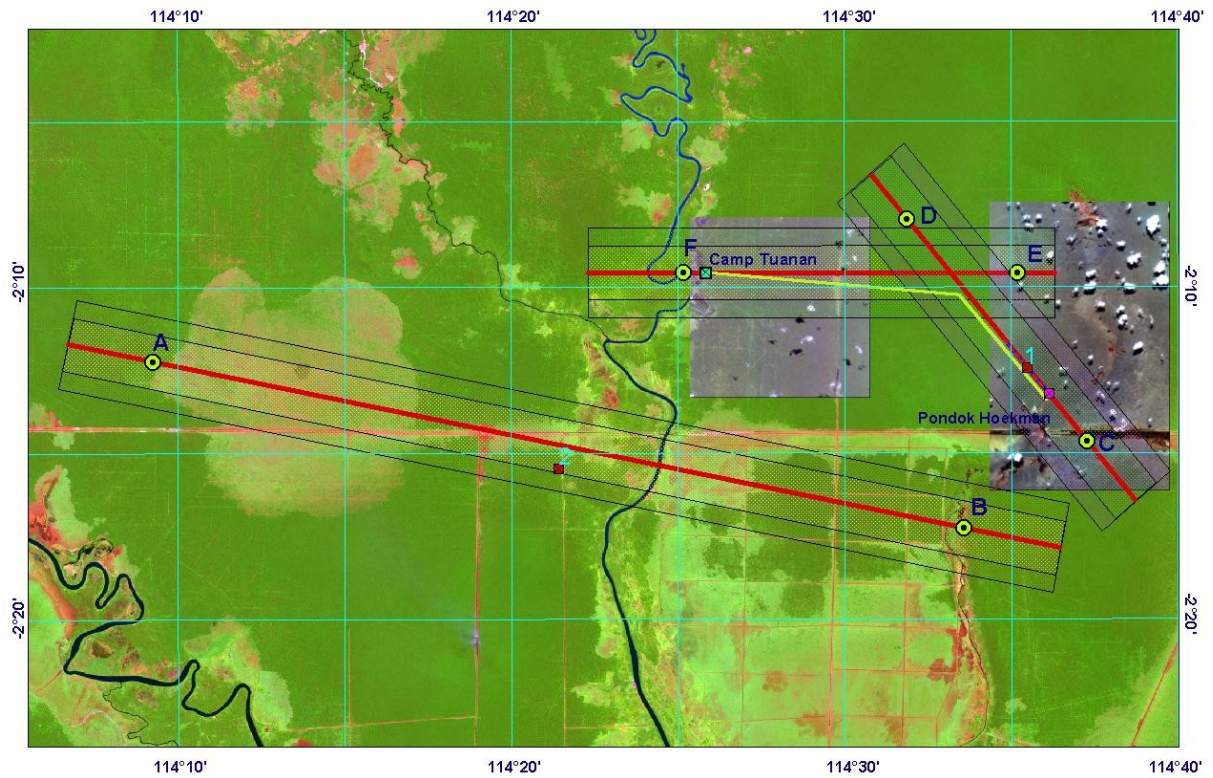
4.4 Test Site Location

In Table 4.1 the proposed coordinates in WGS 84 and the flight track distance of each test site are listed. Correspondingly, the flight areas are displayed on different acquired remote sensing data (see Fig.4.3). The areas covered by the INDREX-I and the PacRim-2 campaign in the Balikpapan area (Mawas was not covered) are indicated in Fig.4.3a and Fig.4.3b, respectively.

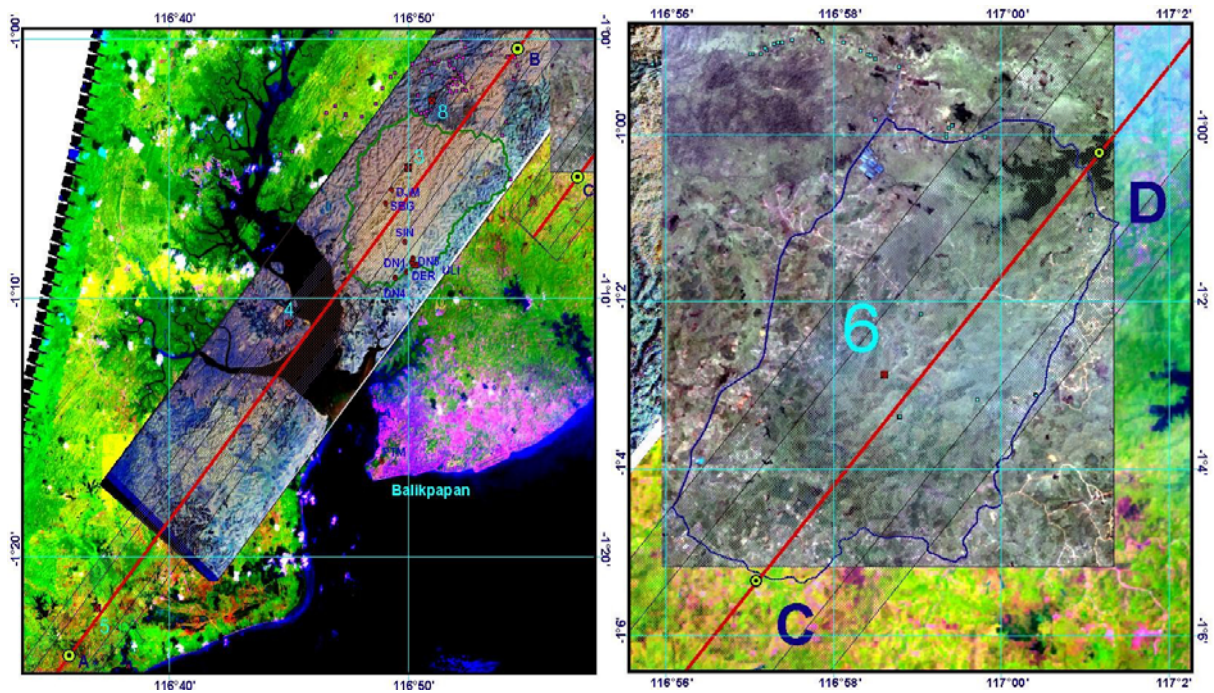
Table 4.1: Coordinates and flight pass distances of the test sites

Test site	Location	Point	Lat	Lon	Length (km)
1	Mawas Reserve (undisturbed part)	C	-2.23611	114.62997	15
		D	-2.12490	114.54050	
	Mawas Reserve (undisturbed part)	E	-2.15187	114.59526	18
		F	-2.15159	114.42887	
2	Mawas Reserve (disturbed part)	A	-2.19601	114.16482	45
		B	-2.27969	114.56836	
3	Sungai Wain Reserve	A	-1.39691	116.59709	55
4	Balikpapan Bay Mangrove area				
5	Penajam Oil Palm Plantation				
8	Rubber Tree Plantation				
6	Samboja Lestari	C	-1.08901	116.95137	12
		D	-1.00370	117.01966	
7	Gunung Meratus Reserve	A	-1.08900	116.29086	30
		B	-0.86059	116.42975	

Fig. 4.4a: Coordinates of each test site are displayed on remote sensing data

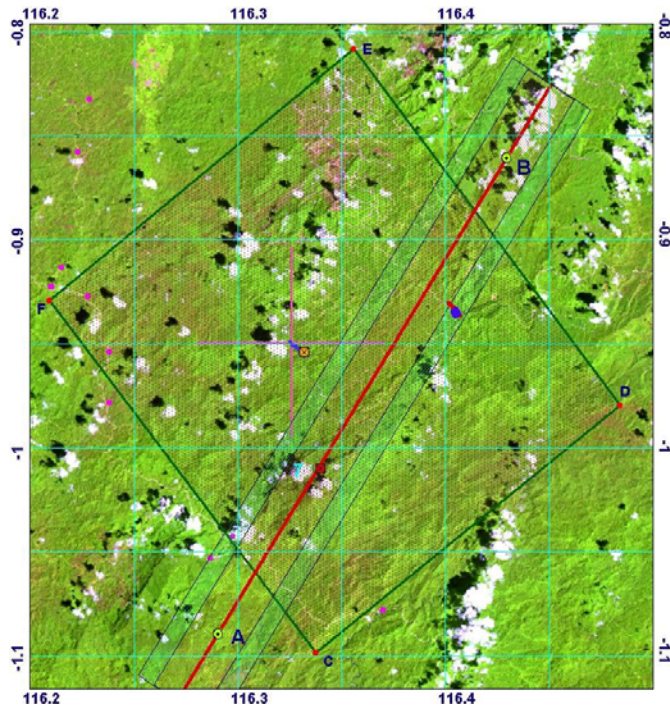


Site 1 and 2: Mawas Area with three flight tracks (background: Landsat-7 16/7/2000; detail Camp Tuanan: IKONOS 11/6/2003; detail Camp Begantung (or Pondok Hoekman): IKONOS 30/7/2003).



Site 3-5 and 8 (left): Sungai Wain Reserve, Balikpapan Bay Mangrove, Penajam Oil Palm Plantation, Rubber Tree Plantation (background: Landsat-7 25/12/2000; detail centre is Sungai Wain: AirSAR 16/9/2000; detail upper-right is Samboja: IKONOS 22/11/2001)

Site 6 (right): Samboja Lestari (background lower-right: Landsat-7 25/12/2000; detail upper-left: AirSAR 16/9/2000; detail centre is Samboja: IKONOS 22/11/2001)



Site 7: Gunung Meratus Reserve (background: Landsat-7 25/12/2000). The large ~20x30 km box indicates the AirSAR 16/9/2000 coverage. The little red square on the ESAR track centre is the top of the Gunung Meratus. The blue spot right of the ESAR track centre is the location of 7 ha tree transect (plot 6000) made for INDREX. The orange dot on the left is the orangutan release camp.

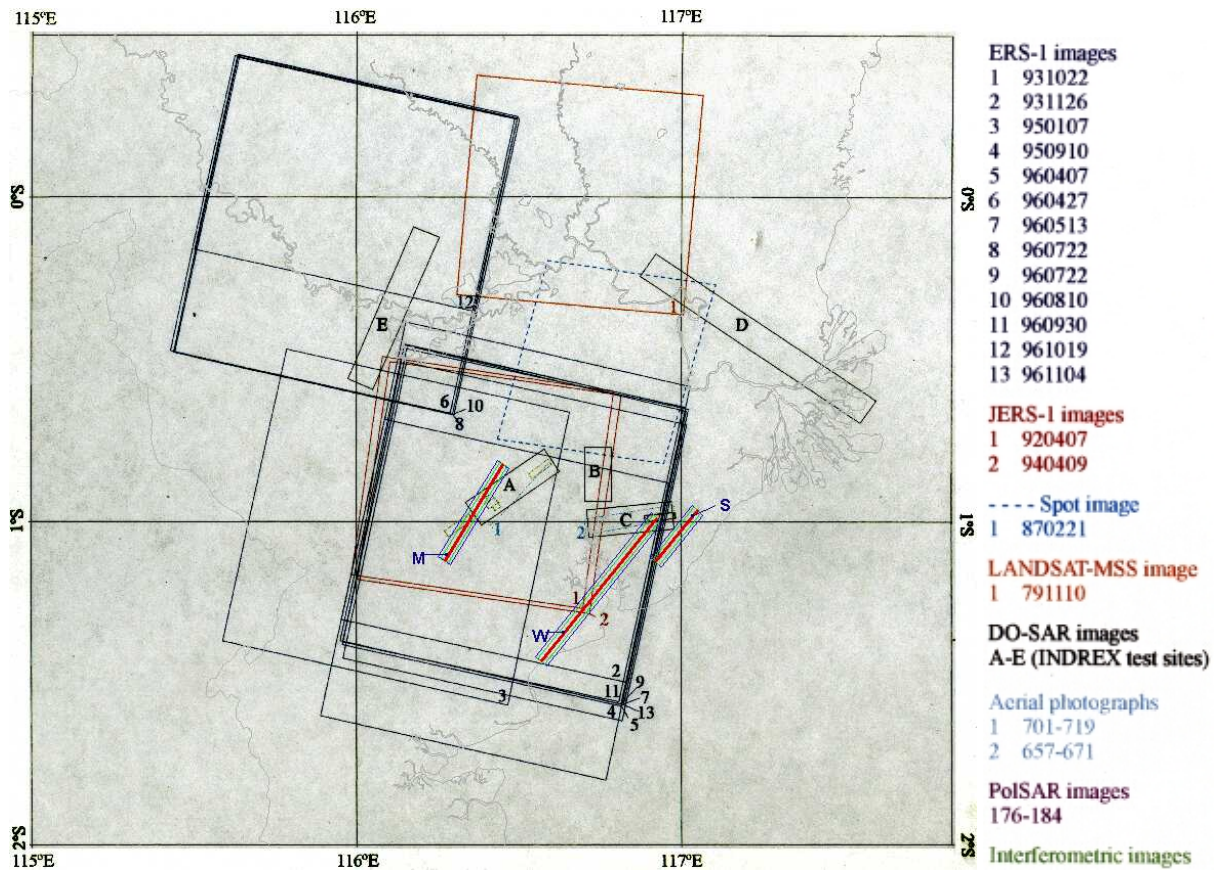


Fig 4b: Overview of the location of **INDREX test sites** and historical satellite data (until 1997) in Kalimantan. The **INDREX-II coverages** are added. **INDREX-II site W** (Sungai Wain) slightly overlaps **INDREX site C** (in Wanariset, ITTO plot). **INDREX-II site M** (G. Meratus) slightly overlaps **INDREX site A** (close to Plot 6000). **INDREX-II site S** (Samboja Lestari) has no overlap with **INDREX sites**.

5 Data Acquisition

In this section the procedure how the ground data has been collection and the effort made for the radar sensor transportation, installation and radar data acquisition are described.

5.1 Ground Data Acquisition

The ground data measurement as described in the INDREX-II experiment plan have been modified and adapted to the field situation during the campaign. These modifications have been discussed and approved by ESA in Balikpapan (November 2004) and have been reported in the INDREX-II data acquisition report. This INDREX-II final report only describes the post-campaign status of ground data collection.

5.1.1 Background Test Sites

The campaign has largely been conducted in areas which are under the permanent management and protection of BOS. This has several advantages: (a) the land cover is in a relatively stable state and can be studied for long periods; (b) ample terrain knowledge is already available; (c) excellent accessibility and logistic support, including 4 ultra-light aircraft; (d) dedicated research and support facilities such as walking bridges, field stations, guest houses and GIS/RS processing centres; (e) good contact and coordination with local authorities and the Ministry of Forestry. Remote sensing research at these sites has been an ongoing activity during the last 10 years. Prototype operational monitoring systems have been developed and are applied to combat illegal logging and secure carbon offset trading. In January 2004 an agreement between BOS and JAXA in the framework of the (ALOS PALSAR) K&C Initiative was established.

5.1.2 In Situ Measurements Performed during the Flight Campaign

The following types of measurement have been made.

(A1) Forest Tree Transects, Dipterocarp

A research area was established in the Sungai Wain Dipterocarp forest, 540 m in length and 286 m wide. Within this research area 26 blocks of 26 m x 32 m (in total 2.1 ha) have been selected. In these blocks each canopy tree with a diameter at breast height (*dbh*) ≥ 10 cm has been measured. These measurements included the following 9 parameters: *x*- and *y*-position, tree height, height to first branch, *dbh* and the crown projection distance in North, East, South and West direction. Also dead trees have been included and indicated as such in the resulting database. In addition the horizontal distance *hd* to the tree at the position of the height measurement taken and another quality parameter *Q* (i.e. is crown well visible? Y/N/Other) are recorded. In 26 sub-blocks of 2 m x 26 m (one in each block) smaller vegetation with a *dbh* ≥ 1 cm (and smaller than 10 cm) and a height ≥ 2 m has been sampled. For these plants the *x*-position, height and *dbh* have been included. Biomass levels have been derived through allometric equations (section 4.1.7).

(A2) Forest Tree Transects, Peat Swamp

In the Mawas peat swamp forests, along the walking bridge, 8 transects with a dimension of 100 m in length and 10 m wide have been measured. Within these transects, for each canopy tree (with *dbh* ≥ 10 cm), the following data have been collected: *x*- and *y*-position, tree height, height to first branch, *dbh* and the crown projection distance in North, East, South and West direction. Also dead trees have been included. In addition, in a 25% sub-sampling area in all transects, for vegetation with *dbh* ≥ 1 cm and *h* ≥ 2 m the *h* and *dbh* have been measured and all *Gringing* plants have been counted. Observations have been made of the tree/plant condition, namely: (A/D, S/L, B (Y/N), C (Y/N) or (Alive, Dead, Straight, Leaning, Buttress, and Climber). The horizontal distance to the tree at the

position of the height measurement taken (hd) and a quality parameter (Q) (see above) are recorded. Biomass levels have been derived through allometric equations (see also section 4.1.7)

(A3) Forest Tree Transects, Mangrove

Because the mangrove is hard to access, but relatively uniform, it was decided to measure three small transects (3 m x 10 m) in order to get some rough estimates.

A more detailed description of tree transect measurements can be found in a document written by Marcela Quiñones on the field data DVD's (section 6: *Tree transects*, folder: *Supporting documents*)

(B) Plantations

Assessments of tree height, height to first branch, age, density and biomass for all plantation areas (sites 5-6-8) were made. These data were collected for the rubber and oil palm plantations in Penajam. In Samboja Lestari plantations including teak, gamelina, meranti and fruit trees, and secondary forest plots and areas of alang-alang grass were sampled.

(C) Inspection from air

It was intended to collect digital geo-referenced (GPS) oblique video recordings from ultra-light aircraft over most sites. Because of problems with aircraft availability, flight and photography licenses, bad weather (rain, bad visibility, low cloud ceilings and high turbulence) and the close vicinity of the international airport Balikpapan these plans had to be adapted frequently. In section 4.1 an overview of the data collected is given. The Mawas centre track has been covered completely using an ultralight aircraft from BOS and a nadir-looking digital photo camera. The resulting strips have stereo coverage and each photograph has a scale and geo-referencing associated. Near Balikpapan parts of the Mawas and Samboja areas could be covered, however, without geo-referencing and mostly oblique.

(D) Hydrological modelling and meteorological data

Along the 23 km research transect in Mawas permanent measurement equipment has been installed to measure water level and soil temperature (15 positions), peat level fluctuations (1 position), air temperature (3 locations) and rainfall (2 positions) every hour. To be able to estimate the flooding percentage at the time of over-flight at each point where soil water levels are measured also soil surface roughness along 40 m transects have been measured.

(E) Future access

The accessibility and continuity of these sites will make it easy to make additional meaningful measurement in the future, e.g. after availability of the E-SAR radar data, or after a first evaluation of the campaign. In fact a first post-campaign visit has already been conducted in October 2005, which included the measurement of 12 additional plots in Sungai Wain.

A brief summary of field data collection measurements is given in table 5.1.

Table 5.1: In situ measurements

Measurement Type	Location
A1: Tree measurements	Sungai Wain (3)
A2: Tree measurements	Mawas undisturbed (1)
A3: Tree measurements	Balikpapan Bay (4)
B: Tree measurements	All plantation areas (5, 6 and 8)
C: Airborne photo survey	Mawas (1, 2), Sungai Wain (3), Samboja Lestari (6)
D: Hydrology / Meteorology	Mawas undisturbed (1), Samboja Lestari (6)
E: Future access	Optional for all sites (1-8)

5.1.3 Some details of measurement approach

Transect accuracy aspects

In Sungai Wain more than 900 big trees have been measured in Dipterocarp forest, in a single large block. This is sufficient to warrant high accuracy of macroscopic quantities. In the case of Mawas less trees per transect need to be measured because the area is uniform and trees are smaller.

To assess the accuracy of the in-situ data a repetition of part of the measurements by a second independent team (from Wageningen) has been carried out.

Ground / undergrowth conditions

During the INDREX-II campaign soil moisture levels have not been measured. In the Mawas peat swamp forests the ground water levels have been measured continuously (every hour), and these may be related to soil moisture conditions. In the rugged terrain of Sungai Wain the soil moisture may be very variable. It also may be too difficult to develop a meaningful sampling strategy (there is little time, moisture conditions change with the hour).

To document ground conditions qualitatively photographs of undercover, soil roughness, rocks and roots have been made.

Derived data and macroscopic forest parameters

For natural forests macroscopic forest parameters can be derived from the transect data, either straightforwardly (dominant height) or indirectly through allometric equations (biomass). Since all original data will be reported, assessment of additional macroscopic parameters, or application of improved allometry, can always be applied in a later stage.

Tree measurement accuracy aspects

Assessment of tree measurement accuracy has been achieved by comparison of the field data (collected by Indonesian staff) with field data collected in the same transect by an independent team (from Wageningen and DLR). This topic will be discussed in some more detail in chapter 4 of this report after the discussion on the allometry needed to translate tree transect data into biomass estimations.

Detailed descriptions of tree transect measurement accuracy, allometry and biomass estimation can be found in several documents written by Marcela Quiñones on the field data DVD's (section 6: *Tree transects*, folder: *Supporting documents*)

5.2 Synthetic Aperture Radar Data Acquisition

5.2.1 Mission Logistics

During the INDREX-II mission the following logistical tasks have been performed:

- organisation of the ferry flight of the Do228 aircraft,
- transfer of the E-SAR equipment,
- installation/reinstallation of the E-SAR system on board the Do228,
- calibration of the E-SAR system,
- main measurements campaign,
- first test processing on site,

For the whole logistic and technical support in Indonesia the handler PT. AIR Ampera, located at Halim airport was responsible. The main tasks that has been performed are the different permission application (Working permission, Aircraft Permission, Radar Permission, Mission Permission, Survey Permission), the support to custom clearance (import and export) for the airfreight and aircraft, support of the Radar equipment transport, support to organise the needed hangars in Jakarta as well as in Balikpapan and the general support which includes the organisation of the transport of the personnel, accommodation, contact to the security officer, etc.

5.2.2 Ferry flight of the Do228

Directly after the airborne acquisition mission in India the INDREX-II mission have been executed without delay. The ferry flight of the Do228 from India (Ahmenabad), via Thailand and Malaysia to Indonesia took approximately 37 flight hours (Fig 5.2.1). The planned stop over in Singapore, to take the security officer on board, could be not made, as the permission procedure for the general over flight permission for the Do228 in Indonesia has been not given in time.

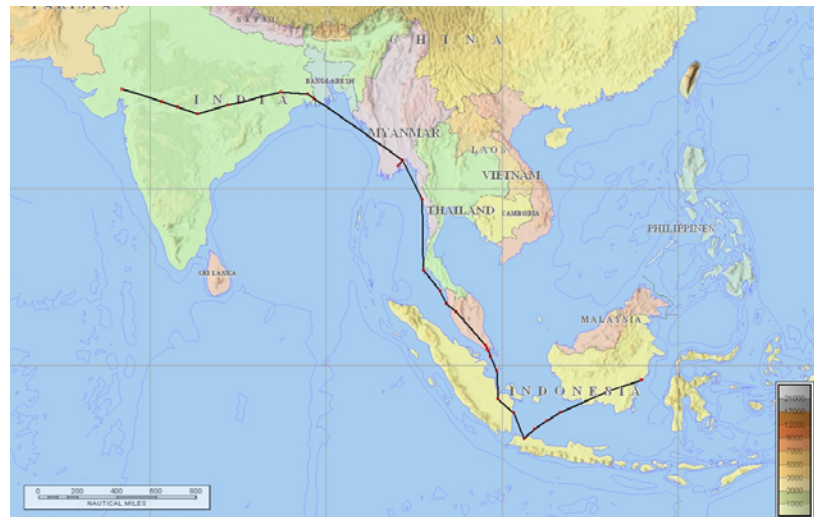


Fig. 5.2.1. Ferry flight of the Do228 from India to Indonesia

The aircraft got the flight permission to land in Jakarta Halim airport just for aircraft maintenance purpose. Here the aircraft maintenance for the 100 h endurance has been performed.

During this time the permission for the over flight could be obtained under the condition that the security officer has to be taken on board from Singapore. The aircraft crew was flying from Halim airport back to Singapore, took the security officer on board, and flew back to Halim Jakarta. At Halim airport the aircraft custom has been performed and two days later the aircraft got the ferry flight permission to the main base in Balikpapan (Fig. 5.2.2). Here a delay of one week had to be accounted

for. In Balikpapan a handler from Biomantara Balikpapan was hired to support the aircraft crew, with flight and landing permissions, flight schedules, refuelling procedures, hangar renting etc. throughout the mission execution.

One ferry flight has been performed to and back to Palangkaraya for the radar measurement campaign. The ferry back to Germany could be executed as planned in the experimental plan. The aircraft was landing after a successful flight at the 19.12.04 in Oberpfaffenhofen.



Fig. 5.2.2. DLR's aircraft Donier 228 after landing in front of the Hanger in Balikpapan, with mounted E-SAR equipment.

5.2.3 Transfer of the E-SAR Equipment

The transfer of the E-SAR hardware system from India has been done by shipping the cargo boxes with a regular aircraft to Jakarta. The custom in Jakarta has been made by MS Cargo, a national cargo company. A delay of one week had to be accounted before the custom clearance for the radar equipment could be obtained. The delays have been caused due to ignorance and disorganisation in the warehouse and by the not precisely defined administrative procedure. One of the critical things was, that the warehouse was opening the DLR's cargo container and was pulling all the equipment out without permission and right to do this (Fig. 5.2.3). The documents delivered to the warehouse were indicating that a sensitive cargo has been delivered. The DLR's technicians needed to pack again the whole container and search for the components distributed in the warehouse (Fig. 5.2.3).



Figure 5.2.3 Left: Radar equipment distributed in the warehouse. Right: Repacking the container with the radar equipment in the warehouse.

After customs at the international airport in Jakarta the E-SAR equipment has been transported by a container truck to Halim airport. At Halim airport the equipment has been stored in the Hercules C-130, operated by the military army, and shipped to Balikpapan by HALIM TRANS. At Balikpapan the equipment has been stored in a hangar at the airport, where also two additional rooms for the laboratory and the processing were available organised by BIOMANTARA. The transport with HALIM TRANS was also critical, as the radar equipment has been transported with 12 huge oil tanks. The radar equipment arrived three days before the aircraft got the permission to land in Balikpapan.

On the way back, we have used a civil cargo transport agency CARDIG AIR, which was just opening his company and had enough space to transport the radar equipment from Balikpapan to Jakarta international. This time no truck transport was necessary. From Jakarta international the radar equipment has been transported directly to the warehouse.

5.2.4 Installation of the E-SAR system on board the Do228

The integration of the E-SAR hardware system and the antennas into the Do228 has been done in a shorter time as planned, so that the test and calibration flight could be done already after one day of the aircraft arrival. No major technical problems occur, so that the radar flight campaign could start as planned.

The reinstallation of the radar has been done after the measurement campaign.

5.2.5 Calibration of the E-SAR system

The test and calibration flight has been done before starting with the measurement flight campaign. Corner reflector of different size (3m and 1.5m) has been installed at the airport (Fig. 5.2.4). Five corner reflectors have been constructed by a workshop operated from the Borneo Orang-Utan Survival foundation. DLR was sending them a construction sketch and they build it accordingly to it. DLR was



Figure 5.2.4: left: Corner reflector of the size 3m for P-band. Right: Corner reflector of the size 1.5m for X-, C-, and L-band. Both positioned along the runway

sending additionally two corner reflectors of the size 1.5m to Balikpapan, in order to compare the construction quality. The corner reflectors are used for the radiometric and geometric calibration of the acquired radar data. They have been precisely levelled and their position measured with a differential GPS (DGPS). The reference point of the DGPS has been allocated on the roof of the airport building (Fig. 5.2.5)

The corner reflector has been installed beside the runway in range direction. The swath width of the E-SAR flight strip has a length of 3 km. In order to measure the system stability in range direction every 250 m a corner reflector has been positioned. In table 5.2.1 the calibration flights and the position, as well as the alignment of the corner reflectors is listed. Altogether three calibration flights have been performed, a pre-calibration, during the measurement flight period and a post-calibration.



Fig. 5.2.5. Differential GPS installed on the airport building above a reference point.

Tabl.5.2.1: Corner reflectors positions and alignment for three calibration flights (CAL 1 to 3)(CR= corner reflector, Az= azimuth direction, El= elevation from ground, NR= near range, FR= far range)

Position [m]	CAL 1 CR+size	Az. [°]	El. [°]	CAL 2 CR+size	Az. [°]	El. [°]	CAL 3 CR+size	Az. [°]	El. [°]
0	Swath NR								
250	CR1 (1.5)	158	28	CR1 (1.5)	158	28	CR1 (1.5)	158	28
500	CR2 (3)	155	15	CR2 (3)	155	15	CR2 (3)	155	15
750	CR3 (1.5)	157	20				CR3 (1.5)	157	20
1250	CR4 (1.5)	156	14	CR4 (1.5)	156	14	CR4 (1.5)	156	14
1500							CR4a (1.5)	156	12
1750	CR5 (1.5)	156	11	CR5 (1.5)	156	11	CR5 (1.5)	156	11
2000							CR5a (1.5)	158	8
2250	CR6 (3)	156	2	CR6 (3)	156	2	CR6 (3)	156	2
2750	CR7 (1.5)	156	4	CR7 (1.5)	156	4	CR7 (1.5)	156	4
3000	Swath FR								

5.2.6 Main Measurement Campaign

The main flight measurement campaign has been executed within 22 days, one week longer as expected. From the beginning of the INDREX-II the campaign execution has been planned with a lot of time buffer, so that at the end with all the difficulties the measurement campaign could be finalised in time. The delay for the measurement time has been caused due to weather restriction and unexpected military training periods.

The camping has been executed during the beginning of the raining season. The flight times had to be shifted several times due to very heavy storm clouds.

Before the flight camping short briefing between the radar operators and the flight crew has been held every day (Fig. 5.2.6).

Each evening the operator and the ground team had a meeting to exchange information.



Fig. 5.2.6 Short briefing before the flight measurement campaign (left to right: Mr. Sauer (second pilot), Mr. Welsler (commander), Mr. Schirmer (aircraft technician), Mr. Horn (radar engineer))

A more detailed description of the flight schedules, system configuration, and flight tracks and data acquisition is given in the following

5.2.7 First Test Processing on Site

A team of two persons have made a first processing of the acquired data on site. For this a small processing room has been installed with a band machine transcribing the data and a PC for survey and data processing (Fig. 5.2.7). First analysis concerning the flights baseline, the radiometric accuracy, the polarimetry and the interferometric coherence has been done on site.

Because of difficult weather conditions one repeat pass flight has been repeated after the flight track investigation. Thus, due to restricting the flights to optimum non-turbulent weather conditions, for most of the flights the nominal tracks could be kept within ± 2 m horizontal and vertical deviations. Even small baselines of 5m could be kept pretty well.

Overall 127 flight tracks have been flown within the 22 days flight measurement campaign corresponding to (were calibration flight tracks 27 of them at the beginning, in between and at the end of the campaign) 200 GByte disc stored raw data. The covered area is about 525 km². The duration of the processing time is expected to take 6 months to complete all the test sites. The estimated data amount of processed radar geometry images (RGI, slant range, multilook and SLC) and geocoded terrain corrected images (GTC) is about 1 Terabyte.

For data processing, long strips are divided into 2-5 overlapping segments in azimuth corresponding to 6 to 10 km length and 3.5 km width. The geocoding is performed onto a 2m grid, WGS-84, UTM projection, zone 50M. Terrain correction is performed using DEMs computed from the X-band single-pass interferometry. All frequencies except of P-band, are delivered with a local incidence range of 25 to 50 degrees, the P-band slant range images will be delivered with a local incidence angle of 18 to 50 degrees.

In order to ensure best radiometric and polarimetric calibration of the data, three calibration flights were conducted. First evaluations of these calibration data confirmed the E-SAR system stability throughout the campaign. The relative deviations measured on the corner reflectors at the Balikpapan Airfield (permanently installed for the duration of the campaign) are within ± 1 dB. First investigations of range profiles in L- and P-band over homogeneous forest areas confirmed this figure.

The results obtained from the evaluation have been discussed each evening during the campaign meeting with the ground team, so that changes, irregularities or problems could be discussed and solutions in the team found.



Fig. 5.2.7 Data processing facility at the hanger in Balikpapan

5.2.8 Flight schedule

The flight schedule of the INDREX-II campaign is given in the following:

Dates	Flight Actions
07.10.04 - 09.10.04	Transfer from Ahmedabad Airport, India to Halim Airport Jakarta, Indonesia
11.10.04 -22.10.04	Aircraft Maintenance at Halim Airport Jakarta, Indonesia
06.11.04	Transfer from Halim to Singapur and back to Halim (taking the Indonesian security officer on board)
09.11.04	Transfer from Halim to Balikpapan, Kalimantan, Indonesia
15.11.04- 25.11.04	Measurements flight campaign at Balikpapan
26.11.04	Transfer from Balikpapan to Palangkaraya
27.11.04 – 30.11.04	Measurement flight campaign at Palangkaraya
01.12.04	Transfer from Palangkaraya to Balikpapan
04.12.04-06.12.04	Measurement flight campaign at Balikpapan
10.12.04-19.12.04	Transfer from Balikpapan to Oberpfaffenhofen, Germany

5.2.9 Measurement flight configuration

For the eight identified test sites two main airbases have been considered, Balikpapan and Palangkaraya. Six test site could be overflown directly from the close located airport in Balikpapan. For two test site the airbase needed to be changed to Palangkaraya, approximately two flight hours away from Balikpapan. For seven of the test flight a total amount of 11 flight passes and for one test site only nine passes has been flown, as described in the following:

For the test site 1-8 (except of 7) the following operation modes has been performed:

E-SAR Mode	Frequency	Pass	Polarisation
Pol-InSAR	L-band	4 pass	quad pol.
Pol-InSAR	P-band	4 pass	quad pol.
InSAR	X-band	1 pass	single pol. (vv)
PoSAR	C-band	2 pass	dual pol. (hh & hv, vv & vh)

For the test site 7 the following operation mode has been performed:

E-SAR Mode	Frequency	Pass	Polarisation
Pol-InSAR	L-band	4 pass	quad pol.
Pol-InSAR	P-band	4 pass	quad pol.
InSAR	X-band	1 pass	single pol. (vv)

The repeat pass baselines for L- and P-band have been chosen correspondingly to the expected volume height on ground. The flown mean heights, baseline and frequency for the different test sites are described in table 5.2.2.

Tab. 5.2.2 Repeat pass baselines and mean flight height for each test site.

Test Site	Mean Flight Height [m]	Baseline [m]	Frequency [band]
Samboja Lestari	3505	0,5,8	L-band
	3505	0,15,30	P-band
Sungai Wain (south)	3660	0,5,8	L-band
	3660	0,15,30	P-band
Sungai Wain (north)	5030	0,5,10,15	L-band
	5030	0,15,30,60	P-band
Meratus	5030	0,5,10,15	L-band
	5030	0,10,20	P-band
Mawas	3500	0,5,15	L-band
	3500	0,15,30,40	P-band

The 3 to 4 passes are chosen in order to be able to extract the vertical forest structure of the illuminated forest. For C-band only two passes are chosen to acquire the full set of available polarisations without interferometric observables. A digital elevation model (DEM) will be calculated from the single pass interferometry using X-band. Additionally in X-band one polarisation amplitude image can be obtained in VV.

The total flight hour of the plane was 2.5 hours during the measuring campaign, as the aircraft is fully equipped with all antennas and hardware on board. The pure measuring time between take off and landing is 120 min. In range direction the width of the measuring path was 3.2 km.

The total flight hours accounting for the whole INDREX-II campaign with including ferry flights were 97 hour, from this 46 hours has been flown over the test areas and 51 hours were needed for ferry flights.

5.3 Data Acquisition Flight Tracks

The flight track flown at Kalimantan is displayed in Fig.5.3.1. The measurements flight was starting with the smallest flight strip in order to get used of the tropical flight conditions. For each test site the radar system configuration as described in 5.2.2. has been flown. The flight time has been scheduled to be performed in the morning starting at 6:00 until 13:00, depending on the airport authority in Balikpapan and the whether conditions. Within the seven flight hours two flights could be performed each with a length of 2.5 hours.

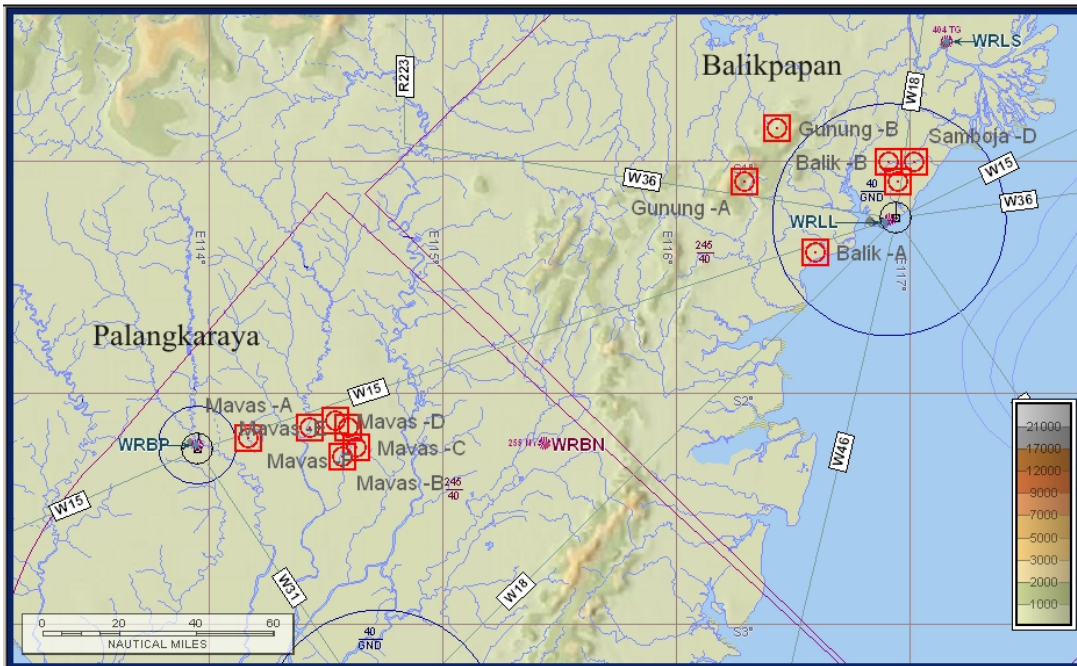


Fig.5.3.1: Flight map with the eight identified test sites.

Order of the performed measuring flights: First performed flight

(6) Samboja Lestari. East Kalimantan, 2,000 ha
 Vegetation: Plantation forest, many species, age: 1-5 year; Some regenerating forest remnants; Alang-alang (grass)
 Topo.: Undulating - Hilly
 Biomass range: **30-150 ton/ha.**
 Height range: **2-15 m.**
 Location centre: 116° 59'E, 1° 02'S
 Extent: +/- 3 km in all directions

Aircraft & Call-Sign Do228 :D-CFFU
Dep./Des.: WRLI
Remark: Shuttling between Samboja C and Samboja D for several times !
Routing: direct Samboja C direct Samboja D direct BPN
Altitude: between FL 090 and FL 120

Point	Coordinates	BPN Radial	BPN Distance
Samboja C	S 01°05' E 116° 57'	003	10 NM
Samboja D	S 01°00' E 117° 01'	018	15 NM



Flight Strip: length 12 km

The second flown flight strip:

(3) Sungai Wain Reserve.

East Kalimantan, 10,000 ha
 Vegetation: Tropical Dipterocarp lowland forest, swamp forest, mangroves
 Topo.: Hilly (lowland forest) to flat (mangrove and swamp forest)
 Biomass range: **100-400 ton/ha.**
 Height range: **10-50 m.**
 Location centre: 116° 50'E, 1° 05'S
 Extent: +/- 10 km in all directions

(4) Balikpapan Bay Mangrove area

Vegetation: Mangrove, Nipah
 Topo.: Flat
 Biomass range: **50-150 ton/ha.**
 Height range: **10-20 m.**
 Location centre: 116° 45'E, 1° 11'S
 Extent: +/- 10 km in all directions

(5) Penajam Oil Palm Plantation

Vegetation: Oil palm, alang-alang (grass)
 Topo.: Flat to undulating
 Biomass range: **20-100 ton/ha.**
 Height range: **5-10 m.**
 Location centre: 116° 37'E, 1° 22'S
 Extent: +/- 5 km in all directions

Aircraft & Call-Sign: Do228/D-CFFU

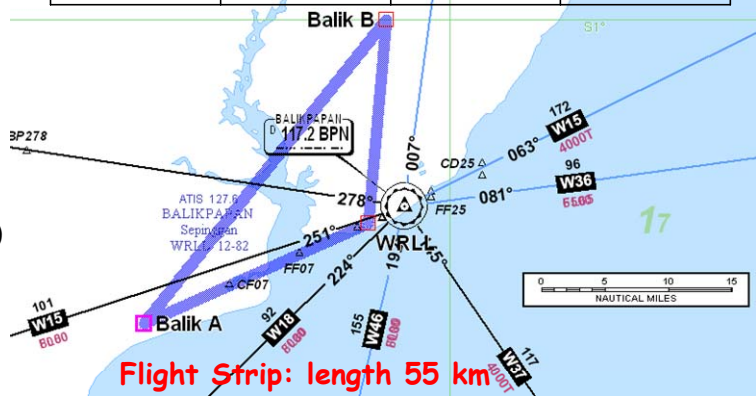
Dep/Des: WRLL

Remark: Shuttling between Balik A and Balik B for several times !

Routing: direct Balik A direct Balik B direct BPN

Altitude: between FL 090 and FL 120

Point	Coordinates	BPN Radial	BPN Distance
Balik A	S 01°24' E 116° 36'	245	22 NM
Balik B	S 01°00' E 116° 55'	355	15 NM



The third flown flight strip is the last flown in the area of Balikpapan:

(7) Gunung Meratus Reserve

Vegetation: Tropical Dipterocarp forest (lowland and mountain)
 Topo.: Hilly to steep
 Biomass range: **100-400 ton/ha.**
 Height range: **10-50 m.**
 Location centre: 116° 15'E, 1° 00'S
 Extent: +/- 20 km in all directions

Point	Coordinates	BPN Radial	BPN Distance
Gunung A	S 01°05' E 116° 17'	285	41 NM
Gunung B	S 00°51' E 116° 26'	308	39 NM

Aircraft & Call-Sign: Do228/D-CFFU

Dep./Des.: WRLL

Remark: Shuttling between Gunung A and Gunung B for several times !

Routing: direct Gunung A direct Gunung B direct BPN

Altitude: between FL 130 and FL 150



Flight Strip: Length 30 km

Further two flight strips has been flown in central Kalimantan, close to Palangkaraya, called Mawas area, where over a disturbed and undisturbed peat forest area data has been acquired.

5.4 Radar Data Acquisition

In table 5.4.1 the acquired radar data are listed with the E-SAR Scene ID, location, date of acquisition, frequency band, polarisation, track ID and radar mode.

Scene-ID	Location	Date of Data Acquis.	Freq.-Band	Polarisation	Track-ID	Radar Mode
CALIBRATION 1						
04indrex0103x1	Bpnairport	15. Nov 04	P	PM	3	4-Kanal,HR-NS,PM
04indrex0104x1	Bpnairport	16. Nov 04	C	DP	3	2-Kanal,HR-NS
04indrex0105x1	Bpnairport	16. Nov 04	C	DP	3	2-Kanal,HR-NS
04indrex0106x1	Bpnairport	16. Nov 04	L	PM	3	4-Kanal,HR-NS,PM
04indrex0107x1	Bpnairport	16. Nov 04	X	VV	2	2-Kanal,HR-NS
04indrex0108x1	Bpnairport	16. Nov 04	X	VV	2	2-Kanal,HR-NS
04indrex0110x1	Bpnairport	16. Nov 04	X	VV	2	2-Kanal,HR-NS
SAMBOJA LESTARI						
04indrex0201x1	Sambojalestari	16. Nov 04	L	PM	2	4-Kanal,HR-NS,PM
04indrex0202x1	Sambojalestari	16. Nov 04	L	PM	3	4-Kanal,HR-NS,PM
04indrex0203x1	Sambojalestari	16. Nov 04	L	PM	4	4-Kanal,HR-NS,PM
04indrex0204x1	Sambojalestari	17. Nov 04	L	PM	2	4-Kanal,HR-NS,PM
04indrex0205x1	Sambojalestari	17. Nov 04	P	PM	2	4-Kanal,HR-NS,PM
04indrex0206x1	Sambojalestari	17. Nov 04	P	PM	5	4-Kanal,HR-NS,PM
04indrex0207x1	Sambojalestari	17. Nov 04	P	PM	6	4-Kanal,HR-NS,PM
04indrex0208x1	Sambojalestari	17. Nov 04	P	PM	2	4-Kanal,HR-NS,PM
04indrex0209x1	Sambojalestari	17. Nov 04	X	VV	8	2-Kanal,HR-NS
04indrex0210x1	Sambojalestari	17. Nov 04	X	VV	7	2-Kanal,HR-NS
04indrex0301x1	Sambojalestari	17. Nov 04	C	DP	2	2-Kanal,HR-NS
04indrex0302x1	Sambojalestari	17. Nov 04	C	DP	2	2-Kanal,HR-NS
04indrex0303x1	Sambojalestari	17. Nov 04	C	DP	2	2-Kanal,HR-NS
SUNGAI WAIN (south)						



04indrex0401x1	Sungai	17. Nov 04	L	PM	2	4-Kanal,HR-NS,PM
04indrex0402x1	Sungai	17. Nov 04	L	PM	3	4-Kanal,HR-NS,PM
04indrex0403x1	Sungai	17. Nov 04	L	PM	4	4-Kanal,HR-NS,PM
04indrex0404x1	Sungai	18. Nov 04	L	PM	2	4-Kanal,HR-NS,PM
04indrex0405x1	Sungai	18. Nov 04	X	VV	7	2-Kanal,HR-NS
04indrex0406x1	Sungai	18. Nov 04	X	VV	8	2-Kanal,HR-NS
04indrex0407x1	Sungai	18. Nov 04	C	DP	2	2-Kanal,HR-NS
04indrex0401x2	Sungai	17. Nov 04	L	PM	2	4-Kanal,HR-NS,PM
04indrex0402x2	Sungai	17. Nov 04	L	PM	3	4-Kanal,HR-NS,PM
04indrex0403x2	Sungai	17. Nov 04	L	PM	4	4-Kanal,HR-NS,PM
04indrex0404x2	Sungai	18. Nov 04	L	PM	2	4-Kanal,HR-NS,PM
04indrex0405x2	Sungai	18. Nov 04	X	VV	7	2-Kanal,HR-NS
04indrex0406x2	Sungai	18. Nov 04	X	VV	8	2-Kanal,HR-NS
04indrex0501x1	Sungai	18. Nov 04	P	PM	2	4-Kanal,HR-NS,PM
04indrex0502x1	Sungai	18. Nov 04	P	PM	5	4-Kanal,HR-NS,PM
04indrex0503x1	Sungai	18. Nov 04	P	PM	6	4-Kanal,HR-NS,PM
04indrex0504x1	Sungai	18. Nov 04	P	PM	2	4-Kanal,HR-NS,PM
04indrex0505x1	Sungai	18. Nov 04	C	DP	2	2-Kanal,HR-NS
04indrex0506x1	Sungai	18. Nov 04	C	DP	2	2-Kanal,HR-NS
04indrex0501x2	Sungai	18. Nov 04	P	PM	2	4-Kanal,HR-NS,PM
04indrex0502x2	Sungai	18. Nov 04	P	PM	5	4-Kanal,HR-NS,PM
04indrex0503x2	Sungai	18. Nov 04	P	PM	6	4-Kanal,HR-NS,PM
04indrex0504x2	Sungai	18. Nov 04	P	PM	2	4-Kanal,HR-NS,PM
04indrex0505x2	Sungai	18. Nov 04	C	DP	2	2-Kanal,HR-NS
04indrex0506x2	Sungai	18. Nov 04	C	DP	2	2-Kanal,HR-NS
SUNGAI WAIN (north)						



04indrex0601x1	Sungai	19. Nov 04	P	PM	2	4-Kanal,HR-NS,PM
04indrex0602x1	Sungai	19. Nov 04	P	PM	5	4-Kanal,HR-NS,PM
04indrex0603x1	Sungai	19. Nov 04	P	PM	6	4-Kanal,HR-NS,PM
04indrex0604x1	Sungai	20. Nov 04	P	PM	2	4-Kanal,HR-NS,PM
04indrex0605x1	Sungai	20. Nov 04	P	PM	9	4-Kanal,HR-NS,PM
04indrex0606x1	Sungai	20. Nov 04	X	VV	8	2-Kanal,HR-NS
04indrex0607x1	Sungai	20. Nov 04	X	VV	7	2-Kanal,HR-NS
04indrex0608x1	Sungai	20. Nov 04	C	DP	2	2-Kanal,HR-NS
04indrex0601x2	Sungai	19. Nov 04	P	PM	2	4-Kanal,HR-NS,PM
04indrex0602x2	Sungai	19. Nov 04	P	PM	5	4-Kanal,HR-NS,PM
04indrex0603x2	Sungai	19. Nov 04	P	PM	6	4-Kanal,HR-NS,PM
04indrex0604x2	Sungai	20. Nov 04	P	PM	2	4-Kanal,HR-NS,PM
04indrex0605x2	Sungai	20. Nov 04	P	PM	9	4-Kanal,HR-NS,PM
04indrex0606x2	Sungai	20. Nov 04	X	VV	8	2-Kanal,HR-NS
04indrex0607x2	Sungai	20. Nov 04	X	VV	7	2-Kanal,HR-NS
04indrex0608x2	Sungai	20. Nov 04	C	DP	2	2-Kanal,HR-NS
04indrex0701x1	Sungai	20. Nov 04	L	PM	2	4-Kanal,HR-NS,PM
04indrex0702x1	Sungai	20. Nov 04	L	PM	3	4-Kanal,HR-NS,PM
04indrex0703x1	Sungai	20. Nov 04	L	PM	4	4-Kanal,HR-NS,PM
04indrex0704x1	Sungai	20. Nov 04	L	PM	5	4-Kanal,HR-NS,PM
04indrex0705x1	Sungai	20. Nov 04	L	PM	2	4-Kanal,HR-NS,PM
04indrex0701x2	Sungai	20. Nov 04	L	PM	2	4-Kanal,HR-NS,PM
04indrex0702x2	Sungai	20. Nov 04	L	PM	3	4-Kanal,HR-NS,PM
04indrex0703x2	Sungai	20. Nov 04	L	PM	4	4-Kanal,HR-NS,PM
04indrex0704x2	Sungai	20. Nov 04	L	PM	5	4-Kanal,HR-NS,PM
04indrex0801x1	Sungai	23. Nov 04	L	PM	2	4-Kanal,HR-NS,PM



04indrex0802x1	Sungai	23. Nov 04	L	PM	3	4-Kanal,HR-NS,PM
04indrex0803x1	Sungai	23. Nov 04	L	PM	4	4-Kanal,HR-NS,PM
04indrex0804x1	Sungai	23. Nov 04	L	PM	5	4-Kanal,HR-NS,PM
04indrex0805x1	Sungai	23. Nov 04	C	DP	2	2-Kanal,HR-NS
04indrex0806x1	Sungai	23. Nov 04	C	DP	2	2-Kanal,HR-NS
04indrex0801x2	Sungai	23. Nov 04	L	PM	2	4-Kanal,HR-NS,PM
04indrex0802x2	Sungai	23. Nov 04	L	PM	3	4-Kanal,HR-NS,PM
04indrex0803x2	Sungai	23. Nov 04	L	PM	4	4-Kanal,HR-NS,PM
04indrex0804x2	Sungai	23. Nov 04	L	PM	5	4-Kanal,HR-NS,PM
04indrex0805x2	Sungai	23. Nov 04	C	DP	2	2-Kanal,HR-NS
04indrex0806x2	Sungai	23. Nov 04	C	DP	2	2-Kanal,HR-NS
CALIBRATION 2						
04indrex0901x1	Bpn	23. Nov 04	P	PM	3	4-Kanal,HR-NS,PM
04indrex0902x1	Bpn	23. Nov 04	P	PM	3	4-Kanal,HR-NS,PM
04indrex0903x1	Bpn	23. Nov 04	P	PM	3	4-Kanal,HR-NS,PM
04indrex0904x1	Bpn	23. Nov 04	C	DP	3	2-Kanal,HR-NS
04indrex0905x1	Bpn	23. Nov 04	C	DP	3	2-Kanal,HR-NS
04indrex0906x1	Bpn	24. Nov 04	L	PM	3	4-Kanal,HR-NS,PM
04indrex0907x1	Bpn	24. Nov 04	L	PM	3	4-Kanal,HR-NS,PM
04indrex0908x1	Bpn	24. Nov 04	X	VV	2	2-Kanal,HR-NS
04indrex0909x1	Bpn	24. Nov 04	X	VV	2	2-Kanal,HR-NS
MERATUS						
04indrex1001x1	Meratus	24. Nov 04	L	PM	2	4-Kanal,HR-NS,PM
04indrex1002x1	Meratus	24. Nov 04	P	PM	2	4-Kanal,HR-NS,PM
04indrex1003x1	Meratus	24. Nov 04	P	PM	4	4-Kanal,HR-NS,PM
04indrex1004x1	Meratus	24. Nov 04	P	PM	10	4-Kanal,HR-NS,PM
04indrex1005x1	Meratus	24. Nov 04	X	VV	8	2-Kanal,HR-NS



04indrex1006x1	Meratus	24. Nov 04	X	VV	7	2-Kanal,HR-NS
04indrex1001x2	Meratus	24. Nov 04	L	PM	2	4-Kanal,HR-NS,PM
04indrex1002x2	Meratus	24. Nov 04	P	PM	2	4-Kanal,HR-NS,PM
04indrex1003x2	Meratus	24. Nov 04	P	PM	4	4-Kanal,HR-NS,PM
04indrex1004x2	Meratus	24. Nov 04	P	PM	10	4-Kanal,HR-NS,PM
04indrex1005x2	Meratus	24. Nov 04	X	VV	8	2-Kanal,HR-NS
04indrex1006x2	Meratus	24. Nov 04	X	VV	7	2-Kanal,HR-NS
04indrex1501x1	Meratus	04. Dez 04	L	PM	2	4-Kanal,HR-NS,PM
04indrex1503x1	Meratus	05. Dez 04	L	PM	4	4-Kanal,HR-NS,PM
04indrex1505x1	Meratus	05. Dez 04	L	PM	3	4-Kanal,HR-NS,PM
04indrex1501x2	Meratus	04. Dez 04	L	PM	2	4-Kanal,HR-NS,PM
04indrex1502x2	Meratus	04. Dez 04	L	PM	3	4-Kanal,HR-NS,PM
04indrex1503x2	Meratus	05. Dez 04	L	PM	4	4-Kanal,HR-NS,PM
04indrex1504x1	Meratus	05. Dez 04	L	PM	5	4-Kanal,HR-NS,PM
04indrex1505x1	Meratus	05. Dez 04	L	PM	3	4-Kanal,HR-NS,PM
MAWAS						
04indrex1101x1	Mawas_a	27. Nov 04	C	DP	2	2-Kanal,HR-NS
04indrex1102x1	Mawas_c	27. Nov 04	C	DP	2	2-Kanal,HR-NS
04indrex1103x1	Mawas_e	27. Nov 04	C	DP	2	2-Kanal,HR-NS
04indrex1104x1	Mawas_a	27. Nov 04	C	DP	2	2-Kanal,HR-NS
04indrex1105x1	Mawas_c	27. Nov 04	C	DP	2	2-Kanal,HR-NS
04indrex1106x1	Mawas_e	27. Nov 04	C	DP	2	2-Kanal,HR-NS
04indrex1107x1	Mawas_e	27. Nov 04	X	VV	8	2-Kanal,HR-NS
04indrex1108x1	Mawas_c	27. Nov 04	X	VV	8	2-Kanal,HR-NS
04indrex1109x1	Mawas_a	27. Nov 04	X	VV	8	2-Kanal,HR-NS
04indrex1201x1	Mawas_c	29. Nov 04	L	PM	2	4-Kanal,HR-NS,PM



04indrex1202x1	Mawas_e	29. Nov 04	L	PM	2	4-Kanal,HR-NS,PM
04indrex1203x1	Mawas_a	29. Nov 04	L	PM	2	4-Kanal,HR-NS,PM
04indrex1204x1	Mawas_c	29. Nov 04	L	PM	3	4-Kanal,HR-NS,PM
04indrex1205x1	Mawas_e	29. Nov 04	L	PM	3	4-Kanal,HR-NS,PM
04indrex1206x1	Mawas_a	29. Nov 04	L	PM	3	4-Kanal,HR-NS,PM
04indrex1207x1	Mawas_c	29. Nov 04	L	PM	5	4-Kanal,HR-NS,PM
04indrex1208x1	Mawas_e	29. Nov 04	L	PM	5	4-Kanal,HR-NS,PM
04indrex1209x1	Mawas_a	29. Nov 04	L	PM	5	4-Kanal,HR-NS,PM
04indrex1210x1	Mawas_c	29. Nov 04	L	PM	4	4-Kanal,HR-NS,PM
04indrex1211x1	Mawas_e	29. Nov 04	L	PM	4	4-Kanal,HR-NS,PM
04indrex1212x1	Mawas_a	29. Nov 04	L	PM	4	4-Kanal,HR-NS,PM
04indrex1213x1	Mawas_a	29. Nov 04	X	VV	8	2-Kanal,HR-NS
04indrex1101x2	Mawas_a	27. Nov 04	C	DP	2	2-Kanal,HR-NS
04indrex1104x2	Mawas_a	27. Nov 04	C	DP	2	2-Kanal,HR-NS
04indrex1109x2	Mawas_a	27. Nov 04	X	VV	8	2-Kanal,HR-NS
04indrex1203x2	Mawas_a	29. Nov 04	L	PM	2	4-Kanal,HR-NS,PM
04indrex1206x2	Mawas_a	29. Nov 04	L	PM	3	4-Kanal,HR-NS,PM
04indrex1209x2	Mawas_a	29. Nov 04	L	PM	5	4-Kanal,HR-NS,PM
04indrex1212x2	Mawas_a	29. Nov 04	L	PM	4	4-Kanal,HR-NS,PM
04indrex1213x2	Mawas_a	29. Nov 04	X	VV	8	2-Kanal,HR-NS
04indrex1101x3	Mawas_a	27. Nov 04	C	DP	2	2-Kanal,HR-NS
04indrex1104x3	Mawas_a	27. Nov 04	C	DP	2	2-Kanal,HR-NS
04indrex1109x3	Mawas_a	27. Nov 04	X	VV	8	2-Kanal,HR-NS
04indrex1203x3	Mawas_a	29. Nov 04	L	PM	2	4-Kanal,HR-NS,PM
04indrex1206x3	Mawas_a	29. Nov 04	L	PM	3	4-Kanal,HR-NS,PM
04indrex1209x3	Mawas_a	29. Nov 04	L	PM	5	4-Kanal,HR-NS,PM



04indrex1212x3	Mawas_a	29. Nov 04	L	PM	4	4-Kanal,HR-NS,PM
04indrex1213x3	Mawas_a	29. Nov 04	X	VV	8	2-Kanal,HR-NS
04indrex1301x1	Mawas_c	30. Nov 04	L	PM	2	4-Kanal,HR-NS,PM
04indrex1302x1	Mawas_e	30. Nov 04	L	PM	2	4-Kanal,HR-NS,PM
04indrex1303x1	Mawas_a	30. Nov 04	L	PM	2	4-Kanal,HR-NS,PM
04indrex1304x1	Mawas_c	30. Nov 04	L	PM	3	4-Kanal,HR-NS,PM
04indrex1305x1	Mawas_e	30. Nov 04	L	PM	3	4-Kanal,HR-NS,PM
04indrex1306x1	Mawas_a	30. Nov 04	L	PM	3	4-Kanal,HR-NS,PM
04indrex1307x1	Mawas_c	30. Nov 04	L	PM	5	4-Kanal,HR-NS,PM
04indrex1308x1	Mawas_e	30. Nov 04	L	PM	5	4-Kanal,HR-NS,PM
04indrex1309x1	Mawas_a	30. Nov 04	L	PM	5	4-Kanal,HR-NS,PM
04indrex1303x2	Mawas_a	30. Nov 04	L	PM	2	4-Kanal,HR-NS,PM
04indrex1306x2	Mawas_a	30. Nov 04	L	PM	3	4-Kanal,HR-NS,PM
04indrex1309x2	Mawas_a	30. Nov 04	L	PM	5	4-Kanal,HR-NS,PM
04indrex1401x1	Mawas	30. Nov 04	P	PM	2	4-Kanal,HR-NS,PM
04indrex1402x1	Mawas	30. Nov 04	P	PM	2	4-Kanal,HR-NS,PM
04indrex1403x1	Mawas_a	30. Nov 04	P	PM	2	4-Kanal,HR-NS,PM
04indrex1404x1	Mawas	30. Nov 04	P	PM	5	4-Kanal,HR-NS,PM
04indrex1405x1	Mawas	30. Nov 04	P	PM	5	4-Kanal,HR-NS,PM
04indrex1406x1	Mawas	30. Nov 04	P	PM	5	4-Kanal,HR-NS,PM
04indrex1407x1	Mawas	30. Nov 04	P	PM	6	4-Kanal,HR-NS,PM
04indrex1408x1	Mawas	30. Nov 04	P	PM	6	4-Kanal,HR-NS,PM
04indrex1409x1	Mawas	30. Nov 04	P	PM	6	4-Kanal,HR-NS,PM
04indrex1410x1	Mawas	30. Nov 04	P	PM	9	4-Kanal,HR-NS,PM
04indrex1411x1	Mawas	30. Nov 04	P	PM	9	4-Kanal,HR-NS,PM
04indrex1403x2	Mawas_a	30. Nov 04	P	PM	2	4-Kanal,HR-NS,PM

04indrex1406x2	Mawas_a	30. Nov 04	P	PM	5	4-Kanal,HR-NS,PM
Extra-Tracks (for Study of Incidence Angle Effects)						
04indrex1601x1	Sungaiwainnorth	05. Dez 04	P	PM	10	4-Kanal,HR-NS,PM
04indrex1602x1	Sungaiwainnorth	05. Dez 04	P	PM	10	4-Kanal,HR-NS,PM
04indrex1603x1	Sambojalestari	05. Dez 04	P	PM	9	4-Kanal,HR-NS,PM
04indrex1604x1	Sambojalestari	05. Dez 04	P	PM	9	4-Kanal,HR-NS,PM
04indrex1601x2	Sungaiwainnorth	05. Dez 04	P	PM	10	4-Kanal,HR-NS,PM
04indrex1602x2	Sungaiwainnorth	05. Dez 04	P	PM	10	4-Kanal,HR-NS,PM
CALIBRATION 3						
04indrex1701x1	Bpn_airport	06. Dez 04	P	PM	3	4-Kanal,HR-NS,PM
04indrex1702x1	Bpn_airport	06. Dez 04	P	PM	3	4-Kanal,HR-NS,PM
04indrex1703x1	Bpn_airport	06. Dez 04	C	DP	3	2-Kanal,HR-NS
04indrex1704x1	Bpn_airport	06. Dez 04	C	DP	3	2-Kanal,HR-NS
04indrex1705x1	Bpn_airport	06. Dez 04	L	PM	3	4-Kanal,HR-NS,PM
04indrex1706x1	Bpn_airport	06. Dez 04	L	PM	3	4-Kanal,HR-NS,PM
04indrex1707x1	Bpn_airport	06. Dez 04	X	VV	2	2-Kanal,HR-NS
04indrex1708x1	Bpn_airport	06. Dez 04	X	VV	2	2-Kanal,HR-NS

Tab. 5.4.1: E-SAR Data Acquisition during the INDREX-II campaign

6 Data Description and Processing

The section describes the acquired ground and radar data, the processing procedure and the storage of the data on CD/DVD and hard disk.

6.1 Ground Data Description

Acknowledgements field data collection

Many people have been involved in field data collection, logistics and coordination. Especially the work of the following persons should be acknowledged.

Marcela Quinones (SarVision) developed the protocol for tree transect measurements, carried out the tree measurement accuracy validation, developed the biomass estimation approaches and made the biomass estimations, and authored the supporting documents for tree transects (section 6 of the database). Florian Kugler (DLR) assisted Marcela with the protocol development and accuracy assessment. Yuyu Ramdhani (SarVision Indonesia) coordinated and carried out the tree transect measurements with his team in Mawas and Bambang Suryokusumo (SarVision Indonesia) had the same task for the Sungai Wain test site (section 6 of the database).

Ruandha Sugardiman (WUR) provided the GIS database (section 1 of the database) and coordinated the aerial photography flights and carried them out in Mawas (section 3 of the database). He was supported by Muljanto Nugroho (former WUR) and Kemal Prakoso (SarVision Indonesia).

Martin Vissers, Vincent Schut, Arjen Vrieling (all SarVision) and Yuyu Ramdhani (SarVision Indonesia) are acknowledged for support during the six missions to Begantung and Tuanan made for setting up hydrological instrumentation (section 2 of the database).

6.1.1 Gross data structure

Types of data

Three types of field data should be distinguished, namely original field data, derived data and supporting data. *Original field data* are data collected in the field from direct measurements such as tree measurements, water levels, GPS readings and photography. *Derived data* are based on these original data. Examples are biomass and forest height (such as h100). Since there is no unique approach to determine the derived data it is of importance that all original data have been included in the field database in order to allow researchers in a later stage to apply their own methodology. It is noted that section 6.1.6 already presents 6x2 different ways to determine biomass levels. Future researchers should still decide which one is the most appropriate, or that still another or new approach is to be preferred. *Supporting data* are data that already existed, mostly in the form of maps and remote sensing images. These are combined in a GIS together with some original field data, such as the position of plots, or camps. These GIS could be easily extended by adding INDREX-II radar data. In such a way the GIS is a useful tool to visualize the relation between different types of data and to support analysis of the INDREX-II data set.

Organization of data on data discs

The INDREX-II ground data discs (3 DVD's) contain six main folders. These are organized by theme and are summarized in Table 6.1.1. These themes will be discussed below. At the second level (first sub-folder level) data are organized by test site.

Table 6.1.1. Contents INDREX-II ground data discs (size 12 Gb).

1st level (types)		size	data disc
1	GIS (supporting data)	691 Mb	1
2	Hydrology Mawas	53 Mb	1
3	Aerial survey	10.0 Gb	1, 2, 3
4	Photographs referenced	561 Mb	1
5	Photographs others	475 Mb	1
6	Tree transects (includes derived data and supporting documents)	20 Mb	1
2nd level (test sites)			
1.1	GIS Mawas		
1.2	GIS Sungai Wain		
etc.			

Relation between ground data sites and radar data strips

The names of the radar strips introduced in the previous chapter do not correspond one-to-one to the names of the test sites. Table 6.1.2 indicates in which images the test sites can be found.

Table 6.1.2. Correspondence between names sites and radar strips.

Sites	Radar strips
1. Mawas Reserve – Undisturbed 1a. Camp Begantung 1b. Camp Tuanan	Mawas C & Mawas E
2. Mawas Reserve – Disturbed	Mawas A
3. Sungai Wain Reserve	Sungai Wain North
4. Balikpapan Bay Mangrove area	Sungai Wain North & South
5. Penajam Oil Palm Plantation	Sungai Wain South
8. Penajam Rubber Tree Plantation	Sungai Wain South
6. Samboja Lestari Plantation	Samboja Lestari
7. Gunung Meratus Reserve	Meratus

6.1.2 GIS data

To use the GIS data standard ArcView 3.3 software is needed, and extensions are not required. The free extension CoordinatesToolBox.avx is recommended for retrieving high precision positions.

The following types of data are included:

- Raster files (all in JPEG format): a selection of SRTM, Landsat, Ikonos, AirSAR and ESAR images
- Vector files such as field work plots, rivers, roads, plantations
- Points such as the location of small plots, photographs, hydrological instruments and camps

The data are organized in four ArvView *.apr project files. These are:

- mawas.apr*, for sites 1 and 2;
- sungaiwain.apr*, for sites 3, 4, 5 and 8;
- sambojalestari.apr*, for site 6;
- meratus.apr*, for site 7

6.1.3 Hydrology data

Hydrological data for the peat swamp forest test sites are measured for two purposes. In the first place data on water levels and flooding percentages may be related to backscatter. Hence they serve to calibrate radar data (such as PALSAR or E-SAR). Secondly, they are useful to model hydrological water flows, i.e. ground water flow and surface run-off, water storage capacity, and spatial patterns. Such hydrological models are crucial for management and restoration of these fragile ecosystems. Hence, in the future, the combination of calibrated space radar monitoring and a good hydrological model may be especially useful. In this report focus is on the first purpose, i.e. the calibration of the radar.

Instruments called divers have been positioned along 15 points of the Mawas research transect to measure water level. The divers measure automatically every hour. Some instruments function already since 1993. The idea is to build up a series of 10 years. At each diver position the soil surface roughness is sampled. The roughness profile serves to estimate the flooding level, i.e. the percentage of terrain flooded. Besides pressure, the diver also measures temperature. The functioning of this system is illustrated in Fig.6.1.1 and Fig.6.1.2.

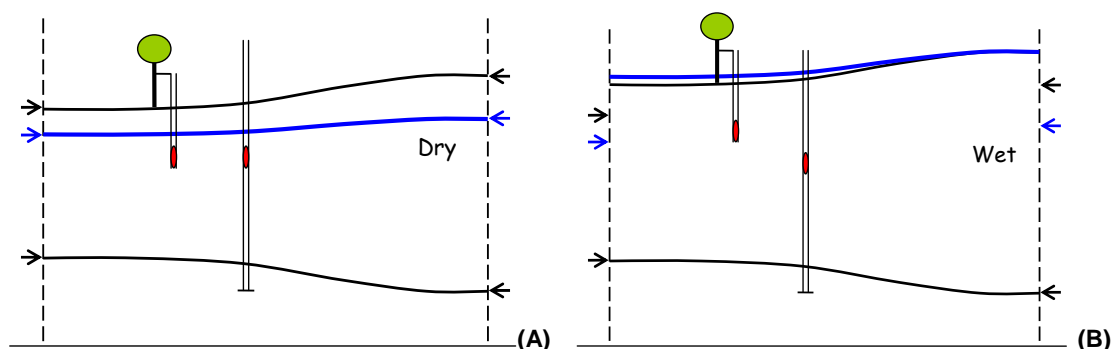


Fig.6.1.1. Principles of water and soil level measurement. The large perforated tube in the centre is pushed through the thick peat layer (up to 15 m) and "anchored" in the mineral soil. A diver (the red spot inside the tube), which in fact is a pressure meter, is located in the tube suspended by a steel wire from the top of the tube. The diver is always under water: in dry season (A) as well as in the wet season (B). The diver measures the sum of the pressure of the water column and atmosphere (or barometric pressure). To compensate for barometric

pressure fluctuations another diver, a so-called baro-diver, is positioned nearby, above the ground, in the base camps. The left tube works according the same principles, however is anchored at a tree. Because the peat layer can swell and shrink, the soil surface altitude changes periodically and the trees, which are shallow rooted move with the surface. Comparison of data from both tubes gives a measurement of soil surface subsidence and swelling.

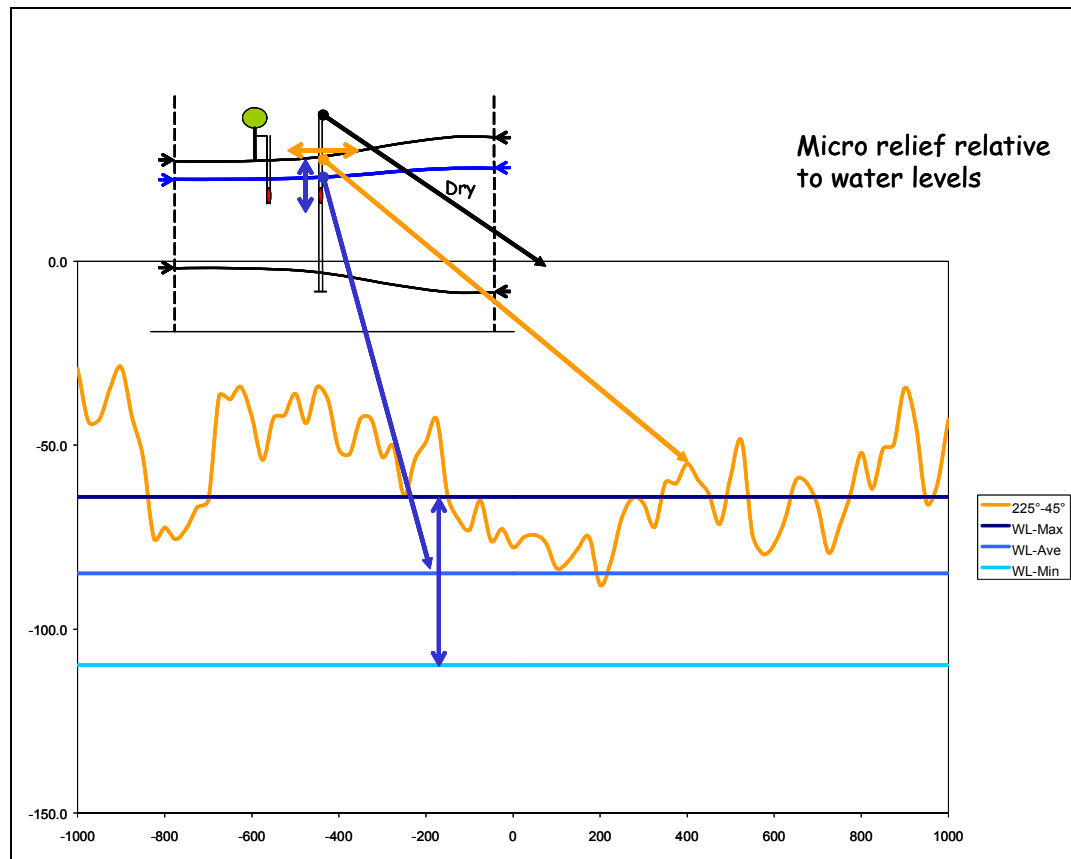
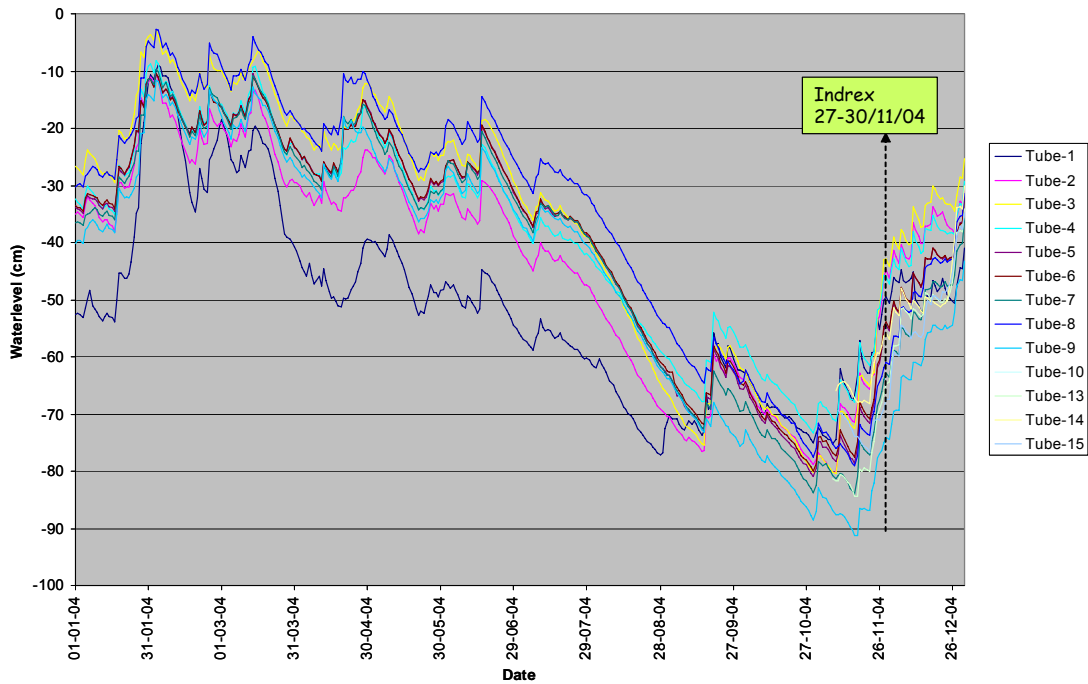


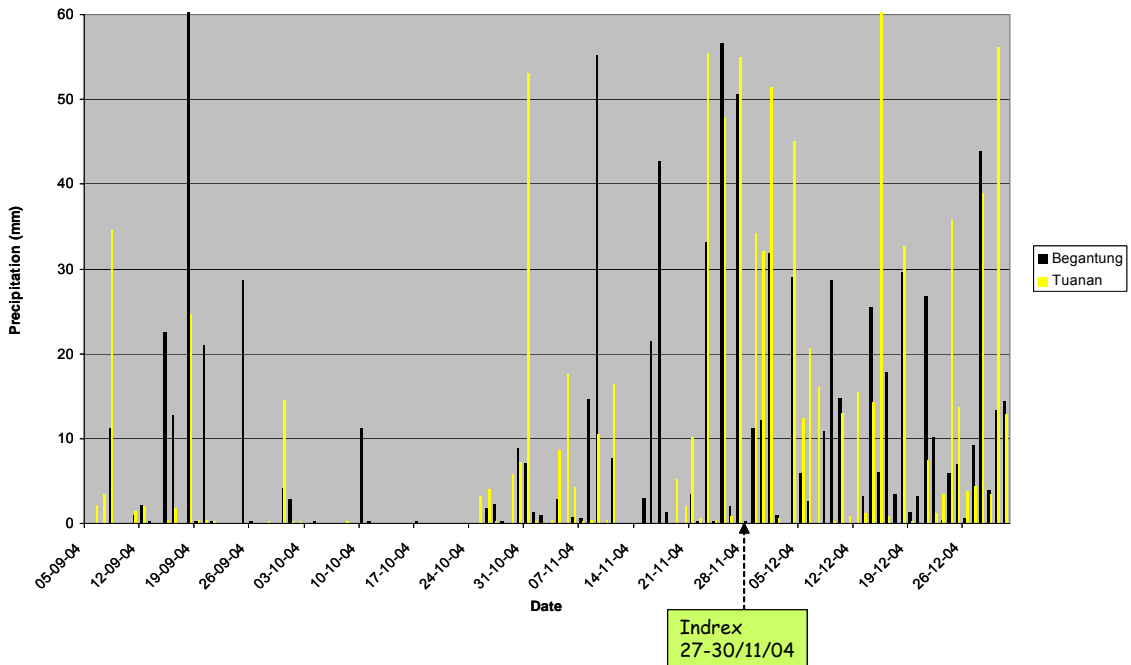
Fig.6.1.2. Principles of flooding fraction estimation. The tube is positioned in the middle (location 0 cm on x-axis) of the soil surface roughness profile (the orange curve) which extends 10 m to the left and the right (-1000 cm and + 1000 cm on x-axis). The height of the soil surface (in cm) relative to the top of the tube is indicated on the y-axis. In this example it ranges from roughly from -25 cm to -75 cm. The three horizontal lines indicate water levels in the tube (these levels are the same in the vicinity of the tube because of the high hydraulic conductivity of the peat. The top line is the maximum water level and the bottom line the minimum water level within a certain measurement period. In the latter case there is no flooding because water level is lower than the deepest pits. During the high water table roughly 30% is flooded. For each diver position soil roughness is sampled along two transects of 20 m.

The INDREX-II database gives this information for every day (averaged) of the year 2004 when available. Some instruments have been placed only during the year 2004, several months in advance of the campaign. Results are summarized in figures 6.1.3-6.



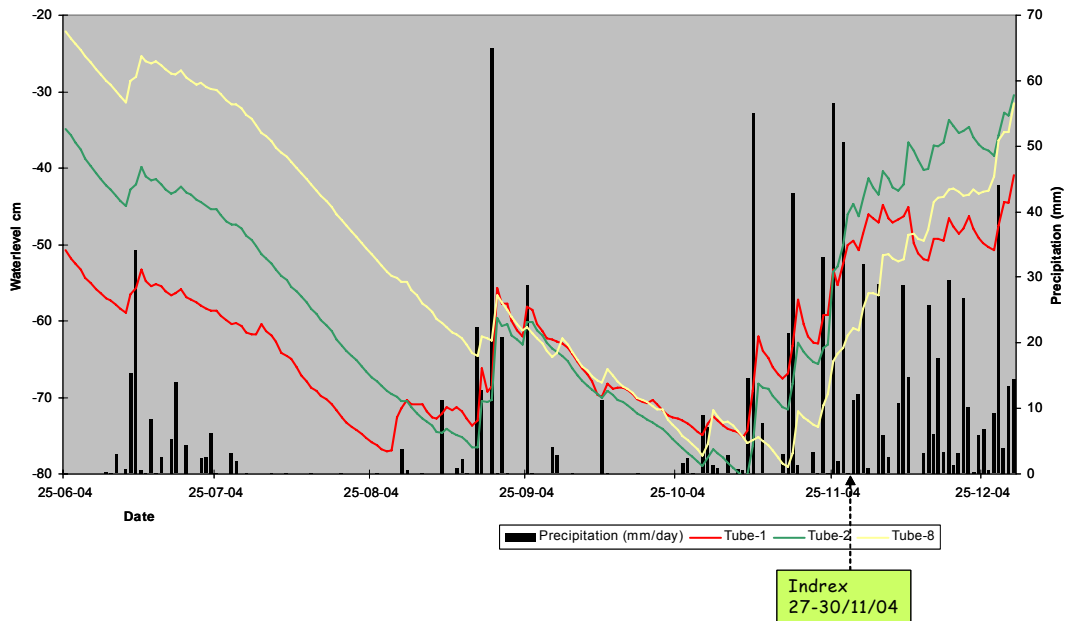
Water level

Fig.6.1.3. Water level variation during the year 2004 relative to the averaged (from the soil surface profile) soil surface height. Note that some curves only start in September 2004. The campaign days are indicated.



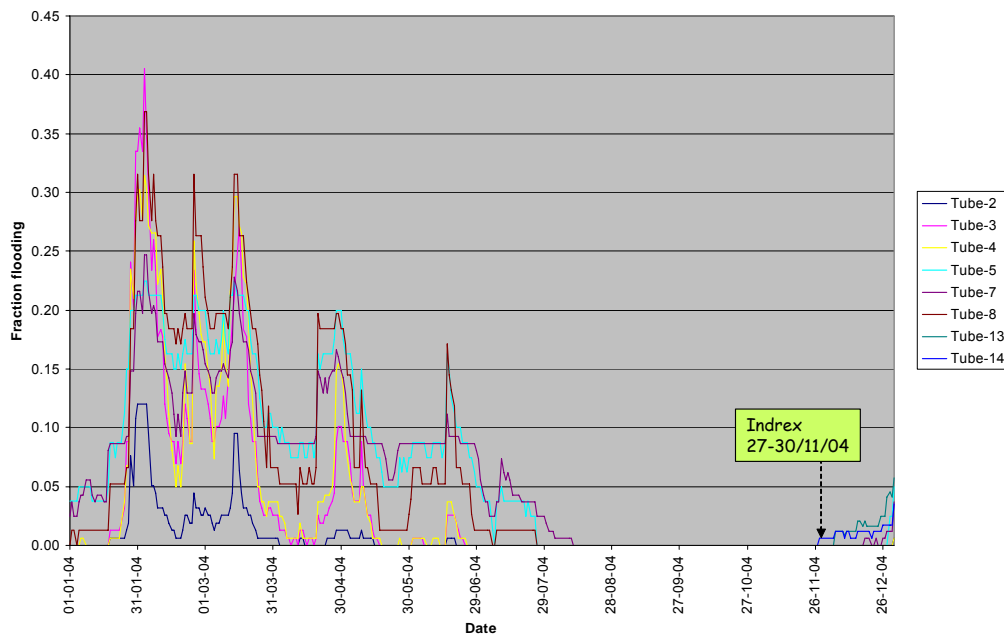
Precipitation

Fig.6.1.4. Daily precipitation as recorded in the base camps. Note the series starts in September 2004. The campaign days are indicated.



Water level and precipitation

Fig.6.1.5. Relating water level and precipitation. It is clearly shown that water levels rise after heavy rainfall. From these data the storage capacity of the soil can be estimated. For example: when after 50 mm of rainfall the soil water level rises 10 cm a storage capacity of 0.5 can be estimated.



Flooding fraction

Fig.6.1.6. Flooding fraction variation during the year 2004. It is evident that during the first half of the year flooding can be substantial. After the dry season and in early wet season (which normally starts around early November) the flooding is absent or almost absent. During INDREX-II the rain period already started (see previous figures) however there was not enough rainfall yet to raise water level sufficiently for flooding.

6.1.4 Aerial photography data

The data discs number 2 and 3 contain the aerial photographs in full resolution in five sub-folders.

- 1) The first flight was executed with the ultralight aircraft over Samboja Lestari at 15 and 16 September 2004 with the photo camera pointing in nadir direction. Because of flying height restrictions it yielded an incomplete sampling (approx. 50%) of the area.
- 2) The flight with a small aircraft over Samboja Lestari at 4 December 2004 yielded oblique photography through the window. No permission was obtained to fly high or to open the door. Also the allowed flying time was very limited. It yielded an incomplete coverage of oblique photography. Nevertheless it is a very useful dataset since it records the actual situation of vegetation condition during the INDREX-II campaign.
- 3) A similar flight over Samboja Lestari was repeated at 7 December 2005. It clearly shows how rapidly the vegetation has developed in certain areas.
- 4) No permission was obtained to fly over Sungai Wain during the INDREX-II campaign. The data disc contains the results of oblique photography collected by Graham Usher at 28 and 29 August 2005 from low flying aircraft.
- 5) In Mawas all INDREX-II radar strips centre line areas have been covered by ultralight aircraft during several flights in the period 13-15 January 2005. It provides a complete coverage in nadir direction with overlap allowing stereo views. Position and height of the camera have been recorded by simultaneous GPS measurements. Since the angle of view of the camera is 53° (in across-flight direction) the height of flight equals the width of the strip covered by the camera.

Data disc number 1 contains a HTML browser for Mawas. The HTML file contains a self explanatory menu. It gives an overview (in the form of maps) of the photography of Mawas, shows the photographs in reduced resolution, and indicates GPS position of the camera and height of flight.

6.1.5 Field photography data

Available field photography has been organised in two separate folders. The first folder contains photographs with a geo-reference (GPS coordinates recorded simultaneously). These coordinates are given in a separate file, often together with auxiliary descriptions. There are sub-folders for the Sungai Wain area, the Samboja Lestari area and the Penajam area. The fourth sub-folder contains a collection for all sites except the Meratus area.

Another folder contains photography without geo-reference or additional descriptions, however these photographs are still organised by site. These sites are Mawas, Sungai Wain, Samboja Lestari and Penajam. A fifth sub-folder contains pictures of the corner reflector deployment at Balikpapan airport.

6.1.6 Tree transect field data

Detailed descriptions of tree transect measurement accuracy, allometry and biomass estimation can be found in several documents written by Marcela Quiñones on the field data DVD's (section 6: *Tree transects*, folder: *Supporting documents*)

Trees and other vegetation have been measured within 63 plots using protocols adapted for the type of vegetation. In October 2005, during a post-campaign mission, 12 additional plots have been measured. An overview of the tree transects measured is given in Table 6.1.3. Figure 6.1.7 shows the location of plots in Sungai Wain. In tables 6.4a-e an overview of the measured parameters is given per site.

Table 6.1.3. Overview of tree transect measurements.

Sites	Number of plots
<i>Mawas</i>	
Begantung	6 plots
Tuanan	2 plots
<i>Sungai Wain</i>	26 plots + 12 plots (Oct 2005)
<i>Samboja Lestari</i>	20 plots
<i>Penajam</i>	
Oil palm	3 plots
Rubber	3 plots
<i>Mangrove</i>	3 plots
<i>Meratus</i>	(no plots)

Table 6.1.4a. Overview of tree transect data collected in Mawas.

Mawas: Begantung & Tuanan
8 Transects, 100 m x 10 m, dbh >10 cm
10 subplots per transect 5 m x 5 m, dbh <10 cm, height >2 m
Species
Location
dbh
Tree height
Height to first branch, crown dimensions
Terrain height- peat depth
Biomass estimations

Table 6.1.4b. Overview of tree transect data collected in Sungai Wain.

Sungai Wain
26 Structural plots, 26 m x 32 m,
Trees, palms, vines dbh >10 cm
26 Subplots of 26*2m, 0< dbh <10 cm
Species
Location
dbh
Total tree height
Height to first branch, crown dimensions
Terrain height (bad quality)
Structural drawing (not yet done)
Biomass estimations
<u>Additionally collected data Oct 2005:</u>
12 Structural plots, 20*20m,
same parameters

Table 6.1.4c. Overview of tree transect data collected in Penajam.

Rubber plantation	Oil palm plantation
3 Plots 20 m x 20 m, trees dbh >10 cm	3 Plots 20 m x 20 m
dbh	dbh
Height	Height
Height of first branch	Height of first branch
Age (8,10,12 years)	Age
Density	Density
Biomass estimations	Biomass estimations

Table 6.1.4d. Overview of tree transects data collected in Samboja Lestari. The plots with trees are mostly 20 m x 20 m in size. For all trees with a dbh in excess of 10 cm the height, the height of the first branch have been measured. For all plots the biomass has been estimated.

Samboja Lestari: Tree plantations and alang-alang	
Secondary forest (4)	
Gamelina (2)	
Acacia (2)	
Teak (10)	
Young fruit trees (1)	
Meranti (1)	
Alang-alang samples (3)	

Table 6.1.4e. Overview of tree transect data collected in the mangroves.

Natural mangrove	
3 transects 10*3m	
dbh	
Height and height of first branch	
Biomass estimations	

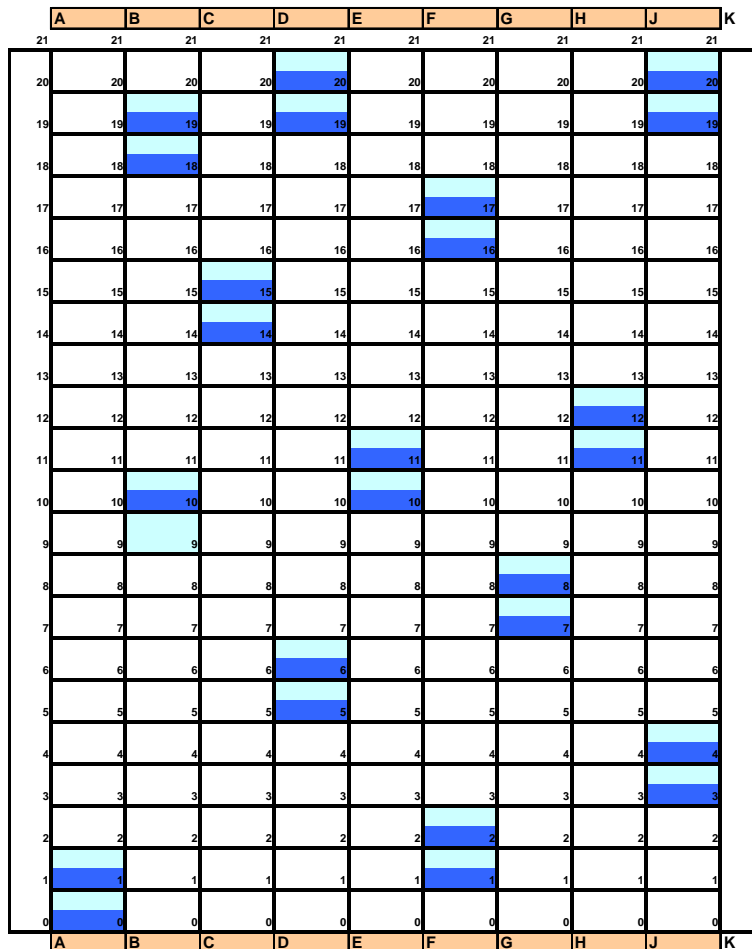


Fig.6.1.7. Location and labelling of the 26 plots in Sungai Wain within the core study area.

6.1.7 Biomass and allometry

Detailed descriptions of tree transect measurement accuracy, allometry and biomass estimation can be found in several documents written by Marcela Quiñones on the field data DVD's (section 6: *Tree transects*, folder: *Supporting documents*)

The following gives a concise summary of definitions and recipes used to define the 6 biomass parameters (i.e. BIO1 to BIO6) developed by Marcela Quiñones for INDREX-II.

Biomass definition

Biomass density is defined as the total amount of above ground living organic matter in trees expressed as oven-dry tons per unit area.

To estimate biomass density from forest inventory data two fundamentally different methods exist. The first is based on allometry, the second on wood volume data.

Biomass density based on allometric equations (parameters BIO 1–4)

When Y is the (oven-dry) biomass per tree in kg, than Y is a function of factors like D (dbh in cm) and H (total tree height in m). Such an allometric expression has a range of validity depending on factors like climatic zone and dbh range. The allometric equations for INDREX-II are summarized in Table 6.1.6.

Table 6.1.6. Allometric equations selected for the INDREX-2 test sites for trees with a dbh ≥ 10 cm.

Biomass parameter	Climatic zone	Equation	Range in dbh (cm)
BIO1/tree	MOIST	$Y = 42.69 - 12.8 D + 1.242 D^2$	5-148
BIO2/tree	MOIST	$Y = \exp(-3.1141 + 0.9719 \ln(D^2H))$	--
BIO3/tree	WET	$Y = \exp(-3.3012 + 0.9439 \ln(D^2H))$	--
BIO4/tree	WET	$Y = 21.297 - 6.953 D + 0.740 D^2$	4-112

Biomass density based on volume data (parameters BIO 5–6)

The general equation for biomass based on volume data is:

$$\text{Biomass density} = \text{VOB} \times \text{WD} \times \text{BEF} \text{ (ton/ha)}$$

where,

VOB = volume over bark (stem volume of all living trees with more than 10 cm diameter at breast height)

WD = volume-weighted average wood density (oven-dry biomass in ton per m³ fresh volume) and

BEF = biomass expansion factor in order to include leaves, twigs, and branches, commonly not measured by the forest inventories (BEF values depend on the value of BV=VOB x WD)

For INDREX-II the following parameters have been used

$$\text{WD} = 0.57$$

$$\text{BEF} = \text{Exp}\{3.213 - 0.506 \times \text{Ln}(\text{BV})\} \text{ for } \text{BV} < 190 \text{ ton/ha}$$

$$\text{BEF} = 1.74 \text{ for } \text{BV} \geq 190 \text{ ton/ha}$$

For INDREX-II biomass parameters BIO 5 and BIO6 have been defined as follows:

Bole volume (for BIO5) = basal area x height to first branch x shape factor

Shape factor (for BIO5) = 0.5

Bole volume (for BIO6) = basal area x total tree height x shape factor

Shape factor (for BIO6) = 0.7

and VOB = Σ Bole volume.

It is noted that for (large) trees with dbh \geq 10 cm the approaches BIO1-4 (allometry) and BIO5-6 (volume) are used. For (small) trees with dbh < 10 cm only approach BIO6 is used. Thus, to arrive at total biomass, the BIO1-6 values (for large trees) and the BIO6 value (of small trees) are added.

As an example the biomass data results for the 8 Mawas plots are given in Tables 6.7a-b. The results shown in Table 6.7a clearly show that the choice of approach (allometry or wood volume based) as well as the choice of the (default) parameters, as described above, has an enormous influence. For example, for plot Begantung Km6-A, the value for BIO1 is almost 600 ton/ha, while for BIO3 it is only 100 ton/ha. It should also be remarked that some of the values are much higher than given in literature. Table 6.7b gives a possible explanation for such high values. In the peat swamp forest 40-80% of the biomass is in the "small plants" (i.e. in trees with a dbh smaller than 10 cm and in undergrowth), which is normally omitted in biomass estimations.

Table 6.1.7a. Total biomass for Mawas plots

Total biomass	BIO1	BIO2	BIO3	BIO4	BIO5	BIO6
Tuanan A	481.46	257.29	171.35	261.49	307.36	386.17
Tuanan B	573.65	255.26	166.77	308.67	303.11	377.71
Begantung Km1-A	542.79	194.56	130.24	286.99	285.86	334.08
Begantung Km1-B	419.66	149.15	100.76	220.80	260.90	283.31
Begantung Km3-A	672.46	198.81	134.00	341.01	291.64	351.24
Begantung Km3-B	554.35	166.03	114.87	278.67	279.22	320.89
Begantung Km6-A	597.56	145.20	100.13	298.64	262.38	303.85
Begantung Km6-B	615.84	179.15	120.65	313.90	283.94	336.66

Table 6.1.7b. Percentage contribution of small trees and plants to the total biomass for the Mawas plots.

% Contribution of small trees/plants	BIO1	BIO2	BIO3	BIO4	BIO5	BIO6
Tuanan A	64.82	28.70	30.44	58.82	49.33	39.25
Tuanan B	61.87	20.95	22.89	55.80	43.22	34.68
Begantung Km1-A	72.76	33.11	35.22	67.47	49.77	42.58
Begantung Km1-B	75.65	37.05	39.02	70.54	51.00	46.97
Begantung Km3-A	83.43	42.07	44.73	79.37	54.56	45.31
Begantung Km3-B	87.54	61.38	63.28	84.15	62.28	54.19
Begantung Km6-A	89.94	58.42	60.64	87.18	61.05	52.72
Begantung Km6-B	82.97	45.48	48.26	79.06	55.47	46.78

6.1.8 Tree transect data quality

Detailed descriptions of tree transect measurement accuracy, allometry and biomass estimation can be found in several documents written by Marcela Quiñones on the field data DVD's (section 6: *Tree transects*, folder: *Supporting documents*)

The tree measurement data quality has been verified by comparing results measured by the Indonesian field teams with data collected by an independent verification team (Marcela Quiñones and Florian Kugler). All original validation data can be found on the data discs. In figures 6.8a-d some examples of the results for the Sungai Wain site are given. Figures 6.8a-b illustrate that the measurement of dbh is fairly accurate. Figures #8c-d illustrate that the measurement of total tree height is also fairly accurate but slightly overestimated. This can be explained by the fact that the error tends to have a bias in positive direction when the angle to the tree top is measured at a distance too close to the tree. Making measurements from a larger distance is tedious and time-consuming because of the increase of tree canopy obscuring sight. As a quality parameter the distance to the tree was also recorded by the Indonesian field teams. Based on this quality parameter (for all plots), the comparison (only for those plots measured by the validation team) and careful evaluation of the results, it was decided to re-measure a number of trees during the October 2005 post-campaign field work.

It should be noted that the remaining measurement error has only a relatively slight influence on the estimation of the biomass level. This is illustrated in Figures #9a-b. The choice of approach, as indicated in section 4.1.7, has a far greater impact.

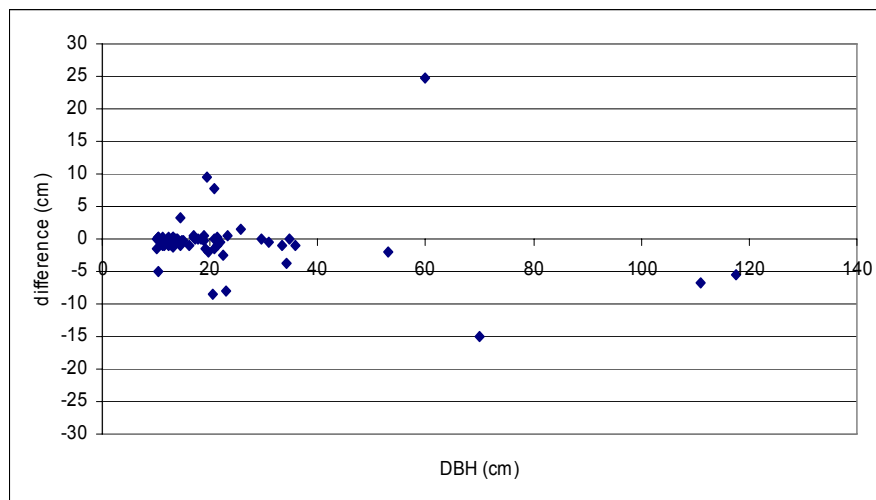


Fig.6.1.8a. Quality assessment of tree transect data. Differences between measurements by the Indonesian field team and the independent validation team of the parameter dbh in Sungai Wain.

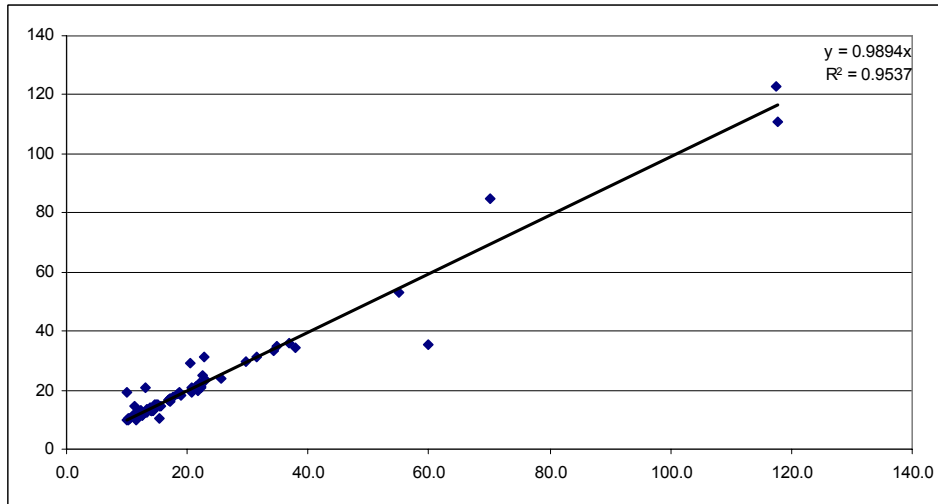


Fig.6.1.8b. Quality assessment of tree transect data. Correlation of measurements by the Indonesian field team and the independent validation team of the parameter dbh in Sungai Wain.

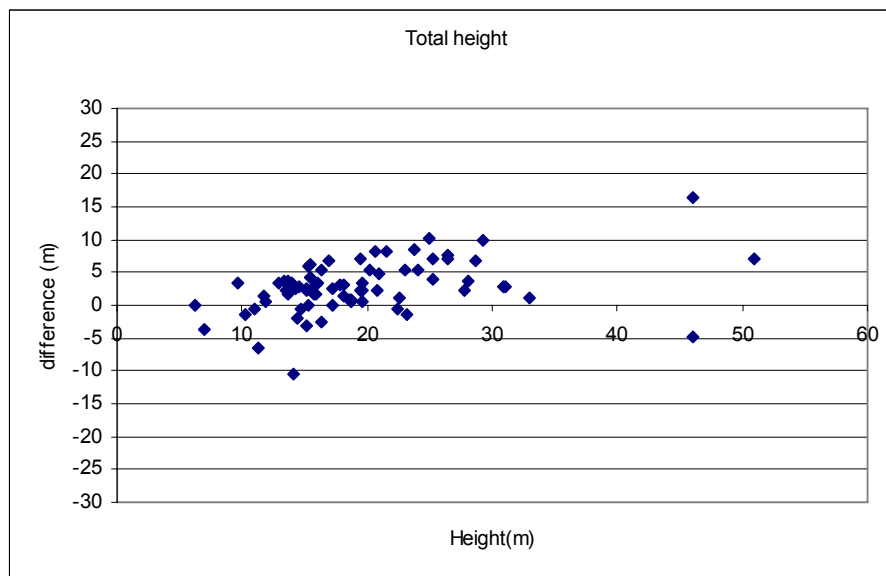


Fig.6.1.8c. Quality assessment of tree transect data. Differences between measurements by the Indonesian field team and the independent validation team of the parameter total tree height in Sungai Wain.

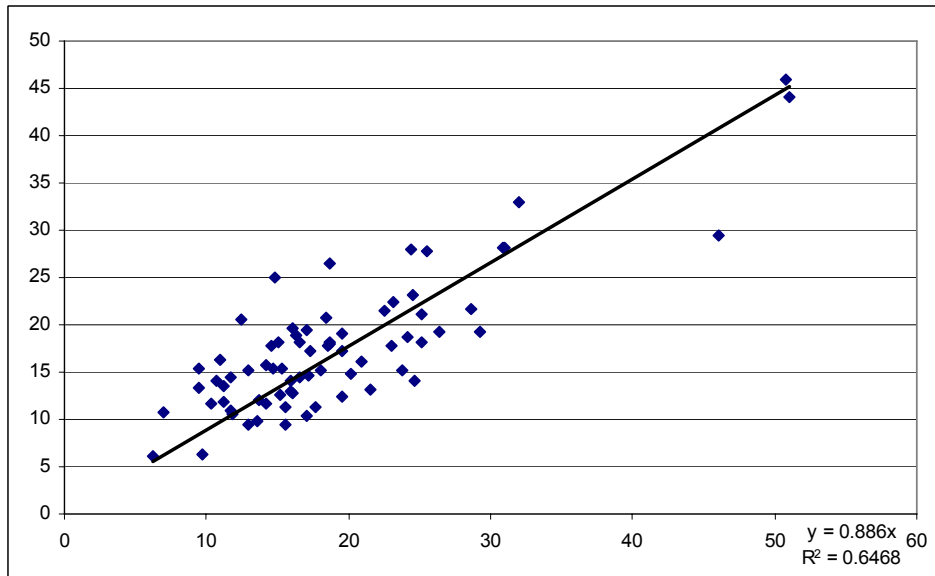


Fig.6.1.8d. Quality assessment of tree transect data. Correlation of measurements by the Indonesian field team and the independent validation team of the parameter total tree height in Sungai Wain.

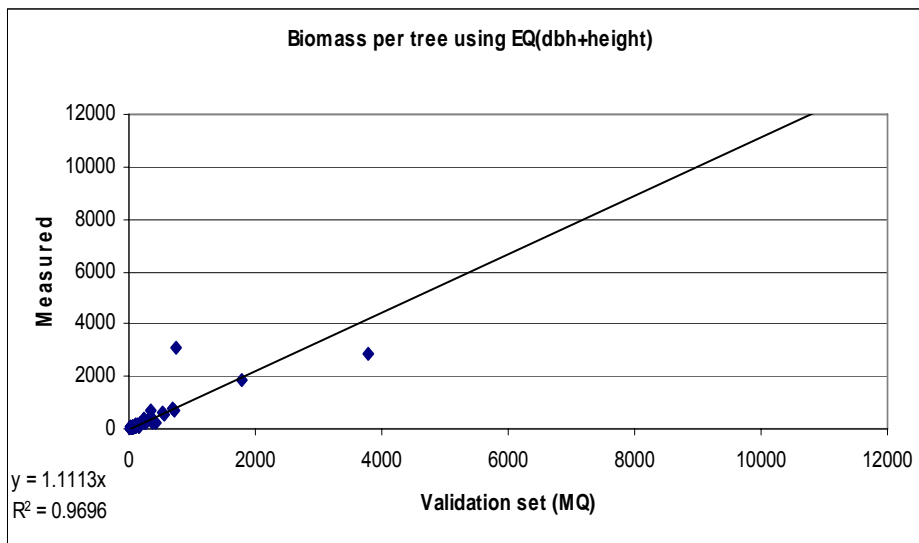


Fig.6.1.9a. Influence of tree transect data quality on biomass estimation in Sungai Wain. Resulting biomass values (BIO3) resulting from tree data collected by the Indonesian field team are compared with biomass values resulting from tree data collected by the validation team.

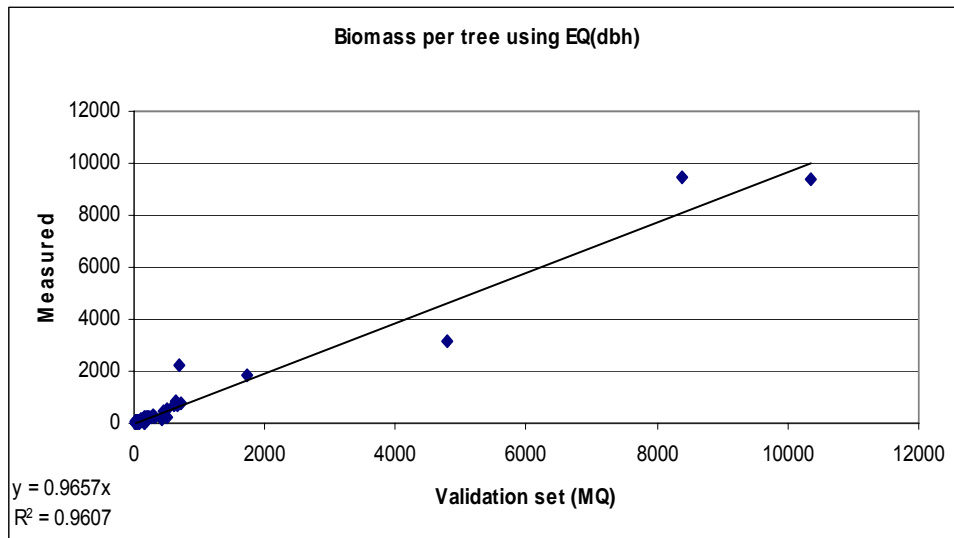


Fig.6.1.9b. Idem, for other biomass parameter (BIO4).

6.1.9 Summary and concluding remarks field data collection

For INDREX-II large tree data sets have been collected. In total approximately 10.000 trees have been measured! The quality of this data set has been verified. Good agreement with independent validation data sets of Mawas and Sungai Wain has been found. Some outliers in the Sungai Wain data set have been re-measured in October 2005. For all sites the biomass density has been determined using two different approaches resulting in six different biomass definitions. Since all original tree data are available scientists could select/study alternative approaches.

Other INDREX-II data include the GIS database which provides an overview of already existing maps and remote sensing images as well as data collected during the INDREX-II campaign. The GIS can be useful to explore relationships or to detect phenomena in the data, and can easily be extended by users of the database. Field photography provides lots of additional qualitative information and shows the situation at the time of the campaign. Aerial survey provides lots of additional information. In particular the stereo coverage of Mawas is useful for additional quantification of forest structure over the entire radar strips. Unique hydrological time series reveal spatial relationships and temporal dynamics of flooding and ground water level.

6.2 Radar Data Processing and Description

This section describes the processing of E-SAR radar data acquired within the INDREX-II campaign and summarizes the obtained radar data products for each test site.

Products are as follows:

- DEM (Digital Elevation Model) products (UTM, WGS84, 2m grid)
- RGI (Radar Geometry Images) and GTC (Geocoded Terrain Corrected) products for single scene processing (multi-frequency and multi-polarisation)
- RGI products from repeat-pass interferometric processing (master & slaves)

Section 6.2.1 gives a brief description on radiometric calibration results and section 6.2.2 explains the adopted processing strategy. Section 4 contains the summary of processed E-SAR data products delivered to the Agency.

6.2.1 Calibration

In November & December 2004 DLR performed measurement flights with its E-SAR system over selected test sites of tropical rain forest on Kalimantan (Borneo), Indonesia. It was the first time the E-SAR system was flown over homogeneous tropical rain forest.

During the INDREX-II campaign, a calibration test site with up to 7 Corner Reflectors (CR) was established on Balikpapan airport, to ensure that the radar system was stable throughout the campaign (3 weeks of effective data acquisition).

This section describes the procedure used to obtain reliable radiometric measurements in all frequency bands operated by the E-SAR system (X, C, L, and P), and summarises the performance on the deployed CR.

6.2.1.1 The calibration test-site

The calibration test-site for the INDREX-II campaign was established on Balikpapan airport. A total of 7 CR was deployed along a line parallel to the runway. Individual CR were separated by about 200-400m. Data acquisition was performed perpendicular to the runway. The C-band SAR image of the CAL-site is shown in Fig. 6.21. The position of the CR is marked with yellow (leg length 150cm) and red circles (leg length 300cm).

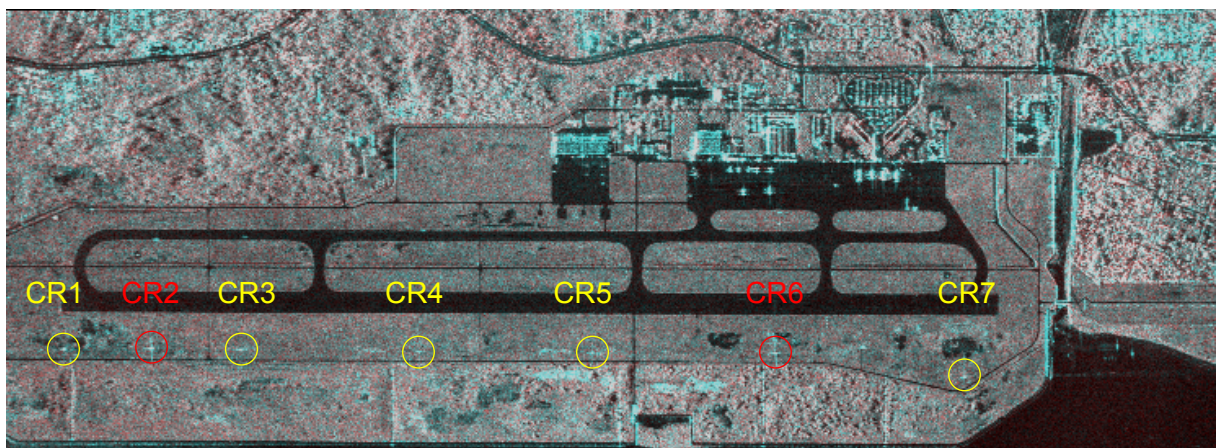


Fig. 6.2.1: INDREX-II CAL-site: dual-pol SAR-image in C-band (cyan C-HH, red C-HV). Near range is on the left.

Fig. 6.2.2 shows one of the deployed 150cm CR and one of the 300cm CR.

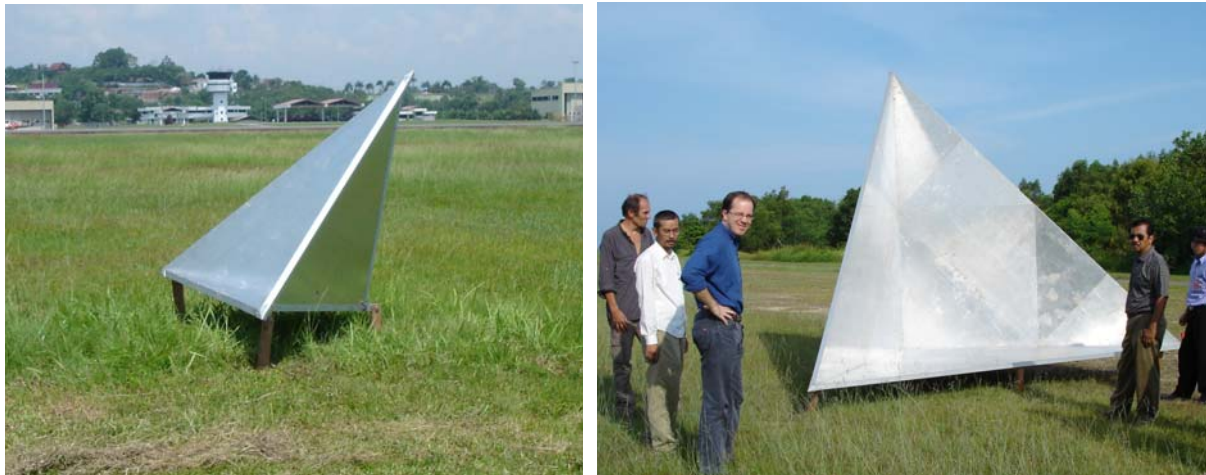


Fig. 6.2.2: Deployed CR for INDREX-II campaign. 150cm leg length reflector (left) vs. 300cm leg length reflector (right).

The geographic position and the orientation of the CR are summarised in Table 6.2.1 below.

	CR1	CR2	CR3	CR4	CR5	CR6	CR7
Latitude [deg]	-1.2740285	-1.2731561	-1.2722923	-1.2705792	-1.2688737	-1.2670848	-1.2657575
Longitude [deg]	116.884165	116.886191	116.888258	116.892415	116.896420	116.900675	116.905261
Height [m]	55.911	56.023	55.805	55.97	55.936	56.056	55.438
Azimuth [deg]	158	158	158	158	158	158	158
Elevation [deg]	28	15	20	14	11	2	4
Size [cm]	150	300	150	150	150	300	150

Table 6.2.1: Geographic position (WGS-84, ellipsoidal heights) and orientation of CR deployed for INDREX-II.

The calibration site was flown three times during INDREX-II, on 16-th and 24-th of November, and on 6-th of December. For the second flight CR3 was removed to serve as reference point for Sungai-Wain test site.

Despite of strong RFI conditions due to airport radars and other signals, especially in L- and P-band, the signatures of the CR are considered to be reliable, due to the high signal level.

6.2.2 Homogeneous tropical rain forest test-site

As mentioned before, within INDREX-II the E-SAR system was flown over tropical rain forest for the first time. Inspection of the acquired data showed, that one of the test-sites, Mawas-E, is extremely flat and homogeneous. This is considered to be the optimum test-site for radiometric calibration of the antenna patterns. Note that Amazon rain forest data are used for this purpose for different satellite SAR systems (ERS-1/2, ASAR, ...).

Fig. 6.2.3(a)-(d) present the  values for the acquired data in X-, C-, L- and P-band just taking into account the nominal antenna patterns of the E-SAR system (except for L-band, which includes already

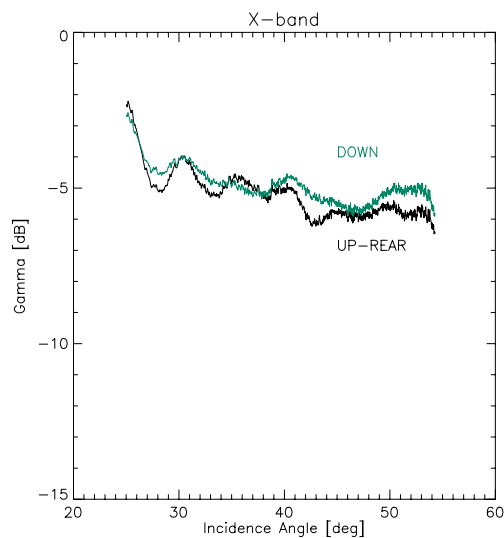
a calibration based on CR deployed at different elevation angles). The relationship between, γ , σ^0 and the radar backscatter coefficient β^0 is given by [19]:

$$\gamma = \frac{\sigma^0}{\cos \theta_i} = \frac{\beta^0 \cdot \sin \theta_i}{\cos \theta_i}$$

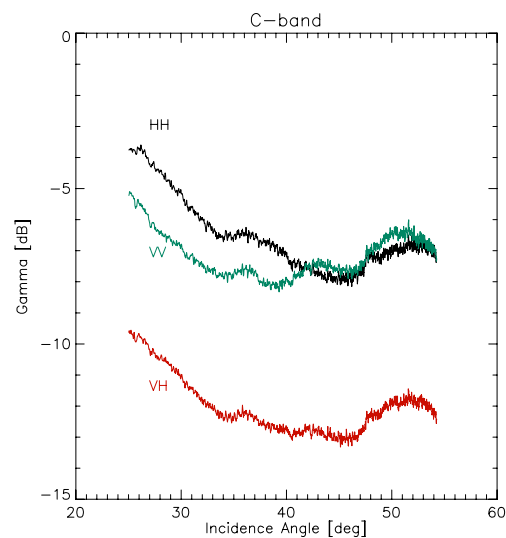
The plots of γ are far from being as expected, i.e. constant. Within the nominal incidence angle range of 25-55 deg, deviations in the order of 2dB are found in every frequency band. In some cases, especially in near range, the deviations are even larger. In P-band the evaluation has been performed down to an incidence angle of 18 deg (ESA's requirement to process steep incidence angles), despite that this angular range is outside the nominal antenna pattern, and therefore not reliable. Also performance is far from being optimum.

The following strategy is adopted to correct the variable incidence angle effects caused by inaccurate antenna patterns / interaction of antenna pattern with aircraft fuselage.

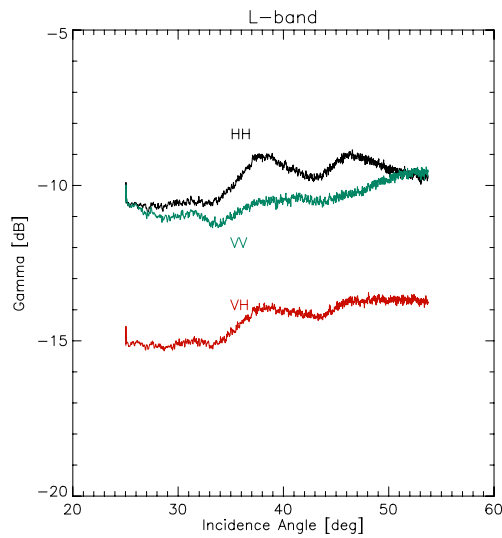
- The variation of the γ factor as a function of incidence angle is filtered to obtain a smooth correction function, which is inverted and applied during the radiometric calibration step as part of the SAR processing.
- The performance is controlled by the signatures of the CR from the calibration flights.
- A proper absolute calibration offset is added, given by the difference of the measured and the theoretical RCS-value of the CR.
- The final performance of the radiometric calibration is checked on all CR for all three calibration flights.



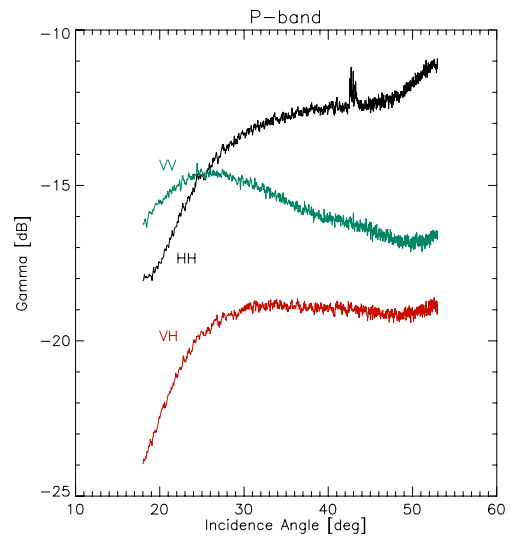
(a)



(b)



(c)



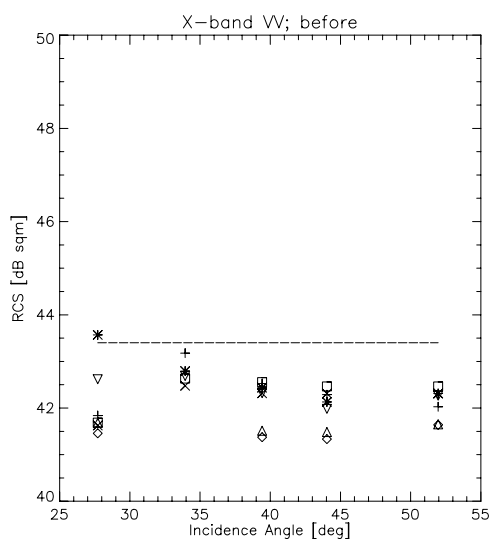
(d)

Fig.6.2.3 Mean backscatter profiles evaluated along homogeneous forest areas, MAWAS test site. X-band (only VV) (a), C-band (b), L-band (c) and P-band (d).

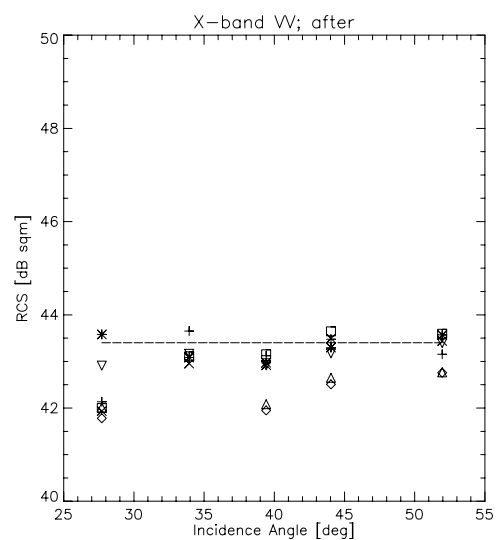
6.2.2.1 Calibration Performance

X-band Validation

The calibration curve obtained from rain forest data was applied to 7 X-band data takes acquired in VV polarisation during the three calibration flights. The RCS has been evaluated for each of the small CR (150cm leg length). The summary of the performance is given in Fig.6.2.4 below, as a comparison of theoretical and measured RCS for each CR. This allows both, a comparison with theoretical values and the check for radiometric stability throughout the campaign.



(a)



(b)

Fig.6.2.4: RCS of CR in X-band before radiometric correction (a) and after radiometric correction (b) with rainforest data derived compensation curve.

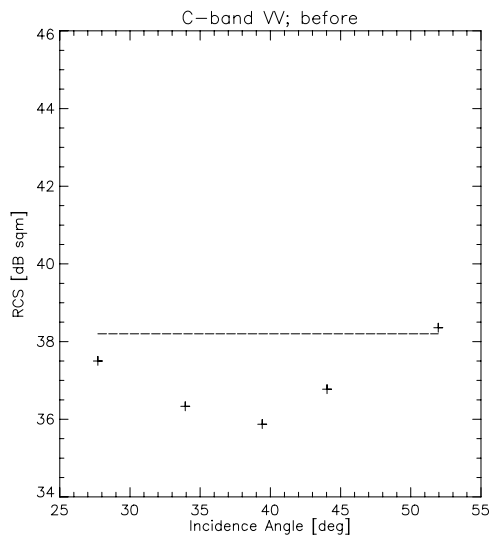
The average RCS is close to the theoretical value and the spread is within 2dB. The remaining deviations are attributed to imperfections in CR manufacturing.

The RCS values of the large CR are about 6dB below the theoretical values. Due to manufacturing inaccuracies in the order of the X-band wavelength, this is reasonable, and therefore they were not considered for validation.

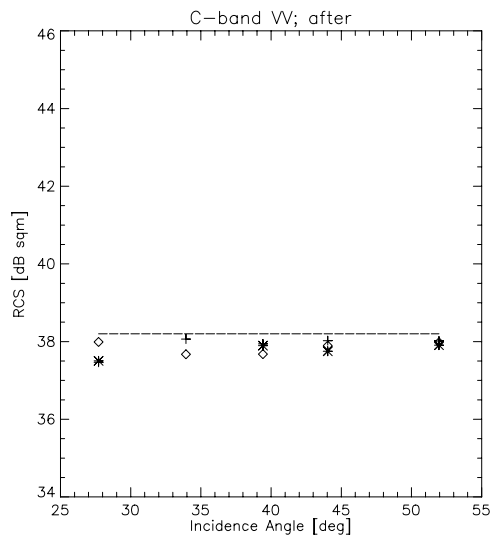
C-band Validation

The calibration curves obtained in HH and VV from rain forest data were applied to 3 C-HH and 3 C-VV data takes acquired during the three calibration flights. The RCS has been evaluated for each of the small CR (150 cm leg length). The summary of the performance is given in Fig.5 below, as a comparison of theoretical and measured RCS for each CR. Again this allows for a comparison with theoretical values and the check for radiometric stability throughout the campaign. A comparison with RCS performance of first calibration flights prior to calibration (Fig.6.2.5(a) and (c)) shows the improvement.

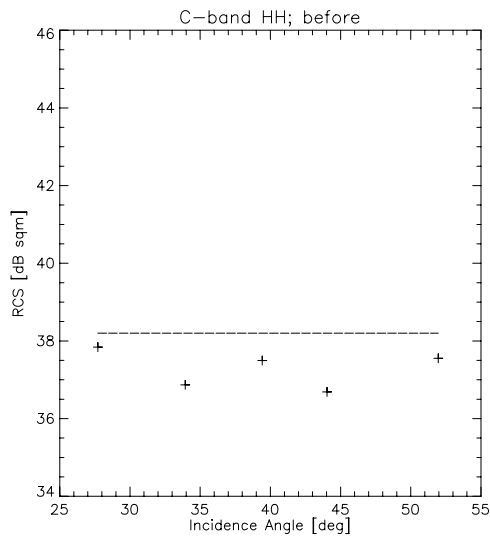
Like in the X-band case, the RCS values of the large CR's are also not considered for C-band validation.



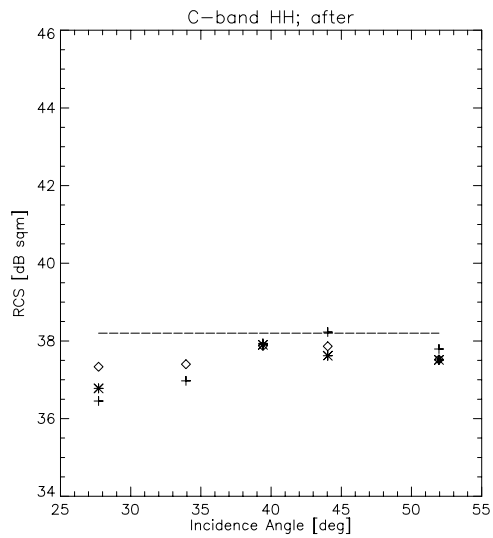
(a)



(b)



(c)



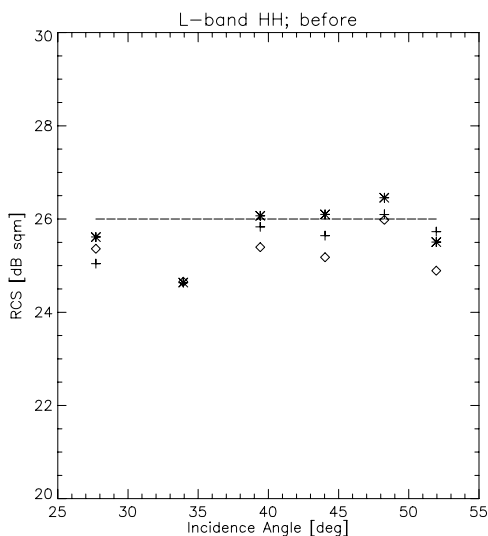
(d)

Fig. 6.2.5: RCS of CR in C-band before radiometric correction ((a) and (c)) and after radiometric correction with rainforest data derived compensation curve ((b) and (d)).

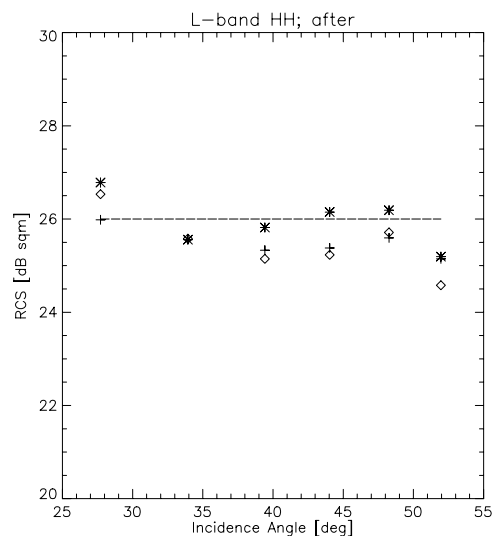
L-band Validation

The calibration curves obtained in HH and VV from rain forest data were applied to 3 L-band quad-pol data takes acquired during the three calibration flights. The RCS has been evaluated for each of the small CR (150cm leg length) and also for the large CR deployed in far range (CR6). The summary of the performance is given in Fig.6 below, as a comparison of theoretical and measured RCS for each CR. Again this allows for a comparison with theoretical values and the check for radiometric stability throughout the campaign.

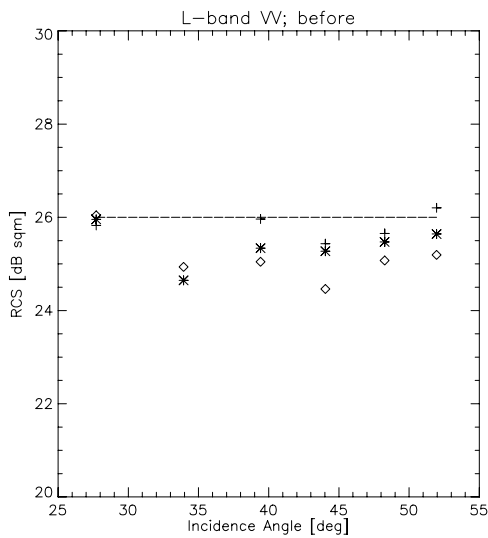
A comparison with RCS performance of first calibration flights prior to calibration (Fig.6.2.6(a) and (c)) shows some improvement in HH and only little in VV. It is not clear whether the calibration curves introduce a bias of about 1dB in the very near range or the RCS estimate on CR1 in L-band is not reliable.



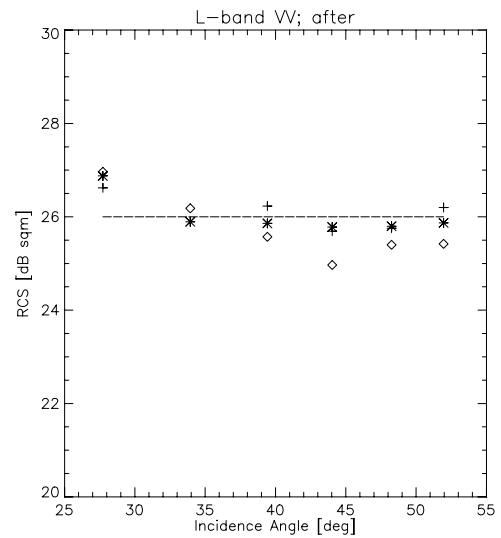
(a)



(b)



(c)



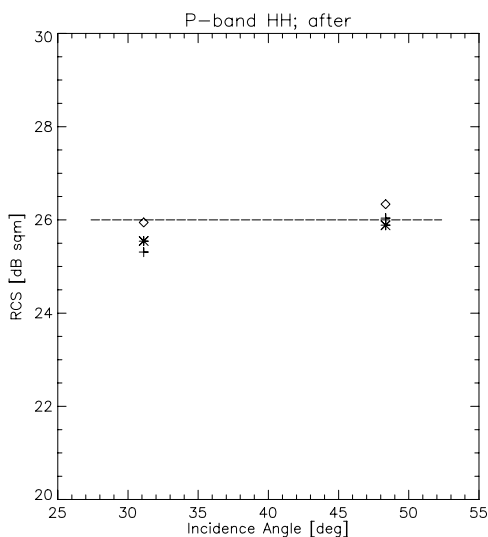
(d)

Fig. 6.2.6: RCS of CR in C-band before radiometric correction ((a) and (c)) and after radiometric correction with rainforest data derived compensation curve ((b) and (d)).

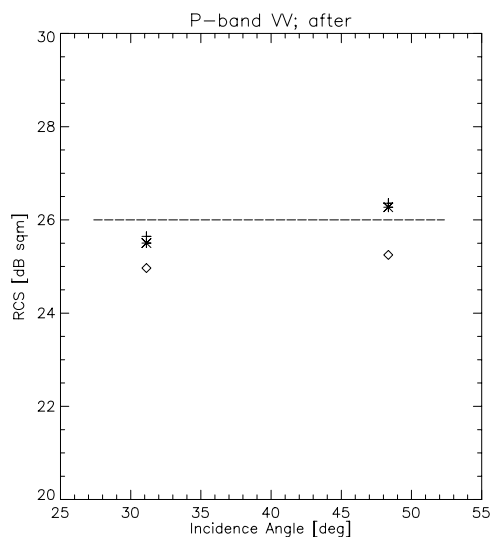
The large CR in near range (CR2) showed decreased RCS by about 2dB, probably due to slight deformations of the metallic plates. It was excluded for L-band validation. We conclude that the E-SAR antenna patterns in L-band are reasonably well calibrated, even without rain forest calibration curves. However, the rainforest calibration curves are used for processing also the L-band INDREX data.

P-band Validation

Opposite to the other frequency bands, the validation of P-band calibration relies only on the large corner reflectors CR2 and CR6 with leg length of 3m. The RCS values estimated from these CR during the 3 measurement flights are summarized in Fig.7.



(a)



(b)

Fig. 6.2.7: RCS of CR in P-band after radiometric correction with compensation curve derived from rainforest data (HH (a) and VV (b)).

Also in this case the profiles estimated from homogeneous rainforest in HH and VV are applied to the data. We found an almost perfect match for the HH signature of the CR (RCS for the near and far range CR within 0.5 dB). However, the signature for the VV polarisation in the two CR was not the same (in near range the RCS was higher by about 1.1 dB). It was decided to trust the CR signatures, and therefore an additional linear compensation was included from near to far range for the VV polarisation.

This means also that the assumption of horizontal γ -profiles in VV-polarisation in the ideal case is not correct. We explain this behaviour with increased surface scattering contributions at steep incidence angles, which overlays the homogeneous scattering (independent of incidence angle) for volume (HV) and double bounce (HH).

Note that for incidence angles steeper than 30 deg the radiometric performance could not be validated.

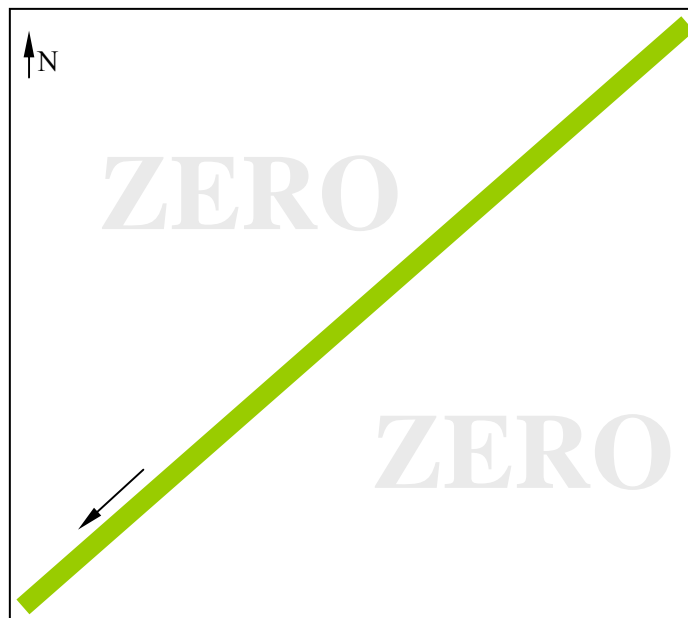
6.2.3 Segmentation and Processing Strategy

6.2.3.1 Large Data Take Handling Problem

Usually, E-SAR data had been acquired such that a data take did not exceed a length of 20 km. This implied easy data handling and data takes could be processed as one segment without major size problems. However, for scenes longer than 10 km and flight directions nearly diagonal in the UTM coordinate system, geocoding becomes inefficient as the data array includes unacceptable many zeros beyond the diagonal.



Geocoded E-SAR data in UTM, swath = 50km x 3km, flight direction = 100°



Geocoded E-SAR data in UTM, swath = 50km x 3km, flight direction = 225°

For INDREX-II E-SAR has flown data takes of up to 50 km length. A swath has 3 km width as the data are acquired in high-resolution narrow-swath (HR-NS) mode.

Such a huge amount of data per data take causes no problem for data transcription from tape to hard disc as file sizes of more than 4GB or even 8GB are allowed, meanwhile, and the E-SAR data transcription has recently been upgraded in hard- and software in order to adapt to the progress which has been evolved in this sector.

Also, processing of large data takes as one segment can be done for INDREX-II as SAR processing calculates overlapping blocks but writes continuously into one file without overlaps.

However, the problem of *geocoding* large data takes with unfavourable flight directions as *one* segment remains - as the example illustrates. The figure depicts schematic examples of geocoded E-SAR data takes in UTM, size 50 x 3 km, with two different flight directions. A ratio of 50:3 is also used in the figures in order to emphasize the issue. It can be seen that data arrays become large and with lots of invalid points for diagonal flight directions.

Furthermore, data with unfavourable shapes as 50:3 are difficult to depict on screens or on posters for



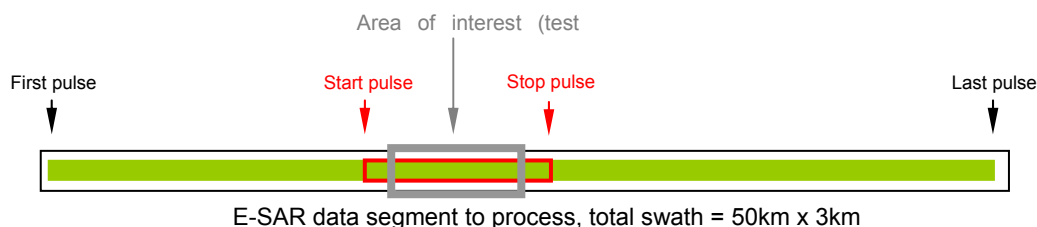
Processed E-SAR data, swath = 50 x 3 km, unfavourable data shape 50:3 for screens / posters

presentation. Smaller data portions are also easier to handle in terms of memory, disk space as well as loading and calculation times.

It is therefore to the favour of the later data evaluation to split large data takes into smaller easy-to-handle segments. The processed image segments should overlap in order to facilitate mosaicking of *geocoded* images in case this is desired.

6.2.4 Segmentation Aspects

Usually, when starting E-SAR processing, the start and stop TRC (Tape Record Counter = pulse number) must be given for processing a tile of data.



So, splitting a data take into segments reduces to determine start/stop TRCs for each data segment. However, several aspects must be considered:

- A constant number of pulses for each segment leads to different length in the geocoded versions due to variable platform velocity.
- Geocoded segments of other data takes (other frequency bands for instance) do badly or even not overlap with corresponding segment of the first data take due to different PRFs, different velocities and different velocity variations.
- Left looking (X-band, C-band, L-band, P-band) and right looking (interferometric X-band) data takes have opposed TRC counting due to opposite flight directions which implies opposite tile numbering and no overlap except in the middle segment compared to left looking scenes.



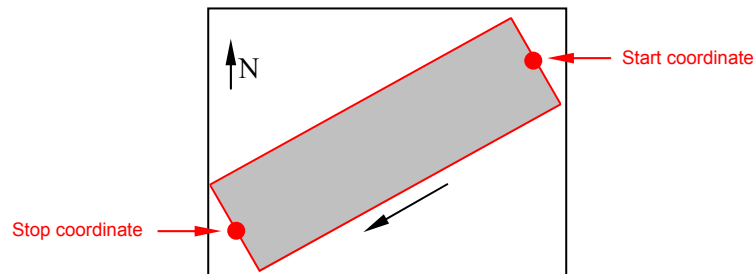
Resulting E-SAR data segmentation with constant number of pulses per data segment

To overcome all these problems, the strategy must be geared towards the geocoded segments:

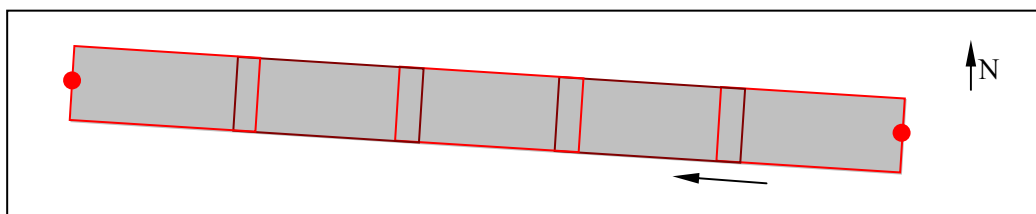
- First a geocoded area of interest must be defined (test site definition).
- The area of interest is segmented if necessary - including overlap for later mosaicking.
- Then each data segment is processed such that the corresponding geocoded area of interest is fully covered.

6.2.5 Test Site Definition and Processing Strategy

Test sites have been defined during E-SAR mission planning prior the campaign via start Longitude/Latitude and stop Longitude/Latitude at mid-range.



Test site definition in WGS84 coordinates via start/stop Longitude/Latitude (area of interest)



Test site segmentation with overlap for later mosaicking

The test site segmentation strategy is as follows:

- For each test site in the campaign we define test site segments if the test site (defined through mission planning) appears to be too long for data handling.
- Test site segments are numbered from 1,...,n according to left-looking scenes for each test site, right-looking scenes are numbered reverse accordingly.

This implies the processing strategy:

- For each data take we process n different overlapping tiles according to the n test sites tiles defined for that test site.
- The processing job for each data segment to process includes the ID number of the test site segment which should be covered (automatically identified through the last digit in the TRY number).
- Test site segment coordinates in UTM are converted into Start/Stop TRCs via lookup tables.
- Start/Stop TRCs are obtained such that they take into account
 - invalid pulses due to half the maximum matched-filter length,
 - invalid pulses due to possible squint and
 - the usual E-SAR processing block size of multiples of 16k pulses.

6.2.6 Other Site Definitions

The strategy explained above has other advantages. It is possible for example to declare other areas than the originally defined test site to an area of interest. These can be:

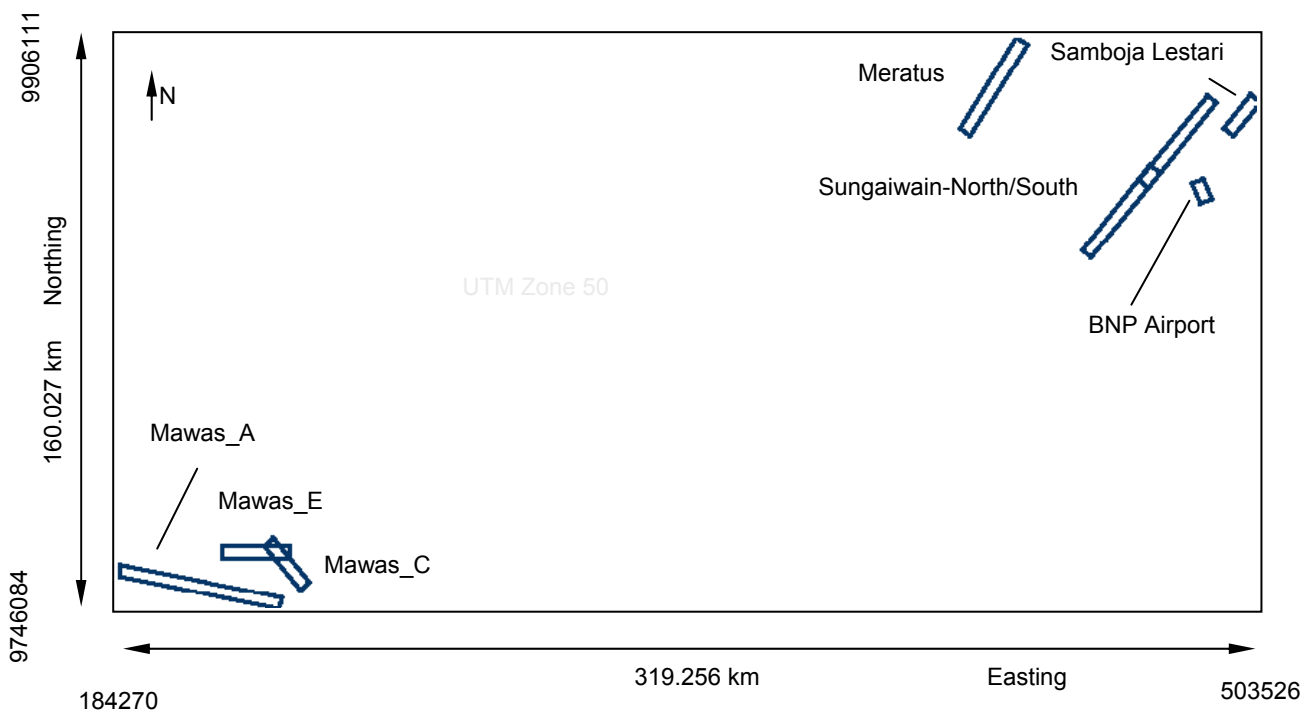
- Calibration sites, i.e. the minimum area where corner reflectors have been installed,
- UTM coordinates of a DEM to be used for terrain correction and geocoding,

- Image corners in UTM coordinates of already processed SAR images,
- Image corners in UTM coordinates of other optical images or
- UTM coordinates read from a map.

A very comfortable feature is that a minimum area covering only the corner reflectors can be processed.

6.2.7 Data Segmentation for INDREX-II

The figure below gives a survey of all acquired data takes in INDREX-II depicted in UTM coordinates.

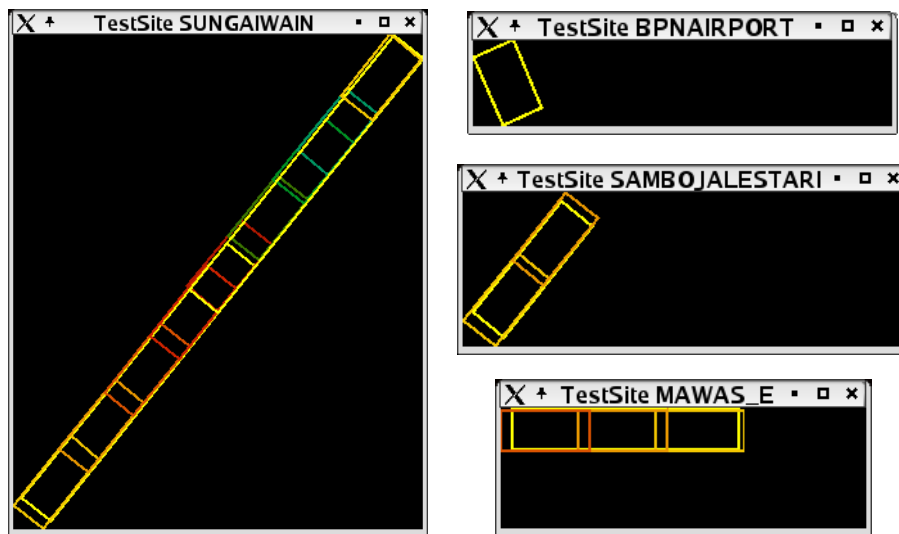


For INDREX-II the following test sites have been covered according to previously acquired data:

- BPN-Airport (calibration site, not segmented),
- Sambojalestari (2 segments),
- Meratus (4 segments),
- Sungaiwain-South (4 segments),
- Sungaiwain-North (5 segments),
- Mawas_A (6 segments),
- Mawas_C (3 segments),
- Mawas_E (3 segments).

Due to reasons given above all test sites except "BPN Airport", which is the calibration site, had to be split. Extreme cases have been "Sungai Wain-South", "Sungai Wain-North", and "Meratus" due to their diagonal flight directions and "MAWAS-A" due to its total length. Additionally, overlap had to be considered for segmentation.

The figure below shows some examples of how defined test sites (yellow) have been split (colored).



Examples of test site segmentations in INDREX-II, no segmentation at BNP-Airport
Yellow: Defined test site through mission planning, **Colored:** Test sites segments

It can be seen that overlaps at Sungai Wain do vary slightly compared to other test site segmentations. This is because we started SAR processing at Sungai Wain when the segmentation software supplement had not been ready developed yet. Splitting here had, therefore, to be done manually and turned out to be time-consuming. This initiated the development of the segmentation tools described in this section.

6.2.8 Summary of Data Delivery

For each segment, data processing is performed using an implementation of the Extended Chirp Scaling Algorithm based on [21]. In addition special care was taken for the implementation of motion compensation in case of repeat-pass interferometric products. In general the compensation corresponds to the three-step strategy described in [20]. The coupling of topography and motion errors (where applicable) is solved via the so called PTA-approach [22] and residual motion errors are compensated using the approach in [23] under consideration of the coregistration method in [24]. However, global 2D (linear) phase errors are not compensated due to the lack of available tie-points. Therefore, DEM-generation from repeat-pass interferometric data products (if intended) will be biased and comparison with DEMs derived from other sources (e.g. single-pass interferometry) must be handled with care.

6.2.9 Test-Site Samboja Lestari

Date of flight: November, 17, 2004.
 Test site dimensions: 3 km x 12 km
 Heading (Track Angle): 39° (219° for X-band)
 Number of segments for processing: 2



6.2.9.1 DEM-Processing

No Radar reflectors were available. The interferometric phase offset was estimated for Segment 1 from GPS-tracks (provided by Wageningen University) by correlating the information with visible roads in the radar image. Interferometric phase offset for segment 2 was estimated via Mosaic Procedure. Expected absolute (horizontal and vertical) accuracy is 5-10m. 2 m grid, reference UTM zone 50 on WGS84 ellipsoid.

Product Name	USB-disc	Remarks
h_geocoded_interp_04indrex0209x1_t01.dat	1	Segment 1: South-west
h_geocoded_interp_04indrex0209x1_t02.dat	1	Segment 2: North-east
h_geocoded_04indrex0209x1_t00_interp.dat	1	Overall DEM (5m posting)

6.2.9.2 Geocoded Image Processing

Segmentation for geocoded products is performed according to segmentation for DEMs (2 segments). DEMs are used for georeferencing (2 m grid). Absolute horizontal position accuracy in the order of 5-10m as no tiepoints available. No radiometric DEM correction of antenna pattern was performed.

Product Name	USB-disc	Remarks
04indrex0201x1_t01	1	L-band (QUAD-POL) – Segment 1

04indrex0201x1_t02	1	L-band (QUAD-POL) – Segment 2
04indrex0205x1_t01	1	P-band (QUAD-POL) – Segment 1, 18°off nadir
04indrex0205x1_t02	1	P-band (QUAD-POL) – Segment 2, 18°off nadir
04indrex1603x1_t01	1	P-band (QUAD-POL) – Segment 1, 18°off nadir 25deg center line for study of inc. angle effects
04indrex1603x1_t02	1	P-band (QUAD-POL) – Segment 2, 18°off nadir 25deg center line for study of inc. angle effects
04indrex0302x1_t01	1	C-band (DUAL-POL, VH-VV) – Segment 1
04indrex0302x1_t02	1	C-band (DUAL-POL, VH-VV) – Segment 2
04indrex0303x1_t01	1	C-band (DUAL-POL, HV-HH) – Segment 1
04indrex0303x1_t02	1 (RGI on 2)	C-band (DUAL-POL, HV-HH) – Segment 2
04indrex0209x1_t11	1	X-band (VV) – Segment 1
04indrex0209x1_t12	1	X-band (VV) – Segment 2

6.2.9.3 Repeat-Pass Interferometric Processing

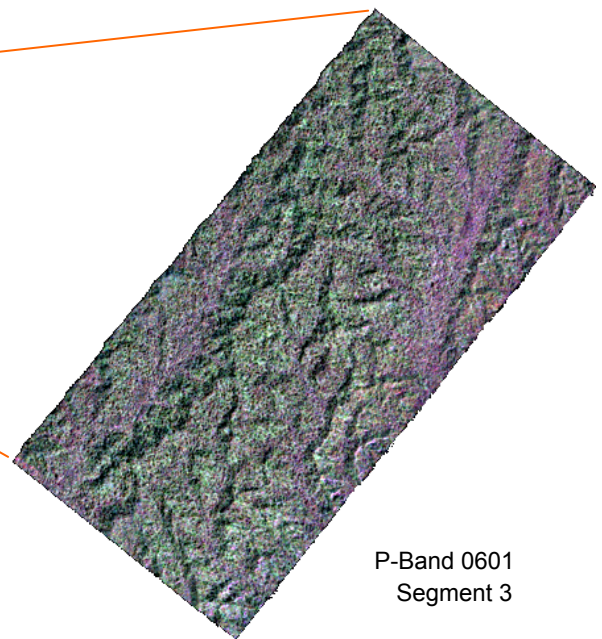
Special Processing:

- L-band: Topographic motion compensation (PTA) & variable Baseline compensation & Radiometric DEM correction of antenna patterns.
- P-band: only variable Baseline compensation

Product Name	USB-disc	Remarks
04indrex0201x1_t01	1	L-band – Segment 1 – MASTER
04indrex0202x1_t01	2	L-band – Segment 1 – 5m Baseline
04indrex0203x1_t01	2	L-band – Segment 1 – 8m Baseline
04indrex0204x1_t01	2	L-band – Segment 1 – 0m Baseline
04indrex0201x1_t02	1	L-band – Segment 2 – MASTER
04indrex0202x1_t02	2	L-band – Segment 2 – 5m Baseline
04indrex0203x1_t02	2	L-band – Segment 2 – 8m Baseline
04indrex0204x1_t02	2	L-band – Segment 2 – 0m Baseline
04indrex0205x1_t11	2	P-band – Segment 1 – MASTER
04indrex0206x1_t11	2	P-band – Segment 1 – 15m Baseline
04indrex0207x1_t11	2	P-band – Segment 1 – 30m Baseline
04indrex0208x1_t11	2	P-band – Segment 1 – 0m Baseline
04indrex0205x1_t12	2	P-band – Segment 2 – MASTER
04indrex0206x1_t12	2	P-band – Segment 2 – 15m Baseline
04indrex0207x1_t12	2	P-band – Segment 2 – 30m Baseline
04indrex0208x1_t12	2	P-band – Segment 2 – 0m Baseline

6.2.10 Sungai Wain (North)

Date of flight: November, 20 and 23 2004
 Test site dimensions: 3 km x 30 km
 Heading (Track Angle): 39° (219° for X-band)
 Number of segments for processing: 5



6.2.10.1 DEM-Processing

Only one radar reflector was positioned in the last segment (segment 5). Interferometric phase offset estimation was based on this tiepoint only. Interferometric phase offset for the other segments via Mosaic Procedure. Linear trend along range possible (baseline tilt could not be calibrated with only one tiepoint). Expected absolute (horizontal and vertical) accuracy is 5-10 m in general, better 1 m close to the Corner reflector. 2 m grid, reference UTM zone 50 on WGS84 ellipsoid.

Product Name	USB disc	Remarks
h_geocoded_interp_04indrex0606x1_t11.dat	1	Segment 5: South-west
h_geocoded_interp_04indrex0606x1_t12.dat	1	Segment 4: middle South-west
h_geocoded_interp_04indrex0606x2_t21.dat	1	Segment 3: middle
h_geocoded_interp_04indrex0606x2_t22.dat	1	Segment 2: middle north-east
h_geocoded_interp_04indrex0606x2_t23.dat	1	Segment 1: north-east
h_geocoded_04indrex0606x0_t00_interp.dat	1	Overall DEM (5m posting)

6.2.10.2 Geocoded Image Processing

Segmentation for geocoded products is performed according to segmentation for DEMs (5 segments). DEMs are used for georeferencing (2 m grid). Absolute horizontal position accuracy in the order of 5-10 m as no tiepoints available (except for segment 5; absolute accuracy better 1m). Radiometric DEM correction of antenna pattern only for C- and L-band.

Product Name	USB disc	Remarks
04indrex0801x1_t11	1 (GTC on 2)	L-band (QUAD-POL) – Segment 1
04indrex0801x1_t12	1 (GTC on 2)	L-band (QUAD-POL) – Segment 2
04indrex0801x2_t21	1 (GTC on 2)	L-band (QUAD-POL) – Segment 3
04indrex0801x2_t22	1 (GTC on 2)	L-band (QUAD-POL) – Segment 4
04indrex0801x2_t23	1 (GTC on 2)	L-band (QUAD-POL) – Segment 5
04indrex0601x1_t01	1	P-band (QUAD-POL) – Segm. 1, 18°off nadir
04indrex0601x1_t02	1	P-band (QUAD-POL) – Segm. 2, 18°off nadir
04indrex0601x2_t03	1	P-band (QUAD-POL) – Segm. 3, 18°off nadir
04indrex0601x2_t04	1	P-band (QUAD-POL) – Segm. 4, 18°off nadir
04indrex0601x2_t05	1	P-band (QUAD-POL) – Segm. 5, 18°off nadir
04indrex1602x1_t01	2	P-band (QUAD-POL) – Segm.1, 18°off nadir 25deg center line for study of inc. angle effects
04indrex1602x1_t02	2	P-band (QUAD-POL) – Segm.2, 18°off nadir 25deg center line for study of inc. angle effects
04indrex1602x1_t03	2	P-band (QUAD-POL) – Segm.3, 18°off nadir 25deg center line for study of inc. angle effects
04indrex1602x2_t04	2	P-band (QUAD-POL) – Segm. 4, 18°off nadir 25deg center line for study of inc. angle effects
04indrex1602x2_t05	2	P-band (QUAD-POL) – Segm. 5, 18°off nadir 25deg center line for study of inc. angle effects
04indrex0805x1_t11	1 (GTC on 2)	C-band (DUAL-POL, HV-HH) – Segment 1
04indrex0805x1_t12	1 (GTC on 2)	C-band (DUAL-POL, HV-HH) – Segment 2
04indrex0805x2_t21	1 (GTC on 2)	C-band (DUAL-POL, HV-HH) – Segment 3
04indrex0805x2_t22	1 (GTC on 2)	C-band (DUAL-POL, HV-HH) – Segment 4
04indrex0805x2_t23	1 (GTC on 2)	C-band (DUAL-POL, HV-HH) – Segment 5
04indrex0806x1_t11	2 (GTC on 1)	C-band (DUAL-POL, VH-VV) – Segment 1
04indrex0806x1_t12	2 (GTC on 1)	C-band (DUAL-POL, VH-VV) – Segment 2
04indrex0806x2_t21	2 (GTC on 1)	C-band (DUAL-POL, VH-VV) – Segment 3
04indrex0806x2_t22	2 (GTC on 1)	C-band (DUAL-POL, VH-VV) – Segment 4
04indrex0806x2_t23	2 (GTC on 1)	C-band (DUAL-POL, VH-VV) – Segment 5
04indrex0606x2_t43	1 (GTC on 2)	X-band (VV) – Segment 1

04indrex0606x2_t42	1 (GTC on 2)	X-band (VV) – Segment 2
04indrex0606x2_t41	1 (GTC on 2)	X-band (VV) – Segment 3
04indrex0606x1_t32	1 (GTC on 2)	X-band (VV) – Segment 4
04indrex0606x1_t31	1 (GTC on 2)	X-band (VV) – Segment 5

6.2.10.3 Repeat-Pass Interferometric Processing

Special Processing:

- L-band: Topographic motion compensation (PTA) & variable Baseline compensation & Radiometric DEM correction of antenna patterns.
- P-band: only variable Baseline compensation; no DEM corrections

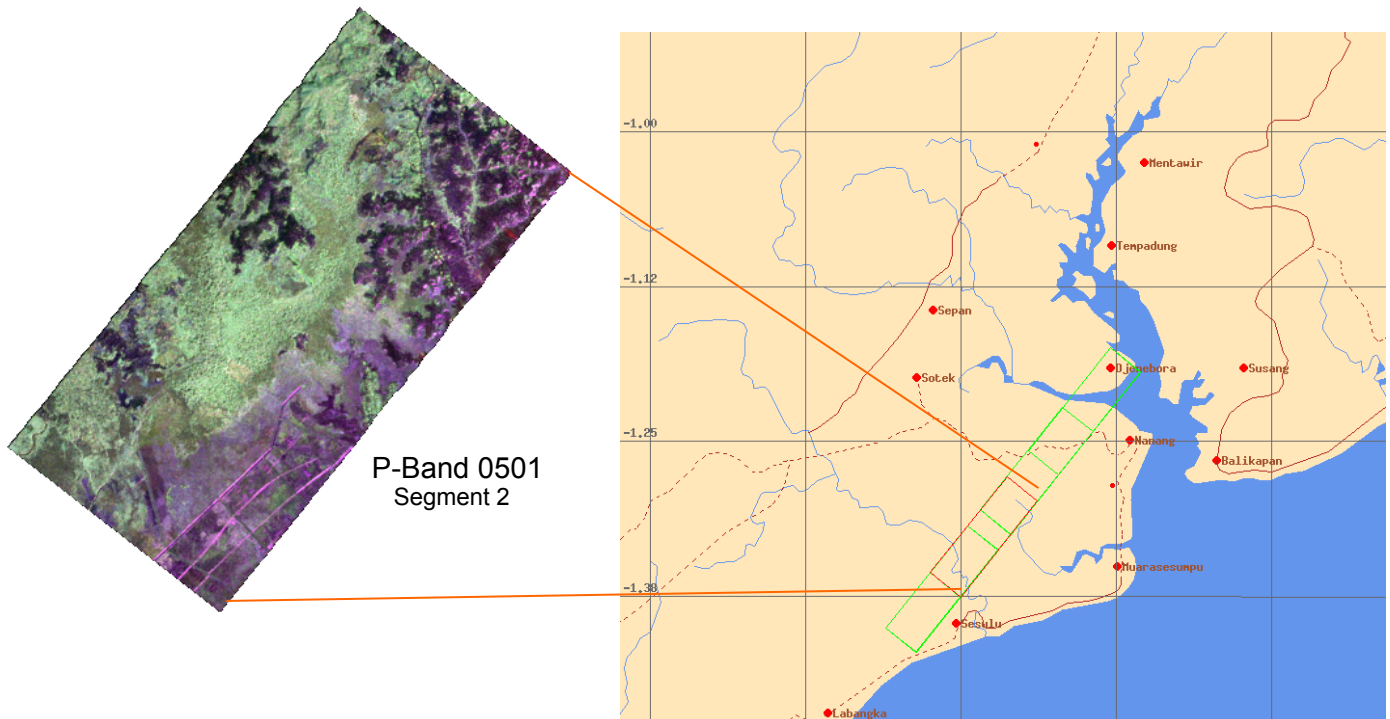
Product Name	USB disc	Remarks
04indrex0801x1_t11	1	L-band – Segment 1 - MASTER
04indrex0802x1_t11	2	L-band – Segment 1 – Baseline 5m
04indrex0803x1_t11	2	L-band – Segment 1 – Baseline 10m
04indrex0804x1_t11	2	L-band – Segment 1 – Baseline 15m
04indrex0801x1_t12	1	L-band – Segment 2 - MASTER
04indrex0802x1_t12	2	L-band – Segment 2 – Baseline 5m
04indrex0803x1_t12	2	L-band – Segment 2 – Baseline 10m
04indrex0804x1_t12	2	L-band – Segment 2 – Baseline 15m
04indrex0801x2_t21	1	L-band – Segment 3 - MASTER
04indrex0802x2_t21	2	L-band – Segment 3 – Baseline 5m
04indrex0803x2_t21	2	L-band – Segment 3 – Baseline 10m
04indrex0804x2_t21	2	L-band – Segment 3 – Baseline 15m
04indrex0801x2_t22	1	L-band – Segment 4 - MASTER
04indrex0802x2_t22	2	L-band – Segment 4 – Baseline 5m
04indrex0803x2_t22	2	L-band – Segment 4 – Baseline 10m
04indrex0804x2_t22	2	L-band – Segment 4 – Baseline 15m
04indrex0801x2_t23	1	L-band – Segment 5 – MASTER
04indrex0802x2_t23	1	L-band – Segment 5 – Baseline 5m (archive retrieval failed; reprocess w/o PTA)
04indrex0803x2_t23	2	L-band – Segment 5 – Baseline 10m
04indrex0804x2_t23	2	L-band – Segment 5 – Baseline 15m
04indrex0601x1_t11	2	P-band – Segment 1 – MASTER
04indrex0602x1_t11	2	P-band – Segment 1 – Baseline 15m
04indrex0603x1_t11	1	P-band – Segment 1 – Baseline 30m



04indrex0604x1_t11	1	P-band – Segment 1 – Baseline 0m
04indrex0605x1_t11	1	P-band – Segment 1 – Baseline 60m
04indrex0601x1_t12	2	P-band – Segment 2 – MASTER
04indrex0602x1_t12	2	P-band – Segment 2 – Baseline 15m
04indrex0603x1_t12	2	P-band – Segment 2 – Baseline 30m
04indrex0604x1_t12	2	P-band – Segment 2 – Baseline 0m
04indrex0605x1_t12	2	P-band – Segment 2 – Baseline 60m
04indrex0601x2_t21	1	P-band – Segment 3 – MASTER
04indrex0602x2_t21	1	P-band – Segment 3 – Baseline 15m
04indrex0603x2_t21	1	P-band – Segment 3 – Baseline 30m
04indrex0604x2_t21	1	P-band – Segment 3 – Baseline 0m
04indrex0605x2_t21	2	P-band – Segment 3 – Baseline 60m
04indrex0601x2_t22	2	P-band – Segment 4 – MASTER
04indrex0602x2_t22	2	P-band – Segment 4 – Baseline 15m
04indrex0603x2_t22	2	P-band – Segment 4 – Baseline 30m
04indrex0604x2_t22	2	P-band – Segment 4 – Baseline 0m
04indrex0605x2_t22	2	P-band – Segment 4 – Baseline 60m
04indrex0601x2_t23	2	P-band – Segment 5 – MASTER
04indrex0602x2_t23	1	P-band – Segment 5 – Baseline 15m
04indrex0603x2_t23	1	P-band – Segment 5 – Baseline 30m
04indrex0604x2_t23	1	P-band – Segment 5 – Baseline 0m
04indrex0605x2_t23	2	P-band – Segment 5 – Baseline 60m

6.2.11 Sungai Wain (South)

Date of flight: November, 18 2004
 Test site dimensions: 3 km x 25 km
 Heading (Track Angle): 39° (219° for X-band)
 Number of segments for processing: 4



6.2.11.1 DEM-Processing

Only one radar reflector was positioned in the last segment (segment 5) of SUNGAI-WAIN NORTH. Interferometric phase offset is found by Mosaic Procedure from continuation of Sungai Wain North scene (04indrex0606x1) towards south-west. Linear trend along range possible (baseline tilt could not be calibrated with only one tiepoint). Expected absolute (horizontal and vertical) accuracy is 5-10 m. 2 m grid, reference UTM zone 50 on WGS84 ellipsoid.

Product Name	USB disc	Remarks
h_geocoded_interp_04indrex0406x2_t01.dat	1	Segment 1: north-east
h_geocoded_interp_04indrex0406x2_t02.dat	1	Segment 2: middle north-east
h_geocoded_interp_04indrex0406x2_t03.dat	1	Segment 3: middle south-west
h_geocoded_interp_04indrex0406x1_t04.dat	1	Segment 4: south-west
h_geocoded_04indrex0400x1_t00_interp.dat	1	Overall DEM (5m posting)

6.2.11.2 Geocoded Image Processing

Segmentation for geocoded products is performed according to segmentation for DEMs (4 segments). DEMs are used for georeferencing (2 m grid). Absolute horizontal position accuracy is in the order of 5-10 m as no tiepoints are available. Radiometric DEM correction of antenna pattern has been only done for X-, C- and L-band.

Product Name	USB disc	Remarks
04indrex0401x1_t01	1	L-band (QUAD-POL) – Segment 1
04indrex0401x1_t02	1	L-band (QUAD-POL) – Segment 2
04indrex0401x2_t03	1	L-band (QUAD-POL) – Segment 3
04indrex0401x2_t04	1	L-band (QUAD-POL) – Segment 4
04indrex0501x1_t01	GTC on 2	P-band (QUAD-POL) – Segm. 1, 18° off nadir
04indrex0501x1_t02	GTC on 2	P-band (QUAD-POL) – Segm. 2, 18° off nadir
04indrex0501x2_t03	GTC on 2	P-band (QUAD-POL) – Segm. 3, 18° off nadir
04indrex0501x2_t04	GTC on 2	P-band (QUAD-POL) – Segm. 4, 18° off nadir
04indrex0501x1_t11	RGI on 1	P-band (QUAD-POL) – Segm. 1, 25° off nadir
04indrex0501x1_t12	RGI on 1	P-band (QUAD-POL) – Segm. 2, 25° off nadir
04indrex0501x2_t13	RGI on 1	P-band (QUAD-POL) – Segm. 3, 25° off nadir
04indrex0501x2_t14	RGI on 1	P-band (QUAD-POL) – Segm. 4, 25° off nadir
04indrex0505x1_t01	1 (GTC on 2)	C-band (DUAL-POL, VH-VV) – Segment 1
04indrex0505x1_t02	1 (GTC on 2)	C-band (DUAL-POL, VH-VV) – Segment 2
04indrex0505x2_t03	1 (GTC on 2)	C-band (DUAL-POL, VH-VV) – Segment 3
04indrex0505x2_t04	1 (GTC on 2)	C-band (DUAL-POL, VH-VV) – Segment 4
04indrex0506x1_t01	1	C-band (DUAL-POL, HV-HH) – Segment 1
04indrex0506x1_t02	1	C-band (DUAL-POL, HV-HH) – Segment 2
04indrex0506x2_t03	1	C-band (DUAL-POL, HV-HH) – Segment 3
04indrex0506x2_t04	1	C-band (DUAL-POL, HV-HH) – Segment 4
04indrex0406x2_t11	1 (GTC on 2)	X-band (VV) – Segment 1
04indrex0406x2_t12	1 (GTC on 2)	X-band (VV) – Segment 2
04indrex0406x2_t13	2	X-band (VV) – Segment 3
04indrex0406x1_t14	1 (GTC on 2)	X-band (VV) – Segment 4

6.2.11.3 Repeat-Pass Interferometric Processing

Special Processing:

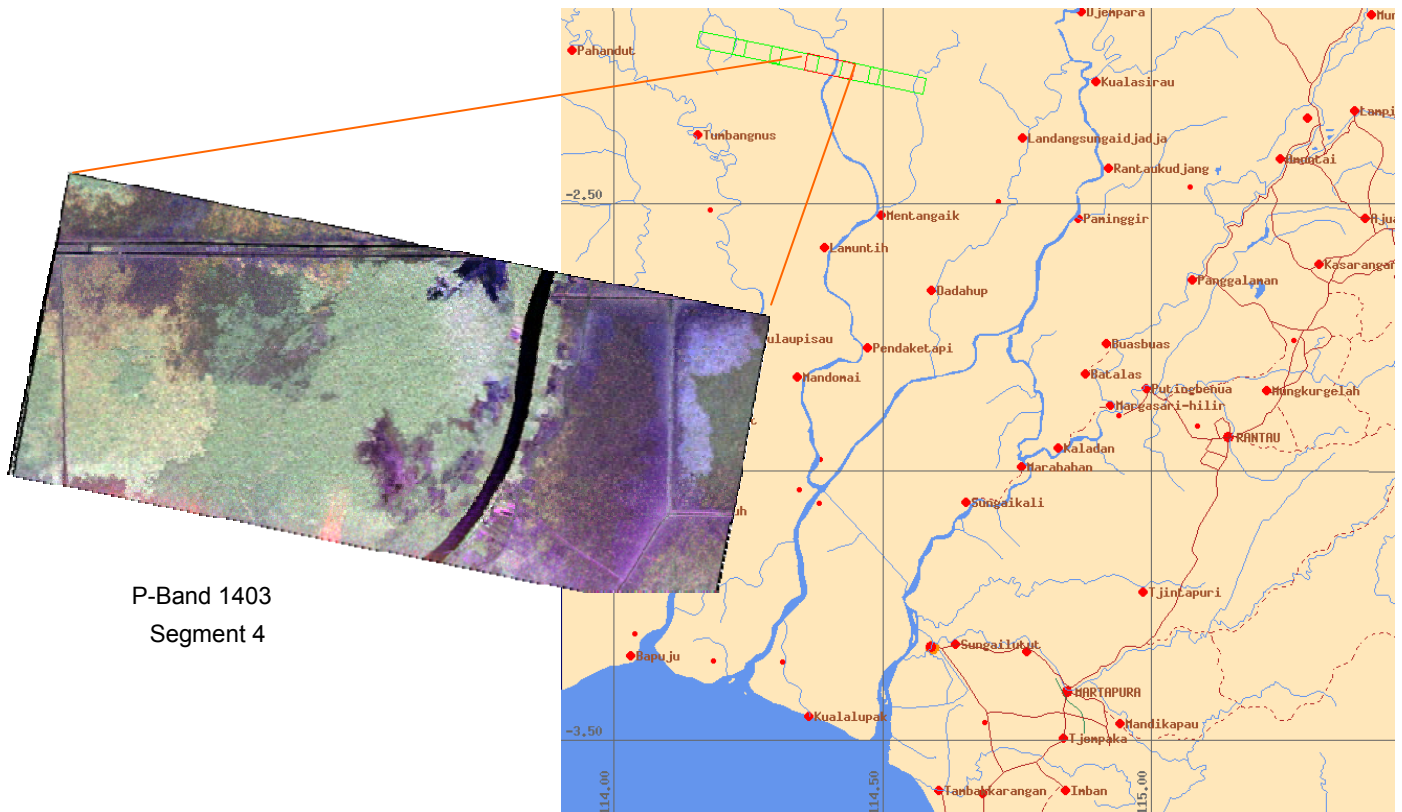
- L-band: Topographic motion compensation (PTA) & variable Baseline compensation & Radiometric DEM correction of antenna patterns.

- P-band: only variable Baseline compensation; no DEM corrections

Product Name	USB disc	Remarks
04indrex0401x1_t01	1	L-band – Segment 1 - MASTER
04indrex0402x1_t01	1	L-band – Segment 1 – Baseline 5m
04indrex0403x1_t01	1	L-band – Segment 1 – Baseline 8m
04indrex0404x1_t01	1	L-band – Segment 1 – Baseline 0m
04indrex0401x1_t02	1	L-band – Segment 2 – MASTER
04indrex0402x1_t02	1	L-band – Segment 2 – Baseline 5m
04indrex0403x1_t02	1	L-band – Segment 2 – Baseline 8m
04indrex0404x1_t02	1	L-band – Segment 2 – Baseline 0m
04indrex0401x2_t03	1	L-band – Segment 3 – MASTER
04indrex0402x2_t03	1	L-band – Segment 3 – Baseline 5m
04indrex0403x2_t03	1	L-band – Segment 3 – Baseline 8m
04indrex0404x2_t03	1	L-band – Segment 3 – Baseline 0m
04indrex0401x2_t04	1	L-band – Segment 4 – MASTER
04indrex0402x2_t04	1	L-band – Segment 4 – Baseline 5m
04indrex0403x2_t04	1	L-band – Segment 4 – Baseline 8m
04indrex0404x2_t04	1	L-band – Segment 4 – Baseline 0m
04indrex0501x1_t11	2	P-band – Segment 1 – MASTER
04indrex0502x1_t11	1	P-band – Segment 1 – Baseline 15m
04indrex0503x1_t11	1	P-band – Segment 1 – Baseline 30m
04indrex0504x1_t11	1	P-band – Segment 1 – Baseline 0m
04indrex0501x1_t12	1	P-band – Segment 2 – MASTER
04indrex0502x1_t12	1	P-band – Segment 2 – Baseline 15m
04indrex0503x1_t12	1	P-band – Segment 2 – Baseline 30m
04indrex0504x1_t12	1	P-band – Segment 2 – Baseline 0m
04indrex0501x2_t13	1	P-band – Segment 3 – MASTER
04indrex0502x2_t13	1	P-band – Segment 3 – Baseline 15m
04indrex0503x2_t13	1	P-band – Segment 3 – Baseline 30m
04indrex0504x2_t13	1	P-band – Segment 3 – Baseline 0m
04indrex0501x2_t14	1	P-band – Segment 4 – MASTER
04indrex0502x2_t14	1	P-band – Segment 4 – Baseline 15m
04indrex0503x2_t14	1	P-band – Segment 4 – Baseline 30m
04indrex0504x2_t14	1	P-band – Segment 4 – Baseline 0m

6.2.12 Mawas-A

Date of flight: November, 27 and 30 2004
 Test site dimensions: 3 km x 40 km
 Heading (Track Angle): 102° (282° for X-band)
 Number of segments for processing: 6



P-Band 1403
Segment 4

6.2.12.1 DEM-Processing

No tiepoints were available for this test site. Interferometric phase offset estimation was based on artificial tiepoints assuming perfectly flat area of constant topographic height at 10m MSL in segment 4. Mosaic procedure was used to obtain smooth conditions at segment boundaries. As weather conditions started to become turbulent, segments 1 and 3 of track 1109 could not be processed. For segment 3 backup track (1213) from next day was successful. Expected absolute (horizontal and vertical) accuracy is 5-10 m. 2 m grid, reference UTM zone 50 on WGS84 ellipsoid.

Product Name	USB-disc	Remarks
Not available	NA	Segment 1
h_geocoded_interp_04indrex1109x2_t02.dat	1	Segment 2
h_geocoded_interp_04indrex1213x2_t03.dat	1	Segment 3
h_geocoded_interp_04indrex1109x2_t04.dat	1	Segment 4
h_geocoded_interp_04indrex1109x1_t05.dat	1	Segment 5
h_geocoded_interp_04indrex1109x1_t06.dat	1	Segment 6
h_geocoded_04indrex1109x1_t00_interp.dat	1	Overall DEM (5m posting)

6.2.12.2 Geocoded Image Processing

Because MAWAS area is extremely flat, geocoding was performed without consideration of DEM information. Also radiometric DEM correction of antenna pattern is not required.

Product Name	USB disc	Remarks
04indrex1203x1_t01	1	L-band (QUAD-POL) – Segment 1
04indrex1203x1_t02	1	L-band (QUAD-POL) – Segment 2
04indrex1203x2_t03	1	L-band (QUAD-POL) – Segment 3
04indrex1203x2_t04	1	L-band (QUAD-POL) – Segment 4
04indrex1203x2_t05	1	L-band (QUAD-POL) – Segment 5
04indrex1203x3_t06	1	L-band (QUAD-POL) – Segment 6
04indrex1403x1_t11	2	P-band (QUAD-POL) – Segm. 1, 18°off nadir
04indrex1403x1_t12	2	P-band (QUAD-POL) – Segm. 2, 18°off nadir
04indrex1403x1_t13	2	P-band (QUAD-POL) – Segm. 3, 18°off nadir
04indrex1403x2_t14	2	P-band (QUAD-POL) – Segm. 4, 18°off nadir
04indrex1403x2_t15	2	P-band (QUAD-POL) – Segm. 5, 18°off nadir
04indrex1403x2_t16	2	P-band (QUAD-POL) – Segm. 6, 18°off nadir
04indrex1101x1_t01	1	C-band (DUAL-POL, VH-VV) – Segment 1
04indrex1101x1_t02	1	C-band (DUAL-POL, VH-VV) – Segment 2
04indrex1101x2_t03	1	C-band (DUAL-POL, VH-VV) – Segment 3
04indrex1101x2_t04	1	C-band (DUAL-POL, VH-VV) – Segment 4
04indrex1101x2_t05	1	C-band (DUAL-POL, VH-VV) – Segment 5
04indrex1101x3_t06	1	C-band (DUAL-POL, VH-VV) – Segment 6
04indrex1104x1_t01	1	C-band (DUAL-POL, HV-HH) – Segment 1
04indrex1104x1_t02	1	C-band (DUAL-POL, HV-HH) – Segment 2
04indrex1104x2_t03	1	C-band (DUAL-POL, HV-HH) – Segment 3
04indrex1104x2_t04	1	C-band (DUAL-POL, HV-HH) – Segment 4
04indrex1104x2_t05	1	C-band (DUAL-POL, HV-HH) – Segment 5
04indrex1104x3_t06	1	C-band (DUAL-POL, HV-HH) – Segment 6
04indrex1213x3_t11	1	X-band (VV) – Segment 1
04indrex1213x3_t12	1	X-band (VV) – Segment 2
04indrex1213x2_t13	1	X-band (VV) – Segment 3
04indrex1213x2_t14	1	X-band (VV) – Segment 4
04indrex1213x1_t15	1	X-band (VV) – Segment 5
04indrex1213x1_t16	1	X-band (VV) – Segment 6

6.2.12.3 Repeat-Pass Interferometric Processing

Because MAWAS area is extremely flat topographic motion compensation and radiometric DEM correction of antenna pattern is not required. Only variable baseline compensation has been performed.

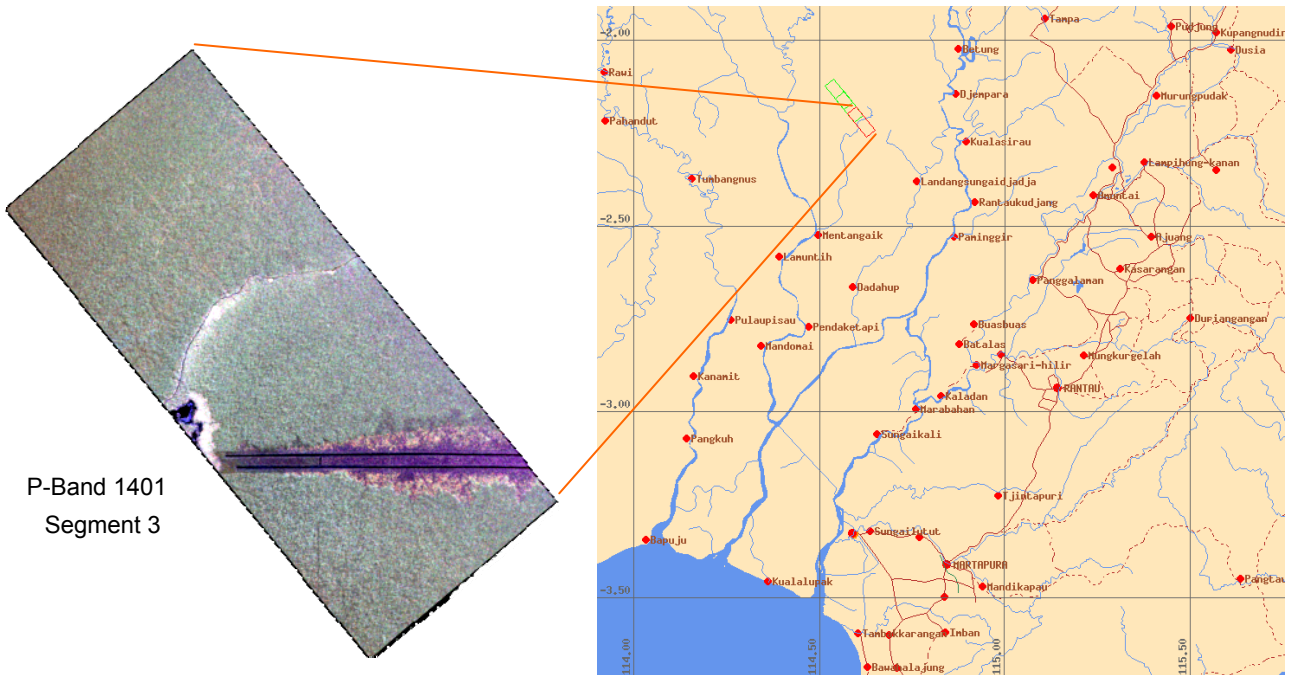
Product Name	USB disc	Remarks
04indrex1203x1_t01	1	L-band – Segment 1 – MASTER
04indrex1206x1_t01	1	L-band – Segment 1 – Baseline 5m
04indrex1209x1_t01	1	L-band – Segment 1 – Baseline 15m
04indrex1212x1_t01	1	L-band – Segment 1 – Baseline 8m
04indrex1203x1_t02	1	L-band – Segment 2 – MASTER
04indrex1206x1_t02	1	L-band – Segment 2 – Baseline 5m
04indrex1209x1_t02	1	L-band – Segment 2 – Baseline 15m
04indrex1212x1_t02	1	L-band – Segment 2 – Baseline 8m
04indrex1203x2_t03	1	L-band – Segment 3 – MASTER
04indrex1206x2_t03	1	L-band – Segment 3 – Baseline 5m
04indrex1209x2_t03	1	L-band – Segment 3 – Baseline 15m
04indrex1212x2_t03	1	L-band – Segment 3 – Baseline 8m
04indrex1203x2_t04	1	L-band – Segment 4 – MASTER
04indrex1206x2_t04	1	L-band – Segment 4 – Baseline 5m
04indrex1209x2_t04	1	L-band – Segment 4 – Baseline 15m
04indrex1212x2_t04	1	L-band – Segment 4 – Baseline 8m
04indrex1203x2_t05	1	L-band – Segment 5 – MASTER
04indrex1206x2_t05	1	L-band – Segment 5 – Baseline 5m
04indrex1209x2_t05	1	L-band – Segment 5 – Baseline 15m
04indrex1212x2_t05	1	L-band – Segment 5 – Baseline 8m
04indrex1203x3_t06	1	L-band – Segment 6 – MASTER
04indrex1206x3_t06	1	L-band – Segment 6 – Baseline 5m
04indrex1209x3_t06	1	L-band – Segment 6 – Baseline 15m
04indrex1212x3_t06	1	L-band – Segment 6 – Baseline 8m
04indrex1403x1_t01	1	P-band – Segment 1 – MASTER
04indrex1406x1_t01	1	P-band – Segment 1 – Baseline 15m
04indrex1409x1_t01	1	P-band – Segment 1 – Baseline 30m
04indrex1403x2_t02	1	P-band – Segment 2 – MASTER
04indrex1406x1_t02	1	P-band – Segment 2 – Baseline 15m
04indrex1409x1_t02	1	P-band – Segment 2 – Baseline 30m
04indrex1403x1_t03	1	P-band – Segment 3 – MASTER



04indrex1406x1_t03	1	P-band – Segment 3 – Baseline 15m
04indrex1409x1_t03	1	P-band – Segment 3 – Baseline 30m
04indrex1403x2_t04	1	P-band – Segment 4 – MASTER
04indrex1406x2_t04	1	P-band – Segment 4 – Baseline 15m
04indrex1409x2_t04	1	P-band – Segment 4 – Baseline 30m
04indrex1403x2_t05	1	P-band – Segment 5 – MASTER
04indrex1406x2_t05	1	P-band – Segment 5 – Baseline 15m
04indrex1409x2_t05	1	P-band – Segment 5 – Baseline 30m
04indrex1403x2_t06	1	P-band – Segment 6 – MASTER
04indrex1406x2_t06	1	P-band – Segment 6 – Baseline 15m
04indrex1409x2_t06	1	P-band – Segment 6 – Baseline 30m

6.2.13 Mawas-C

Date of flight: November, 27 and 30 2004
 Test site dimensions: 3 km x 15 km
 Heading (Track Angle): 321° (141° for X-band)
 Number of segments for processing: 3



6.2.13.1 DEM-Processing

No tiepoints were available for this test site. Interferometric phase offset estimation was based on artificial tiepoints assuming perfectly flat area of constant topographic height at 7m MSL in segment 1. Mosaic procedure was used to obtain smooth conditions at segment boundaries. Expected absolute (horizontal and vertical) accuracy is 5-10 m. 2 m grid, reference UTM zone 50 on WGS84 ellipsoid.

Product Name	USB disc	Remarks
h_geocoded_interp_04indrex1108x1_t01.dat	1	Segment 1
h_geocoded_interp_04indrex1108x1_t02.dat	1	Segment 2
h_geocoded_interp_04indrex1108x1_t03.dat	1	Segment 3
h_geocoded_04indrex1108x1_t00_interp.dat	1	Overall DEM (5m posting)

6.2.13.2 Geocoded Image Processing

Because MAWAS area is extremely flat, geocoding was performed without consideration of DEM information. Also radiometric DEM correction of antenna pattern is not required.

Product Name	USB disc	Remarks
04indrex1301x1_t01	1	L-band (QUAD-POL) – Segment 1
04indrex1301x1_t02	1	L-band (QUAD-POL) – Segment 2
04indrex1301x1_t03	1	L-band (QUAD-POL) – Segment 3
04indrex1401x1_t11	2	P-band (QUAD-POL) – Segm. 1, 18°off nadir
04indrex1401x1_t12	2	P-band (QUAD-POL) – Segm. 2, 18°off nadir
04indrex1401x1_t13	2	P-band (QUAD-POL) – Segm. 3, 18°off nadir
04indrex1102x1_t01	1	C-band (DUAL-POL, VH-VV) – Segment 1
04indrex1102x1_t02	1	C-band (DUAL-POL, VH-VV) – Segment 2
04indrex1102x1_t03	1	C-band (DUAL-POL, VH-VV) – Segment 3
04indrex1105x1_t01	1	C-band (DUAL-POL, HV-HH) – Segment 1
04indrex1105x1_t02	1	C-band (DUAL-POL, HV-HH) – Segment 2
04indrex1105x1_t03	1	C-band (DUAL-POL, HV-HH) – Segment 3
04indrex1108x1_t11	1	X-band (VV) – Segment 3
04indrex1108x1_t12	1	X-band (VV) – Segment 2
04indrex1108x1_t13	1	X-band (VV) – Segment 1

6.2.13.3 Repeat-Pass Interferometric Processing

Because MAWAS area is extremely flat topographic motion compensation and radiometric DEM correction of antenna pattern is not required. Only variable baseline compensation has been performed.

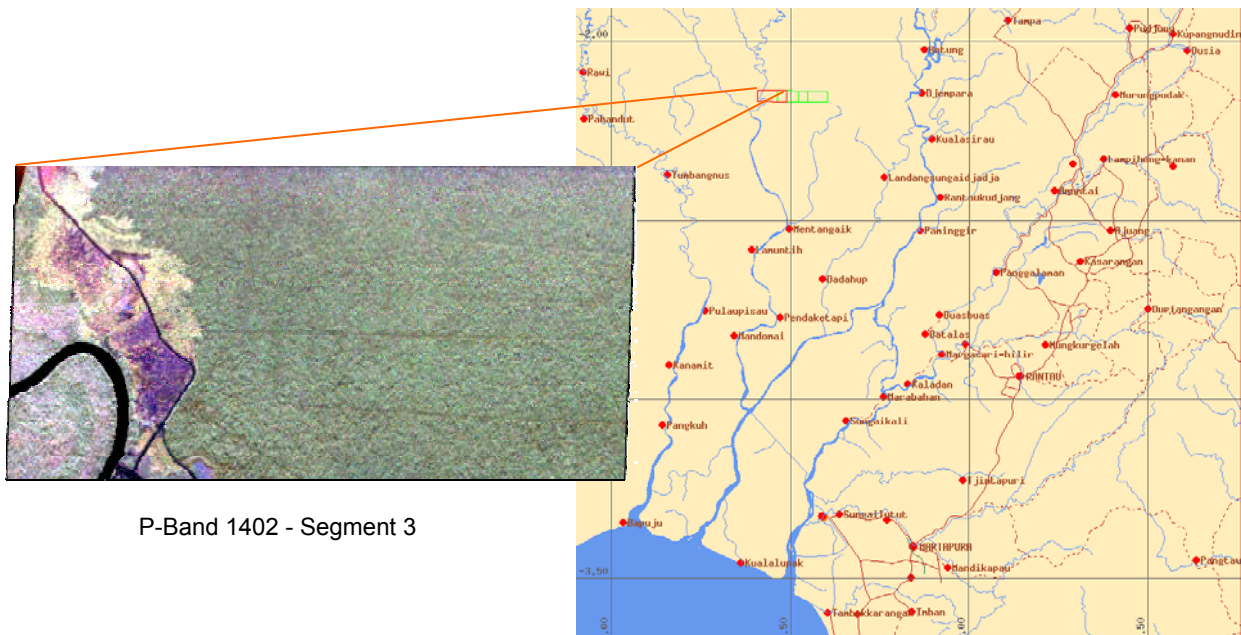
Product Name	USB-disc	Remarks
04indrex1301x1_t01	1	L-band – Segment 1 – MASTER
04indrex1304x1_t01	2	L-band – Segment 1 – Baseline 5m
04indrex1307x1_t01	2	L-band – Segment 1 – Baseline 15m
04indrex1301x2_t02	1	L-band – Segment 2 – MASTER
04indrex1304x1_t02	2	L-band – Segment 2 – Baseline 5m (archive retrieval failed; reprocessed)
04indrex1307x1_t02	2	L-band – Segment 2 – Baseline 15m
04indrex1301x1_t03	1	L-band – Segment 3 – MASTER
04indrex1304x1_t03	2	L-band – Segment 3 – Baseline 5m (archive retrieval failed; reprocessed)
04indrex1307x1_t03	2	L-band – Segment 3 – Baseline 15m
04indrex1401x1_t01	1	P-band – Segment 1 – MASTER
04indrex1404x1_t01	2	P-band – Segment 1 – Baseline 15m



04indrex1407x1_t01	2	P-band – Segment 1 – Baseline 30m (archive retrieval failed; reprocessed without variable baseline compensation)
04indrex1410x1_t01	2	P-band – Segment 1 – Baseline 40m
04indrex1401x2_t02	1	P-band – Segment 2 – MASTER
04indrex1404x1_t02	2	P-band – Segment 2 – Baseline 15m
04indrex1407x1_t02	2	P-band – Segment 2 – Baseline 30m
04indrex1410x1_t02	2	P-band – Segment 1 – Baseline 40m
04indrex1401x1_t03	1	P-band – Segment 3 – MASTER
04indrex1404x1_t03	2	P-band – Segment 3 – Baseline 15m
04indrex1407x1_t03	2	P-band – Segment 3 – Baseline 30m
04indrex1410x1_t03	2	P-band – Segment 3 – Baseline 40m

6.2.14 Mawas-E

Date of flight: November, 27 to 30 2004
 Test site dimensions: 3 km x 15 km
 Heading (Track Angle): 270° (90° for X-band)
 Number of segments for processing: 3



P-Band 1402 - Segment 3

6.2.14.1 DEM-Processing

No tiepoints were available for this test site. Interferometric phase offset estimation was based on artificial tiepoints assuming perfectly flat area of constant topographic height at 6m MSL in segment 3. Mosaic procedure was used to obtain smooth conditions at segment boundaries. Expected absolute (horizontal and vertical) accuracy is 5-10 m. 2 m grid, reference UTM zone 50 on WGS84 ellipsoid.

Product Name	USB disc	Remarks
h_geocoded_interp_04indrex1107x1_t01.dat	1	Segment 1
h_geocoded_interp_04indrex1107x1_t02.dat	1	Segment 2
h_geocoded_interp_04indrex1107x1_t03.dat	1	Segment 3
h_geocoded_04indrex1107x1_t00_interp.dat	1	Overall DEM (5m posting)

6.2.14.2 Geocoded Image Processing

Because MAWAS area is extremely flat, geocoding was performed without consideration of DEM information. Also radiometric DEM correction of antenna pattern is not required.

Product Name	USB disc	Remarks
04indrex1302x1_t01	1	L-band (QUAD-POL) – Segment 1
04indrex1302x1_t02	1	L-band (QUAD-POL) – Segment 2
04indrex1302x1_t03	1	L-band (QUAD-POL) – Segment 3
04indrex1402x1_t11	2	P-band (QUAD-POL) – Segm. 1, 18°off nadir
04indrex1402x1_t12	2	P-band (QUAD-POL) – Segm. 2, 18°off nadir
04indrex1402x1_t13	2	P-band (QUAD-POL) – Segm. 3, 18°off nadir
04indrex1103x1_t01	1	C-band (DUAL-POL, VH-VV) – Segment 1
04indrex1103x1_t02	1	C-band (DUAL-POL, VH-VV) – Segment 2
04indrex1103x1_t03	1	C-band (DUAL-POL, VH-VV) – Segment 3
04indrex1106x1_t01	1	C-band (DUAL-POL, HV-HH) – Segment 1
04indrex1106x1_t02	1	C-band (DUAL-POL, HV-HH) – Segment 2
04indrex1106x1_t03	1	C-band (DUAL-POL, HV-HH) – Segment 3
04indrex1107x1_t11	1 (GTC on 2)	X-band (VV) – Segment 1
04indrex1107x1_t12	1 (GTC on 2)	X-band (VV) – Segment 2
04indrex1107x1_t13	1 (GTC on 2)	X-band (VV) – Segment 3

6.2.14.3 Repeat-Pass Interferometric Processing

Because MAWAS area is extremely flat topographic motion compensation and radiometric DEM correction of antenna pattern is not required. Only variable baseline compensation has been performed.

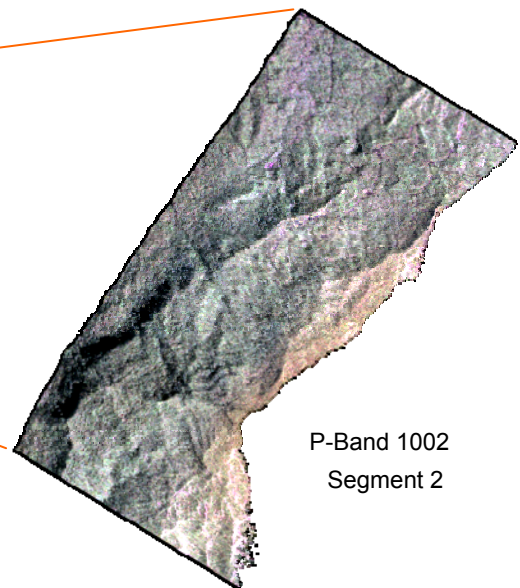
Product Name	USB disc	Remarks
04indrex1302x1_t01	1	L-band – Segment 1 – MASTER
04indrex1305x1_t01	2	L-band – Segment 1 – Baseline 5m
04indrex1308x1_t01	2	L-band – Segment 1 – Baseline 15m
04indrex1302x2_t02	1	L-band – Segment 2 – MASTER
04indrex1305x1_t02	2	L-band – Segment 2 – Baseline 5m
04indrex1308x1_t02	2	L-band – Segment 2 – Baseline 15m
04indrex1302x1_t03	1	L-band – Segment 3 – MASTER
04indrex1305x1_t03	2	L-band – Segment 3 – Baseline 5m
04indrex1308x1_t03	2	L-band – Segment 3 – Baseline 15m
04indrex1402x1_t01	1	P-band – Segment 1 – MASTER
04indrex1405x1_t01	2	P-band – Segment 1 – Baseline 15m
04indrex1408x1_t01	2	P-band – Segment 1 – Baseline 30m
04indrex1411x1_t01	2	P-band – Segment 1 – Baseline 40m



04indrex1402x2_t02	1	P-band – Segment 2 – MASTER
04indrex1405x1_t02	2	P-band – Segment 2 – Baseline 15m
04indrex1408x1_t02	2	P-band – Segment 2 – Baseline 30m
04indrex1411x1_t02	2	P-band – Segment 1 – Baseline 40m
04indrex1402x1_t03	1	P-band – Segment 3 – MASTER
04indrex1405x1_t03	2	P-band – Segment 3 – Baseline 15m
04indrex1408x1_t03	2	P-band – Segment 3 – Baseline 30m
04indrex1411x1_t03	2	P-band – Segment 3 – Baseline 40m

6.2.15 Meratus

Date of flight: November, 24 and December, 5 2004
 Test site dimensions: 3 km x 30 km
 Heading (Track Angle): 32° (212° for X-band)
 Number of segments for processing: 4



P-Band 1002
Segment 2

6.2.15.1 DEM-Processing

As Meratus test-site is a mountaneous area, interferometric X-band acquisition was performed from opposite look directions to avoid excessive shadow and layover areas. The mosaic procedure was used to obtain DEMs for the 4 sections. Interferometric phase offset was estimated from the only known elevation point on top of the mountain (i.e. 1230 m MSL). Total height variations in this test site are about 1000 m. Expected absolute (horizontal and vertical) accuracy is 5-10 m. 2 m grid, reference UTM zone 50 on WGS84 ellipsoid.

Product Name	USB disc	Remarks
h_geocoded_04indrex1000x1_t01_interp.dat	1	Segment 1
h_geocoded_04indrex1000x1_t02_interp.dat	1	Segment 2
h_geocoded_04indrex1000x1_t03_interp.dat	1	Segment 3
h_geocoded_04indrex1000x1_t04_interp.dat	1	Segment 4
h_geocoded_04indrex1000x1_t00_interp.dat	1	Overall DEM (5m posting)

6.2.15.2 Geocoded Image Processing

For geocoded terrain correction, the DEMs computed for the 4 segments were used. Radiometric DEM correction of antenna patterns is performed for all frequency bands. Without tiepoints, the expected absolute horizontal accuracy is in the order of 5-10 m.

Product Name	USB disc	Remarks
04indrex1001x1_t01	2	L-band (QUAD-POL) – Segment 1
04indrex1001x1_t02	2	L-band (QUAD-POL) – Segment 2
04indrex1001x2_t03	2	L-band (QUAD-POL) – Segment 3
04indrex1001x2_t04	2	L-band (QUAD-POL) – Segment 4
04indrex1002x1_t11	2	P-band (QUAD-POL) – Segm. 1, 18° off nadir
04indrex1002x1_t12	2	P-band (QUAD-POL) – Segm. 2, 18° off nadir
04indrex1002x2_t13	2	P-band (QUAD-POL) – Segm. 3, 18° off nadir
04indrex1002x2_t14	2	P-band (QUAD-POL) – Segm. 4, 18° off nadir
Not acquired	NA	C-band
04indrex1005x1_t11	2	X-band (VV) – Segment 1
04indrex1005x1_t12	2	X-band (VV) – Segment 2
04indrex1005x2_t13	2	X-band (VV) – Segment 3
04indrex1005x2_t14	2	X-band (VV) – Segment 4

6.2.15.3 Repeat-Pass Interferometric Processing

Special Processing for L- and P-band:

- Topographic motion compensation (PTA) &
- variable Baseline compensation &
- Radiometric DEM correction of antenna patterns.

Product Name	USB disc	Remarks
04indrex1501x1_t01	1	L-band – Segment 1 – MASTER
04indrex1502x1_t01	1	L-band – Segment 1 – Baseline 5m
04indrex1503x1_t01	1	L-band – Segment 1 – Baseline 10m
04indrex1504x1_t01	1	L-band – Segment 1 – Baseline 15m
04indrex1505x1_t01	1	L-band – Segment 1 – Baseline 5m
04indrex1501x1_t01	1	L-band – Segment 2 – MASTER
04indrex1502x1_t02	1	L-band – Segment 2 – Baseline 5m
04indrex1503x1_t02	1	L-band – Segment 2 – Baseline 10m
04indrex1504x1_t02	1	L-band – Segment 2 – Baseline 15m

04indrex1505x1_t02	1	L-band – Segment 2 – Baseline 5m
04indrex1501x2_t03	1	L-band – Segment 3 – MASTER
04indrex1502x2_t03	1	L-band – Segment 3 – Baseline 5m
04indrex1503x2_t03	1	L-band – Segment 3 – Baseline 10m
04indrex1504x2_t03	1	L-band – Segment 3 – Baseline 15m
04indrex1505x2_t03	1	L-band – Segment 3 – Baseline 5m
04indrex1501x2_t04	1	L-band – Segment 4 – MASTER
04indrex1502x2_t04	1	L-band – Segment 4 – Baseline 5m
04indrex1503x2_t04	1	L-band – Segment 4 – Baseline 10m
04indrex1504x2_t04	1	L-band – Segment 4 – Baseline 15m
04indrex1505x2_t04	1	L-band – Segment 4 – Baseline 5m
04indrex1002x1_t01	1	P-band – Segment 1 – MASTER
04indrex1003x1_t01	1	P-band – Segment 1 – Baseline 15m
04indrex1004x1_t01	1	P-band – Segment 1 – Baseline 30m
04indrex1002x1_t02	1	P-band – Segment 2 – MASTER
04indrex1003x1_t02	1	P-band – Segment 2 – Baseline 15m
04indrex1004x1_t02	1	P-band – Segment 2 – Baseline 30m
04indrex1002x2_t03	1	P-band – Segment 3 – MASTER
04indrex1003x2_t03	1	P-band – Segment 3 – Baseline 15m
04indrex1004x2_t03	1	P-band – Segment 3 – Baseline 30m
04indrex1002x2_t04	2	P-band – Segment 4 – MASTER
04indrex1003x2_t04	2	P-band – Segment 4 – Baseline 15m
04indrex1004x2_t04	2	P-band – Segment 4 – Baseline 30m

6.2.16 Summary

Data processing of INDREX-II E-SAR data could be performed successfully on all test-sites. The encountered problems due to lack of tiepoints could be solved by a priori information on terrain topography. Radiometric calibration was refined based on homogeneous rainforest data - and validated based on corner reflectors - for all frequency bands and polarisations. To allow for efficient processing (also repeat-pass interferometric processing) of the long data takes acquired during the campaign, a new segmentation procedure has been implemented. Single-pass interferometric processing was used to obtain DEMs for each test site. Repeat-pass interferometric and fully-polarimetric products were generated in L- and P-band. Finally, P-band images (non-interferometric) have been obtained also for incidence angles down to 18 deg off-nadir (steepest nominal incidence angle is 25 deg) to allow assessment of potential future space-borne SAR in P-band.

In this way, roughly 550 GByte of processed data have thus been generated and delivered to the evaluating scientists and to the European Space Agency.

7 Data Analysis

In the following preliminary analysis concerning radar backscattering analysis, classification and Pol-InSAR processing for forest parameter derivation will be presented, in order to answer the short term questions posed in section 2.

7.1 Radar Backscattering Evaluation

7.1.1 Mawas research transect

Backscatter values have been extracted around the 15 diver positions and around the 8 tree transect plots. Figure 7.1.1 illustrates the relation between biomass level BIO6 and the backscatter in L- and P-band with HH- and HV- polarization for the 8 tree transect plots. It is believed that the BIO6 measure is the most realistic. No clear relationships show up however. It is noted that these biomass levels are all high and already in the so-called saturation zone. Of course different relationships may be found when one of the other five sets of biomass levels (i.e. BIO1 to BIO5) would be used, or new equations will be developed. This is still a matter of research. Figure 7.1.2 shows there is a clear relationship with ground water level though. As noted in earlier chapters important applications exist in hydrology, peat swamp forest management and restoration.

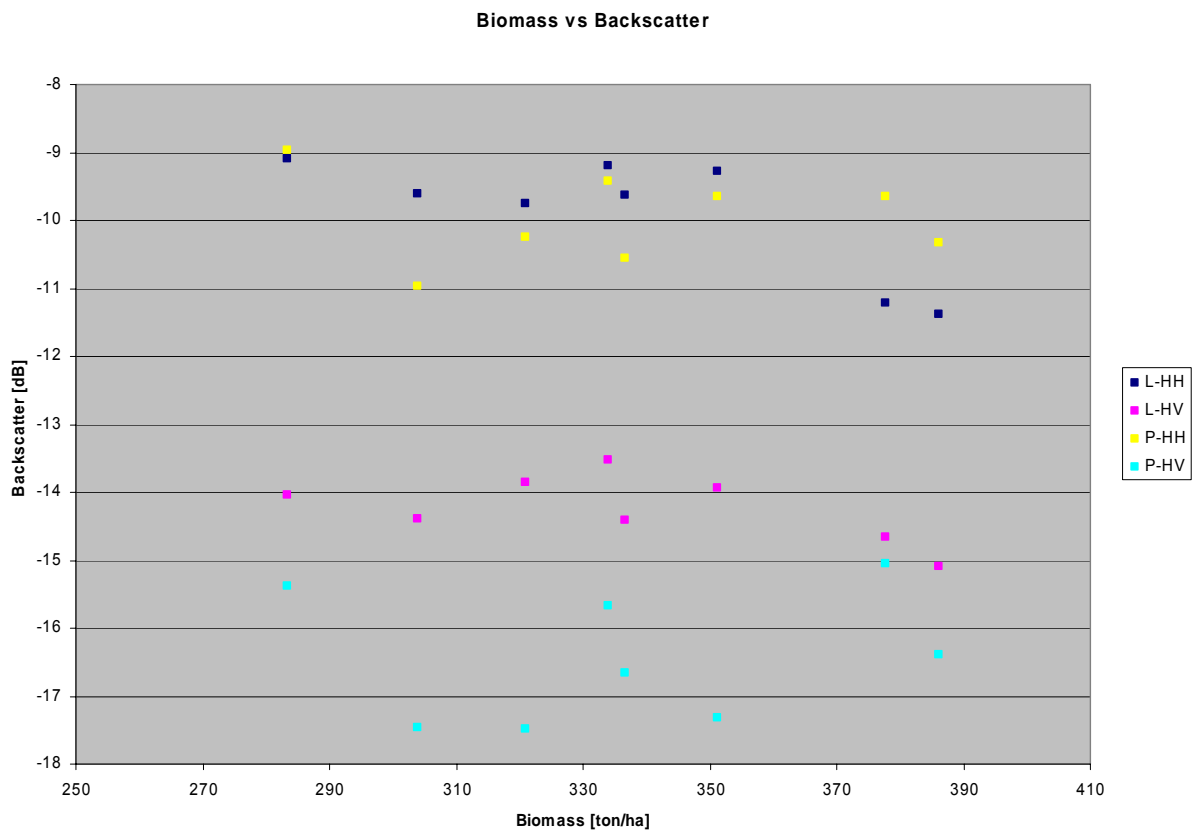


Fig.7.1.1. Relation backscatter vs. biomass in Mawas. These data indicate neither L- or P-band is sensitive to biomass (expressed as BIO6) variation in the 270 – 390 ton/ha range.

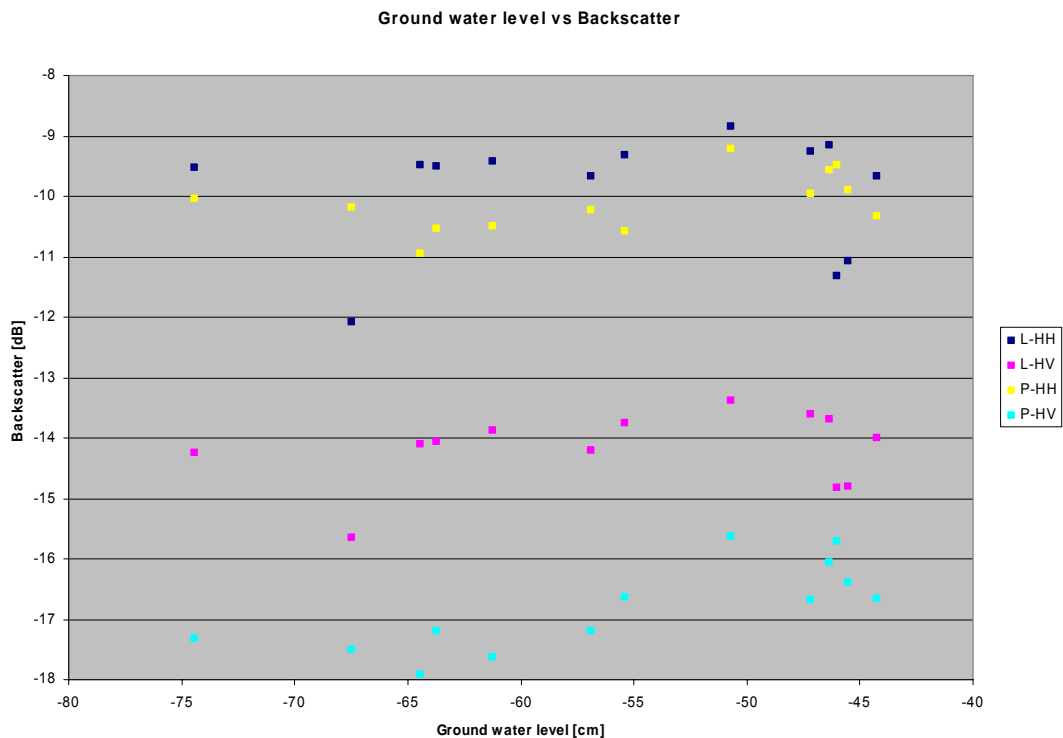


Fig. 7.1.2. Relation backscatter vs. ground water level in Mawas. These data indicate P-band is sensitive to deep (!) ground water level variation in peat swamp forests.

7.1.2 Balikpapan sites

Also for the Balikpapan area backscatter values have been derived carefully for the tree transects in Samboja Lestari, the mangrove area and Penajam. An overview of biomass and backscatter values is given in Table 7.1.1. It is noted that for palm trees another biomass equation (BIO8) has been used. The results are shown in Figure 7.1.3.

These data indicate that neither L- or P-band is sensitive to biomass when expressed with the parameter BIO6. Probably the structure of the vegetation has to be accounted for better. P-band is mainly sensitive for large trunks and, moreover, in a non-linear way. It is noted that the values (i.e. of BIO6) given here include the small trees and plants (which may account for a large biomass fraction) for which notably the P-band is hardly sensitive. Moreover, the range of structures is large as it comprises "normal" trees, palms, mangroves and open vegetation. Other measures (such as forest height or others related to forest structure) may yield better relationships but still have to be studied.

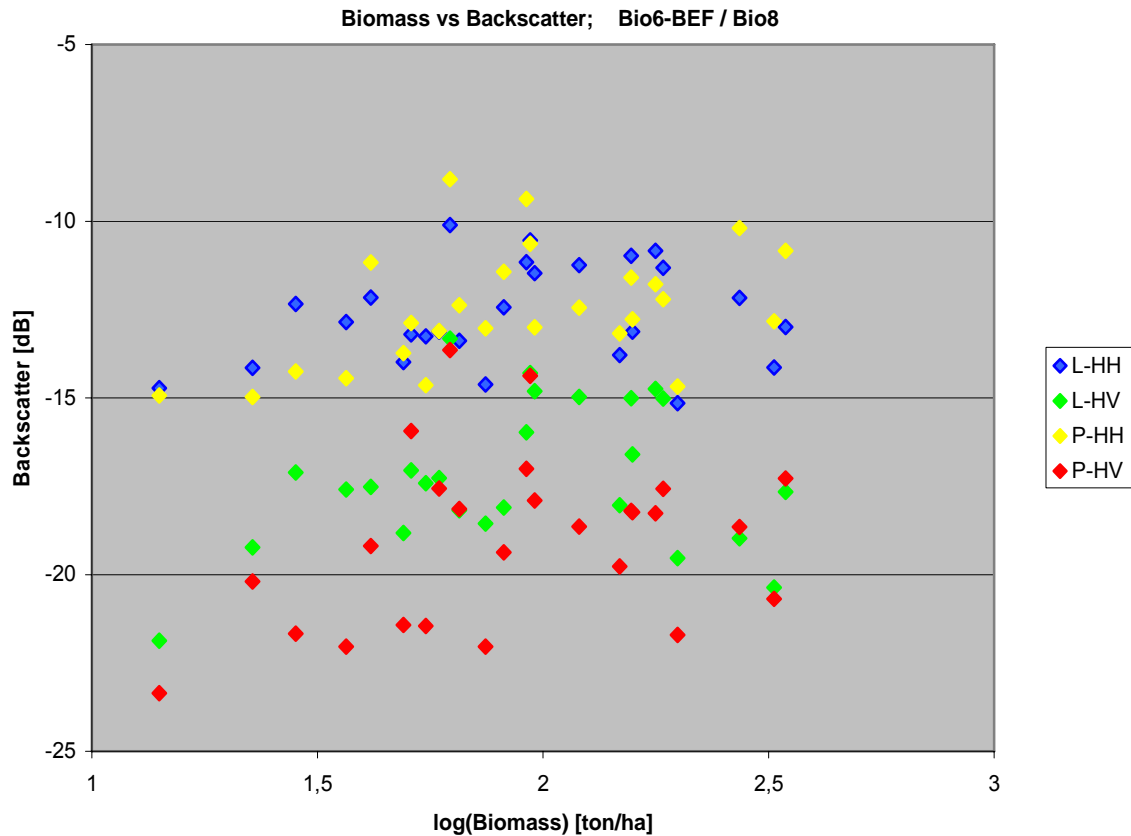


Fig.7.1.3. Relation backscatter vs. biomass in the Balikpapan sites. These data indicate neither L- or P-band is sensitive to biomass when expressed with the parameter BIO6. Probably the structure of the vegetation has to be accounted for better. It is noted that the values given here include the small trees and plants (which may account for a large fraction) for which notably the P-band is less sensitive. The scale is logarithmic: 1 (10 tons/ha); 2 (100 tons/ha); 2.5 (300 tons/ha).

Table 7.1.1. Biomass (in ton/ha) and backscatter values for the plots of the Balikpapan sites.

Plot	BIO6	BIO8	Backscatter intensity (dB)			
			L-HH 16Nov04	L-HV 16Nov04	P-HH 17Nov04	P-HV 17Nov04
Samboja Lestari						
Gameлина	120.2		-11.24	-14.97	-12.45	-18.64
Acacia	157.9		-13.13	-16.60	-12.78	-18.24
Secondary forest 1	93.7		-10.54	-14.30	-10.64	-14.38
Secondary forest 2	62.2		-10.11	-13.33	-8.81	-13.65
Secondary forest 3	95.8		-11.47	-14.81	-13.00	-17.90
Young fruit plantation	28.3		-12.34	-17.11	-14.25	-21.67
Teak 1-top	22.7		-14.15	-19.23	-14.97	-20.19
Teak 1-slope	51.0		-13.20	-17.05	-12.88	-15.94
Teak 1-valley	58.9		-13.13	-17.27	-13.11	-17.56
Teak 2-top	49.0		-13.99	-18.82	-13.73	-21.42
Teak 2-slope	74.6		-14.62	-18.56	-13.03	-22.04
Teak 2-valley	41.5		-12.16	-17.52	-11.17	-19.19
Teak 3-top	81.8		-12.44	-18.10	-11.43	-19.37
Teak 3-slope	65.2		-13.38	-18.18	-12.38	-18.14
Teak 3-valley	91.8		-11.16	-15.97	-9.37	-17.01
Teak-10	55.0		-13.26	-17.41	-14.64	-21.45
Alang-alang	14.1		-14.73	-21.87	-14.93	-23.35
Meranti	36.6		-12.85	-17.59	-14.44	-22.04



Penajam						
Oil palm 1; 3 yr	--	272.7	-12.17	-18.97	-10.19	-18.65
Oil palm 2; 6 yr	--	324.9	-14.14	-20.36	-12.83	-20.69
Oil palm 3; 1-2 yr	--	--	-19.10	-25.02	-20.54	-29.70
Rubber 1	184.5		-11.32	-15.02	-12.21	-17.57
Rubber 2; 12 yr	177.4		-10.84	-14.74	-11.78	-18.26
Rubber 3; 8 yr	156.9		-10.98	-15.01	-11.59	-18.20
Mangrove						
Mangrove 1	198.8		-15.15	-19.53	-14.68	-21.71
Mangrove 2	344.5		-12.99	-17.66	-10.84	-17.28
Mangrove 3	147.9		-13.79	-18.04	-13.17	-19.77

7.2 Classification Analysis

A preliminary visual classification has been made for the Samboja Lestari and Sungai Wain South radar images. For the Sungai Wain South area a mosaic of four radar frames had to be made. Since it appeared hard to co-registrare frames of different frequency bands it was decided to use only P-band data. Figure 7.2.1 indicates positions of most of the main land cover types (in letters) as well as all the field plots (in numbers). For Samboja Lestari a total power image in C-, L- and P-band could be made as a mosaic of 2 radar frames (Figure 7.2.2).

Note that these areas are very large compared to the size of the tree transect areas and, consequently, the tree transect are not well visible. For this reason a full resolution version of Figures 7.2.1 and 7.2.2 are provided on the data discs.

Legend of Figure 7.2.1

Plots	Cover types
1 : Oilpalm	A : Paddy fields
2 : Oilpalm	B : Low biomass wastelands
3 : Oilpalm	C : Alang-alang
4 : Rubber	D : Mixed gardens (Kebun)
5 : Rubber	E : Rubber and oilpalm estates
6 : Rubber	
7 : Mangrove	
8 : Mangrove	
9 : Mangrove	

Legend of Figure 7.2.2.

Plots	Plots	Cover types
1 : Gamelina	10 : Teak 2-top	A : Alang-alang
2 : Acacia	11 : Teak 2-slope	B : Vegetated lake
3 : Secondary forest 1	12 : Teak 2-valley	C : Base camp
4 : Secondary forest 2	13 : Teak 3-top	D : Orang-utan islands
5 : Secondary forest 3	14 : Teak 3-slope	E : Lake
6 : Young fruit plantation	15 : Teak 3-valley	F : Secondary forest
7 : Teak 1-top	16 : Teak-10	G : Sun bear sanctuary forest
8 : Teak 1-slope	17 : Alang-alang	
9 : Teak 1-valley	18 : Meranti	

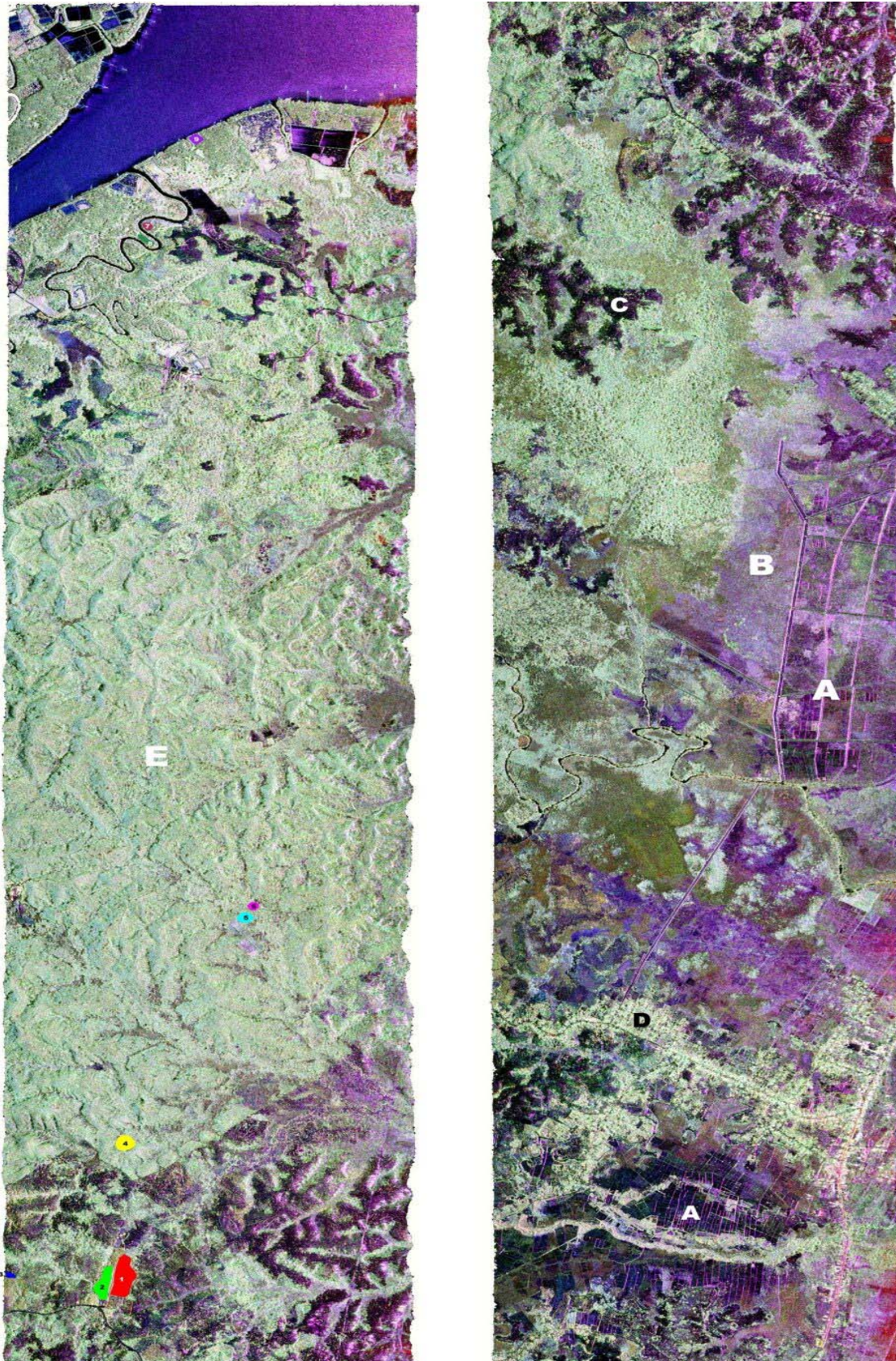


Figure 7.2.1. The Sungai Wain South radar image shows the Penajam and mangrove areas. It is a P-band sigma-nought image (with HH/HV/VV polarization in Red/Green/Blue) and a mosaic from 4 frames.

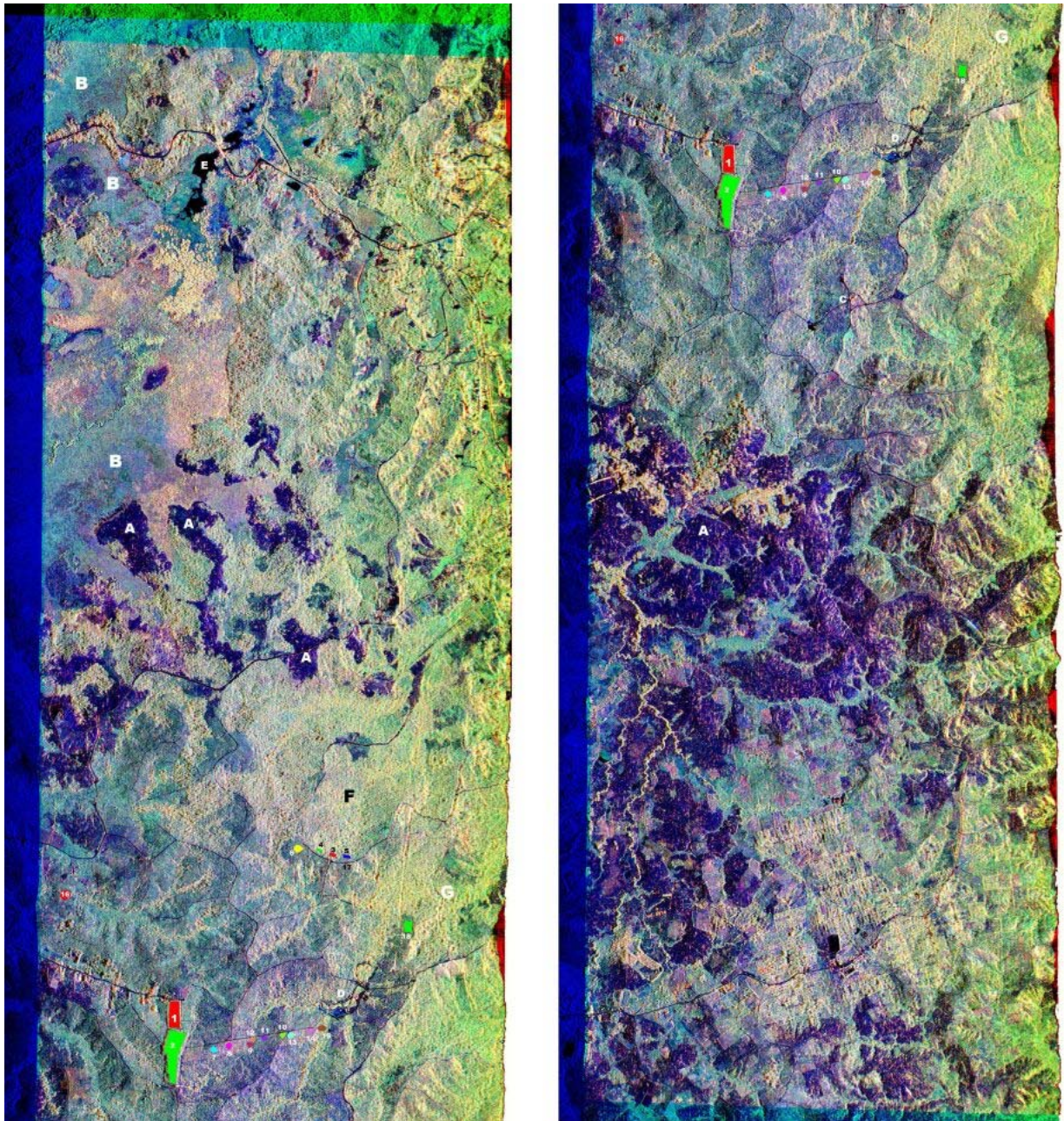


Figure 7.2.2. The Samboja Lestari radar image is a C-, L- and P-band total power image (with the P/L/C bands in Red/Green/Blue) and is a mosaic from 2 frames.

7.3 Polarimetric SAR and Interferometric SAR Analysis

7.3.1 Test Sites and Data Selection

From the test sites acquired in the frame of INDREX-II four test sites - Sungai Wain, Mawas and Samboja Lestari - have been chosen for the following Pol-InSAR analysis and discussion. The flown configurations and the available data sets are summarised in Table 7.3.1. At L in general three spatial baselines of about 5 m, 10 m, and 15 m have been acquired with a maximum temporal baseline of about 60 min for all test sites except for the Samboja Lestary test site where only two spatial baselines (5 m and 8 m) have been acquired due to low vegetation level. Also at P Band three spatial baselines of about 15 m 30 m, and 60 m (i.e., scaled by a factor of three compared to L band) have been acquired with approximately the same temporal baseline of max. 60 min. For all scenes a single pass X Band observation with a spatial baseline of 0.8 m was additionally acquired.

Table 7.3.1: E-SAR modes for each test site

Test Site	L – Band Quad Pol		P – Band Quad Pol		X- Band VV
	Baseline		Baseline		Baseline
	temporal [min]	spatial [m]	temporal [min]	spatial [m]	spatial [m]
Sungai Wain	15,30,45	5,10,15	15,30,45	15,30,60	0,8
Mawas	20,40,60	5,10,15	20,40,60	15,30,60	0,8
Samboja Lestari	10,20	5,8	10,20	15,30,60	0,8
Meratus	15,30,45	5,10,15	15,30,45	15,30	0,8

7.3.2 Pol-InSAR Processing Flow

The Pol-InSAR processing flow is schematically shown in Figure 7.3.1. Input data are the co-registered SLC (single look complex) data files at the three polarisations (i.e., HH, VV and HV). In a first step the complex interferometric coherences (including interferometric correlation and phase) at different polarisation states (obtained a linear combinations of HH, VV and HV) are generated and the Lagrangian coherence optimisation algorithm was applied as described in [1].

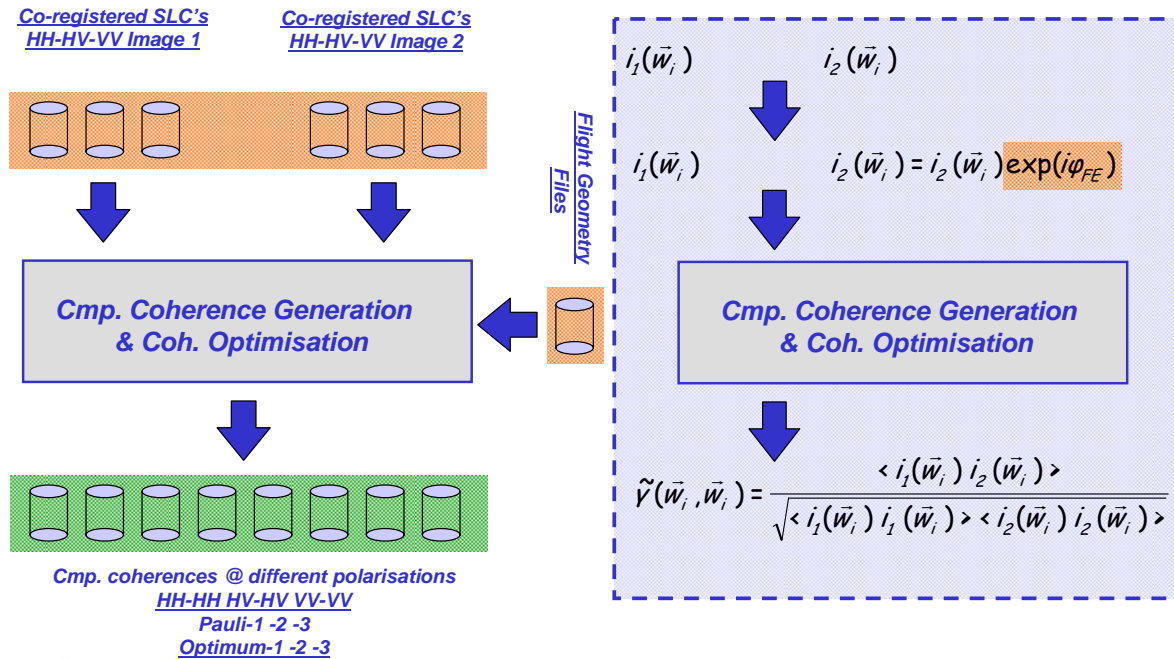


Figure 7.3.1: Pol-InSAR Processing flow

The output is a series of complex coherences at different polarisations. The discussion in the following will focus primarily on the three lexicographic (i.e. HH-HH, VV-VV, and HV-HV) and the three optimised coherences.

7.3.3 Pol-InSAR Data Discussion

The fact that the interferometric coherence is sensitive to the vertical structure of the individual scatterers allows discriminating between surface and volume scatterers:

- **Surface Scatterers** have a Dirac-like vertical distribution and therefore the interferometric coherence are (after range spectral filtering) independent of baseline and - in the absence of system or temporal decorrelation effects - independent of polarisation and equal to one. However, in the presence of SNR-decorrelation the coherence over bare surfaces becomes polarisation dependent and non-unity

$$\gamma_{Total} = \gamma_{SNR} \gamma_{Volume} \quad \text{where} \quad \gamma_{Volume} = 1 \quad \text{Eq. 1}$$

- **Volume Scatterers** have an extended vertical distribution of effective scatterers and therefore the interferometric coherence decreases with baseline. The coherence can vary with polarisation when the effective vertical distribution of scatterers changes with polarisation: In forests this can be the case when the ground scattering component changes with polarisation – and/or when the propagation through the forest-layer is polarisation dependent. However this second effect is at L band less distinct so that a variation of coherence with polarisation can be used as an indicator for the presence of the ground under the forest.

Based on this, the coherence images obtained from the Pol-InSAR data processing will be discussed in the following:

Mawas E – L-band

Figure 7.3.2 shows the data corresponding to the 5m spatial baseline. On the upper left image of Figure 7.3.2 the HH amplitude image of the scene is shown: In the upper part a river (low backscatter) meanders through the scene and a peat swamp (surface scatterer) neighbouring the river appears darker. The rest of the image is covered with forest. The corresponding interferometric phase and vertical wave-number (k_z) images are shown on the left. The small and smooth phase variations indicate the flatness of the terrain; the phase difference in the transition between peat swamp to forest (known as vegetation bias) is clearly visible. The vertical wave-number image reflects the 2-D baseline variation typical for the airborne case: from near to far range due to the wide incidence angle variation and along azimuth due to the deviation of the platform from the nominal track. The strong variations along azimuth are typical for an airborne system configuration at small spatial baselines as performed here. The interferometric coherence images in the HH, HV, and VV polarisations - scaled from 0 to 1 - are shown in the middle. In accordance with the considerations above, the peat swamp area is characterised by high coherence values (close to 1) while the river decorrelates completely (coherence close to 0) as a result of temporal decorrelation. The forest is characterised by volume decorrelation that varies with baseline (i.e. from near to far range - as indicated by the vertical wave-number image). Note that in contrast to the amplitude images where the dynamic range over the forest is limited; forest structures (as for example logging trails) become visible in the coherence images due to the sensitivity of the coherence to vertical structure variation. On the bottom of Figure 7.3.2, the three optimum coherence images are shown, indicating the range of coherence variation with polarisation. The wide range of variance is a direct indicator for the visibility of the ground scattering contribution under the forest layer **Fehler! Verweisquelle konnte nicht gefunden werden..**

In Figure 7.3.3 the corresponding images for the 10m spatial baseline are shown. As expected, with increasing baseline the volume decorrelation over the forested areas increases. The coherence decreases (stronger at near range) because of the larger effective baseline. In contrast to the forest, the coherence over the surface scatterers remains the same. Looking on the phase image now, the vegetation bias becomes more evident due to the increased height sensitivity of the larger baseline. A smaller relative variation of the vertical wave-number within the scene (especially along azimuth) can be observed.

Going to the 15m baseline in Figure 7.3.4 the coherence decreases dramatically (especially in near range values gets close to 0), in consequence to high volume decorrelation. Coherences over surfaces stay still at very high levels. The relative variations of the vertical wave-number along azimuth further declines.

The high coherence levels obtained over the peat swamp area at all baselines indicate a high system acquisition and data processing quality of the data set.

Mawas E - P Band

Figure 7.3.5 shows the same test site for the 15 m spatial baseline at P band (corresponding to a 5 m baseline at L band). The amplitude (HH), interferometric phase and vertical wavenumber images are shown on the top from left to right. The logging trails - invisible in the L band amplitude image - become visible at P band image that has a higher dynamic than the corresponding L band image. In the phase image the vegetation bias is clearly present indicating the presence of a vegetation bias and pointing to the fact that the scattering center at P band is not located on (or very close) to the ground. The relative variation of the vertical wave-number (across range and azimuth) is reduced compared to

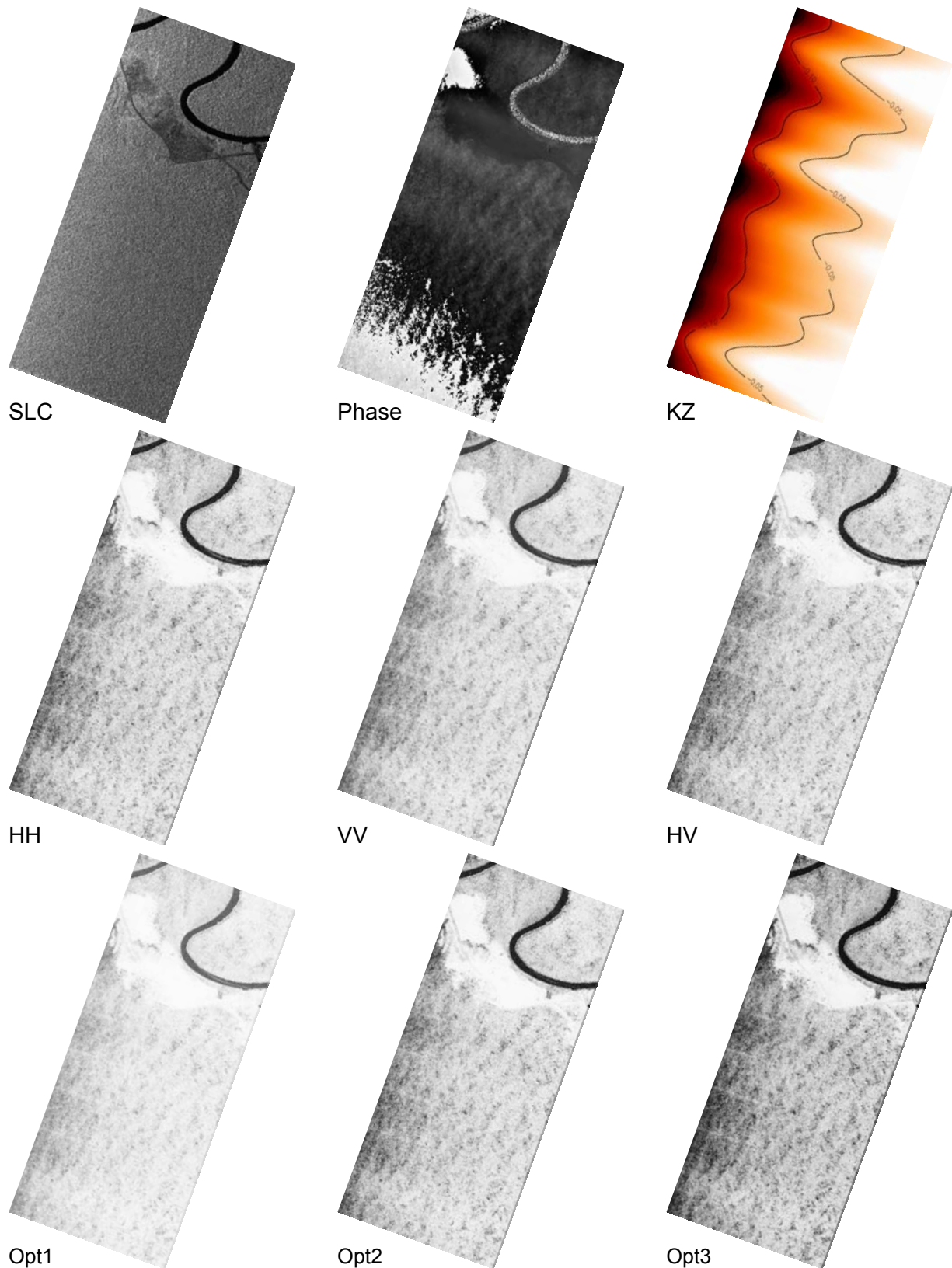


Figure 7.3.2: Test Site Mawas E; Interferometric coherences for a 5m spatial baseline in L Band; from left to right upper part: amplitude image (HH polarisation), interferometric phase (HH polarisation), vertical wave-number (kz); from left to right middle part: coherence in HH, VV, and XX polarisation; from left to right lower part: optimized coherence 1 to 3

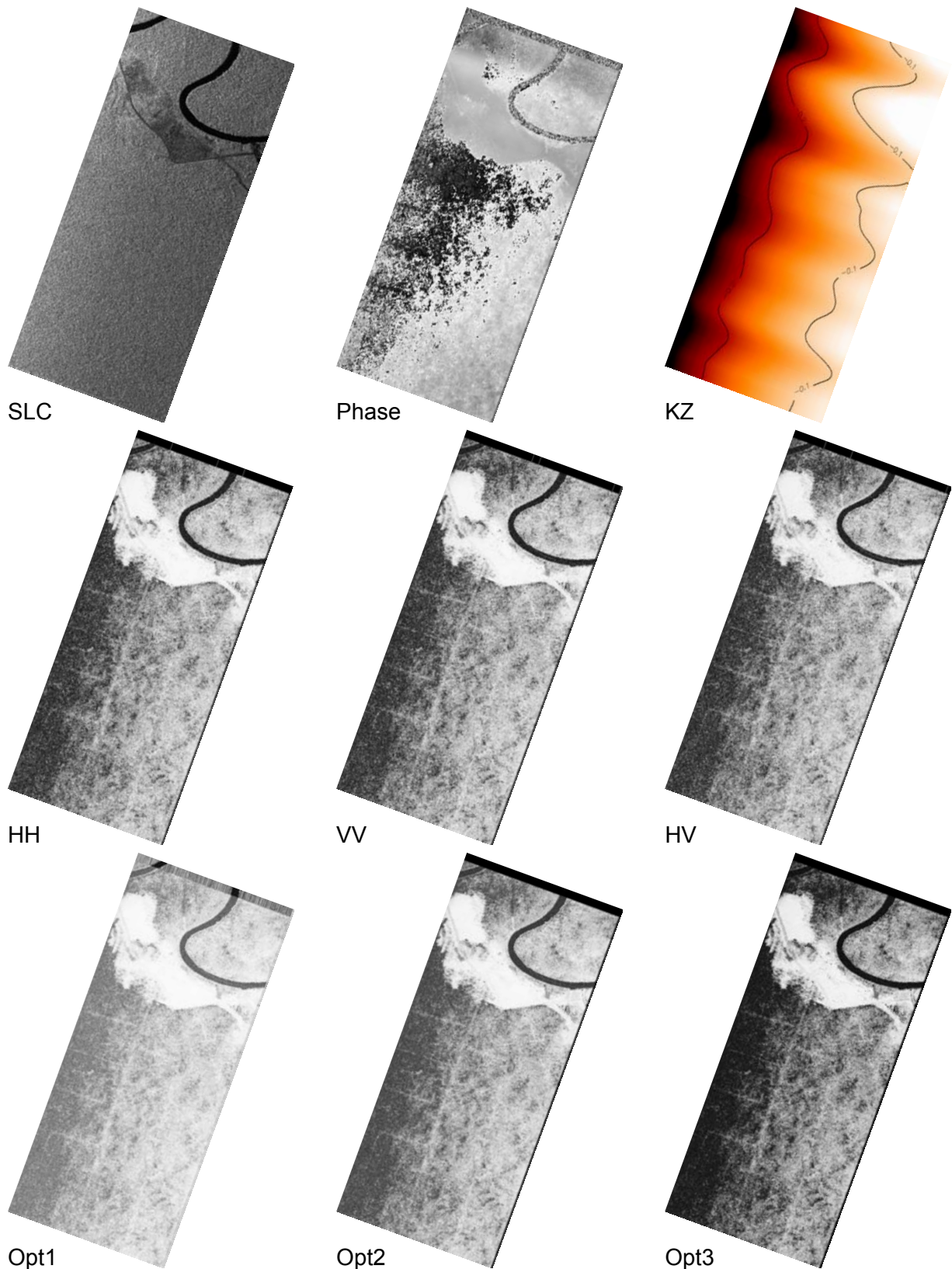


Figure 7.3.3: Test Site Mawas E; Interferometric coherences for a 10m spatial baseline in L Band; from left to right upper part: amplitude image (HH polarisation), interferometric phase (HH polarisation), vertical wave-number (kz); from left to right middle part: coherence in HH, VV, and XX polarisation; from left to right lower part: optimized coherence 1 to 3

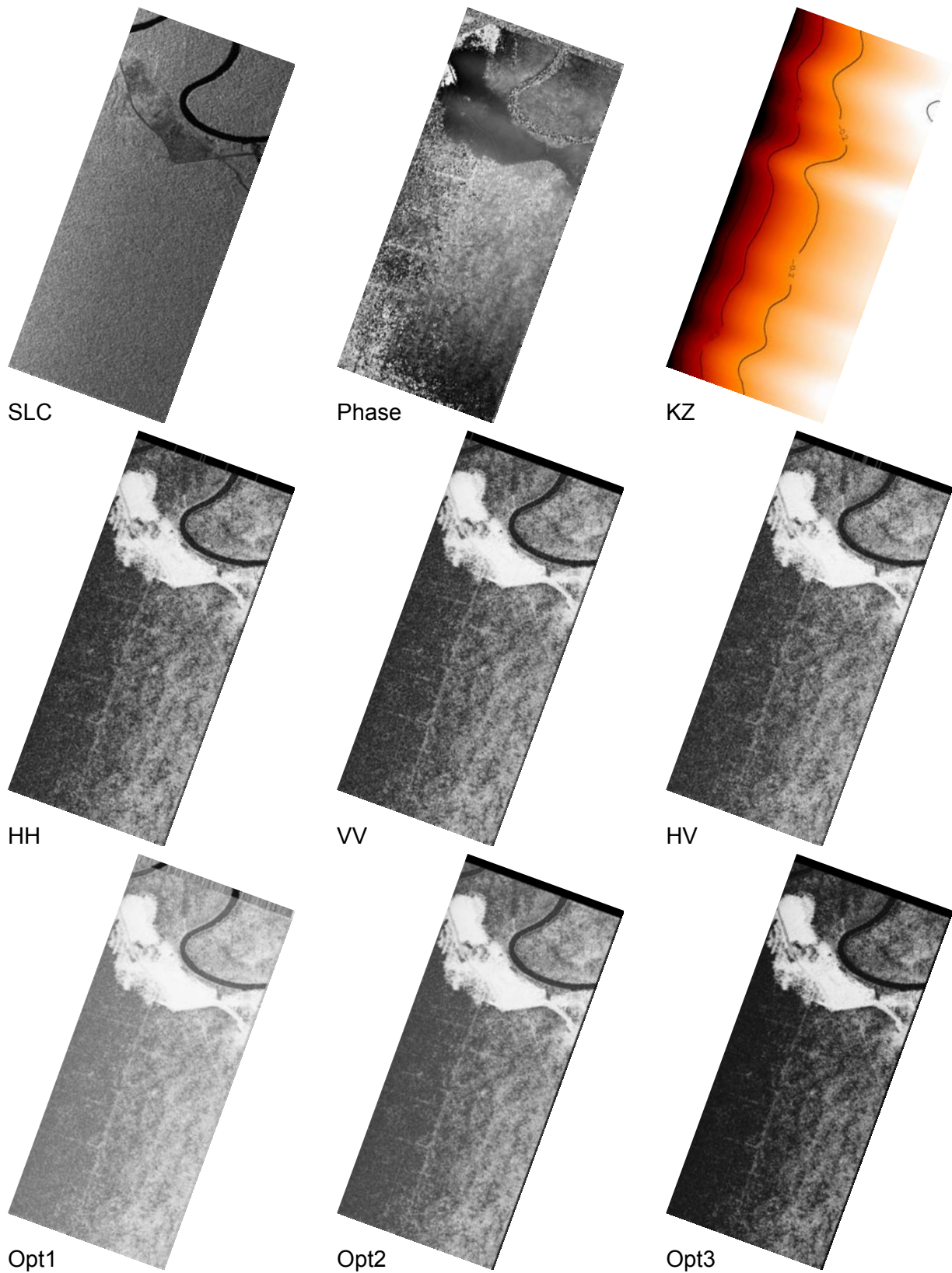


Figure 7.3.4: Test Site Mawas E; Interferometric coherences for a 15m spatial baseline in L Band; from left to right upper part: amplitude image (HH polarisation), interferometric phase (HH polarisation), vertical wave-number (kz); from left to right middle part: coherence in HH, VV, and XX polarisation; from left to right lower part: optimized coherence 1 to 3

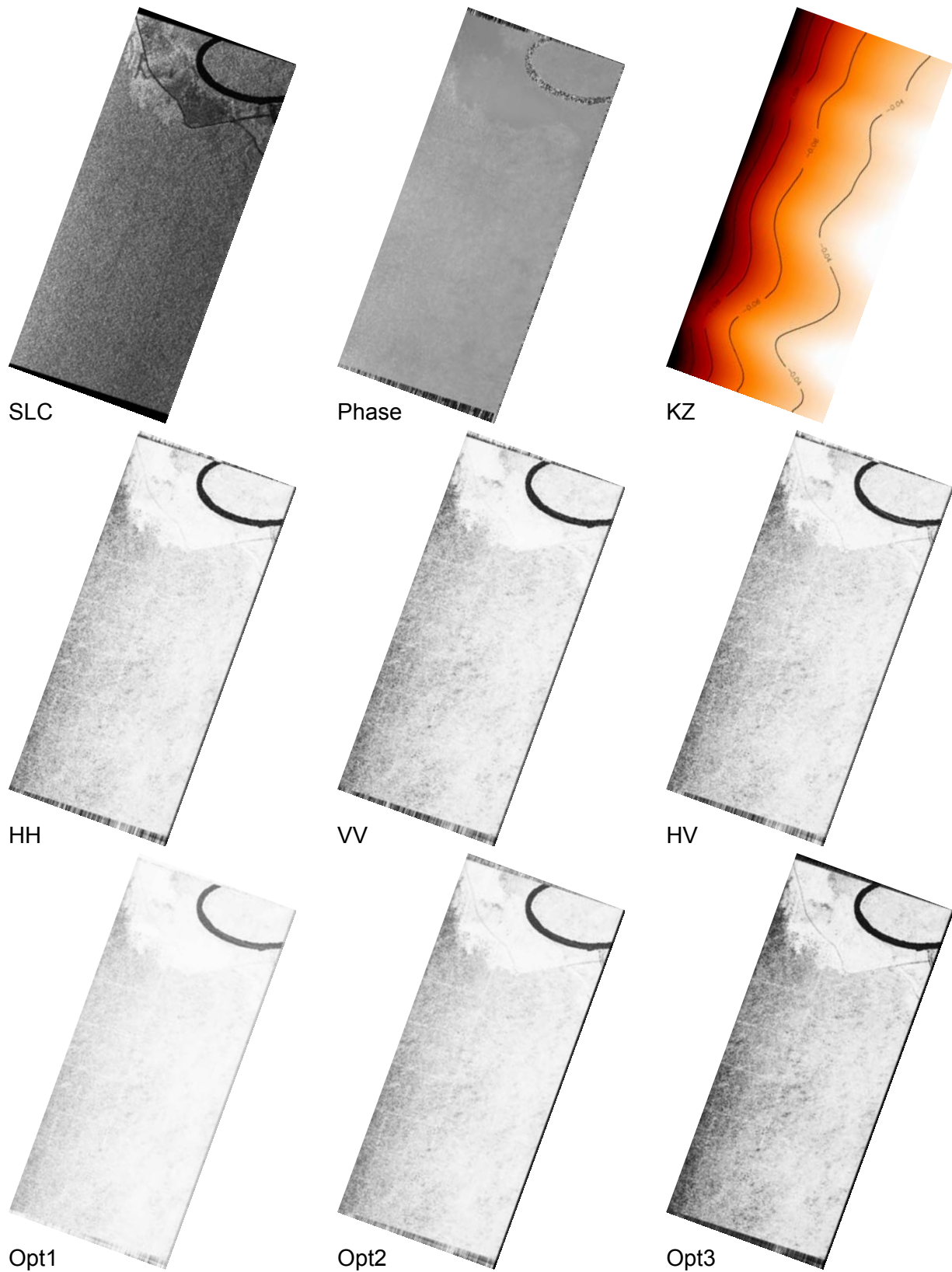


Figure 7.3.5: Test Site Mawas E; Interferometric coherences for a 15m spatial baseline in P Band; from left to right upper part: amplitude image (HH polarisation), interferometric phase (HH polarisation), vertical wave-number (kz); from left to right middle part: coherence in HH, VV, and XX polarisation; from left to right lower part: optimized coherence 1 to 3

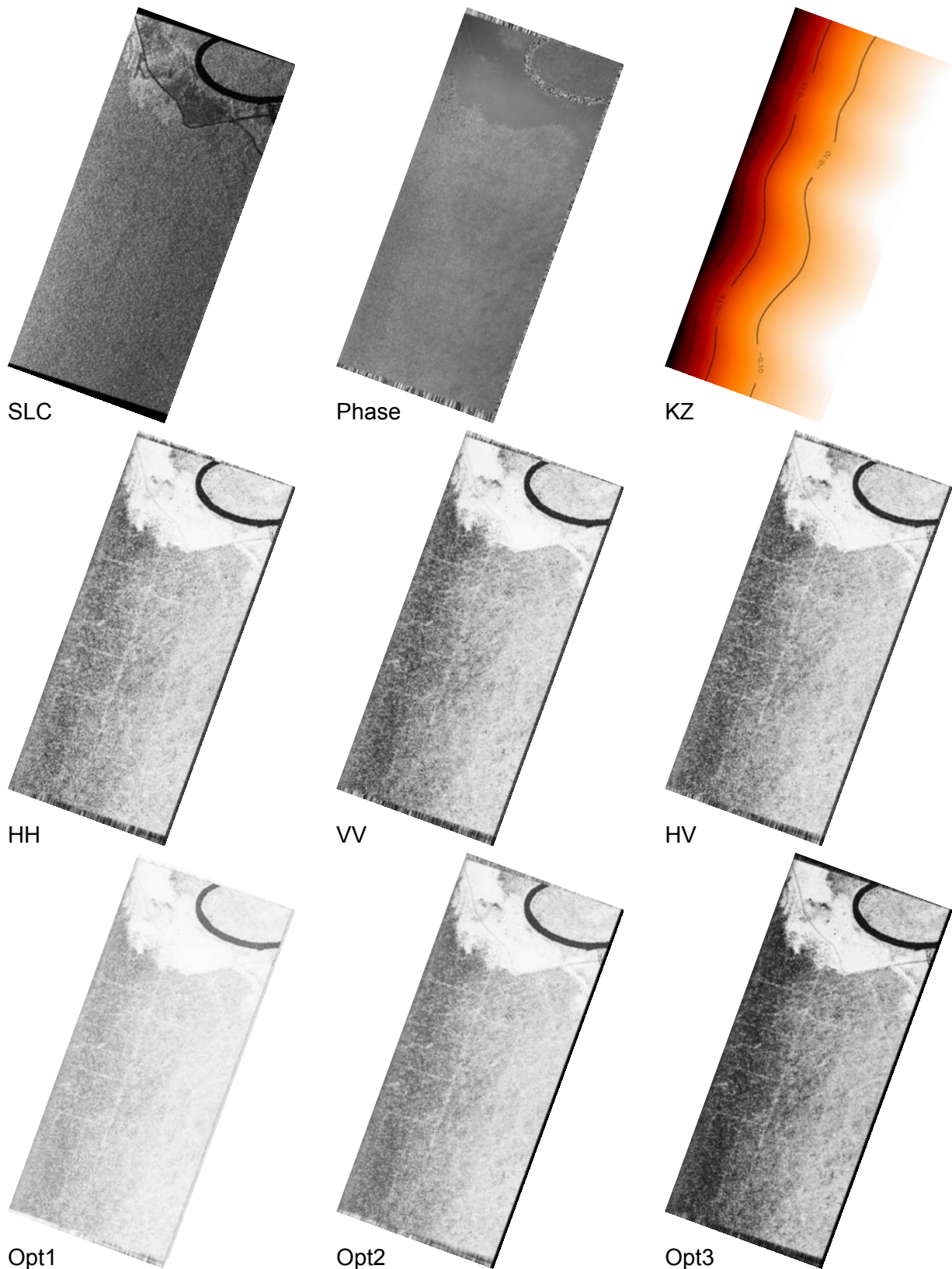


Figure 7.3.6: Test Site Mawas E; Interferometric coherences for a 30m spatial baseline in P Band; from left to right upper part: amplitude image (HH polarisation), interferometric phase (HH polarisation), vertical wave-number (kz); from left to right middle part: coherence in HH, VV, and XX polarisation; from left to right lower part: optimized coherence 1 to 3

the one obtained at the corresponding L band baseline (5m see Figure 7.3.2). The coherences at the lexicographic polarisations are shown in the middle: Surfaces (i.e. the peat swamp) have not anymore coherences close to one due to the increased Signal to Noise ratio (SNR) decorrelation. The forest appears also at P band as a volume scatterer characterised by the baseline dependent (over range) volume decorrelation contribution. The optimum coherences shown on the bottom indicate a wide range of coherence variation with polarisation indicating the presence of a strongly polarised ground scattering component.

With increasing baseline to 30 m (see Figure 7.3.6) the vegetation bias (peat swamp – forest transition) becomes more evident due to the increases phase-2-height sensitivity. On the other hand the coherence level over the forest decreases due to the increased volume decorrelation contribution (stronger in near range than in far range). In contrast to the forest, coherence over surface scatterer remains constant but significantly lower than one.

Mawas C - L Band

Mawas C is part of the undisturbed peat swamp forest area. In the amplitude image (HH) shown in Figure 7.3.7 can be seen that the scene is predominantly covered by forest. A small river is crossing the image in the middle of the scene covered by the trees on the riverside and can be recognised by the high dihedral scattering component (a phenomenon also known from flooded tropical forests). On the lower part of the image a channel system (characterised by low backscattering) crosses the scene, surrounded by deforested areas characterised by surface scattering. Looking on the interferometric phase image the vegetation offset on the transition from the deforested to the forested area appears clearly. In the coherence images now (shown in the middle row), the river shows high coherences because of the strong dihedral scattering contribution that has its scattering centre located on the ground and behaves therefore as a surface scatterer. The deforested surfaces have a high coherence (close to one) while the forested areas decorrelate due to volume decorrelation. Obvious is the modulation of the interferometric coherence with the baseline indicated by the red box on the kz and on the coherence images in Figure 7.3.7).

With increasing spatial baseline to 10m (see Figure 7.3.8) and 15m (see Figure 7.3.9) the relative variation of the vertical wavenumber decreases. The coherence over the surface scatterers remains constant at a high level, while decreases over the forested parts.

Mawas C - P Band

Comparing the L and P band amplitude images, one can see the (slightly) higher dynamic range of the P band image over the forested areas. This is due to the higher saturation level expected at P band. Looking on the interferometric coherences now, (15m / 30m baseline images are shown in Figure 7.3.10 / Figure 7.3.11 respectively) surface scatterers are characterised by high and baseline independent coherence levels close to one while the forest is characterised by a baseline varying volume decorrelation contribution. An (radio frequency) interference (RFI) induced decorrelation (!!!) is visible in the HH channel, indicated by the red box.

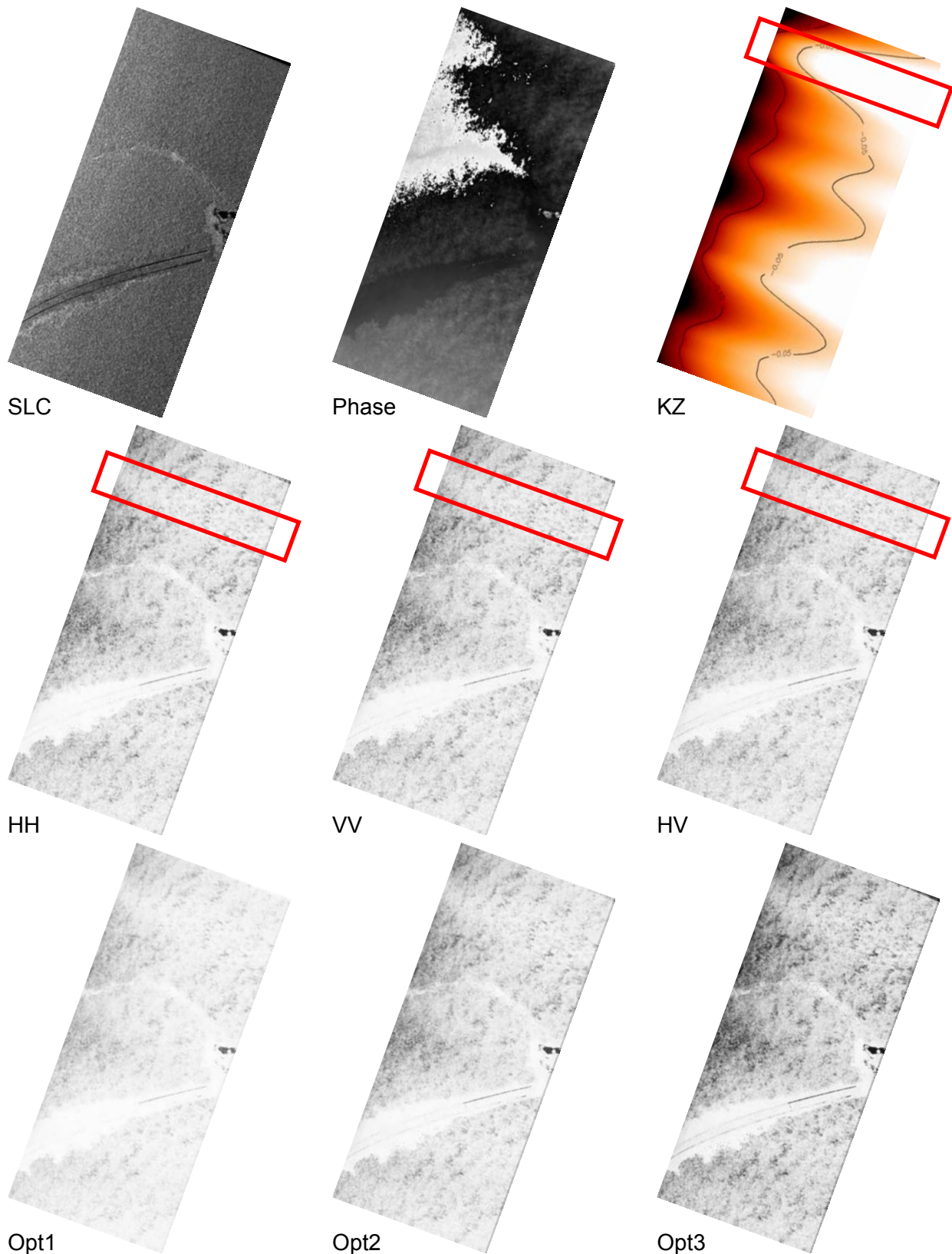


Figure 7.3.7: Test Site Mawas C; Interferometric coherences for a 5m spatial baseline in L Band; from left to right upper part: amplitude image (HH polarisation), interferometric phase (HH polarisation), vertical wave-number (kz); from left to right middle part: coherence in HH, VV, and XX polarisation; from left to right lower part: optimized coherence 1 to 3; red box highlights impact of small baseline on coherence

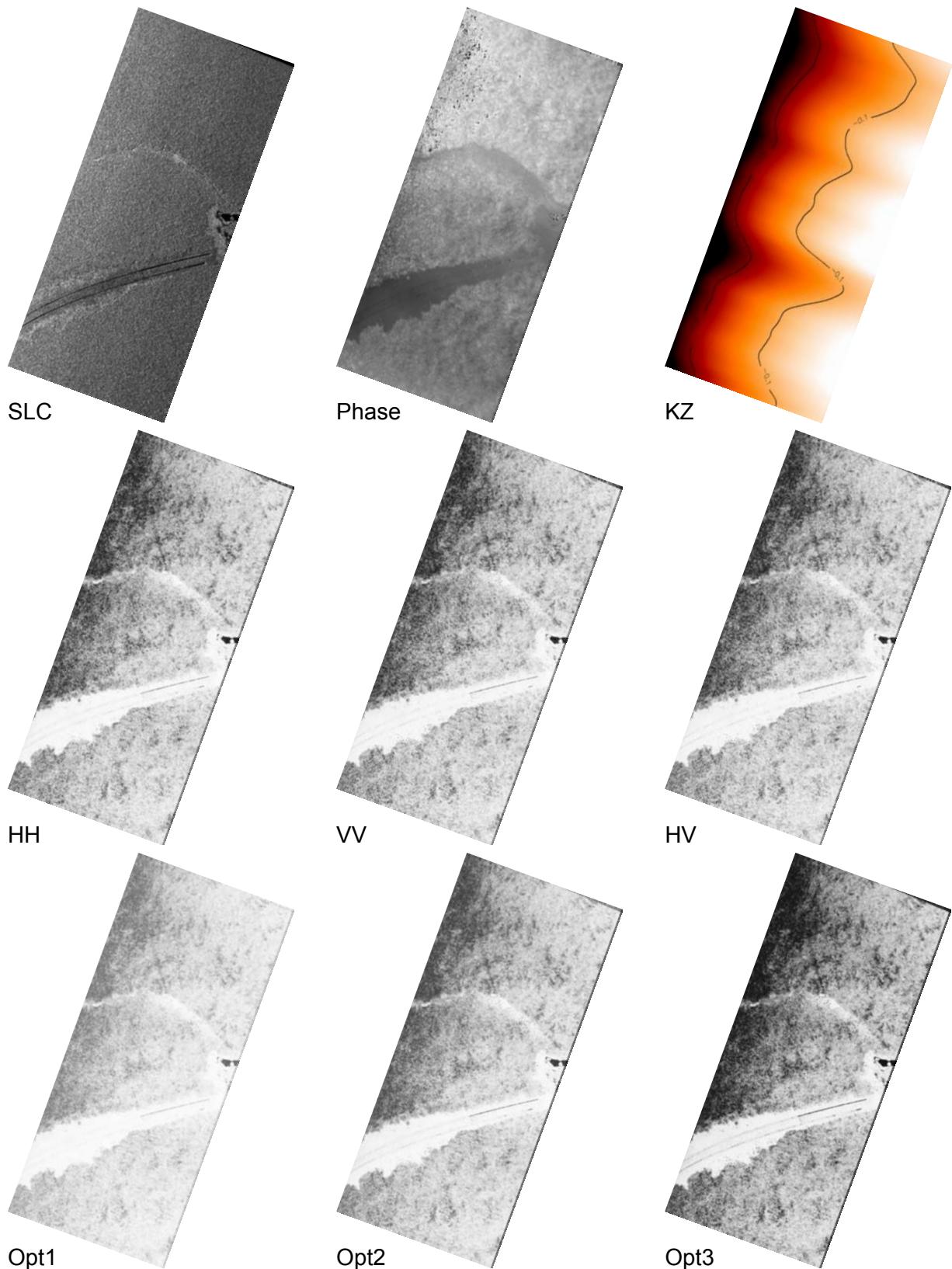


Figure 7.3.8: Test Site Mawas C; Interferometric coherences for a 10m spatial baseline in L Band; from left to right upper part: amplitude image (HH polarisation), interferometric phase (HH polarisation), vertical wave-number (kz); from left to right middle part: coherence in HH, VV, and XX polarisation; from left to right lower part: optimized coherence 1 to 3

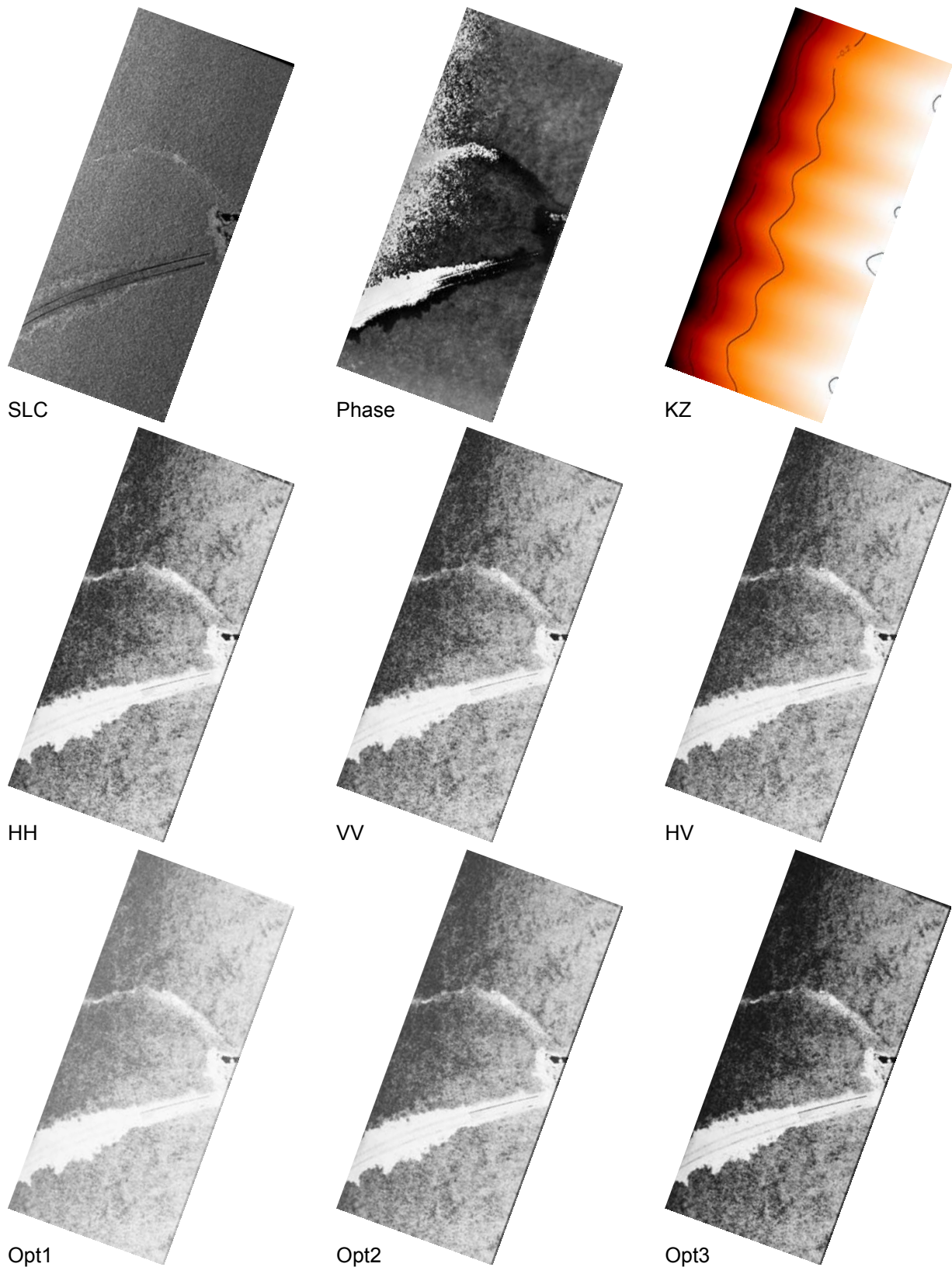


Figure 7.3.9: Test Site Mawas C; Interferometric coherences for a 15m spatial baseline in L Band; from left to right upper part: amplitude image (HH polarisation), interferometric phase (HH polarisation), vertical wave-number (kz); from left to right middle part: coherence in HH, VV, and XX polarisation; from left to right lower part: optimized coherence 1 to 3

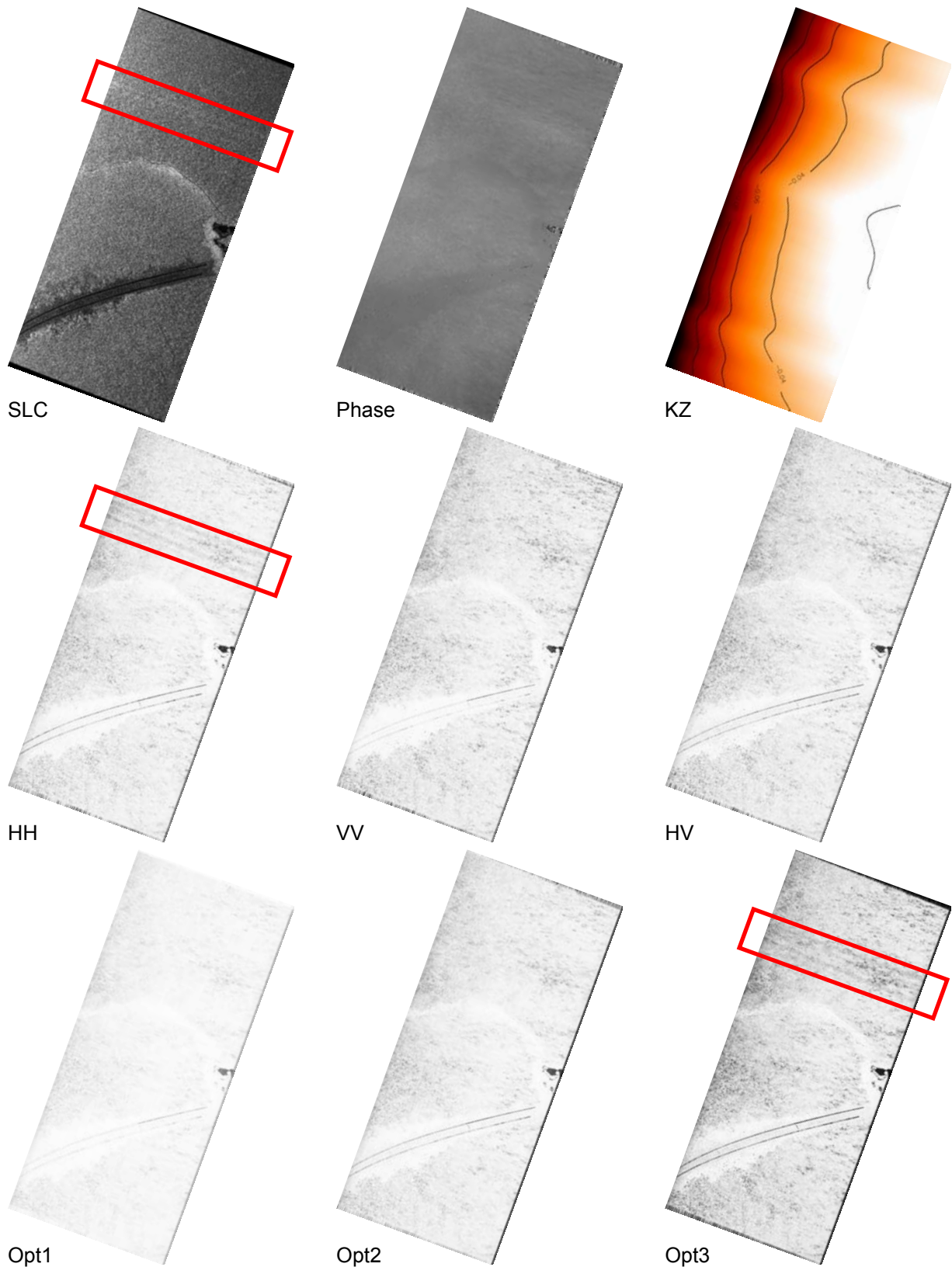


Figure 7.3.10: Test Site Mawas C; Interferometric coherences for a 15m spatial baseline in P Band; from left to right upper part: amplitude image (HH polarisation), interferometric phase (HH polarisation), vertical wave-number (kz); from left to right middle part: coherence in HH, VV, and XX polarisation; from left to right lower part: optimized coherence 1 to 3; Red box highlights RFI in HH Channel

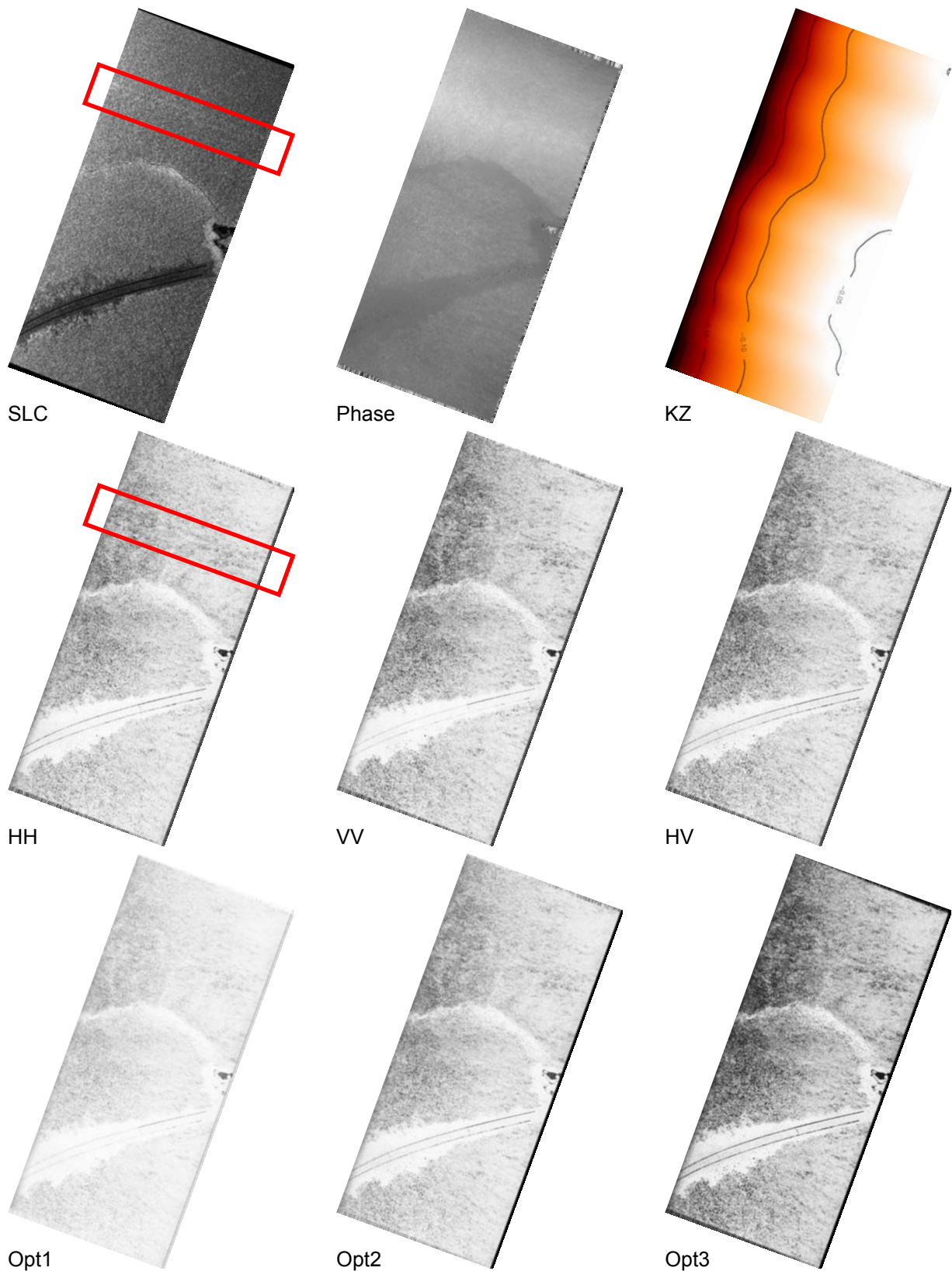


Figure 7.3.11: Test Site Mawas C; Interferometric coherences for a 30m spatial baseline in P Band; from left to right upper part: amplitude image (HH polarisation), interferometric phase (HH polarisation), vertical wave-number (kz); from left to right middle part: coherence in HH, VV, and XX polarisation; from left to right lower part: optimized coherence 1 to 3; Red box highlights RFI in HH Channel

Sungai Wain - L Band

An important test site is the dipterocarp forest of Sungai Wain. This type of forest is much higher (up to 60m) and denser than the peat swamp forest of Mawas. Furthermore, the area of Sungai Wain has (unlike Mawas) strong topographic variations. Figure 7.3.12 shows (from left to right and top to bottom) the amplitude (HH), interferometric phase (HH-HH), vertical wavenumber, X-band Digital Elevation Model (DEM) and the lexicographic / optimum coherence images obtained at the 5m spatial baseline on the Sungai Wain test site. The amplitude image makes clear that the whole scene is covered by forest. The X band DEM makes the hilly character of the test site with terrain variations from 60m to 180m evident. This reflects not only on the interferometric phase image but (surprisingly) also on the amplitude image where the terrain modulation of the backscattering coefficient is clearly visible. This is already a first (indirect) indication for the visibility of the ground under the forest at L band in this dense tropical forest environment.

Looking on the interferometric coherence images now, it becomes clear that - in general - the obtained coherence level is much lower than the coherence level obtained in Mawas, due to the higher (taller) forest conditions in Sungai Wain. Because of the higher and denser forest conditions, the ground contribution is expected to be strongly attenuated. Indeed, this becomes evident in the range of coherence variation with polarisation and by the difference between the optimal coherences. However there are still differences that indicate the visibility of the polarised ground scattering contribution. The dependency of the interferometric coherence with the baseline is also here visible (see the red boxes in Figure 7.3.12).

Looking on the 10m baseline (Figure 7.3.13), the coherence decreases faster with baseline than in the Mawas case – again due to the much higher forest. In the 15m baseline (Figure 7.3.14) the forest is almost completely decorrelated.

Sungai Wain - P Band

Similar to L band, the variations in the amplitude image of P band (see Figure 7.3.15) reflect also the variation of the underlying topography. The 15m baseline shows - compared to L Band - a higher variance of coherence with polarisation indicating (as expected) a stronger ground contribution at P band than at L band. Comparing Figure 7.3.15 with Figure 7.3.16 (i.e. the 15m with the 30m baseline) the baseline dependency of the volume decorrelation contribution at P band becomes clear.

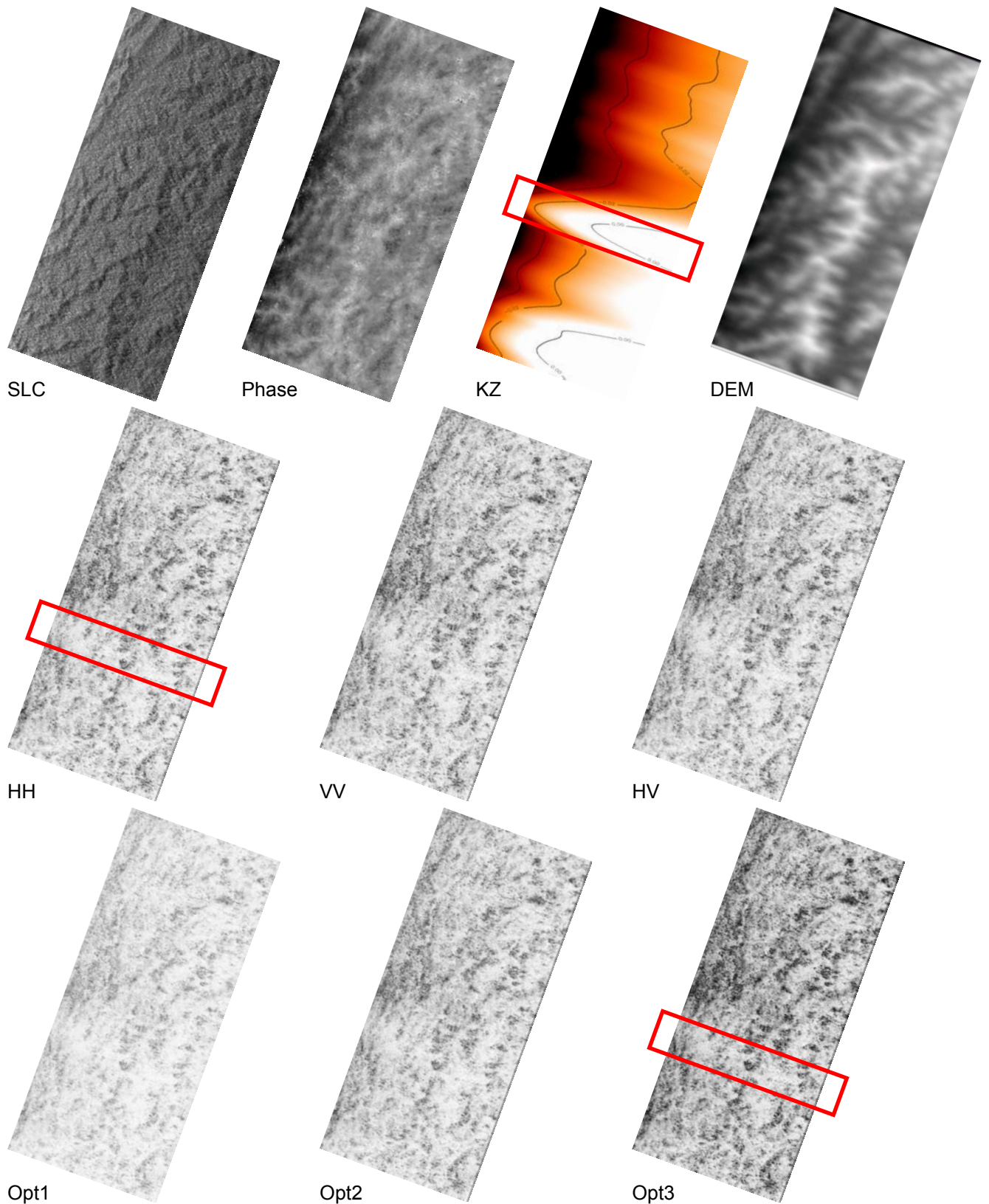


Figure 7.3.12: Test Site Sungai Wain; Interferometric coherences for a 5m spatial baseline in L Band; from left to right upper part: amplitude image (HH polarisation), interferometric phase (HH polarisation), vertical wave-number (kz), X Band Digital Elevation Model (DEM); from left to right middle part: coherence in HH, VV, and XX polarisation; from left to right lower part: optimized coherence 1 to 3

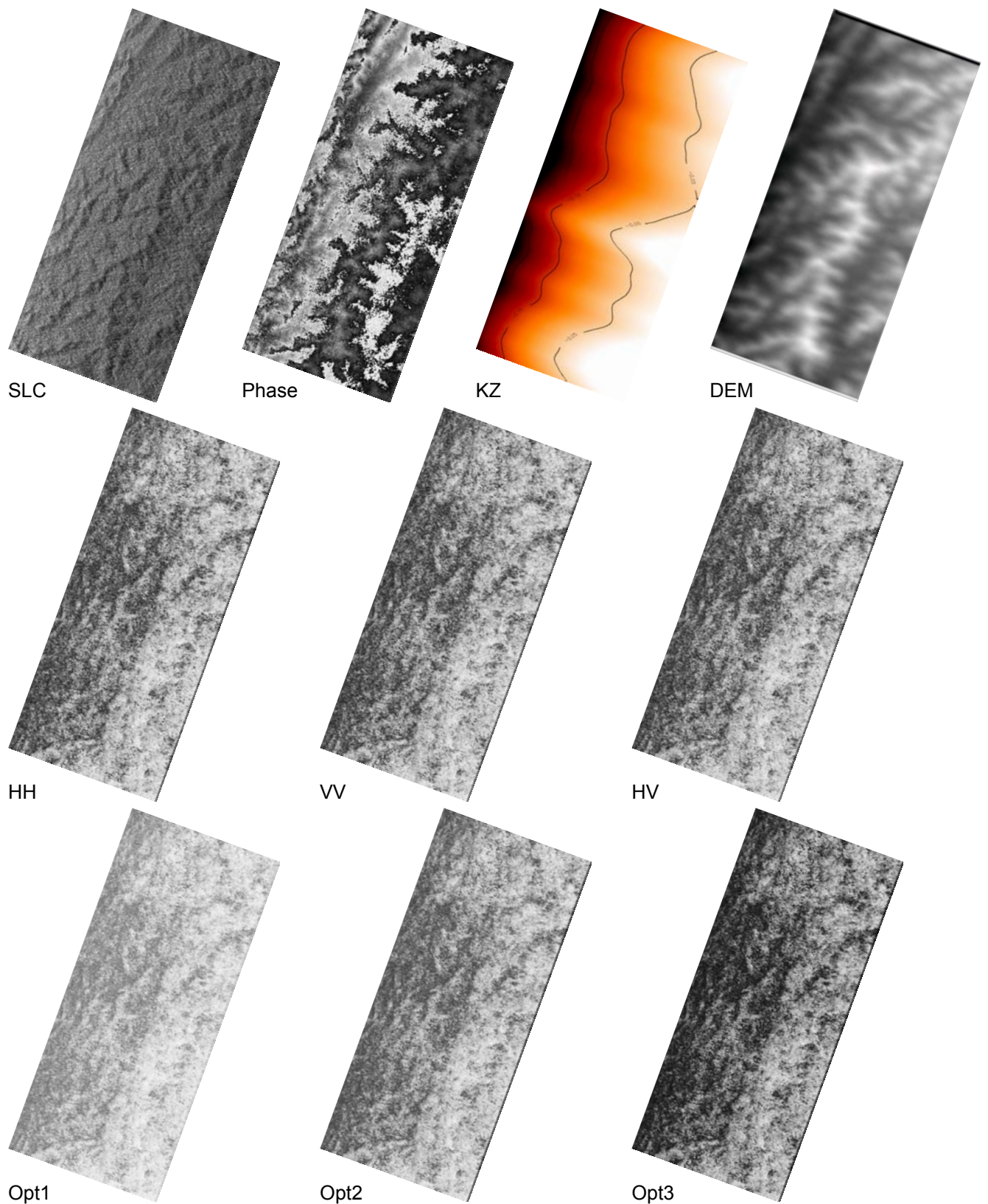


Figure 7.3.13: Test Site Sungai Wain; Interferometric coherences for a 10m spatial baseline in L Band; from left to right upper part: amplitude image (HH polarisation), interferometric phase (HH polarisation), vertical wave-number (kz), X Band Digital Elevation Model (DEM); from left to right middle part: coherence in HH, VV, and XX polarisation; from left to right lower part: optimized coherence 1 to 3

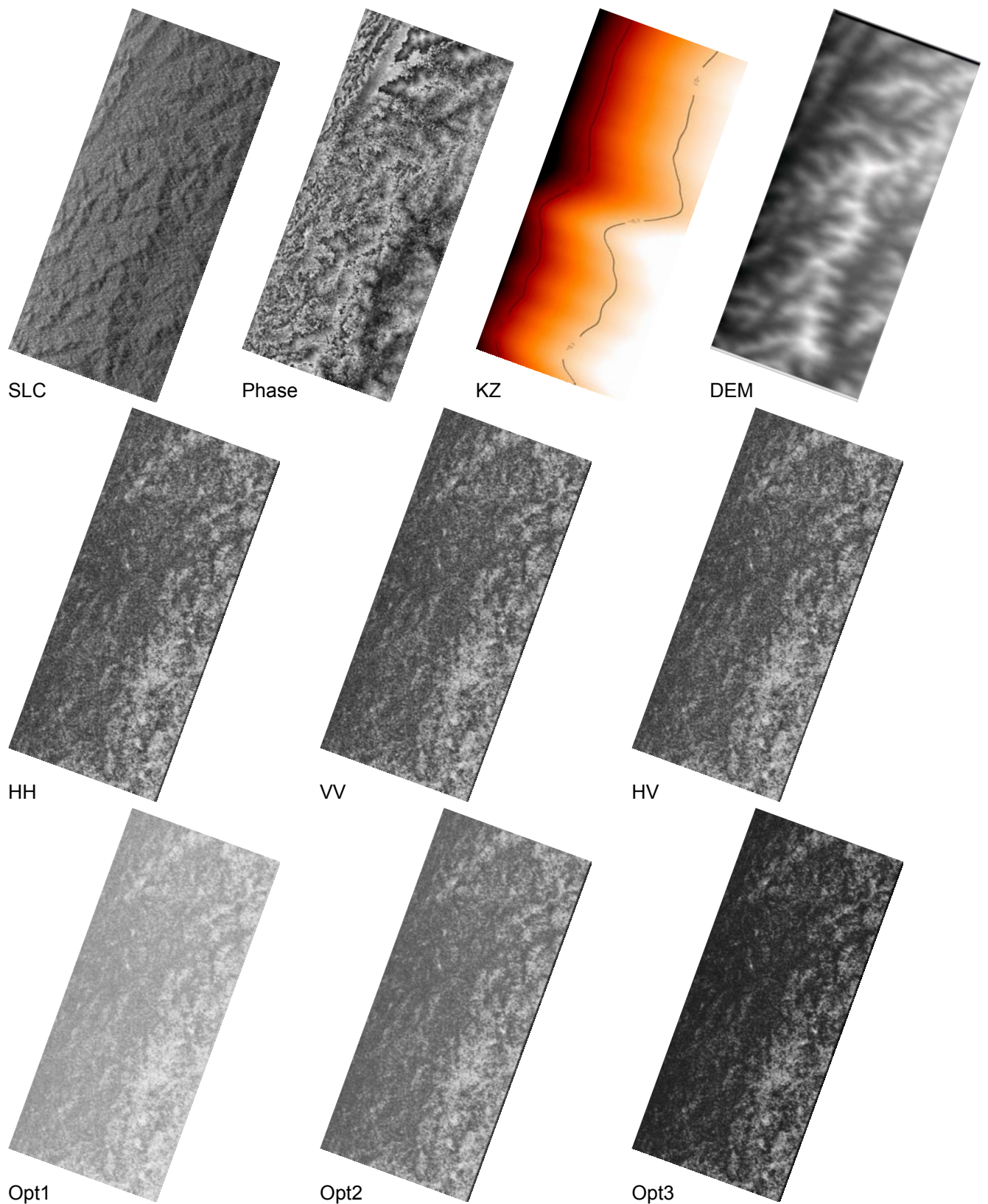


Figure 7.3.14: Test Site Sungai Wain; Interferometric coherences for a 15m spatial baseline in L Band; from left to right upper part: amplitude image (HH polarisation), interferometric phase (HH polarisation), vertical wave-number (kz), X Band Digital Elevation Model (DEM); from left to right middle part: coherence in HH, VV, and XX polarisation; from left to right lower part: optimized coherence 1 to 3

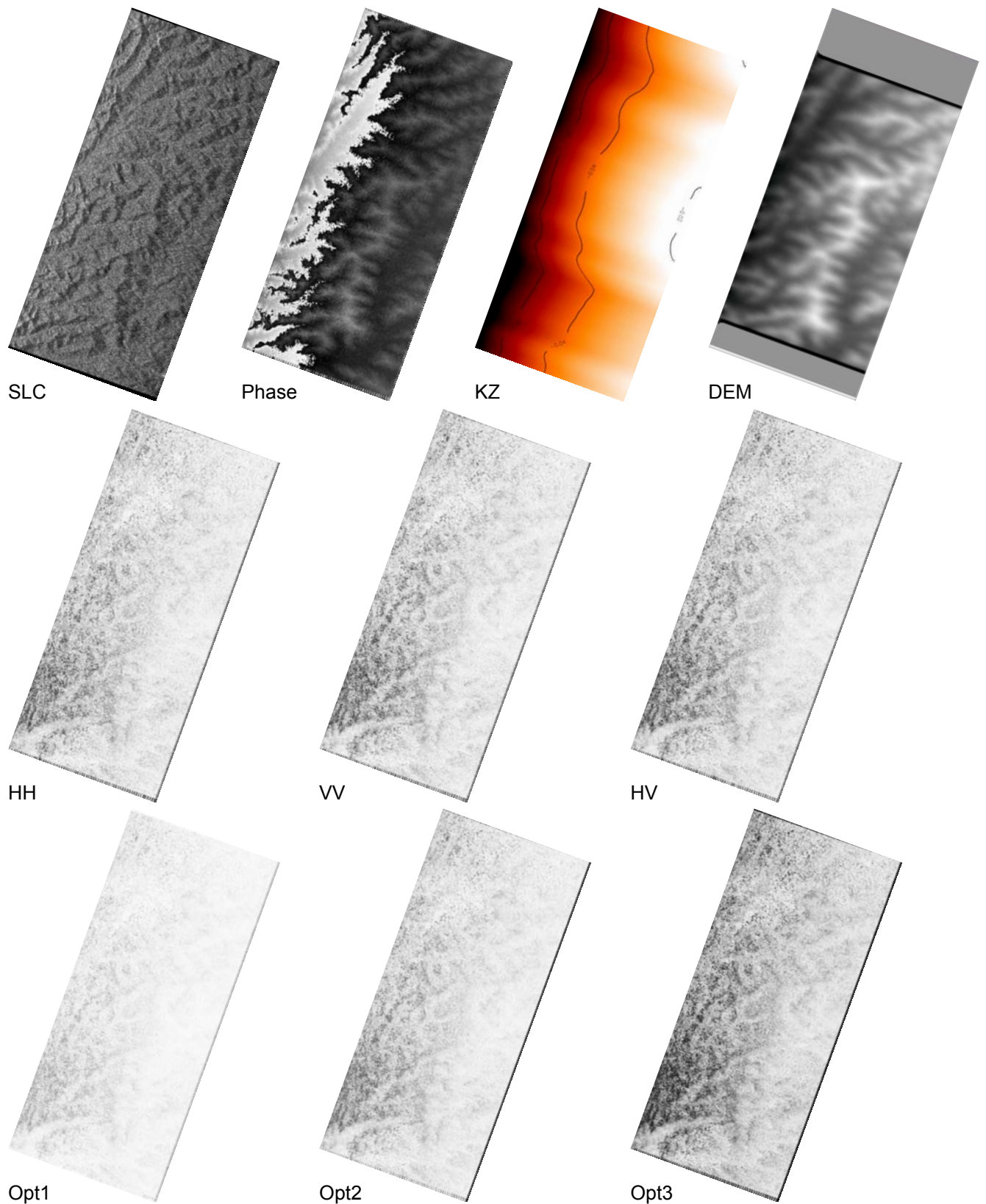


Figure 7.3.15: Test Site Sungai Wain; Interferometric coherences for a 15m spatial baseline in P Band; from left to right upper part: amplitude image (HH polarisation), interferometric phase (HH polarisation), vertical wave-number (kz), X Band Digital Elevation Model (DEM); from left to right middle part: coherence in HH, VV, and XX polarisation; from left to right lower part: optimized coherence 1 to 3

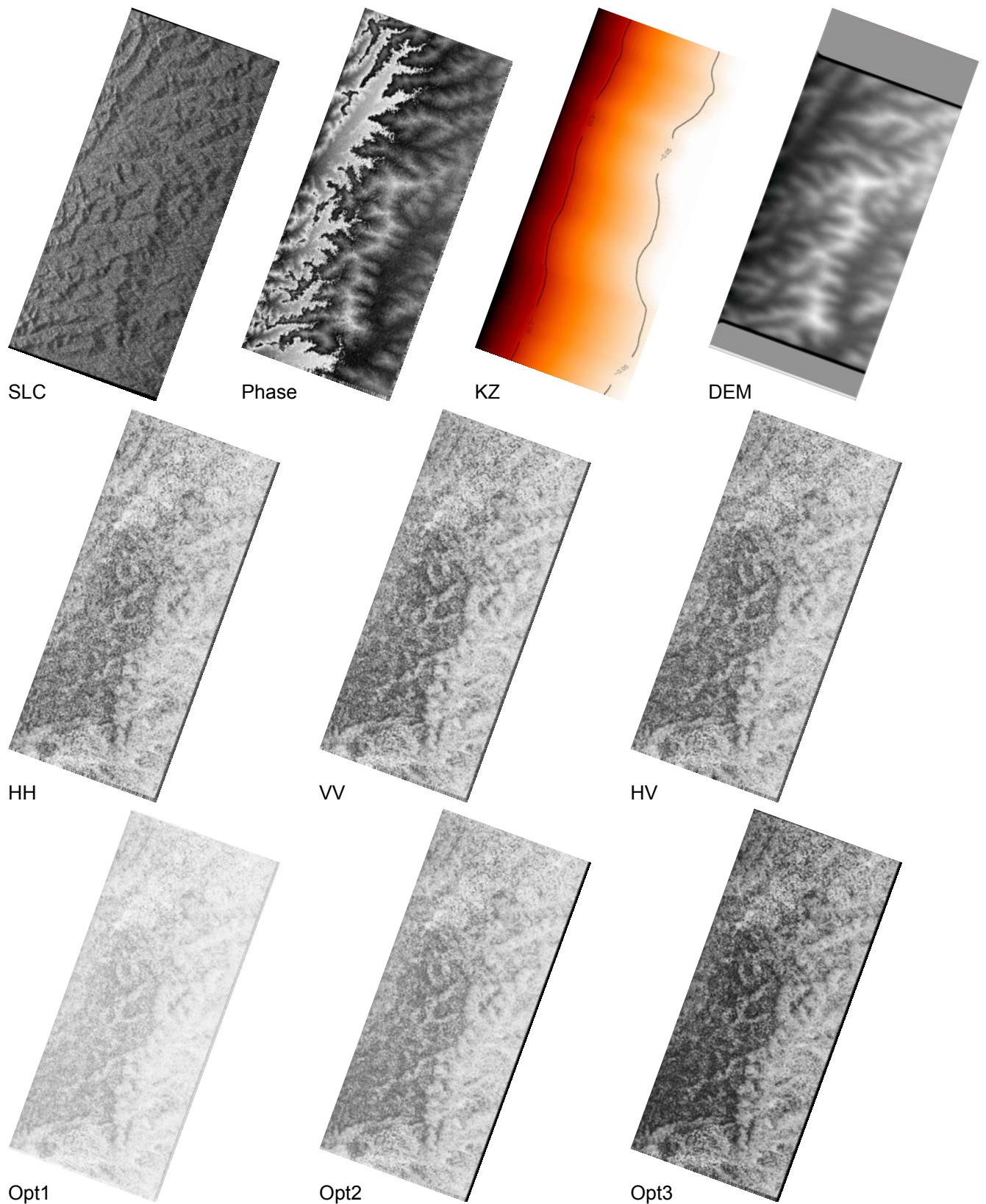


Figure 7.3.16: Test Site Sungai Wain; Interferometric coherences for a 30m spatial baseline in P Band; from left to right upper part: amplitude image (HH polarisation), interferometric phase (HH polarisation), vertical wave-number (kz), X Band Digital Elevation Model (DEM); from left to right middle part: coherence in HH, VV, and XX polarisation; from left to right lower part: optimized coherence 1 to 3

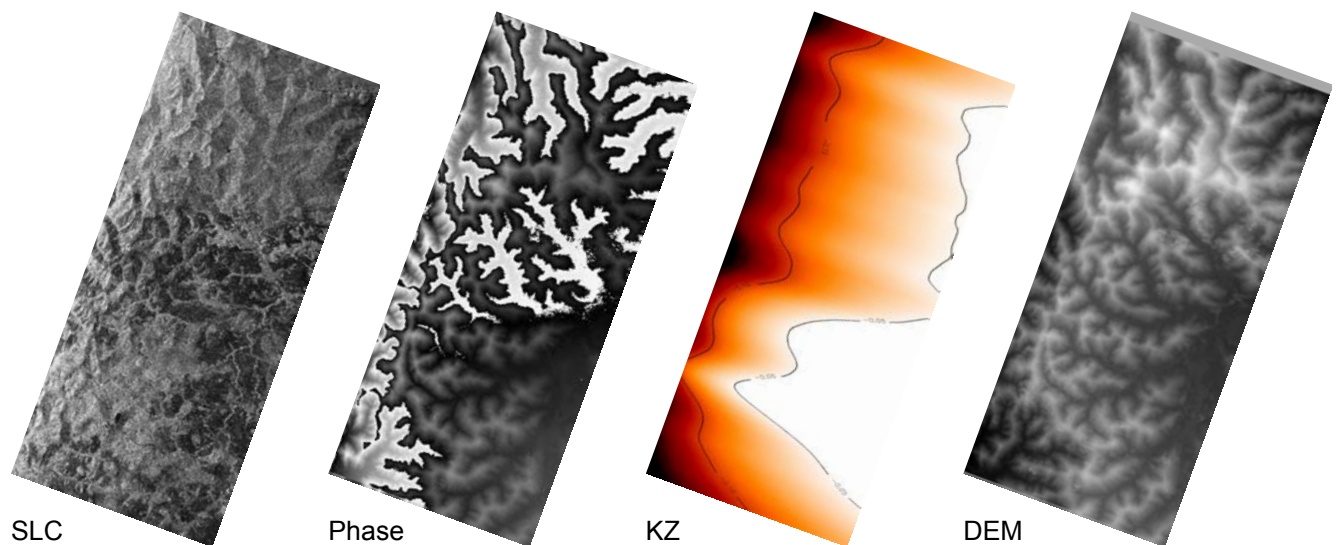
Samboja Lestari - L Band

The last test site discussed here is Samboja Lestari, characterised by rather low and sparse vegetation conditions that reflect on the amplitude (HH) image shown in Figure 7.3.17. As it can be seen in the interferometric phase and X band DEM image of the test site the terrain is quite hilly with variations between 30m and 150m a.s.l. Compared to the scenes discussed before, the interferometric coherence reaches a higher level due to low / sparse vegetation. The variance of the interferometric coherences with polarisation is of course higher because of stronger ground/surface scattering contributions.

With increasing baseline (see in Figure 7.3.18 the corresponding images for the 8m baseline) a variable amount of volume decorrelation – depending on the individual vegetation heights (and local baseline values kz) can be observed.

Samboja Lestari - P Band

Similar as at L band, the amplitude image at P band (see in Figure 7.3.19) evince the diverse scattering processes occurring. The interferometric coherence decreases in far range due to SNR decorrelation. The polarisation dependence of the interferometric coherences is stronger at P band than at L band. For the larger spatial baseline of 30m (see in Figure 7.3.20) volume decorrelation increases over the vegetated areas while the coherence over the surfaces (primarily contributed by SNR decorrelation) remain on the same level.



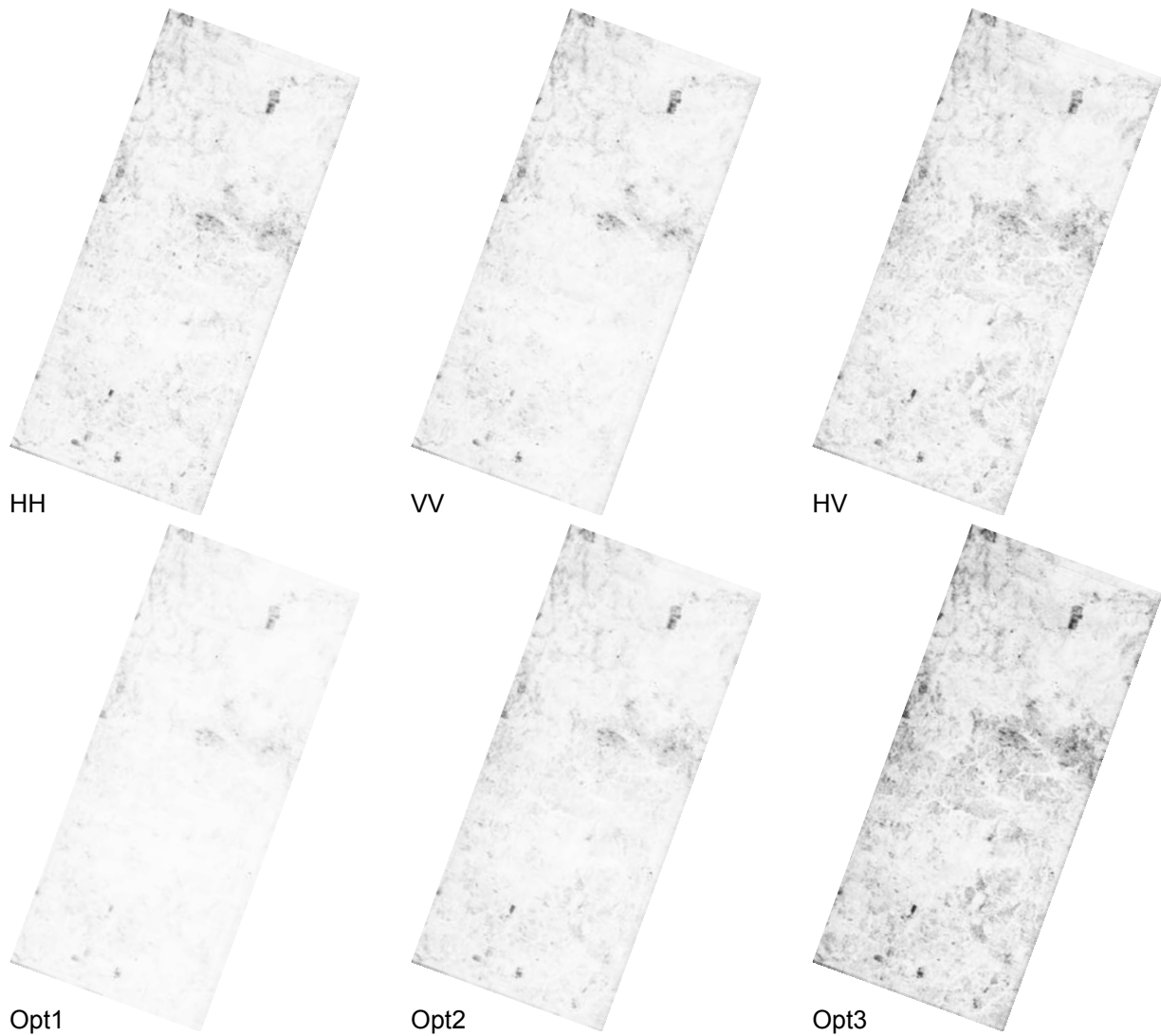


Figure 7.3.17: Test Site Samboja Lestari; Interferometric coherences for a 5m spatial baseline in L Band; from left to right upper part: amplitude image (HH polarisation), interferometric phase (HH polarisation), vertical wave-number (kz), X Band Digital Elevation Model (DEM); from left to right middle part: coherence in HH, VV, and XX polarisation; from left to right lower part: optimized coherence 1 to 3

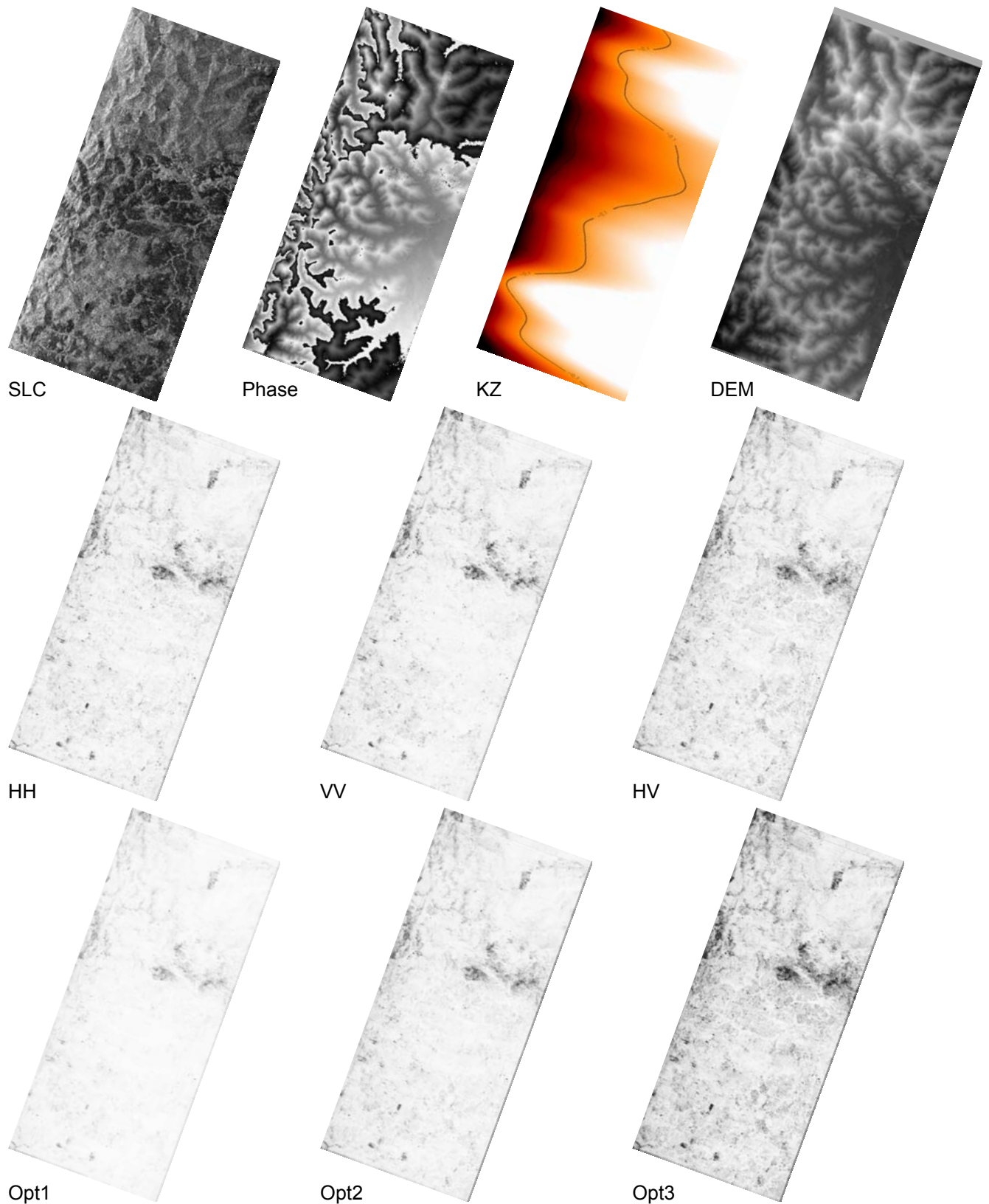


Figure 7.3.18: Test Site Samboja Lestari; Interferometric coherences for a 8m spatial baseline in L Band; from left to right upper part: amplitude image (HH polarisation), interferometric phase of HH polarisation, vertical wave-number (kz), X Band Digital Elevation Model (DEM); from left to right middle part: coherence in HH, VV, and XX polarisation; from left to right lower part: optimized coherence 1 to 3

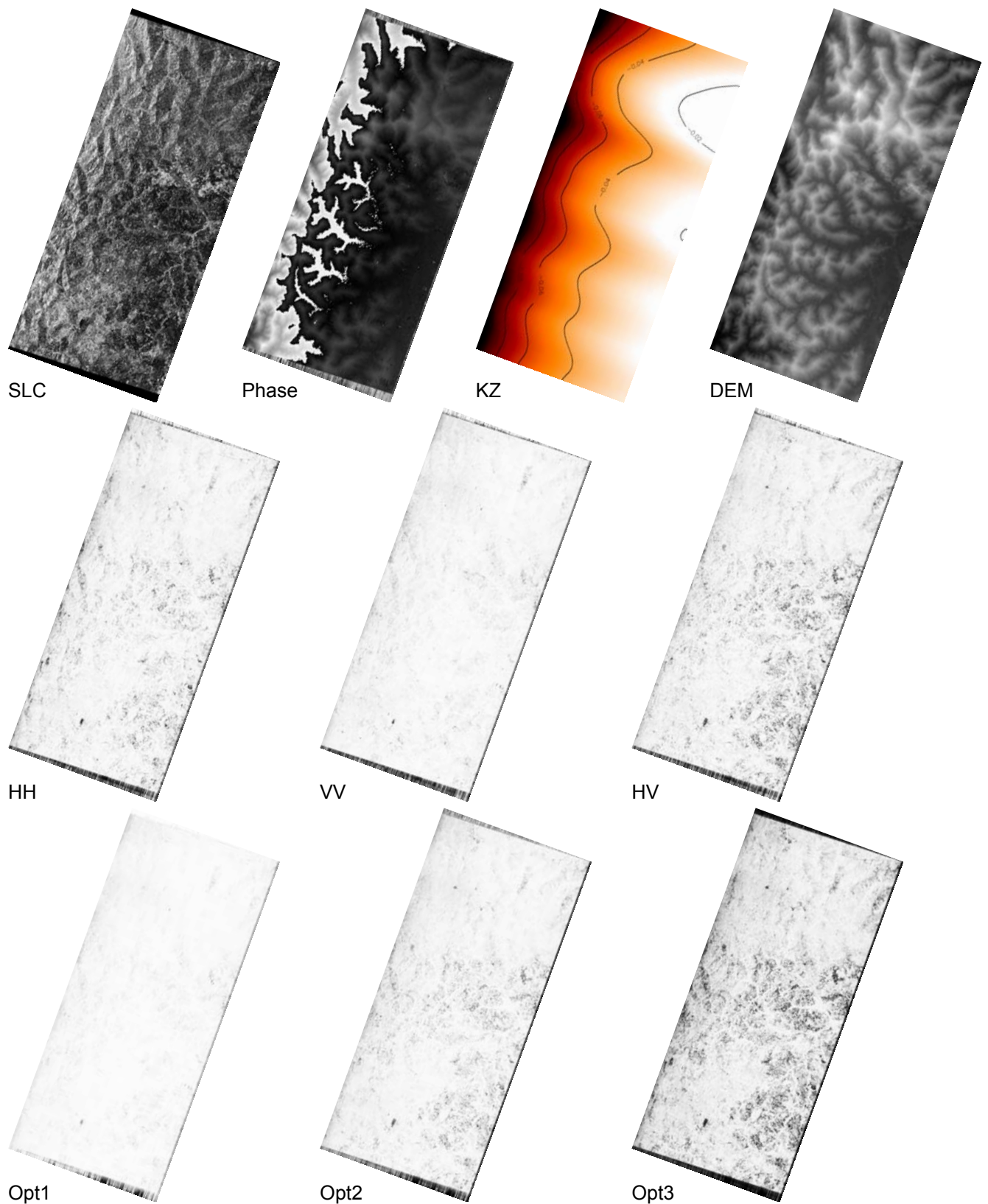


Figure 7.3.19: Test Site Samboja Lestari; Interferometric coherences for a 15m spatial baseline in P Band; from left to right upper part: amplitude image (HH polarisation), interferometric phase (HH polarisation), vertical wavenumber (kz), X Band Digital Elevation Model (DEM); from left to right middle part: coherence in HH, VV, and XX polarisation; from left to right lower part: optimized coherence 1 to 3

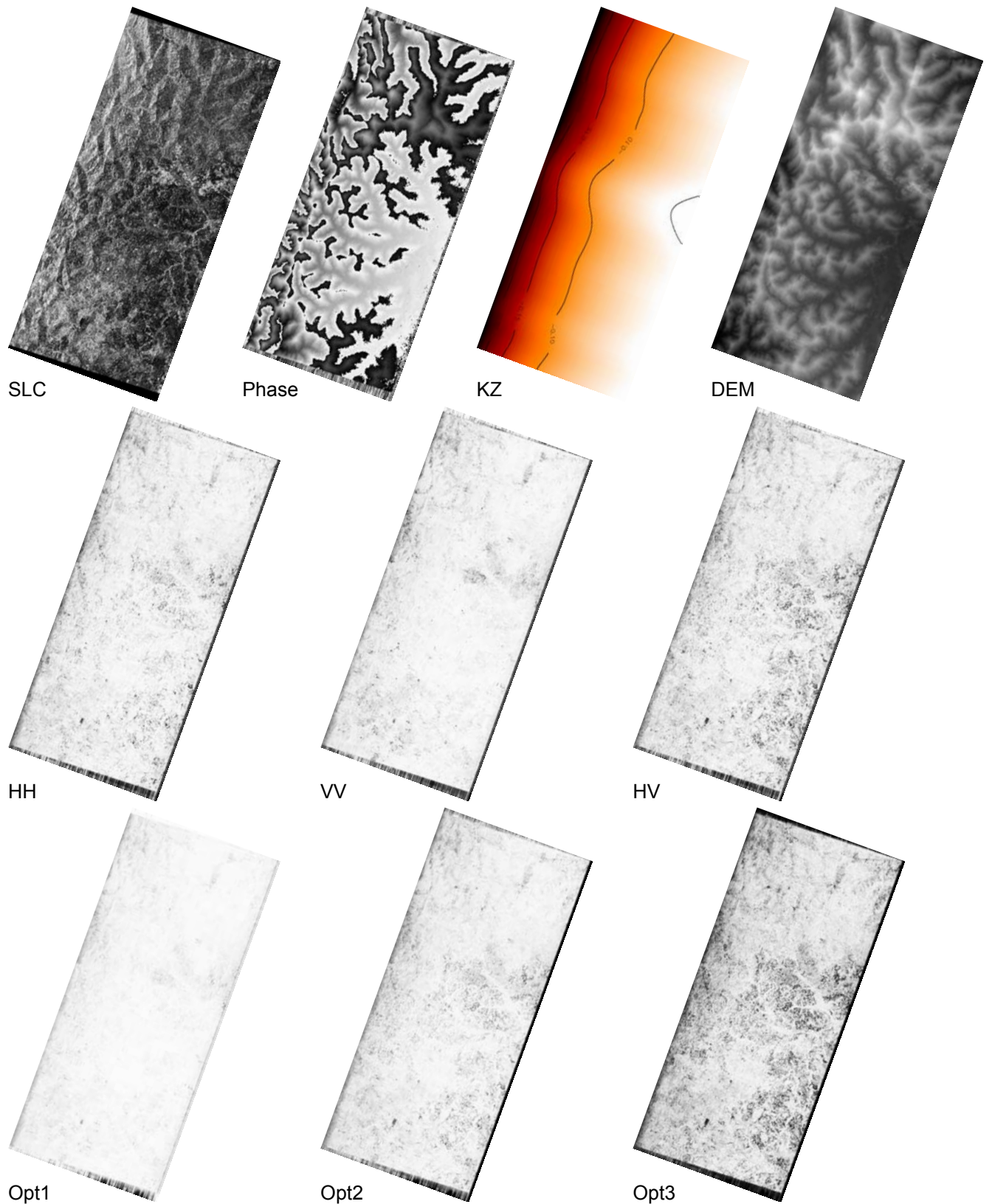


Figure 7.3.20: Test Site Samboja Lestari; Interferometric coherences for a 30m spatial baseline in P Band; from left to right upper part: amplitude image (HH polarisation), interferometric phase (HH polarisation), vertical wave-number (kz), X Band Digital Elevation Model (DEM); from left to right middle part: coherence in HH, VV, and XX polarisation; from left to right lower part: optimized coherence 1 to 3

7.3.4 Conclusions

The high interferometric coherence levels reached over surface-like scatterers across all analysed scenes / baselines and at both frequencies (L and P band) indicate a high system acquisition and data processing quality of the data sets. There was only one site (Mavas C) affected by a weak external RF interference (see Figure 7.3.10 and Figure 7.3.11).

The flight tracks have been flown as accurate as possible under the given conditions. For the Sungai Wain and Samboja Lestari sites the flight conditions where (in general) very good resulting into optimum flight tracks (deviations are on the order of $\pm 2\text{m}$ in horizontal and $\pm 2\text{-}5\text{m}$ in the vertical direction). This is an excellent performance. For the Mawas test site the weather conditions where rougher (Monsoon storm/wind) affecting off course the flight performance with deviations on the order of up to 5m in horizontal and about 5m in the vertical direction.

The impact of the flight-track deviations on the vertical-wavenumber - which is the key parameter for the interpretation / inversion of the interferometric phase and coherence data - depends on the actual baseline configuration. Small baselines are stronger affected than large ones. In consequence at L-band the smaller spatial baselines (primarily the 5m baselines) are stronger affected than the larger ones (10 and 15m) as it can be seen in the kz images in Figure 7.3.7, Figure 7.3.12, Figure 7.3.17 and Figure 7.3.18. At P band the (nominal) baselines have been selected to be by a factor of three larger than at L band the impact of the flight track deviations is of secondary importance.

On the other hand, some of the baselines led to maybe too low coherences levels due to the high vegetation heights (see Figure 7.3.4, Figure 7.3.9 and Figure 7.3.14) and may complicate quantitative inversion. Also in this case the L band data appear to be more affected because of the weaker ground scattering component. However, in all of these cases the smaller baselines provide sufficient high coherence levels.

7.3.5 Quantitative Pol-InSAR Data Analysis

Forest Height Inversion

It is known that the (complex) volume decorrelation contribution $\tilde{\gamma}_V$ of the interferometric coherence is directly linked to the vertical distribution of scatterers $F(z)$ through a (normalized) Fourier transformation relationship [15]

$$\tilde{\gamma}_V = \exp(i\kappa_z z_0) \frac{\int_0^{h_V} F(z') \exp(i\kappa_z z') dz'}{\int_0^{h_V} F(z') dz'} \quad -2)$$

where κ_z is the effective vertical (interferometric) wavenumber that depends on the imaging geometry and the radar wavelength λ

$$\kappa_z = \frac{\kappa \Delta\theta}{\sin(\theta_0)} \quad \text{and} \quad \kappa = \frac{4\pi}{\lambda} \quad -3)$$

and $\Delta\theta$ is the incidence angle difference between the two interferometric images induced by the baseline. z_0 is a reference height.

The estimation of vertical forest structure parameters from interferometric measurements can be addressed as a two step process: In the first step (modelling) $F(z)$ is parameterized in terms of a more or less limited set of physical forest parameters that are related through Eq. 2 to the interferometric coherence. In the second step (inversion), the volume contribution of the measured interferometric coherence is then used to estimate $F(z)$ and to derive the corresponding parameters. A widely and successfully used model for $F(z)$ is the so called Random Volume over Ground (RvoG), a two layer model consisting of a volume and a ground layer [16][8]

$$F(z) = \tilde{m}_V \exp\left(\frac{2\sigma}{\sin(\theta_0)} z\right) + m_G \delta(z - z_0) \quad -4)$$

where m_V and m_G are the ground and volume scattering amplitudes and σ a mean extinction coefficient. Eq. 2 leads to

$$\tilde{\gamma}_V = \exp(i\kappa_z z_0) \frac{\tilde{\gamma}_{V0} + m}{1 + m} \quad -5)$$

where $\varphi_0 = \kappa_z z_0$ is the phase related to the ground topography z_0 and m the effective ground-to-volume amplitude ratio accounting for the attenuation through the volume

$$m = \frac{m_G}{m_V I_0} \quad -6)$$

$\tilde{\gamma}_{V0}$ is the volume decorrelation caused in the absence of the ground layer (i.e. $m_G = 0$)

$$\tilde{\gamma}_{V0} = \exp(i\kappa_z z_0) \frac{\int_0^{h_V} \exp(i\kappa_z z') \exp\left(\frac{2\sigma z'}{\cos\theta_0}\right) dz'}{\int_0^{h_V} \exp\left(\frac{2\sigma z'}{\cos\theta_0}\right) dz'} \quad -7)$$

Neglecting temporal decorrelation and assuming a sufficient calibration/compensation of system (e.g. SNR) and geometry (range/azimuth spectral shift) induced decorrelation contributions Eq. 7 can be inverted in terms of a quad-pol single baseline acquisition [8], **Fehler! Verweisquelle konnte nicht gefunden werden..** In this case the (regularised) inversion problem is balanced with five unknowns $(h_V, \sigma, m_{1-2}, \phi_0)$ and three measured complex coherences $[\tilde{\gamma}(\bar{w}_1) \tilde{\gamma}(\bar{w}_2) \tilde{\gamma}(\bar{w}_3)]$ each for any independent polarization channel providing estimates for forest height **Fehler! Verweisquelle konnte nicht gefunden werden..**

$$\min_{h_V, \sigma, m_1, \phi_0} \left\| [\tilde{\gamma}(\bar{w}_1) \tilde{\gamma}(\bar{w}_2) \tilde{\gamma}(\bar{w}_3)]^T - [\tilde{\gamma}_V(h_V, \sigma, m_1) \tilde{\gamma}_V(h_V, \sigma, m_2) \tilde{\gamma}_{V0} \exp(i\phi_0)]^T \right\| \quad -8)$$

Eq. 8 is used to invert Pol-InSAR data sets from the Sungai Wain and Mawas test sites at L- and P-band.

Coherence Calibration

As discussed in the previous section, the inversion of forest height is based on the evaluation of the volume decorrelation contribution of the interferometric coherence. Non-volumetric decorrelation contributions bias the obtained height estimates.

The plots in Figure 7.3.22 quantify the estimation error due to un-compensated non-volumetric decorrelation contributions: On the left hand side the height error for a 20m volume is plotted as a function of the baseline (expressed in form of the vertical wavenumber kZ) for different decorrelation contributions. Accordingly, already a small decorrelation contribution of 0.95 causes at a kZ of 0.1 a height error larger than 10%. Furthermore, the plot indicates that small baselines are stronger affected than large baselines and require therefore a more accurate coherence calibration. On the right hand side, the height error is plotted as a function of forest height for a constant baseline ($kZ=0.1$) for different decorrelation contributions. Similar, the plot indicates that lower forest-heights are stronger affected than higher ones.

The measured/estimated interferometric coherences are in general affected by additional system and/or processing induced decorrelation effects, that have to be calibrated/compensated before inversion. The individual decorrelation contributions are presented in Figure 7.3.21. The most relevant ones effecting the available E-SAR data sets are the Range Spectral (γ RG), SNR (γ SNR), Coregistration (γ COR), and Temporal (γ TEMP) decorrelation contributions as well as - - the Estimation Bias (γ BIAS) contribution. These individual contributions/corrections are discussed in the following.

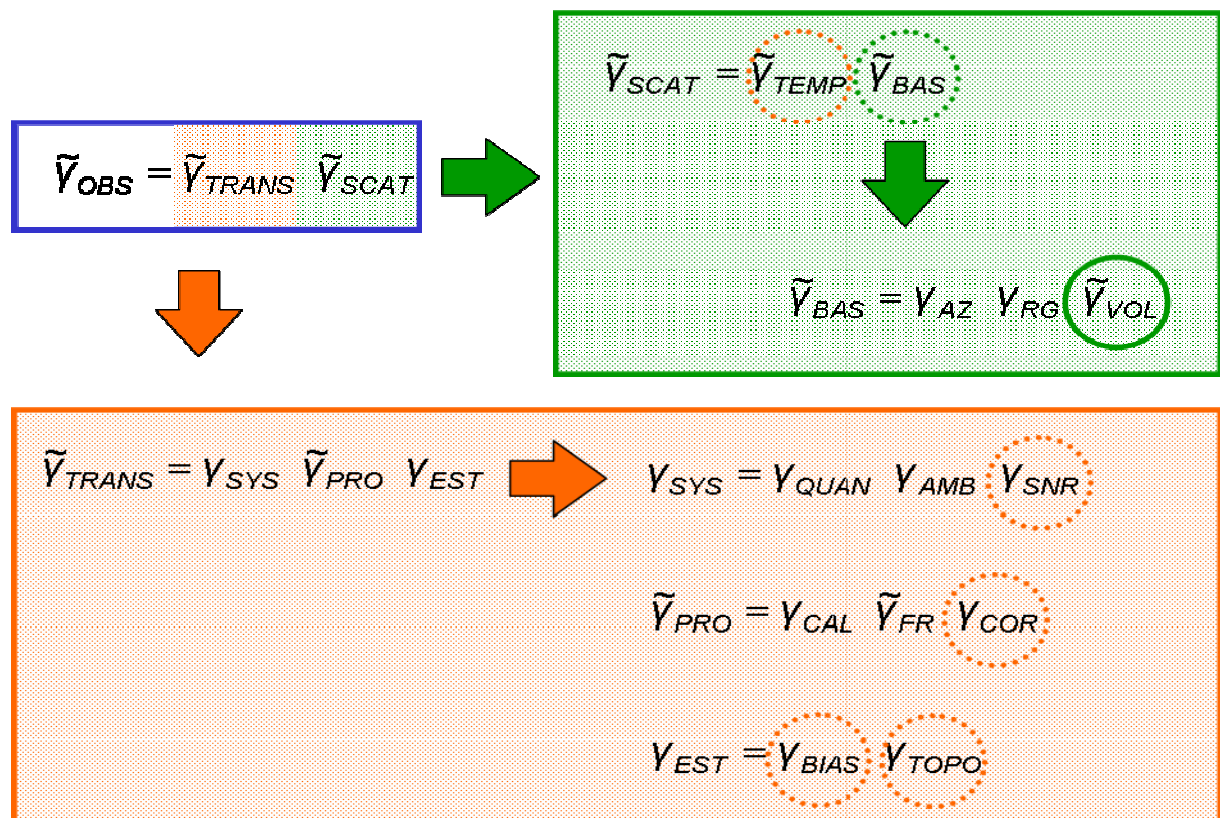


Figure 7.3.21: Decorrelation Effects: γ SCAT=Scatterer Induced Decorrelation: γ TEMP=Temporal Decorrelation, γ BAS=Baseline Decorrelation, γ AZ=Doppler Spectral Decorrelation, γ RG=Range Spectral Decorrelation, γ VOL=Volume Decorrelation. γ SYS=System Induced Decorrelation: γ QUAN =Quantisation Decorrelation, γ AMB=Ambiguities Decorrelation, γ SNR =SNR Decorrelation. γ PRO=Processing Decorrelation: γ CAL=Calibration, Decorrelation, γ FR=Faraday Rotation Compensation, (not relevant for airborne systems), γ EST=Coherence Estimation Bias, γ COR=Coregistration Decorrelation. γ EST=Estimation Bias: γ BIAS=Coherence Estimation Bias, γ TOPO=Topography Induced Coherence Bias.

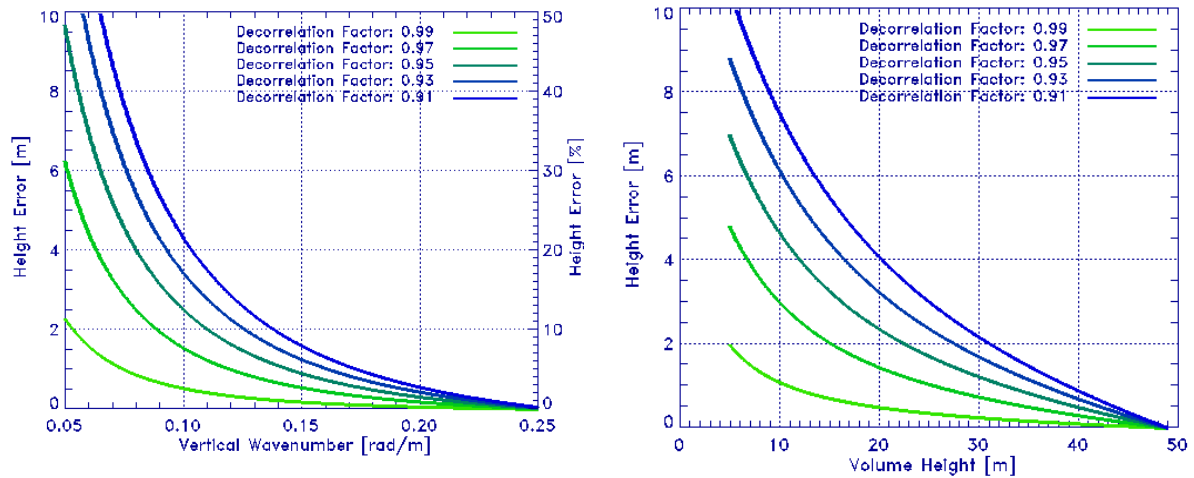


Figure 7.3.22: Impact of uncompensated decorrelation effects. Left: Height error against vertical wavenumber for different decorrelation factors assuming a constant volume height of 20m. Right: Height error against volume height for different decorrelation factors for a constant vertical wavenumber of 0.1.

SNR Decorrelation: γ_{SNR} is defined as Fehler! Verweisquelle konnte nicht gefunden werden.

$$\gamma_{SNR} = \frac{1}{1 + (SNR)^{-1}} \quad \text{with} \quad 0 \leq \gamma_{SNR} \leq 1 \quad -9)$$

where

$$SNR = \frac{\text{Signal Power}}{\text{Noise Power}} \quad -10)$$

Accordingly, a SNR ratio of 0dB results in a decorrelation factor of 0.5 as displayed on the left hand side of Figure 7.3.23.

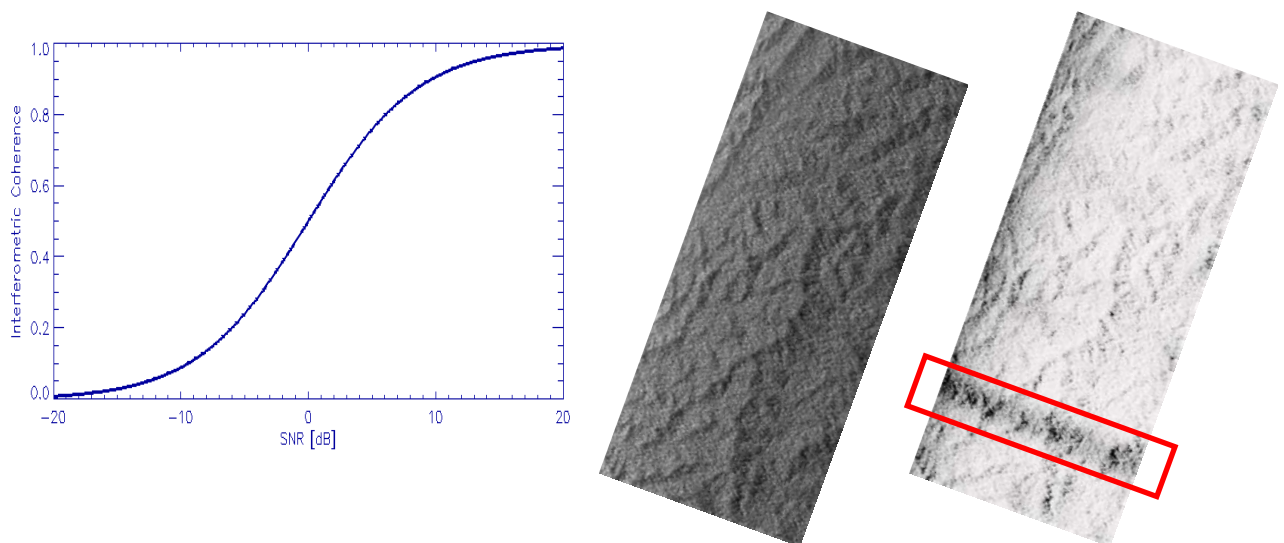


Figure 7.3.23: SNR Decorrelation; left: interferometric coherence against SNR, middle: Amplitude image of Sungai Wain scene; right: SNR Decorrelation of Sungai Wain scene scaled from 0.9=black to 1=white, red box shows disturbance in the signal due to a motion compensation error.

SNR can't be estimated –within the required accuracy – in a direct way so that the approach proposed in Fehler! Verweisquelle konnte nicht gefunden werden. has been applied. Accordingly, for reciprocal scatterers the correlation between the cross-pol channels HV and VH is only disturbed by the noise component. The HV-VH coherence obtained for the Sungai Wain scene at L band is shown in Figure 7.3.23. The red box marks a distortion due to a motion compensation error.

Range Spectral Decorrelation & Terrain Compensation: Range spectral decorrelation is caused by the (slightly) different projection of the ground-range (spectral) component into the two band-limited SAR images. Assuming a rectangular transfer function in range the correlation decreases linearly with increasing angular baseline $\Delta\theta$

$$\gamma_{RG} = 1 - \frac{|\Delta f_{RG}|}{W_{RG}} \quad -11)$$

where $\Delta f_{RG} = f_0 \Delta\theta / \tan(\theta_0 - \alpha)$ is the range spectral shift where W_{RG} is the (range) system bandwidth f_0 the central frequency, θ_0 the incident angle and α the terrain slope angle. In the case of airborne SAR systems range spectral decorrelation varies across range due to the variation of the incident angle θ_0 (see Figure 7.3.24 left hand side) and with topography due to the variation of α .

α is estimated from the X band DEM, (a low-pass filter has to be applied to reduce the vegetation induced DEM variation and obtain the low-frequency terrain variation). Figure 7.3.24 on the right shows the range spectral decorrelation after terrain compensation.

Vertical Wavenumber Correction: As already mentioned, terrain variation implies a change of the incidence angle. The fact that the vertical wavenumber that scales phase to height differences

$$KZ = \frac{k\Delta\Theta}{\sin(\Theta - \alpha)}, \quad k = \frac{4\pi}{\lambda} \quad -12)$$

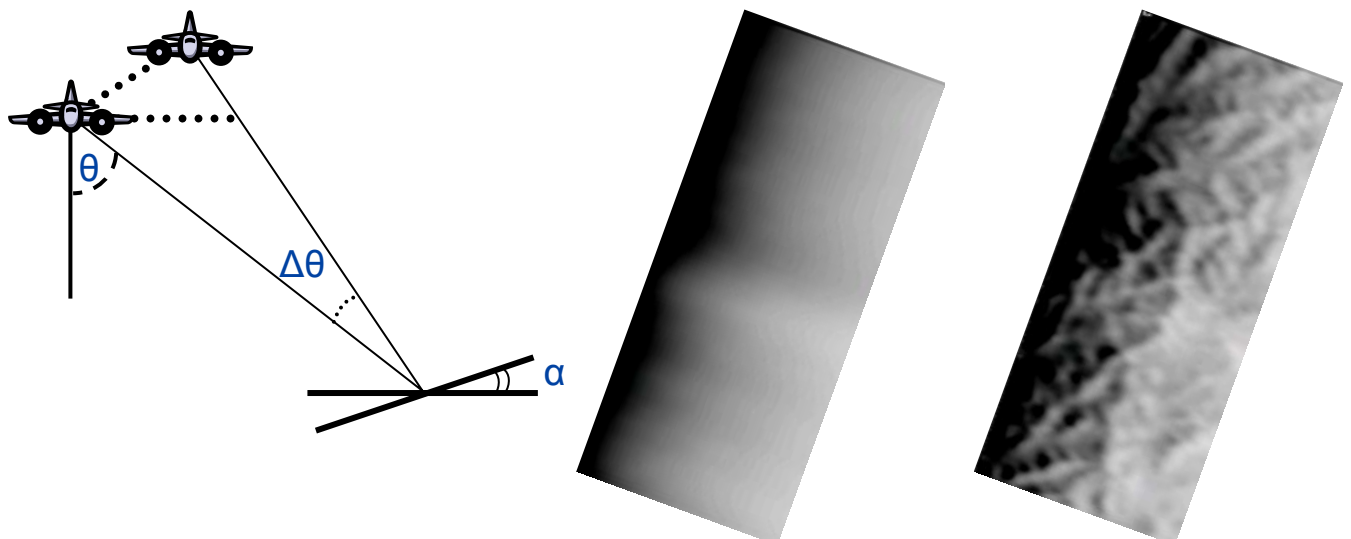


Figure 7.3.24: Example of range spectral decorrelation for the Sungai Wain scene in L Band; left: Acquisition geometry, θ =incidence angel, $\Delta\theta$ =difference in incidence angle, α =terrain slope; middle: range decorrelation for Sungai Wain scene; right: terrain corrected range decorrelation

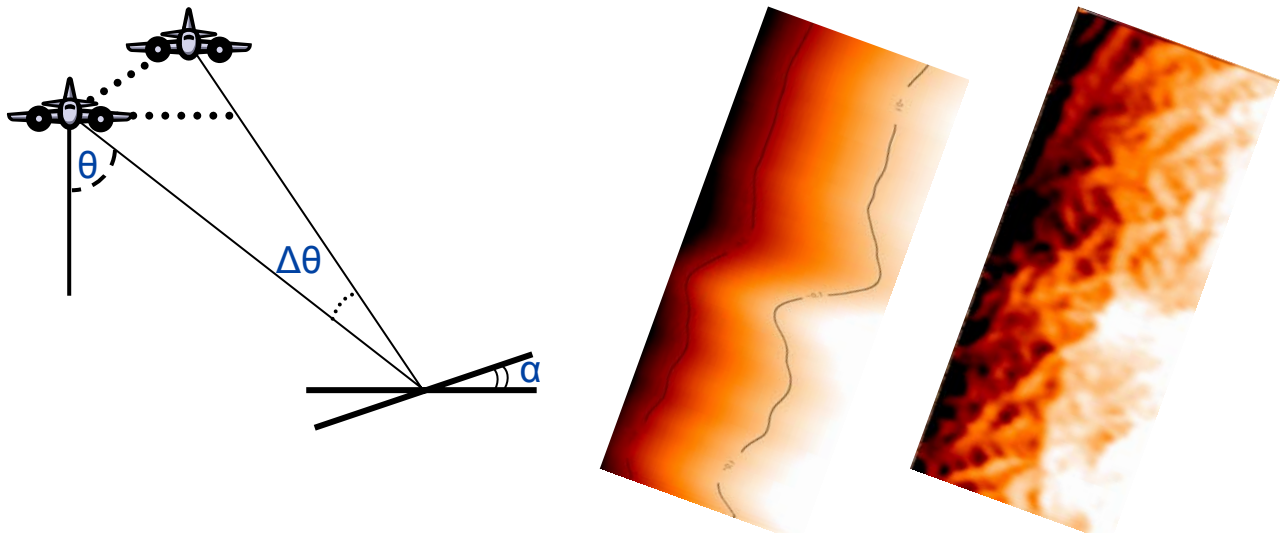


Figure 7.3.25 Example of vertical wavenumber terrain correction for the Sungai Wain scene at L band. Left: Acquisition geometry: θ =incidence angel, $\Delta\theta$ =difference in incidence angle, α =terrain slope. Middle: Vertical wavenumber scaled from 0.9=black to 1=white; Right: Terrain corrected vertical wavenumber.

is a function of the incidence angle θ makes a terrain correction necessary. As an example, the vertical wavenumber images for the Sungai Wain scene are shown in Figure 7.3.25 before (left) and after terrain correction (right).

Coregistration Decorrelation: The miss-registration of the interferometric images causes a decorrelation according to:

$$\gamma_{COR} = \frac{\sin(\pi\delta_{AZ})}{\pi\delta_{AZ}} \frac{\sin(\pi\delta_{AZ})}{\pi\delta_{AZ}} \quad -13)$$

where δ_{AZ} and δ_{RG} is the relative shift between the images in azimuth and range respectively. It is obvious that a shift of a full resolution cell leads to a total decorrelation. Assuming a coregistration accuracy of about 1/10 of an image pixel leads to $\gamma_{COR} = 0.97$. Note that the coregistration accuracy depends locally on the coherence level. In low coherence areas the coregistration performance decreases increasing (locally) the decorrelation.

Mask Generation: Even after coherence calibration, geometrical and coherence constrains still may limit the inversion performance. To avoid this, before inversion, ill-conditioned regions have to be masked out. In this sense, three different criteria have been applied:

1. Coherence Criterion: Low coherences are affected by large phase variance **Fehler! Verweisquelle konnte nicht gefunden werden.** making accurate inversion at a reasonable spatial resolution not-possible. Therefore, areas with coherences lower than 0.3 have been excluded. The corresponding mask is shown in Figure 7.3.26 (Image 2), and acts across the whole image.

2. Large kZ Criterion: At large effective baselines (i.e. large kZ values) the sensitivity of the coherence to forest height can saturate at heights lower than the forest heights in the scene. Such areas are masked out. The corresponding mask (threshold: $kZ < 0.15$) is shown in Figure 7.3.26 (Image 3). The mask acts primarily in near range.

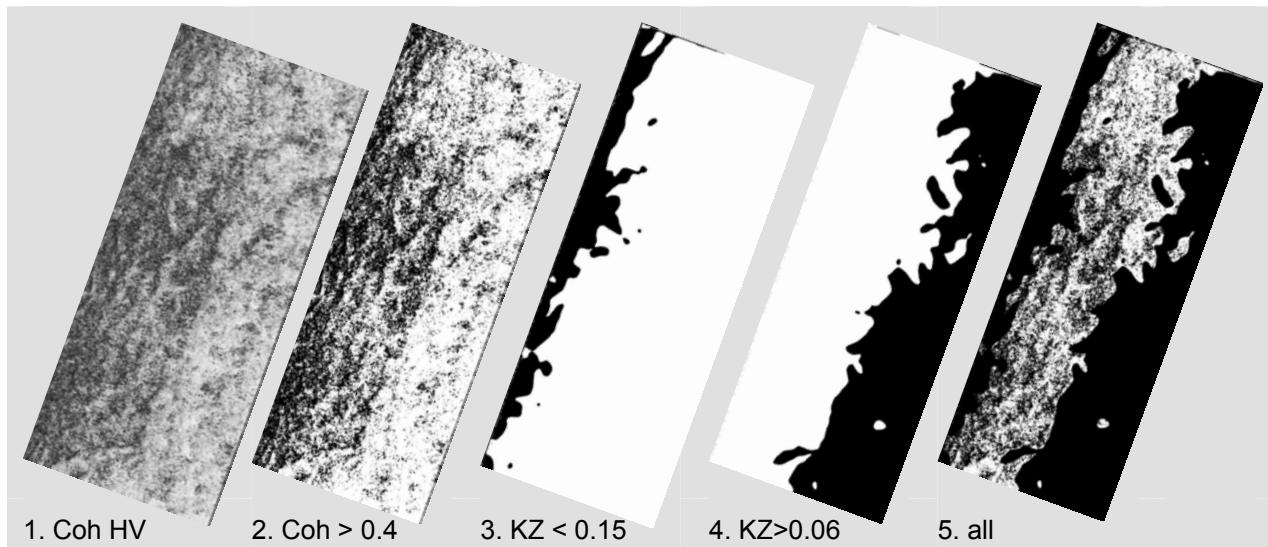


Figure 7.3.26: Mask generation for an L Band scene of Sungai Wain 1. Coherence image of HV Polarisation, 2. Coherence mask, 3. KZ mask for low values, 4. KZ mask for high values, 5. Combination of all masks, valid points are white

3. Low kZ Criterion: At small effective baselines (i.e small kZ values) the unfavourable coherence to height scaling leads to high height errors for small residual non-volumetric decorrelations. Such areas are also masked out. The corresponding mask (threshold: $kZ > 0.05$) is shown in Figure 7.3.26 (Image 4). The mask acts primarily in near range.

The combination of all three masks is finally shown in Figure 7.3.26 (Image 5).

Forest Height Validation - Sungai Wain Test Site.

After height inversion and masking out of non valid points, the obtained forest height maps at L and P band are shown in Figure 7.3.27, where on the left are the L and on the right the P band estimates. Both height maps are scaled from 0 to 60 m. The comparison of the obtained heights does not show up significant differences. Both images cover the same height range and reflect a similar forest height structure. The height variance is higher at L band than at P band because of the lower coherence level.

A detail of the obtained forest height maps is shown in Figure 7.3.28 (also scaled from 0 to 60m and black are the masked areas). As the mask applies in both images at different pixels a direct comparison between the L and P band estimates can only be performed on the basis of the common points. Figure 7.3.29 shows a pixel based comparison between the L and P band heights. Obviously, both measurements are well correlated (with a correlation about 0.84, i.e. $P \text{ Height} = 0.84 \text{ L Height}$). In other words, the height estimates in P band are (constantly) about 16% lower than the ones at L band. The corresponding height histograms follow almost a Gaussian distribution with mean value at L band of about 34m and at P band about 29m.

There are two possible reasons for this behavior: The first one is the reduced sensitivity of P band to (volume) height variations caused by the low extinction values. This can lead to an underestimation of forest height at P band in less dense forest environments. The second one is the impact of temporal (or other) decorrelation at the L band that can lead to an overestimation of forest height.

The white rectangle in the height map of Figure 7.3.27 indicates the location of the ground measurement plot with forest height varying mainly between 15m and 40m. The available ground measurements are represented in three graphs in Figure 7.3.30: The plot on the right represents the

structure and height of the Sungai Wain forest; The upper left plot the height distribution of all measured trees; and the lower left plot the diameter at breast height against (DBH) the forest height.

The first plot shows that most of the heights are between 10m and 20m, much lower than the estimated

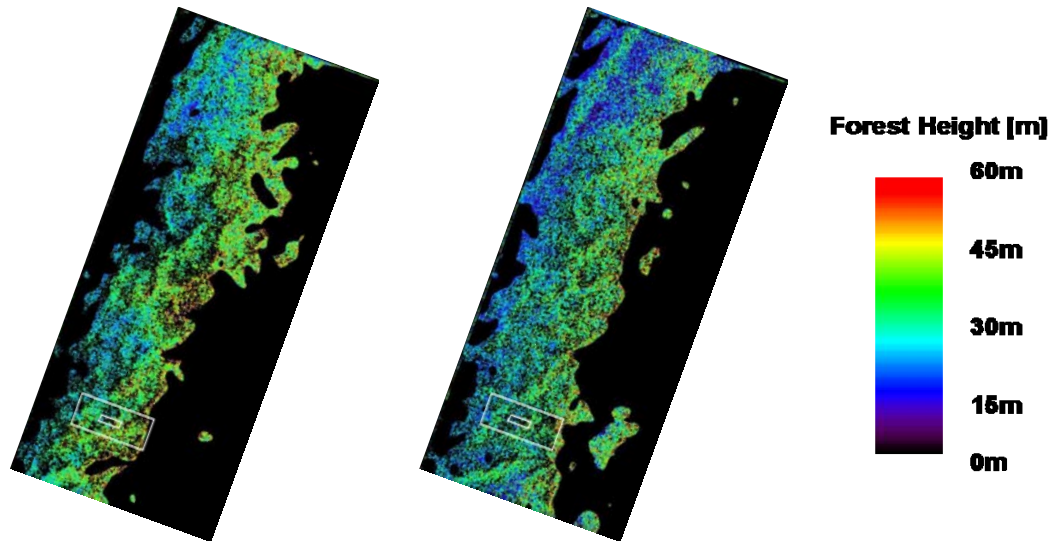


Figure 7.3.27: Height map for the Sungai Wain forest: left: L-band 10m baseline, right: P-band 30m baseline. Black are the masked areas; the white rectangle indicates the position of the ground measurements plot

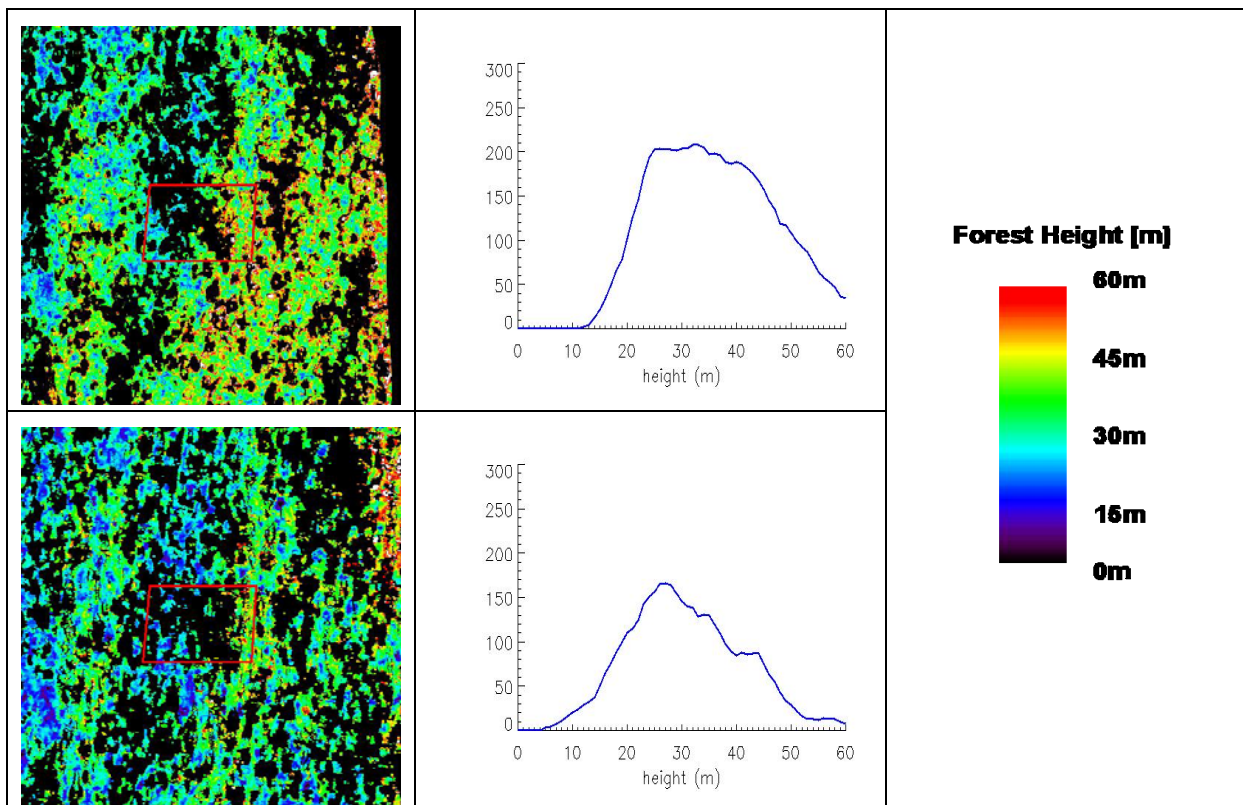


Figure 7.3.28: Detail of height maps for the Sungai Wain forest: top: L-band 10m baseline, bottom: P-band 30m baseline; masked areas are black

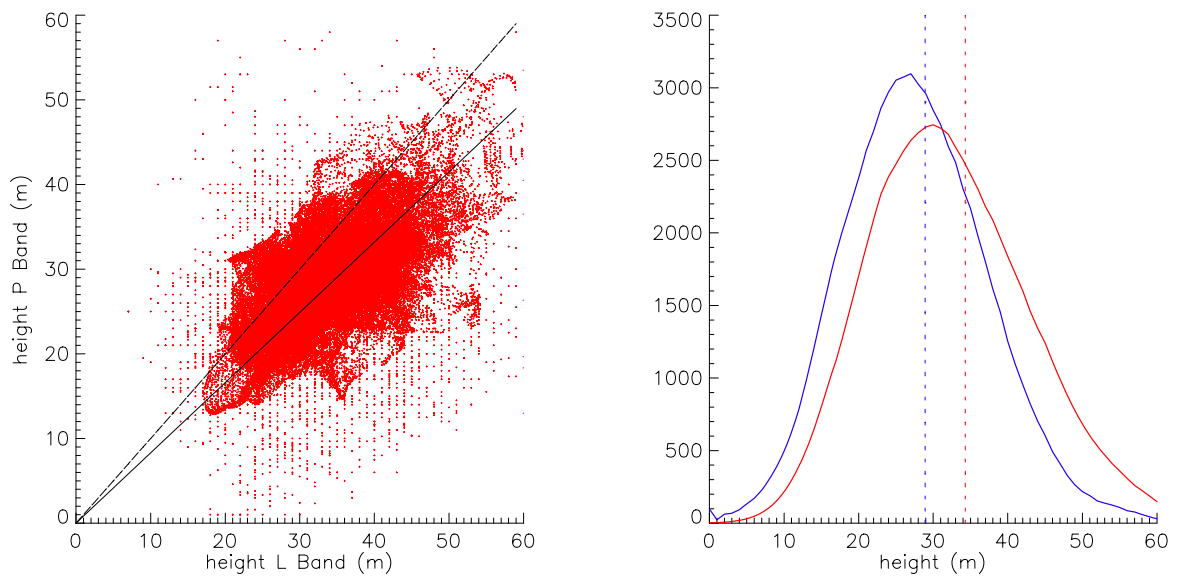


Figure 7.3.29: Comparison L and P Band heights for Detail (Figure 7.3.28) of Sungai Wain; left: Plot L Band heights against P Band heights (low pass filtered); right: histogram, P Band=blue, L Band=red

forest heights. However, looking on the other two plots it becomes clear that the estimated radar heights do not correspond to every single tree: Furthermore, they reflect the height of the higher trees which form the upper canopy layer. Assuming that the diameter at breast height (DBH) reflects

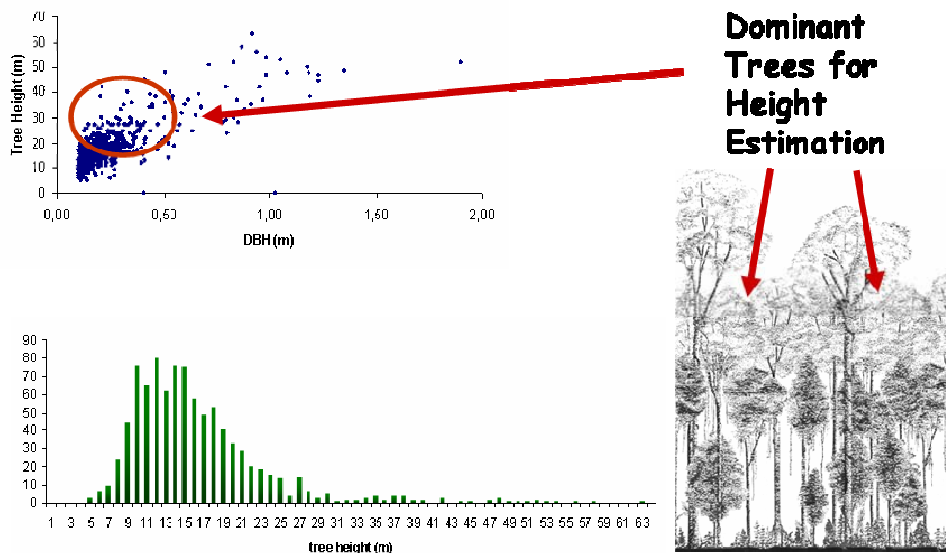


Figure 7.3.30: Ground measurements of Sungai Wain plot; upper left: DBH (diameter in breast height) – height distribution; lower left: stem number – tree height distribution; lower right: structural sketch of lowland dipterocarp forest; the red circle in the upper left shows the dominant trees which represent the height of the forest

the dominance of a tree within the forest, one can conclude that the canopy of an uneven aged forest is formed by a small number of trees, as indicated by the red circle in the upper left plot of Figure 7.3.30. The height of these trees fits to the estimated height from the radar data.

Forest Height Validation - Mawas Test Site.

Height inversion at L and P band was also performed for the Mawas test site. The obtained estimates are shown in Figure 7.3.31. Also here, both L and P band cover the same range of forest heights, which is lower in the Mawas region than in Sungai Wain. Forest structures like logging trails and skirts of the wood can be clearly detected at both frequencies.

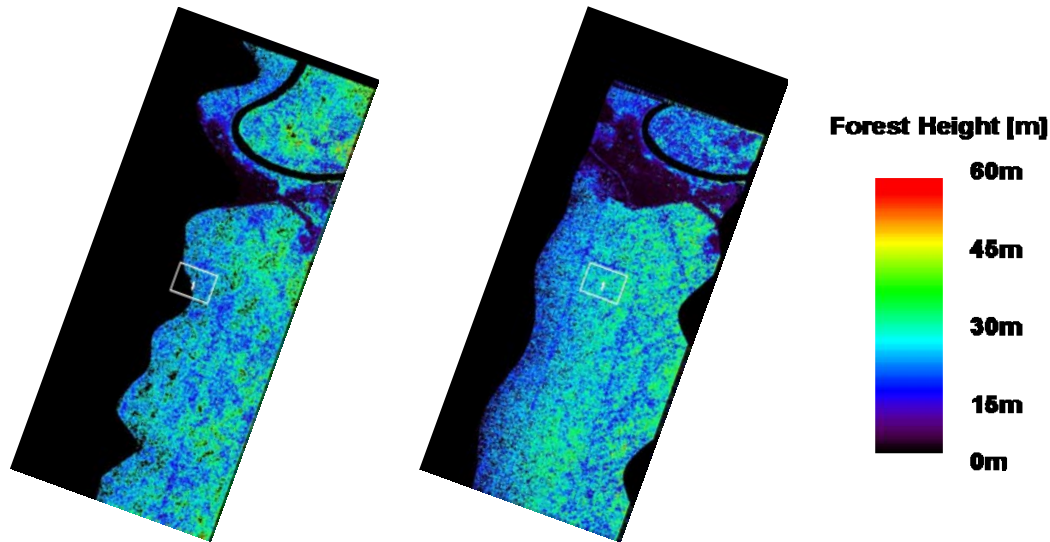


Figure 7.3.31: Height map for the Mawas forest: left: L-band 10m baseline, right: P-band 30m baseline. Black are the masked areas; the white rectangle indicates the position of the ground measurement plot.

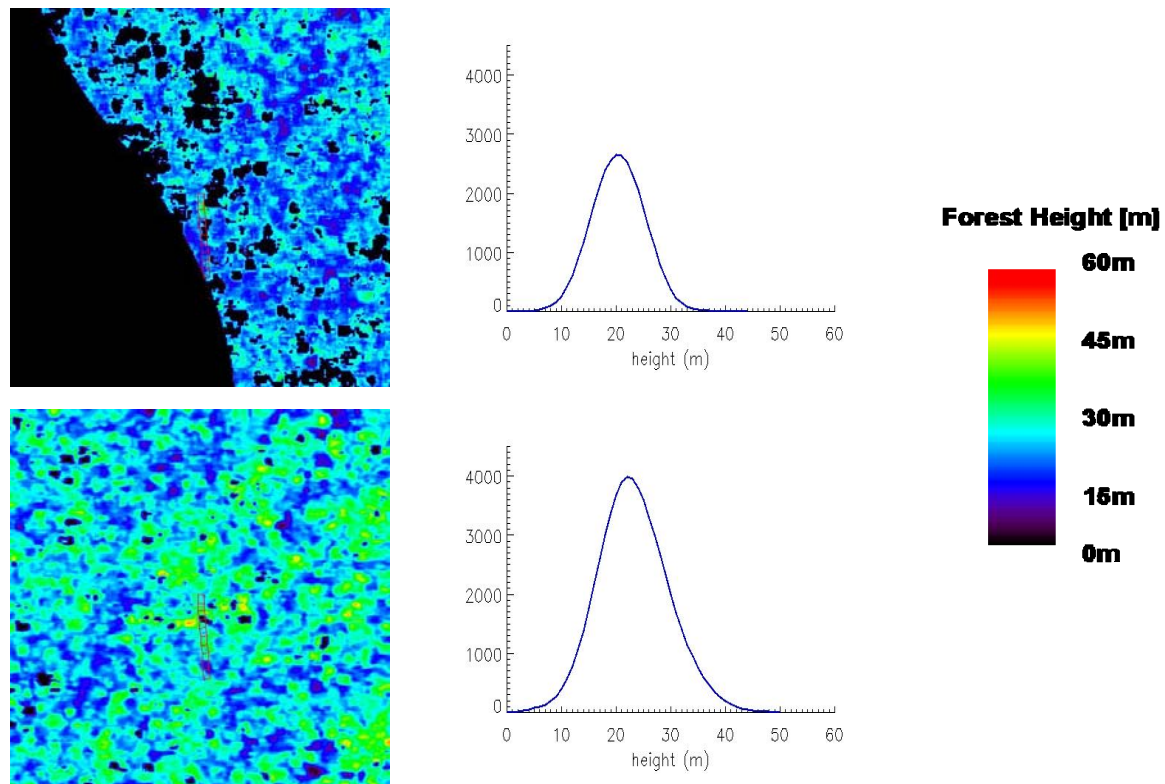


Figure 7.3.32: Detail of height maps for Mawas forest: top: L-band 10m baseline, bottom: P-band 30m baseline; masked areas are black

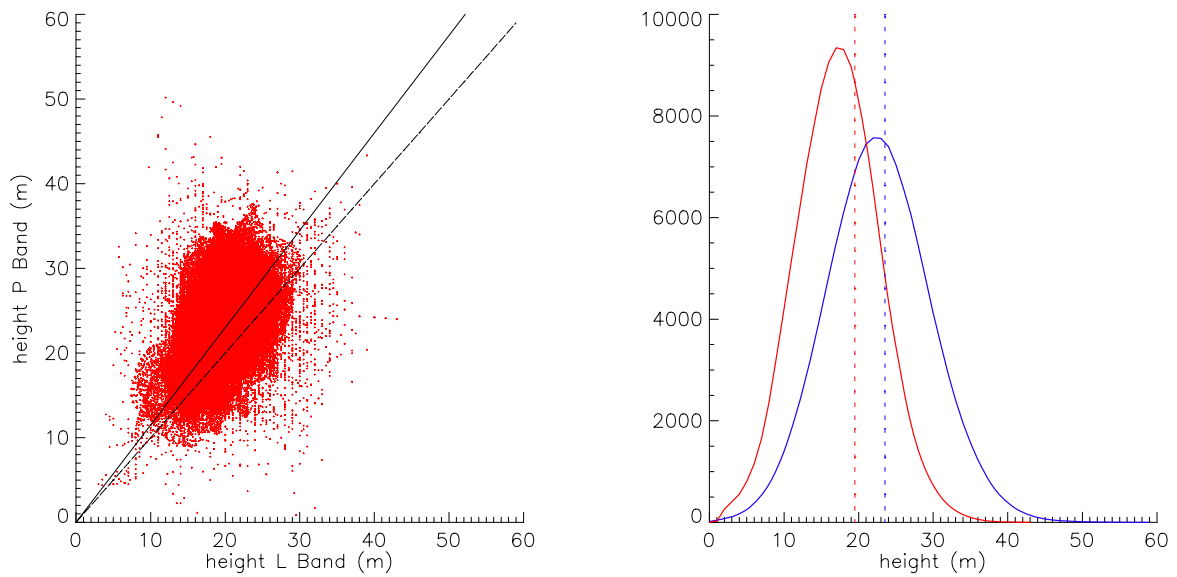


Figure 7.3.33: Comparison L and P Band heights for Detail (Figure 7.3.32) of Mawas; left: Plot L Band heights against P Band heights (low pass filtered); right: histogram, P Band=blue, L Band=red

For the plot indicated in Figure 7.3.32 the height estimations at P band (mean value: 22.5m) are in average 3m higher than the one obtained at L band (mean value: 19.5m). A common pixel based comparison indicates the strong correlation between the obtained L band and P band heights (see Figure 7.3.33). Finally the histograms of the obtained heights are shown in Figure 7.3.33 and Figure 7.3.32.

Temporal Decorrelation

A critical decorrelation source in repeat-pass interferometry is temporal decorrelation. Temporal effects are difficult to quantify and can appear in a more or less stochastic fashion within the scene. Temporal decorrelation decreases the interferometric coherence, increases the variance of interferometric phase and biases forest height estimates. A decomposition of temporal and volume decorrelation is – due to the stochastic nature of temporal disturbance effects – difficult if not impossible.

The Mawas data acquisition flights had to be performed under windy conditions. In consequence, some of the repeat-pass acquisitions (at L and P band) are affected by wind induced temporal decorrelation. Assuming a scalar temporal decorrelation that affects only the volume (canopy) part and the measured interferometric coherence becomes according to [17]

$$\tilde{\gamma}(\vec{w}) = \exp(i\kappa_z z_0) \frac{\gamma_{Temp} \tilde{\gamma}_{V0} + m(\vec{w})}{1 + m(\vec{w})} \quad -14)$$

An inversion by means of Eq. 6 without accounting for γ_{Temp} leads to a critical overestimation of forest height [17].

One way to evaluate γ_{Temp} is to make use of the available single-pol (VV) single-pass X band acquisition as it is unaffected by temporal decorrelation. The high extinction values at X band allows a simplification $F(z)$ by ignoring completely the ground scattering component (assuming $m=0$) and fixing the extinction to a given (non-zero) value. This leads to a determined inversion problem [18]

$$\min_{h_V, \phi_0} \left\| \tilde{\gamma}^X(\vec{w}) - \tilde{\gamma}_V^X(h_V, \phi_0 \mid \sigma = \sigma_0) \right\| \quad -15)$$

Eq. 15 can be further reduced to a single parameter problem by neglecting the ground phase

$$\min_{h_V} \left\| |\tilde{\gamma}^X(\vec{w})| - |\tilde{\gamma}_V^X(h_V, \phi_0 \mid \sigma = \sigma_0)| \right\| \quad -16)$$

Eq. 16 can be inverted by a single interferometric channel providing forest height estimates – as shown in Figure 7.3.34. Of course a generalisation of Eq. 16 is critical: The maximum volume height that can be estimated is limited by the penetration depth that decreases with increasing extinction. With further increasing height the interferometer do not "see" anymore the whole volume and the height estimation "saturates". However, the Mawas test site is characterised by very low and less dense forest conditions leading to moderate extinction values for X band.

The obtained forest height estimates are now used to approximate the volume decorrelation contribution at L (and P) band for the HV channel. Assuming a zero extinction (i.e. $\sigma_L = 0$) and a zero ground scattering (i.e., $m(HV) = 0$) the volume decorrelation is given by

$$|\tilde{\gamma}_V^L(HV)| = |\tilde{\gamma}_{V0}^L(HV)| = \text{sinc}\left(\frac{\kappa_z^L h_V}{2}\right) \quad -17)$$

where $\text{sinc}(x) = \sin(x)/x$. The obtained results for the L band coherences are shown in Figure 7.3.35. Having an estimate of the (absolute) volume decorrelation contribution at HV permits now to estimate the temporal decorrelation contribution at L (and P) band

$$\gamma_{Temp} = |\tilde{\gamma}(HV)| / |\tilde{\gamma}_{V0}^L(HV)| \quad -18)$$

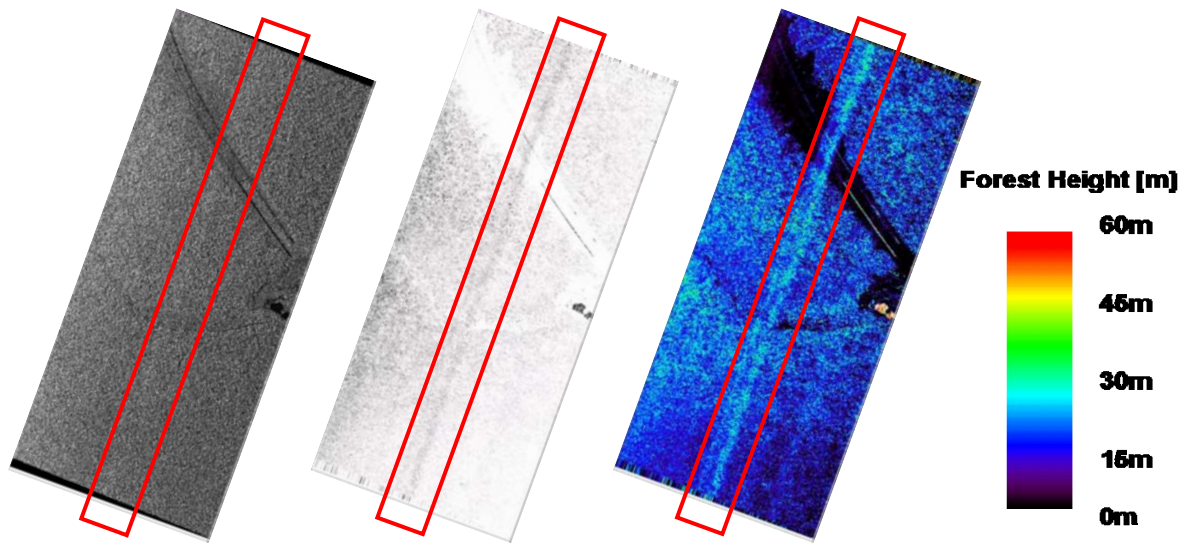


Figure 7.3.34: Inversion X Band; from left to right: Amplitude (VV), Coherence (VV), Height map, Legend; red boxes mark disturbances due to an antenna error (only in X Band)

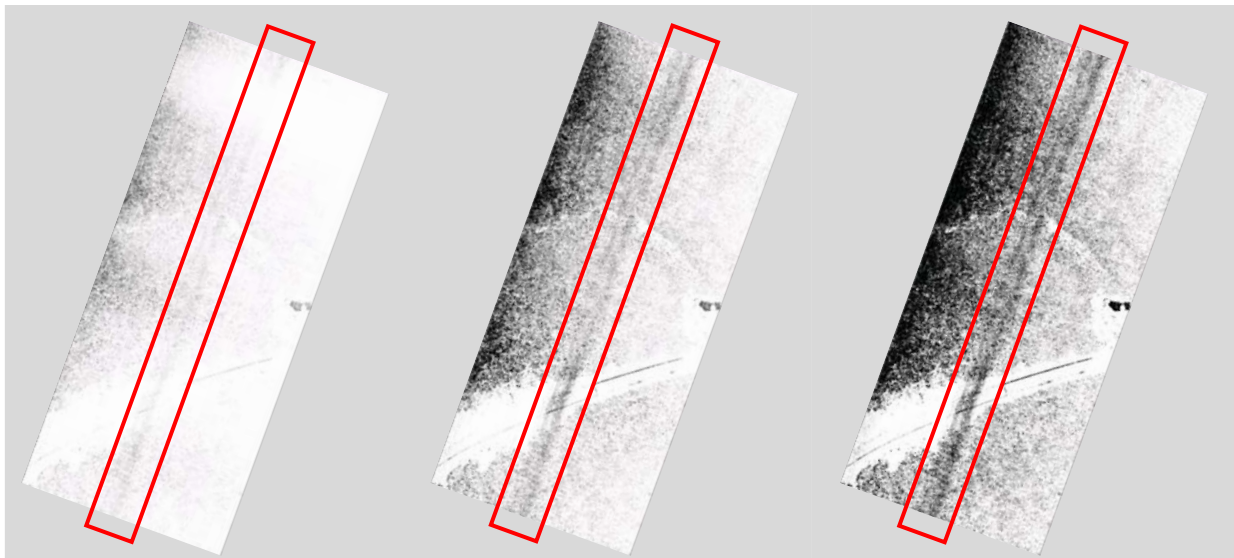


Figure 7.3.35: Volume coherence of X Band heights in L Band Geometry; left: 5m Baseline, middle: 10m Baseline; right 15m Baseline; red boxes mark disturbances due to an antenna error (only in X Band)

The obtained γ_{Temp} maps with the corresponding histograms are shown in Figure 7.3.36. At L band γ_{Temp} is about 0.90 while at P band it is 0.95 – as expected – lower at about 0.05. The temporal baseline was about 20 minutes for both frequencies.

Note that a potential underestimation of the forest height used in Eq. 11 (because of saturation for example) will bias the volume decorrelation estimation and leads to an underestimation of the temporal decorrelation. In contrary, an overestimation of the forest height (due to an underestimated extinction) will lead to an overestimation of the temporal decorrelation or even to ratios larger than one.

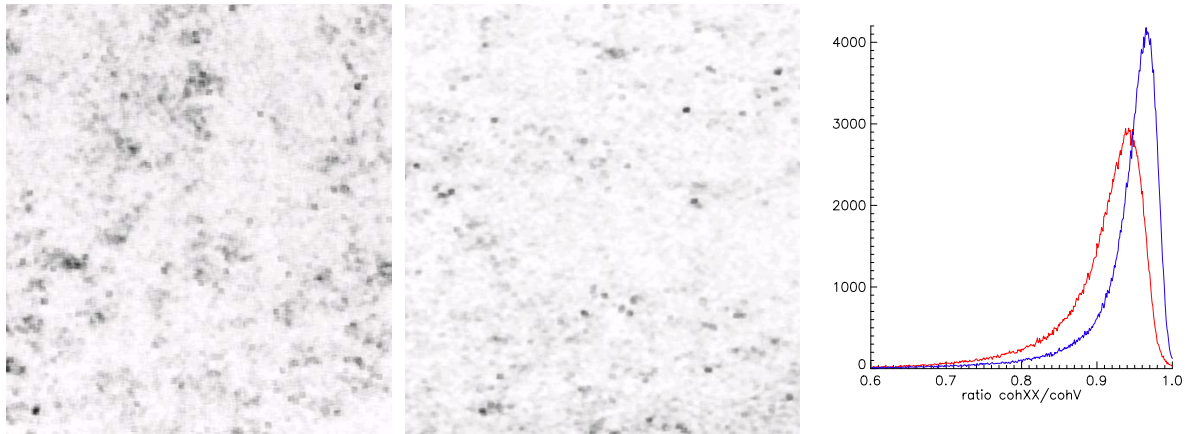


Figure 7.3.36: Estimated temporal decorrelation at L band (left) and P band (middle) for the Mawas test site: Scaled from black: $\gamma_{Temp}=0$ to white: $\gamma_{Temp}=1$; Histogram of estimated γ_{Temp} (scaled from 0.6 to 1): L band=red, P band=blue.

The localised high decorrelation “points “ visible at L band and even more at P band are due to single large trees that are underestimated when inverting the X band coherence leading therefore to high temporal decorrelation ratios.

7.3.6 Performance Comparison and Discussion

Regarding the RVoG inversion performance by means of single-baseline Pol-InSAR data at L and P band following points can be made based on the obtained results:

1. L band (and of course P band) seems - as far as it can be validated with the available data - to penetrate the vegetation layer even in the densest forested INDREX-II test sites, and to provide a sufficient ground contribution for Pol-InSAR data inversion. This is an important result as this was one of the main mission objectives of INDREX-II.
2. L and P band have a similar inversion performance. The RVoG inversion performance in terms of a single baseline depends - primarily - on the length of the "visible line segment" in the data. On the one hand P band has a higher penetration capability through vegetation layers than L band. This leads to a wider ground scattering spectrum and potentially longer "visible line segments". On the other hand is P band less sensitive to the vegetation layer that again may shorten the visible line segment.
3. The L band estimates are in average about 5m higher than the estimates at P band. This can be interpreted by the reduced sensitivity of P band to the top vegetation layer and/or by a higher sensitivity of L band to decorrelation effects (as temporal decorrelation) which introduce a bias resulting in overestimated heights.
4. The direct validation (i.e. line test) as well as the achieved inversion results made clear that the RVoG model is applicable on tropical vegetation. Further, there were no indications for any limitation with respect to its application on the P band data sets.

Note that a fair comparison between L and P band Pol-InSAR inversion performance has to account the wavelength induced geometric scaling factor: In order to achieve the same vertical wavelength (kZ) the L band baseline has to be about 3-4 times smaller than at P band. In the case of the E-SAR System for example, the realisation of $kz = 0.1$ requires at P band a 15m while at L band a 5m horizontal baseline (at 3 km flight height above ground and an incidence angle of about 30°).

The inversion performance at L band is expected to be less sensitive to topographic variations within the scene than P band due to the strong topographic dependency of the dihedral scattering component that is the dominant ground scattering component at P band. However, L-band can be indirectly affected by topographic variations: Terrain slopes modulate the effective baseline at L-band by a factor of three (i.e. the P to L band wavelength ratio) stronger than at P band (for the same spatial baseline) increasing the decorrelation level on positive slopes at L-band. However, no topography induced effects - neither at P nor at L band - could be demonstrated, probably due to the limitations on the available ground-measurements.

5. For the same number of effective looks, the variance of the obtained estimates is related to the overall coherence level in the formed interferograms. For the available baselines - especially the smaller ones - the coherence level at P band is, in general, higher than at L band (for the same kZ values) due to the larger ground-to-volume scattering amplitude ratios at P-band. Accordingly, the variance of the estimates obtained at L band is somewhat higher than at P band. This can be compensated either by increasing the number of effective looks - at the expense of spatial resolution - or better by using smaller baselines.

However, the realisation of small baselines by means of an air-borne repeat-pass configuration is limited by the flight track accuracy. In the case of the E-SAR the achieved track accuracy is on the order of $\pm 2m$ (in good conditions) up to $\pm 5m$ (in poor conditions) limiting the realisation (or the quality) of baselines smaller than 4-10m. The strong variation of the effective baseline leads to the strong variation of kZ in the small-baseline interferograms at L-band as observed in the INDREX-II data sets.

In consequence, the inversion performance dependency on the baseline is significantly larger at L band than at P band affecting the obtained estimates. However, it is important to make clear that this is a limitation that arises from the specific system design and acquisition implementation rather than a physical limitation.

There are still two points that have to be mentioned:

6. Spatial Resolution: The availability of a certain (relative large - depending on the actual coherence level) number of looks is essential for reaching acceptable accuracy levels in almost all interferometric applications. This makes the use of high resolution systems essential for reaching the spatial resolution requirements and/or to recover the spatial inhomogeneity of forest structures. In the case of INDREX-II both L and P band data have been acquired / processed to the same range (100MHz) / azimuth bandwidths and the same number of looks has been used in the inversion process. A reduced spatial resolution of the original data lead to a reduced inversion performance.
7. Temporal Decorrelation: P band is of course characterised by a higher temporal stability than L band. However, temporal decorrelation effects had to be accounted / compensated in both frequencies.

Finally note that as reference height the height of the trees which form the upper canopy of the forest should be used. For even aged single species temperate forests this corresponds to the so called h100 [7] that have been successfully used for POI-InSAR validation. However, tropical forests don't fulfil necessarily that criterion, as they are composed of many different tree species with unequal age and a complex vertical structure. Therefore, a forest height for validation needs still to be defined.

8 Summary and Conclusions

INDREX-II was under several aspects a challenging airborne radar campaign; the challenges that needed to be faced where in the domain of management, logistics, permission application barriers, cultural aspects and not to forget the tropical end of Monsoon weather. In all this aspects the DLR and WUR team was strongly supported by the Indonesian partners and Indonesians not being explicitly mentioned here. The continuous support throughout the campaign helped to keep the tight time schedule of the experiment and to perform the airborne and ground measurements smoothly and without any major interruption or technical problems.

The ground measurements have been performed under extreme tropical conditions during a period of almost a year at the different INDREX-II forest test sites. A huge - for tropical conditions - amount of measurements have been performed under the lead of WUR and supported by the Indonesian partners. The data have been delivered accordingly to ESA (Section 5).

The performance of the radar measurements was challenging too. First, DLR's E-SAR airborne radar system has to be transported to Indonesia in containers, separately from the aircraft. The reason for this was the limited flight range of the aircraft (Do228) with the system on board. The customs for both systems have been done in Jakarta, then both have been then separately transported to Balikpapan, that was the main base of the campaign. In a hunger at the Balikpapan airport the E-SAR system has been mounted into the Do228 aircraft (Section 5).

The test and calibration site has been deployed on the Balikpapan airport. Several corner reflectors, of small 1.5m and big 3m have been installed beside the runway. In order to check the (first order) calibration and data quality on site a mobile processing facility has been installed in the hanger. These first quality checks performed on site indicated already a good radiometric and interferometric quality of the acquired data. Identified problematic deviations from the nominal tracks - caused by the sometimes turbulent weather conditions - initiated the repetition of some of the flights in order to assure optimal interferometric data quality. It happens that one flight needed to be repeated, as from the processing it could be already seen that a forest height derivation from a repeat pass track would be nearly impossible with the strong flight line deviations.

The acquired SAR raw data has been processed at DLR in Germany under the supervision of an Indonesian security officer. In Section 6 the processing procedure is described in detail. In summary it can be stated that the overall radar data quality - accounting from radiometric accuracy over at the different frequencies to interferometric quality and the flight accuracy - is very good. The absolute radiometric accuracy is ranging between 1 and 3 dB depending on the different frequencies, the relative radiometric accuracy is about 1dB or even better. All data have been processed with an incidence angle range from 25 to 55 degrees. In addition, after ESA's request, P-band data have been processed also for a steeper incidence angle range from 18 to 50 degrees. However, these data sets should be used carefully, as no calibration control could be done for the steeper incidence angle range. In order to be able to process the huge amount of acquired data and modes, an automatic processing procedure, that cuts the data and process it with an overlap has been developed. Finally, two hard disks have been delivered to ESA with about 550 Gbyte on processed data.

In order to answer some of the questions posed at the begin of the study the first order results obtained in the frame of this project are summarised in the following:

1. *Is there an empirical relation between the radar backscatter and the forest biomass using L- and/or P-band?*

No relation between the radar backscatter, nor at L- either at P-band and biomass level could be found. One potential reason for this is that the biomass levels in tropical forest is much

higher than the reported (expected) saturation levels at L- or P-band (270 - 390 t/ha). But also at the low biomass test sites no clear relation between radar backscatter at L- or P-band to biomass could be validated (14 – 158 t/ha).

The biomass level at the different test sites has been evaluated from the ground measurements by using standard allometric equations. Several equations have been analysed and the input parameter carefully checked. High deviations of the obtained biomass estimates between the different allometric equations have been obtained. As reference for further analysis within this project one standard allometric equation corresponding to Indonesian forest types has been finally selected.

2. ***Does L or/and P-band penetrate through the dense tropical forest and shows reflection from the ground?***

Yes they do. L band (and of course P band) appear - as far as it can be validated with the available data - to penetrate the vegetation layer even in the densest forested INDREX-II test sites, and to provide a sufficient ground contribution for Pol-InSAR data inversion. This has been validated indirectly, by analysing amplitude and Pol-InSAR forest signatures, but also in a direct way by validating the obtained forest height inversion results. This is an important result as this was one of the main mission objectives of INDREX-II

3. ***Is it possible to estimate forest height by means of Pol-InSAR over tropical forest sites?***

Yes it is. Forest height has been successfully estimated using single-baseline quad-pol repeat-pass L-band P-band. This has been demonstrated for two INDREX-II test sites and validated against the ground measurements. In order to compare the achieved results at the two frequencies the baselines have been selected to account for the ratio of the wavelengths (i.e. the P-band baselines are about a factor of three larger compared to L-band baselines). This is important for obtaining the same sensitivity to the volume layer and to guarantee a fair comparison.

The results obtained at both frequencies are similar (see Section 7) The L-band estimates are on average about 5m higher than the estimates at P-band. This can be interpreted by the reduced sensitivity of P-band to the top vegetation layer and/or by a higher sensitivity of L-band to decorrelation effects (as temporal decorrelation) which introduce a bias resulting in overestimated heights.

A detailed validation against the full ground measurement basis is still open and is recommended for further investigations. The main problem here is to define which height is the height that radar 'sees' and is sensitive to. A preliminary analysis showed, that there is a correspondence to the ground measured heights, but this needs still to be confirmed and validated. In temperate forest the so called h100 (the highest 100 trees) method has been used, where high correlation could be observed. In tropical forest this is not possible, as the forest is very heterogeneous and needs other height definitions.

The INDREX-II data sets are a unique data basis for a wide spectrum of investigations relevant to many different scientific domains as ecology, forestry and remote sensing community that may allow to improve our understanding of tropical forests ecosystems. And only if humans start to understand better then they will be - maybe - able to care and sustain these fragile ecosystems.

9 Recommendation

9.1.1 Ground measurements and Radar backscattering analysis

Mawas

- The quantification of forest structure along the Mawas research transect using the aerial photo stereo coverage is very useful and will open the way for the extraction of relationships between forests parameters and backscatter along the complete range of conditions found in the radar strips.
- A study of the dynamic aspects of flooding and ground water level using additional PALSAR data.

Balikpapan

- Trees in the Dipterocarp forest, such as at the Sungai Wain and Meratus test sites, can be very large. Canopy trees up to 70 m frequently occur. Moreover many species are present and the canopy is very rough. In high resolution radar images such as those from E-SAR or AirSAR such trees show up individually and have distinct radar signatures. More fieldwork is needed to study such radar data sets especially at the individual tree level.

Biomass

- The question how to derive biomass from field data has to be addressed in far more detail for these complex tropical surroundings.

The question how to retrieve biomass information from radar data still needs a lot of attention. It could be done through (1) direct relationships (i.e. biomass vs. backscatter) or (2) through prior classification of forest structure, and subsequently relating structure to biomass. An unsupervised polarimetric classification of forest structure is a promising approach in this respect.

9.1.2 Pol-InSAR analysis

In order to evolve forest product generation by means of Pol-InSAR from local/regional to large scale/global applications two critical issues remain to be faced:

1. The product generation performance has to be demonstrated/validated in tropical forest environments because of the enormous ecological importance of the tropical ecosystems;
2. A successful implementation in a space-borne framework has to be demonstrated.

Both aspects could not be covered up to know

- a) because appropriate Pol-InSAR data over tropical forests are not available, and
- b) because of the delay of the ALOS launch.

The success of the INDREX-II campaign and the successful launch of ALOS in January 2006 open now the way for the investigation of both aspects. Combining expertise in polarimetric SAR interferometry (Pol-InSAR) calibration, processing, modelling and inversion algorithms, radar system design and technology, as well as directing expertise in tropical forest ecology we propose to address and evaluate both aspects in the frame of this project.

It is recommended, that the methodology for forest height derivation developed in the frame of the *Pol-InSAR Mission and Application Study* is applied and evaluated on selected test sites of the INDREX-II campaign. Pol-InSAR product need then to be assessed for the most important tropical forest types as

undisturbed and disturbed primary/secondary forest, mangrove forest and palm plantations. The selected Pol-InSAR data sets should be inverted and the generated products need to be validated against ground measurements and other available reference data. The availability of dual- and quad-Pol-InSAR data sets at different frequencies (X-, L- and P-band) challenges a performance comparison of Pol-InSAR products generated at the different frequencies. This will provide a validation of the critical assumptions drawn in the product generation methodology and will allow conclusions about optimum frequency selection.

Further it is recommended to evaluate the effect of temporal decorrelation on the individual Pol-InSAR products, which need to be quantified using as reference the ground measurements and the products generated by using the airborne data. Depending on the impact of temporal decorrelation the product generation methodology need be adjusted, modified or extended to account for the ALOS-PaISAR data characteristics. The performance of ALOS-PaISAR for forest height derivation needs to be investigated.

Finally, the “lessons learned” from the analysis of the INDREX-II and the ALOS-PaISAR data sets are important in order to extrapolate it on large scale and to conclude about the potential the forest height product generation and as well as about and possible/realistic future mission scenarios. In addition new application areas and development directions of Pol-InSAR technology are possibly identified and new proposition will be made – accounting user perspective requirements and needs.

10 Publications

1. Irena Hajsek, Florian Kugler, Konstantinos Papathanassiou, Rolf Scheiber , Ralf Horn, Alberto Moreira , Dirk Hoekman , Malcolm Davidson , and Evert Attema, ‘INDREX II: Indonesian Airborne Radar Experiment Campaign over Tropical Forest’, Proceedings of ESA Workshop on Applications of SAR Polarimetry and Polarimetric Interferometry, PolinSAR 2005, Frascati, p. 6.
2. I. Hajsek, F. Kugler, K. Papathanassiou, R. Horn, R. Scheiber, A. Moreira, D. Hoekman and M. Davidson, ‘INDREX II – Indonesian Airborne Radar Experiment Campaign over Tropical Forest in L-and P-band: First Results’, IGARSS2005, Seoul, South-Korea, July. 2005, IEEE, Proceedings IGARSS, vol. VII, pp.4335-4339, (2005)
3. F. Kugler, K. Papathanassiou, I. Hajsek, D. Hoekman, INDREX-II Tropical Forest Height Estimation with L- and P-band Polarimetric Interferometric SAR
4. Microwaves and Radar Home page, <http://www.dlr.de/hr>

11 Reference

- [1] Shane, R. C. Papathanassiou, K. P. "Polarimetric SAR Interferometry", IEEE Transactions on Geoscience and Remote Sensing, VOL. 36, NO. 5, September 1998, pp. 1551 – 1565
- [2] Papathanassiou, K., & Cloude, S.; "Single Baseline Polarimetric SAR Interferometry"; IEEE Transactions on Geoscience and Remote Sensing, 2001, vol. 39, no. 11, pp. 2352-2363
- [3] Cloude, S.R. Papathanassiou, K.P. "A 3-Stage Inversion Process for Polarimetric SAR Interferometry" IEEE Proceedings Radar Sonar & Navigation, vol 150, issue 3, 2003
- [4] Just D. Bamler, R. "Phase Statistics of Interferograms with Applications to Synthetic Aperture Radar", Applied Optics, Vol.33, Nr.20, S. 4361-4368, Juli 1994.
- [5] Bamler, R. Hartl, P. "Synthetic aperture radar interferometry", Inverse Problems 14, R1-R45, UK, 1998
- [6] Hajnsek, I. Papathanassiou, K.P. Cloude, S.R. "Removal of Additive Noise in Polarimetric Eigenvalue Processing", Proceedings IGARSS'01, Sydney Australia, 2001
- [7] Mette, T., Papathanassiou, K & Hajnsek, I., 'Biomass estimation form polarimetric SAR interferometry over heterogenous forest terrain', Proc. IGARSS04, 20.-24. Sept. 2004, Anchorage, vol. I ,pp. 511-514
- [8] Papathanassiou, K. & Cloude, S. "Single Baseline Polarimetric SAR Interferometry", Transactions on Geoscience and Remote Sensing, vol. 39, no. 11, pp. 2352-2363, 2001
- [9] Cloude, S.R. Papathanassiou, K.P. "A 3-Stage Inversion Process for Polarimetric SAR Interferometry" IEEE Proceedings Radar Sonar & Navigation, vol 150, issue 3, 2003
- [10] Hajnsek, I., Kugler, F., Papathanassiou, K., Scheiber, R., Horn, R. Moreira, A., Hoekman, D., Davidson, M., INDREX – Indonesian Airborne Radar Experiment Campaign over tropical forest in L- and P-band, Workshop PolinSAR, ESA, ESRIN, Italy, January 2005, <http://earth.esa.int/cgi-bin/confpol.pl?abstract=193>
- [11] Mette, T., Papathanassiou, K & Hajnsek, I., "Biomass estimation form polarimetric SAR interferometry over heterogenous forest terrain", Proc. IGARSS04, 20.-24. Sept. 2004, Anchorage, vol. I ,pp. 511-514
- [12] Kugler, F. Hajnsek, I. Papathanssiou, K. Hoekman, D. "INDREXII – Indonesian Airborne Radar Experiment Campaign over Tropical Forest In L- and P-band Polarimetric interferometric SAR", Proc. 3D Remote Sensing in Forestry, Vienna, 14.2 – 15.2.2005,
- [13] Kugler, F. Papathanssiou, . Hajnsek, I K. Hoekman, D. "INDREX-II – Tropical Forest Height estimation with L and P band Polarimetric interferometric SAR", Proc. EUSAR, Dresden, 16-18.5.2006
- [14] Kugler, F. Hajnsek, I. Papathanassiou P. K. Horn, R. Scheiber, R. Moreira, A. Hoekman, D. Davidson, M. "INDREX II – Indonesian Airborne Radar Experiment Campaign over Tropical Forest in L- and P-band: First results" IGARSS2005, Seoul, South Korea, 2005-07-25 - 2005-07-29
- [15] Bamler, R. & Hartl, P. "Synthetic Aperture Radar Interferometry", Inverse Problems, vol. 14, pp. R1-R54, 1998.
- [16] Treuhaft, R.N. and Siqueira P.R.. "The Vertical Structure of Vegetated Land Surfaces from Interferometric and Polarimetric Radar", Radio Science, vol. 35, no. 1, pp. 141-177, 2000.

- [17] K.P. Papathanassiou and S.R. Cloude, "The Effect of Temporal Decorrelation on the Inversion of Forest Parameters from Pol-InSAR Data", Proceedings IGARSS'03 (CD-ROM), Toulouse, France, 2003.
- [18] Kugler, F. Koudogbo, N. F. Gutjahr, K. Papathanassiou, K. P. "Frequency effects in PolInSAR Forest Height Estimation", Proc. EUSAR, Dresden, 16-18.5.2006
- [19] R.K. Raney, T. Freeman, R.W. Hawkins, and R. Bamler: "A Plea for Radar Brightness", Proc. IGARSS, pp. 1090-1092, Pasadena, 1994.
- [20] A. Moreira, J. Mittermayer, R. Scheiber: "Extended Chirp Scaling Algorithm for Air- and Spaceborne SAR Data Processing in Stripmap and ScanSAR Imaging Modes", IEEE Trans. Geosc. Rem. Sens., vol.34, no. 5, pp. 1123-1136, September 1996.
- [21] R. Scheiber and A. Moreira: „Coregistration of Interferometric SAR Images using Spectral Diversity“, IEEE Trans. Geosc. Rem. Sens., vol.38, no. 5, pp. 2179-2191, September 2000.
- [22] A. Reigber: „Correction of residual motion errors in airborne SAR interferometry“, Electronics Letters, vol. 37, no. 17, August 2001.
- [23] R. Scheiber: „A Three step phase correction approach for airborne repeat-pass interferometric SAR“, Proc. IGARSS, Toulouse, July 2003.
- [24] K.A.Câmara de Macedo and R. Scheiber: "Precise Topography and Aperture Dependent Motion Compensation for Airborne SAR", IEEE Geosc. Rem. Sens. Letters, vol.2 no.2, pp.172-176, April 2005.